Identifying novel drugs for the treatment of rhabdomyosarcoma

---

Jenna Bleloch

BLLJEN010

Supervisor:

Professor Sharon Prince

This thesis is presented for the degree of

DOCTOR OF PHILOSOPHY IN MEDICAL CELL BIOLOGY

Division of Cell Biology

Department of Human Biology

Faculty of Health Sciences

University of Cape Town

South Africa

11th February 2019

Declaration

I, Jenna Susan Bleloch, hereby declare that the work on which this thesis is based is my original work (except where acknowledgements indicate otherwise) and that neither the whole work nor any part of it has been, is being, or is to be submitted for another degree in this or any other university. I empower the university to reproduce for the purpose of research either the whole or any portion of the contents in any manner whatsoever.

Signed by candidate

11th February 2019

Acknowledgements

I would like to express my sincerest gratitude to my PhD supervisor, **Professor Sharon Prince**, for her constant sport, guidance and encouragement. I am so grateful for all the time she has so generously invested in me and her commitment to developing me in all spheres of academia. I hold her in high regard for what she has achieved as a woman in science and I have been inspired by her work ethic and strive for excellence.

A special thank you to the members of the **Prince Laboratory** who collectively contributed to a stimulating, productive and collegial working environment. It has been inspiring to be surround by so much passion for science and the past 4 years have been truly fulfilling and memorable. To my PhD contemporaries, **Alexis Mufweba** and **Rehana Omar,** I cannot thank you enough for all your support and positivity on this journey and to previous Prince Lab members and my friends, **Danica Sims**, **George Cooper** and **Brittany Jacobs,** thank you for adding so much colour to my life inside the lab and outside - this journey of mine has been so much richer for having you in it.

I would like to thank **Professor Colin Goding** at the Ludwig Institute for Cancer Research at the University of Oxford for welcoming me into his laboratory for a few months and for his supervision and guidance on an exciting aspect of my PhD project. Thank you to the members of the **Goding Laboratory** for their kindness and making me feel so a part of the lab with a special thanks to **Sizhu Lu** who I so enjoyed working with and appreciated sharing the lows and highs of our high throughput drug repurposing project. Thank you to **Daniel Ebner**, **Dr Val Millar** and **Elena Seraia** from the High Throughput Screening Group at the Target Discovery Institute for their time, assistance and patience with developing and optimising our high throughput drug screen.

My gratitude is extended to **Dr Ben Loos** from the University of Stellenbosch for his insightful feedback and advice on our autophagy research and for his combined contribution with **André Du Toit** to generating the data in Fig. 3.8. **Dr Lubbe Wiesner** and **Dr Liezl Gibhard** from the Division of Clinical Pharmacology at the University of Cape Town must be thanked for

their in vivo pharmacokinetic research of AJ-5 depicted in Fig. 3.11 and Table 3.1. Our inorganic chemistry collaborators from Stellenbosch University, **Professor Selwyn Mapolie**, **Dr Angelique Blanckenberg** and **Annick van Niekerk**, must be thanked for synthesising and providing AJ-5 and BTC2. My gratitude is expressed to **Professor Musa Mhlanga** from the University of Cape Town for his invaluable input and suggestions on specific aspects of my PhD project. My deepest thanks go to this lab members **Loretta Magagula** for so generously assisting with experiments involving the Tet-On Cas9 iPSCs (Fig. 4.17) and **Dr Jerolen Naidoo** for his time and patience with teaching me how to use HC StratoMiner and interpret the data. My sincere thanks to **Saif Khan** for his enthusiasm in pursuing our 'hit' drugs for the treatment of TBX2/3 driven cancers and for providing feedback on CHAPTER 4 of this thesis. Gratitude is due to **Associate Professor Dirk Lang** and **Susan Cooper** for their confocal microscopy assistance and **Ronnie Dreyer** for assisting me with all my **FACS** experiments.

This work was generously supported by the **National Research Foundation**, **Newton Fund** and **Research Council UK**, **Struwig-Germeshuysen Trust**, **Ernst and Ethel Erikson Trust**, and the **University of Cape Town**. Thank you for the funding and financial support that enabled this research.

On a personal note, I would like to thank my parents **Sue** and **Grant Gush** and **Mark Bleloch** and **Leigh De Decker** who have always believed in me, encouraged me and supported me; my brother, **James Bleloch,** for his genuine interest and engagement in my research; and my grandparents **Lionel** and **Rosemary Falcon** for always checking in on me and my PhD. I would also like to extend my gratitude to **Ashley** and **John Bestbier** and **Michèle Betty** for their consistent support and encouragement throughout this scientific endeavour. Lastly, I would like to thank my partner **Nicholas Bestbier**. Words will never be enough to describe how grateful and appreciative I am for his unconditional support. This PhD journey has been filled with wonderful and exciting moments, but also difficult and challenging times and I could not have wished for a better partner to celebrate in my successes and encourage and believe in me when times were tough. I would not have been able to achieve this without him.

Research Outputs from this PhD

Original Publications

Bleloch, J.S., Lu, S., Khan, S.F., Goding, C. and Prince, S. 2019. A high throughput screen to identify FDA-approved drugs that target the oncogenic TBX2 and TBX3 for anti-cancer activity. In preparation.

Bleloch, J.S., Du Toit, A., Gibhard, L., Kimani, S., Ballim, R.D., Lee, M., Blanckenberg, A., Mapolie, S., Wiesner, L., Loos, B. and Prince, S. 2019. The palladacycle complex AJ-5 induces apoptotic cell death while reducing autophagic flux in rhabdomyosarcoma cells. *Cell Death Discovery,* 5(1): 60.

Bleloch, J.S., Ballim, R.D., Kimani, S., Parkes, J., Panieri, E., Willmer, T., and Prince, S. 2017. Managing sarcoma: where have we come from and where are we going? *Therapeutic Advances in Medical Oncology*, 9(10), 637–659.

Aliwaini, S., **Bleloch, J.**, Kimani, S. and Prince, S. 2016. Induction of Autophagy and Apoptosis in Melanoma Treated with Palladacycle Complexes. In: Hayat, M.A. ed. *Autophagy: Cancer, Other Pathologies, Inflammation, Immunity, Infection, and Ageing, Volume 10*. Chennai: Elsevier Inc.

Patent

Enabler on the following patent:
Mapolie S., Blanckenberg A., van Niekerk A., and Prince S. (2018) Binuclear palladacycles and their use in the treatment of cancer. PA168462/ZA, filed 16 February 2018. Patent pending.

National and International Conferences

Bleloch, J., Lu, S., Ebner, D., Goding, C. and Prince, S. 2018. Repurposing FDA-approved drugs that target transcription factors for their use in cancer therapy. Oral presentation at the international ICGEB Workshop 'Transcription factors in cancer therapy,' 2018, Cape Town, South Africa, 8-10 October 2018.

Bleloch, J., Lu, S., Ebner, D., Millar, V., Seraia, E., Goding, C. and Prince, S. 2018. A high throughput screen to identify FDA-approved drugs that target the oncogenic TBX2 and TBX3 for anti-cancer activity. Oral presentation at the Newton Fund Networking Meeting for the Biomedical Sciences Exchange PhD Studentship Programme between the University of Cape Town and the University of Oxford, Cape Town, South Africa, 25-26 September 2018.

Bleloch, J., Du Toit, A., Gibhard, L., Ballim, R., Blanckenberg, A., Mapolie, S., Wiesner, L., Loos, B. and Prince, S. 2018. The palladacycle complex AJ-5 induces apoptotic and necroptotic cell death while reducing autophagic flux in rhabdomyosarcoma cells. Oral presentation at the University of Cape Town Department of Human Biology Research Day, 12 September 2018. *Award for best oral presentation.*

Bleloch, J., Lu, S., Ebner, D., Millar, V., Seraia, E., Goding, C. and Prince, S. 2017. A high throughput screen to identify FDA-approved drugs that target the oncogenic TBX2 and TBX3 for anti-cancer activity. Oral presentation at the University of Cape Town Health Sciences Faculty Postgraduate Research Day, 27 September 2017. *Award for best oral presentation.*

Bleloch, J., Ballim, R., Aliwaini, S., Blanckenberg, A., Mapolie, S., Kimani, S. and Prince, S. 2017. A novel palladacycle complex with anti-cancer activity against breast cancer and melanomas also exhibits potent cytotoxicity in a range of sarcomas. Poster presentation at the AACR-EACR-SIC 2nd Special Conference, The Challenges of Optimizing Immuno- and Targeted Therapies: From Cancer Biology to the Clinic, Florence, Italy, 25-27 June 2017.

Bleloch, J., Ballim, R., Aliwaini, S., Blanckenberg, A., Mapolie, S., Kimani, S. and Prince, S. 2017. A novel palladacycle complex with anti-cancer activity against breast cancer and melanomas

also exhibits potent cytotoxicity in a range of sarcomas. Poster presentation at the AACR International Conference: New Frontiers in Cancer Research, Cape Town, South Africa, 18-22 January 2017.

Bleloch, J., Ballim, R., Aliwaini, S., Blanckenberg, A., Mapolie, S., Kimani, S. and Prince, S. 2016. Investigating novel binuclear palladacycle complexes for anti-cancer activity in rhabdomyosarcoma cells. Oral presentation at the 25th South African Society of Biochemistry and Molecular Biology, East London, South Africa, 10-14 July 2016.

Bleloch, J., Ballim, R., Aliwaini, S. and Prince, S. 2016. Investigating novel binuclear palladacycle complexes for anti-cancer activity in rhabdomyosarcoma cells. Poster presentation at the EACR Conference Series, A Matter of Life or Death: Mechanisms and Relevance of Cancer Cell Death for Cancer Biology and Treatment, Amsterdam, Netherlands, 28-30 January 2016.

Bleloch, J., Ballim, R., Aliwaini, S. and Prince, S. 2016. Investigating novel binuclear palladacycle complexes for anti-cancer activity in rhabdomyosarcoma cells. Oral presentation at the University of Cape Town Health Sciences Faculty Postgraduate Research Day, 2 September 2015. *Award for 2nd best oral presentation.*

Table of Contents

List of Figures

List of Tables

List of Abbreviations

%	percentage
°C	degrees Celsius
ACTN1	alpha-actinin-1
ADP	adenosine triphosphate
AIF	apoptosis-inducing factor
AKT	protein kinase B
ALK	anaplastic lymphoma kinase
AMP	adenosine monophosphate
AMPK	5′ AMP-activated protein kinase
APAF1	apoptotic protease activating factor 1
ARMS	alveolar rhabdomyosarcoma
ATG	autophagy related
ATM	ataxia telangiectasia mutated
ATP	adenosine triphosphate
ATR	ATM-Rad3-related
AUC	area under the curve
BA	bioavailability
BCL-2	B-cell lymphoma 2
BCL-XL	Bcl-extra large
BCOR	BCL-6 corepressor
bHLH	basic helix–loop–helix
BSA	bovine serum albumin
BTC2	Bridged Tethered Complex 2
CDK	cyclin-dependent kinase
CDKI	CDK inhibitor
cGMP	cyclic guanosine monophosphate
ChIP-seq	chromatin immunoprecipitation-coupled high throughput sequencing
CHK1	checkpoint kinase 1
CHK2	checkpoint kinase 2

cIAP	cellular inhibitor of apoptosis protein
CL	clearance
cm	centimetres
C_{max}	maximum concentration
COG	Children's Oncology Group
CRISPR	clustered regularly interspaced short palindromic repeats
CST6	cystatin 6
Cy3	cyanine 3
CYLD	cylindromatosis
DAI	DNA-dependent activator of interferon
DAPI	4',6-diamidino-2-phenylindole
DDR	DNA damage response
DES	desmin
DISC	death-inducing signalling complex
DMEM	Dulbecco's Modified Eagle's Medium
DMSO	dimethyl sulfoxide
DNA	deoxyribonucleic acid
DNMT	DNA methyltransferase
Dox	doxycycline
DRAM	damage-regulated modulator of autophagy
DSBs	double stranded DNA breaks
dsDNA	double stranded DNA
EED	embryonic ectoderm development
EGF	epidermal growth factor
EGFR	epidermal growth factor receptor
EGR1	early growth response 1
EMT	epithelial-mesenchymal transition
ERBB2	epidermal growth factor receptor 2
ERMS	embryonal rhabdomyosarcoma
EtOH	ethanol
EZH2	enhancer of zeste homolog 2
FACS	fluorescence activated cell sorting

FADD	FAS-associated death domain
FBS	foetal bovine serum
FBXW7	F-Box and WD repeat domain containing 7
FDA	Food and Drug administration (USA)
FGF4	fibroblast growth factor 4
FGFR4	fibroblast growth factor receptor 4
FITC	fluorescein isothiocyanate
FLIP	FLICE-like inhibitory protein
FOV	field of view
FOXO1	forkhead box O1
FRS2	fibroblast growth factor receptor substrate 2
g	gram
GOI	gene of interest
Gy	gray
H3K27	histone H3 lysine 27
HDAC	histone deacetylase
HRP	horseradish peroxidase
IC_{50}	half maximal inhibitory concentration
IGF1	insulin-like growth factor 1
IGF1R	insulin-like growth factor 1 receptor
IGF2	insulin-like growth factor 2
IGF2R	insulin-like growth factor 2 receptor
IGFBP3	IGF-binding protein 3
IKK	inhibitor of kappa B kinase
IL	interleukin
INK	inhibitor of cyclin-dependent kinase
IP	intraperitoneal
iPSCs	induced pluripotent stem cells
IRS	Intergroup Rhabdomyosarcoma Study
IRSG	Intergroup Rhabdomyosarcoma Study Group
ITR	inverted terminal repeat sequence
IV	intravenous

IκBα	inhibitor of NFκB-α
JAK/STAT	janus kinase /signal transducer and activator of transcription
JARID2	jumonji and AT-rich interaction domain containing 2
JDP2	jun dimerization protein 2
KIP	kinase inhibitory protein
LC3	microtubule-associated protein 1A/1B-light chain 3
LMOD2	leiomodin 2
M	molar
MAPK	mitogen-activated protein kinase
Mb	mega base pairs
MCK	muscle creatine kinase
MDM2	mouse double minute 2 homolog
MEC	mammary epithelial cells
MEF	mouse embryonic fibroblast
MEF2	myocyte enhancer factor-2
MET	mesenchymal-epithelial transition factor
MIR17HG	micro-RNA cluster miR-17-92
mL	millilitre
MLKL	mixed lineage kinase domain-like protein
mm	millimetre
MOMP	mitochondrial outer membrane permeabilization
MPT	mitochondrial permeability transition
MRF	myogenic regulatory factor
MST1/2	mammalian Ste20-like kinases 1/2
mTOR	mammalian target of rapamycin
MTT	3-(4,5-dimethylthiazol-2-yl)-2,5-diphenyl tetrazolium bromide
MYH	myosin heavy chain
MYLPF	myosin light chain phosphorylatable fast skeletal muscle
NCOA1	nuclear receptor coactivator 1
ND	not determined
NDGR1	N-MYC down-regulated gene 1
NF1	neurofibromatosis type I

NFIC	nuclear factor IC
NF-κB	nuclear factor-kappa B
ng	nanogram
nm	nanometre
NS	not significant
PARP	poly (ADP-ribose) polymerase
PAX3	paired box 3
PAX7	paired box 7
PB	piggyBAC
PBS	phosphate buffered saline
PBS/T	phosphate buffered saline /tween
PCD	programmed cell death
PDE5	phosphodiesterase type 5
PDGF	platelet derived growth factor
PDGFR	platelet derived growth factor receptor
PE	phosphatidylethanolamine
PI	propidium iodide
PI3K	phosphatidylinositol 3-kinase
PIK3CA	catalytic component of the phosphatidylinositol 3-kinase complex
PK	pharmacokinetic
PKR	protein kinase R
PO	per os (oral administration)
p	phosphorylated
pRB	retinoblastoma
PRC2	polycomb repressor complex 2
PS	phosphatidylserine
PTEN	phosphatase and tensin homolog
PUMA	p53-upregulated modulator of apoptosis
qRT-PCR	quantitative real-time PCR
RASSF4	Ras association domain family member 4
RIPK1	receptor-interacting serine/threonine-protein kinase 1
RIPK2	receptor-interacting serine/threonine-protein kinase 3

RMS	rhabdomyosarcoma
RNA	ribonucleic acid
RNase	ribonuclease
RPMI	Roswell Park Memorial Institute Medium
RT	room temperature
RTK	receptor tyrosine kinase
rtTA	reverse tetracycline transactivator
RUNX1	runt-related transcription factor 1
SDS-PAGE	sodium dodecyl sulphate-polyacrylamide gel electrophoresis
SEM	standard error of the mean
shRNA	short hairpin RNA
SI	selectivity index
siRNA	small interfering RNA
SOI	site of interest
SRPK3	SRSF protein kinase 3
SRSF	serine and arginine rich splicing factor
SSDM	strictly standardized mean difference
SUZ12	suppressor of zeste 12 homolog
SWI/SNF	SWItch/Sucrose Non-Fermentable
T ½	half-life
TAB	TAK1 binding protein
TAK	TGFβ-activated kinase
TAZ	transcriptional coactivator with PDZ-binding motif
TBS	tris buffered saline
TBS/T	tris buffered saline/tween
TBX2	T-box transcription factor 2
TBX3	T-box transcription factor 2
Tet-On	tetracycline-controlled transcriptional activation
TGF-β	transforming growth factor-β
T_{max}	time at maximum concentration
TNFR	tumour necrosis factor

TNFR	tumour necrosis factor receptor
TNNI2	troponin 1 type 2
TRADD	TNFR1 associated death domain
TRAF	TNFR associated factor
TRE	tetracycline response element
U	unit
UV	ultraviolet
V	vehicle
V	volt
VAC	vincristine, dactinomycin (actinomycin D) and cyclophosphamide
Vd	volume of distribution
VEGF	vascular endothelial growth factor
VEGFR	vascular endothelial growth factor receptor
YAP	yes-associated protein
YY1	ying yang 1
ZO1	zonula occulens
µg	microgram
µL	microlitre
µM	micromolar

Abstract

Rhabdomyosarcoma (RMS) forms in skeletal muscle and is the most common soft tissue sarcoma in children and adolescents. Current treatment is associated with debilitating side effects and treatment outcomes for patients with metastatic disease are dismal. Other than a need for alternative and more effective therapies there is also a growing appreciation for the need to understand the molecular underpinnings of RMS with the aim of identifying, in part, novel targets to develop highly specific and effective treatments with negligible adverse effects. The aim of this study was to identify novel drugs for the treatment of the two major RMS subtypes viz alveolar (ARMS) and embryonal (ERMS) RMS and to do so it adopted a two-pronged approach. Firstly, a novel binuclear palladacycle, AJ-5, was investigated for its anti-cancer activity and its mechanism(s) of action in RMS cells. The second approach involved a target-based drug repurposing strategy where a library of FDA-approved drugs was screened to identify leads that were able to negatively regulate the oncogenic TBX2 and TBX3 transcription factors that are known drivers of RMS.

The binuclear palladacycle, AJ-5, was recently shown to exert potent cytotoxicity in melanoma and breast cancer and to present with negligible adverse effects in mice. To investigate the anti-cancer activity of AJ-5 in RMS cells, MTT assays were firstly performed in ERMS and ARMS as well as 'normal' cells. IC_{50} values determined from these experiments showed values of ≤ 0.2μM for the RMS cells and a favourable selectivity index of > 2. Clonogenic and migration assays showed that AJ-5 inhibited the ability of RMS cells to survive and migrate respectively. Western blotting revealed that AJ-5 induced levels of key DNA damage response proteins (γH2AX, p-ATM and p-Chk2) and the p38/MAPK stress pathway. This correlated with an upregulation of p21 and a G_1 cell cycle arrest. Annexin V–FITC/propidium iodide staining revealed that AJ-5 induced apoptotic and necrotic cell death. Apoptosis was confirmed by the detection of cleaved PARP and increased levels and activity of cleaved caspases-3, -7, -8 and -9. Increased levels of necroptotic markers p-RIP3 and p-MLKL and inhibition of necroptosis with necrostatin-1 with a corresponding significant increase in cell viability suggests that AJ-5 is also capable of triggering a form of programmed necrosis. Furthermore, AJ-5 reduced autophagic flux as shown by reduced LC3II accumulation in the presence of bafilomycin A1, and a significant reduction in autophagosome flux *J*. Pharmacokinetic studies in mice show that AJ-5 has a promising half-life and that its volume of distribution is high, its clearance low and its intraperitoneal absorption is good. With the intention of improving the drug-like properties of AJ-5, specifically its water solubility, a derivative of AJ-5, BTC2, was synthesised and identified to display comparable anti-

cancer activity against ERMS and ARMS cells. Together these findings suggest that AJ-5 and BTC2 may be effective chemotherapeutics with a desirable and novel mechanism of action for treating drug-resistant and advanced RMS.

The highly homologous T-box transcription factors TBX2 and TBX3 have both been implicated as key drivers of RMS and they have been identified as novel therapeutic targets for the treatment of this sarcoma subtype. Indeed, TBX2 or TBX3 overexpression in normal myoblasts inhibits muscle differentiation and overexpression and knock-down cell culture and mouse models show that RMS cells are addicted to them for their cancer phenotype. However, targeting transcription factors is notoriously challenging because unlike enzymes they do not have catalytic activity and deep binding pockets to which small molecule inhibitors can be designed which is further exacerbated by the length of time and costs associated with de novo drug development. Therefore, this study adopted a novel strategy to circumvent these challenges by combining a drug repurposing with a targeted approach to TBX2/3. Briefly, a high throughput cell-based immunofluorescence screen was designed and conducted to identify FDA-approved drugs that could negatively regulate TBX2 and/or TBX3 protein levels or nuclear localisation. Cells were engineered to express induced exogenous FLAG-tagged TBX2 and TBX3 using a Tet-On system and they were screened with the Pharmakon 1600 drug library at a concentration of 10µM. 'Hits' were identified by z-scores and amongst these, niclosamide, piroctone olamine and pyrvinium pamoate were validated to be potent inhibitors of TBX2/3 and were shown to display anti-cancer activity in RMS. These drugs have the potential to be repurposed for the treatment of RMS and other TBX2/3 driven cancers either as single agents or in combination with currently used chemotherapeutics.

CHAPTER 1

Literature Review

1.1 Introduction

Cancer is a large group of complex diseases consisting of over 200 different types named according to their tissue type of origin and can be broadly classified as carcinoma, sarcoma, melanoma, lymphoma and leukaemia. In an ever-ageing society the cancer burden is rising globally exerting significant strain on populations and healthcare systems worldwide. In 2010 cancer was estimated to cost the world $2.5 trillion calculated from the direct costs related to the prevention and treatment of the disease with the added long-term costs to patients and their families (Soerjomataram et al., 2012). The World Health Organization (WHO) predicted 18.1 million new cancer cases globally for 2018 and this number is expected to double by 2035. WHO also predicted 9.6 million cancer deaths globally for 2018 which translates to 1 in 6 cancer related deaths. This exceeds the number of deaths from HIV/AIDS, malaria and tuberculosis combined. Of concern are reports that 75% of cancer related deaths occur in low-income and middle-income countries (Prager et al., 2018). Despite the advancements of almost half a century of oncology research, cancer continues to present a serious health problem due to late diagnosis, lack of advanced diagnostic modalities and ineffective cancer therapies (Arruebo et al., 2011).

1.2 Sarcoma

Sarcomas are aggressive highly diverse mesenchymal malignancies of the bone, cartilage, muscle, peripheral nerves and adipose or fibrous connective tissues (Skubitz & D'Adamo, 2007). Approximately 80% of these tumours are classified as soft tissue sarcomas and 20% as bone sarcomas (Hui, 2016). Sarcomas account for approximately 1% of all cancers in adults, 8% in adolescents and 10% in children (Amankwah, Conley, & Reed, 2013). They contribute to a considerable loss of years of life in comparison to other cancers as they affect mainly children, adolescents and young adults. Historically, sarcomas have been classified based on the tissue type they resemble but more recently, classifications have been revised to include

molecular features and genetic profiles (Francis et al., 2007; Helman & Meltzer, 2003; Jain, Xu, Prieto, & Lee, 2010). From a molecular point of view, sarcomas may be broadly classified into two types: (I) sarcomas with simple karyotypes characterised by chromosomal translocations or specific mutations and (II) sarcomas with complex aneuploidy karyotypes, consisting of numerous losses, gains and amplifications (Osuna & de Alava, 2009). While the vast majority of sarcomas fall in the complex karyotype subgroup, approximately only 15-20% fall within the simple karyotype subgroup (Matushansky et al., 2005; Oda & Tsuneyoshi, 2009). Although the ultimate cells of origin of sarcoma subtypes remain unclear, there is increasing evidence that they arise de novo from mesenchymal pluripotent stem cells (Lye, Nordin, Vidyadaran, & Thilakavathy, 2016; Xiao et al., 2013). An extension of this theory would be that alteration(s) in mesenchymal stem cell genetics can give rise to several sarcomas including osteosarcoma, Ewing's sarcoma, synovial sarcoma, chondrosarcoma, rhabdomyosarcoma, fibrosarcoma and liposarcoma (Teicher, 2012) (Fig. 1.1).

While localised sarcoma tumours can be effectively treated with surgery in combination with pre- or post-operative therapies, metastatic tumours are poorly responsive to chemotherapy and radiation. This is particularly problematic because metastases occur in one-third of all patients and approximately 20% of sarcomas recur (Hui, 2016). The problem is further exacerbated by the fact that more than 100 histological sarcoma subtypes have been identified and they all vary in pathology, molecular characteristics, clinical presentation and response to treatment (D'Adamo, 2011). A major challenge in sarcoma research has thus been to identify the molecular mechanisms underpinning sarcoma with the goal to identify novel subtype-specific diagnostic markers and treatment strategies (Demicco, Maki, Lev, & Lazar, 2012; Heymann & Rédini, 2013; Teicher, 2012).

1.3 Rhabdomyosarcoma

Rhabdomyosarcoma (RMS) is an aggressive cancer of the skeletal muscle and is the most common soft tissue sarcoma that affects children and adolescents. Globally, it accounts for 3% of childhood cancers and 2% of adolescent cancers and it has an annual incidence of 4.4-4.5 cases per million (Perez et al., 2011; Ward, DeSantis, Robbins, Kohler, & Jemal, 2014). Approximately 350 new cases are diagnosed in individuals younger than 20 years of age each

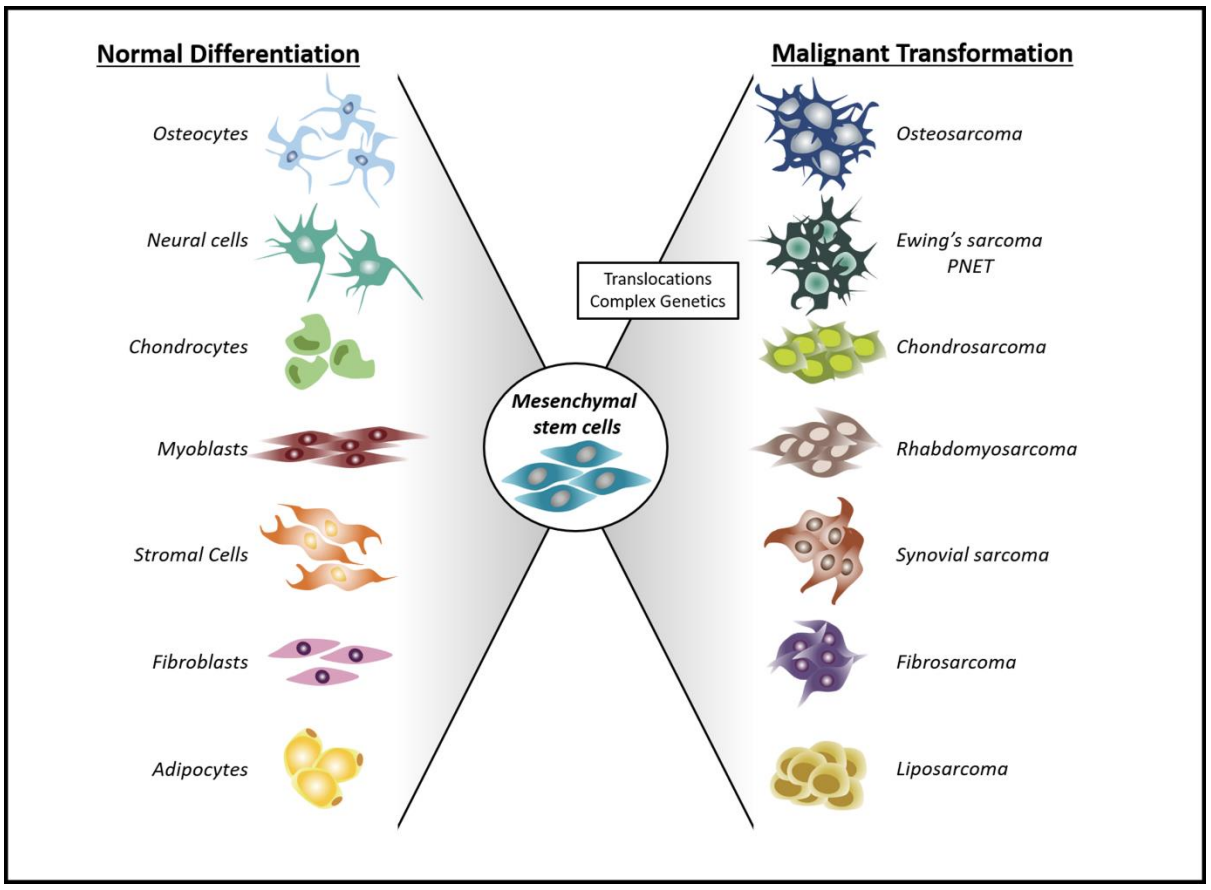

Fig. 1.1 Schematic showing the pluripotency of mesenchymal stem cells. *Mesenchymal stem cells reside in all tissues and can differentiate into a number of cell types as indicated. When chromosomal translocations or complex genetic alterations occur, mesenchymal stem cells can transform into a range of sarcomas (adapted from Teicher 2012).*

year in the United States (Ferrari et al., 2011). This soft tissue sarcoma commonly originates from skeletal muscle progenitor cells, however, there is evidence that they can also originate from non-skeletal muscle precursors (Abraham et al., 2014; Hatley et al., 2012). RMS is classified into two main subtypes viz embryonal (ERMS) and alveolar (ARMS) and they exhibit different histological, molecular and pathological characteristics. ERMS predominantly affects infants and children comprising approximately 67% of RMS cases with common sites of tumourigenesis including the head, neck and genitourinary system. ARMS, occurs primarily in adolescents and young adults and accounts for approximately 30% of RMS cases with arms and legs often being sites of primary disease (Perez et al., 2011; Wachtel et al., 2006; Ward et al., 2014). ERMS is commonly localised and thus associated with a more favourable prognosis while ARMS is more often aggressive with a greater risk of recurrence and metastasis and is thus associated with a poorer prognosis (Punyko et al., 2005). More recently, the WHO has also recognized two more rare RMS subtypes viz pleomorphic RMS and spindle cell/sclerosing

RMS. Whereas pleomorphic RMS is a morphological variant of RMS that typically occurs in adults, the spindle cell/sclerosing RMS variant is seen in children. Similar to ERMS, unifying molecular genetic aberrations in pleomorphic RMS are not yet clear. Spindle cell/sclerosing RMS tumours arise in the head and/or neck region and seem to be more likely to carry specific somatic mutations and have a poorer prognosis (Rudzinski et al., 2015). Due to the focus of this thesis, the following section will only describe information related to ARMS and ERMS.

1.3.1 RMS risk factors

It has been challenging to define risk factors in RMS as it is a rare cancer type with a relatively low incidence rate. However, there is evidence in the literature to suggest that genetic susceptibility and environmental factors play a part in RMS development (Skapek et al., 2019). Few studies have characterised the role of germline DNA mutations on disease susceptibility, but somatic mutations that predispose children and adolescents to RMS have been identified through whole-exome and whole-genome sequencing (Seki et al., 2015).

Numerous studies have reported that children with certain genetic disorders are more likely to develop RMS compared to their unaffected peers. Syndromes that are most commonly associated with ERMS include Li–Fraumeni syndrome (germline mutation of the tumour suppressor, *TP53*), neurofibromatosis type I (deletions in *NF1*), Costello syndrome (*HRAS* mutation), Noonan syndrome (germline genetic variants activating RAS–mitogen-activated protein kinase pathways), Beckwith–Wiedemann syndrome and DICER1 syndrome (germline *DICER1* mutations) (Diller, Sexsmith, Gottlieb, Li, & Malkin, 1995; Hartley, Birch, Marsden, Harris, & Blair, 1988; Kratz, Rapisuwon, Reed, Hasle, & Rosenberg, 2011a; Shuman, Beckwith, & Weksberg, 1993; Yang et al., 1995). Interestingly, these cancer predisposition syndromes appear to be more frequent in patients with ERMS than in those with ARMS (Estep, Tidyman, Teitell, Cotter, & Rauen, 2006; Kratz, Rapisuwon, Reed, Hasle, & Rosenberg, 2011b; Ognjanovic, Olivier, Bergemann, & Hainaut, 2012; Yang et al., 1995).

Several environmental factors have also been implicated in RMS risk in children. Many published reports are based on a large epidemiological case–control study of RMS that was enabled through the former Intergroup Rhabdomyosarcoma Study Group (IRSG) and current

Children's Oncology Group (COG), which drive therapeutic studies for 80–85% of all children with RMS in North America (Grufferman, Delzell, & Delong, 1984). In this study, 322 patients with RMS aged ≤20 years at the time of diagnosis and 322 control individuals matched by sex, age and ethnicity were enrolled between April 1982 and July 1988. The study reported that several environmental and clinical factors are correlated with risk of RMS development including prenatal X-ray exposure, parental recreational drug use, use of fertility medications, birth defects, childhood allergies, vaginal bleeding during pregnancy, premature birth, a first-degree relative with RMS and paternal exposure to Agent Orange (Grufferman, Schwartz, Ruymann, & Maurer, 1993; Seymour Grufferman et al., 2014; Seymour Grufferman, Ruymann, Ognjanovic, Erhardt, & Maurer, 2009; Lupo et al., 2015; Lupo, Danysh, et al., 2014; Lupo, Zhou, et al., 2014; Yang et al., 1995).

1.3.2 Genetics of RMS

The genetic alterations in RMS described in this section are summarised in Fig. 1.2. Approximately 75% of ARMS tumours are classified as having a simple karyotype because they exhibit characteristic pathogenomic chromosome translocations which, 60% of the time, occur between chromosome 2 and 13 [t(2;13)(q35;q14)] and 10-15% of the time occur between chromosome 1 and 13 [t(1;13)(p36;q14)]. These translocations lead to the fusion of the 3' end of the forkhead box O1 (*FOXO1*) locus on chromosome 13 with the paired box (PAX) transcription factors *PAX3* (chromosome 2) or *PAX7* (chromosome 1) (Galili et al., 1993; Netto & Kaul, 2018; Soleimani & Rudnicki, 2011; Tiffin, Williams, Shipley, & Pritchard-Jones, 2003). This results in the formation of the PAX3-FOXO1 and the PAX7-FOXO1 fusion proteins. Additional PAX fusions have also been identified in a small subset of ARMS tumours including fusions between *PAX3* and nuclear receptor coactivator 1 (*NCOA1*) and *PAX3* and a subunit of the ATP dependent chromatin remodelling complex, *INO80D* (Shern et al., 2014). PAX fusion proteins exhibit potent transcriptional activity which modifies growth, differentiation and apoptosis pathways leading to cellular transformation and oncogenesis (Anderson, Ramsay, Gould, & Pritchard-Jones, 2001; Lam, Sublett, Hollenbach, & Roussel, 1999). Indeed, ectopic expression of PAX3-FOXO1 in fibroblasts causes transformation and anchorage-independent growth and knockdown of PAX3-FOXO1 decreased the proliferation rate of RH30 ARMS cells and reduced the metastatic ARMS phenotype observed in corresponding xenograft models

(Kikuchi et al., 2008; Scheidler, Fredericks, Rauscher, Barr, & Vogt, 1996). Targeted sequencing and microarray analyses revealed that PAX gene fusion-positive tumours have an extremely low overall mutation rate (0.1 protein-coding mutation/Mb) (Shern et al., 2014). In these tumours the most commonly amplified genomic regions are 2p24, which contains the *MYCN* oncogene, and 12q13-q14, which includes cyclin-dependant kinase (CDK) 4 (Gordon et al., 2000). The amplification of MYCN occurs in 28% of fusion-positive cases and it has been more commonly associated with the PAX3-FOXO1 fusion-positive ARMS (Barr et al., 2009; Schwab, 2004). Another frequently amplified chromosomal region, commonly associated with PAX7-FOXO1 fusion-positive ARMS, is 13q31-32. This amplification is associated with a poorer failure-free survival and contains the *C12ORF25* gene which encodes the oncogenic micro-RNA cluster miR-17-92 (*MIR17HG*) (Gordon et al., 2000; Weber-Hall et al., 1996; Williamson et al., 2007). Upregulation of several tyrosine kinase molecules important for cell growth have been reported to be upregulated by PAX-FOXO1 fusion proteins. These include fibroblast growth factor receptor 4 (FGFR4), anaplastic lymphoma kinase (ALK), and mesenchymal-epithelial transition factor (MET) (Khan et al., 1999; Riccardo Taulli et al., 2006; van Gaal et al., 2012).

ERMS, also referred to as fusion-negative RMS, is classified as having complex karyotypes. While they display a wide range of chromosomal aberrations, the loss of heterozygosity at the 11p15.5 locus is the most unifying feature of ERMS. This locus houses the tumour suppressor genes CDK inhibitor 1C (*CDKN1C*), which encodes $p57^{KIP2}$ (kinase inhibitory protein) and *H19*. Furthermore, lack of imprinting of proto-oncogenes housed in this region such as insulin-like growth factor 2 (*IGF2*) and *HRAS* result in their overexpression which contributes to ERMS oncogenesis (Kratz et al., 2007; Scrable et al., 1989). Multiple studies have also reported recurrent gains of chromosomes 2, 7, 8, 12, and 13, but the impact of this on the ERMS phenotype has not been described (Bridge et al., 2000; Bridge et al., 2002; Weber-Hall et al., 1996). In addition, there have been reports of focal losses at 9q32-34, which includes *CDKN2A* (encodes tumour suppressors $p16^{INK4a}$ (inhibitor of cyclin-dependent kinase) and $p14^{ARF}$ (alternate reading frame)), and 17p, which harbours the tumour suppressor *TP53* and the Ras GTPase-activating protein *NF1* loci. One recurrent focal amplification event that occurs in ERMS is the high copy gain of the 12q14-15 locus which contains the mouse double minute 2 homolog (*MDM2*) and fibroblast growth factor receptor substrate 2 (*FRS2*). MDM2

is an E3 ubiquitin protein ligase which ubiquitinates p53 targeting it for degradation and FRS2 is a mediator of FGF signalling and also a negative regulator of p53 (Kakazu, Yamane, Miyachi, Shiwaku, & Hosoi, 2014; Leach et al., 1993).

Compared to ARMS, ERMS displays more causative mutations of which the most frequent mutation occurs within one of the Ras genes (*NRAS*>*KRAS*>*HRAS*) which are involved in regulating cell growth, differentiation and survival (Asati, Mahapatra, & Bharti, 2016). Indeed, 75% of high-risk and 45% of intermediate-risk ERMS tumours, tested, harboured a Ras isoform mutation and a subset of tumours also harbour *NF1* mutations which potentially lead to aberrant Ras signalling (Chen et al., 2013). Importantly, in vitro and in vivo models have confirmed the central role for aberrant Ras activity in ERMS tumorigenesis and thus "RAS-opathy" is often used to describe ERMS tumours (Hinson et al., 2013; Linardic, Downie, Qualman, Bentley, & Counter, 2005; Storer et al., 2013; Tsumura, Yoshida, Saito, Imanaka-Yoshida, & Suzuki, 2006). For example, zebrafish embryos injected with oncogenic *KRAS* at the single cell stage develop tumours that histologically resemble ERMS (Shern, Yohe, & Khan, 2015). Other genes reported to be mutated in ERMS include the catalytic component of the phosphatidylinositol 3-kinase complex (*PIK3CA*), *TP53*, the ubiquitin ligase F-Box and WD repeat domain containing 7 (*FBXW7*), the proto-oncogene *CTNNB1* encoding β-catenin, BCL-6 corepressor (*BCOR*) gene which encodes a transcriptional repressor that interacts with histone deacetylases (HDACs) and growth factor receptor tyrosine kinases such as *FGFR4*, platelet derived growth factor receptors α and β (*PDGFRα/β*) and epidermal growth factor receptor 2 (*ERBB2*) (Paulson et al., 2011; Shern et al., 2014). Copy number alterations in *IGF1R*, have also been identified as recurrent oncogenic alterations in ERMS (Shern et al., 2014; Tiash & Chowdhury, 2015).

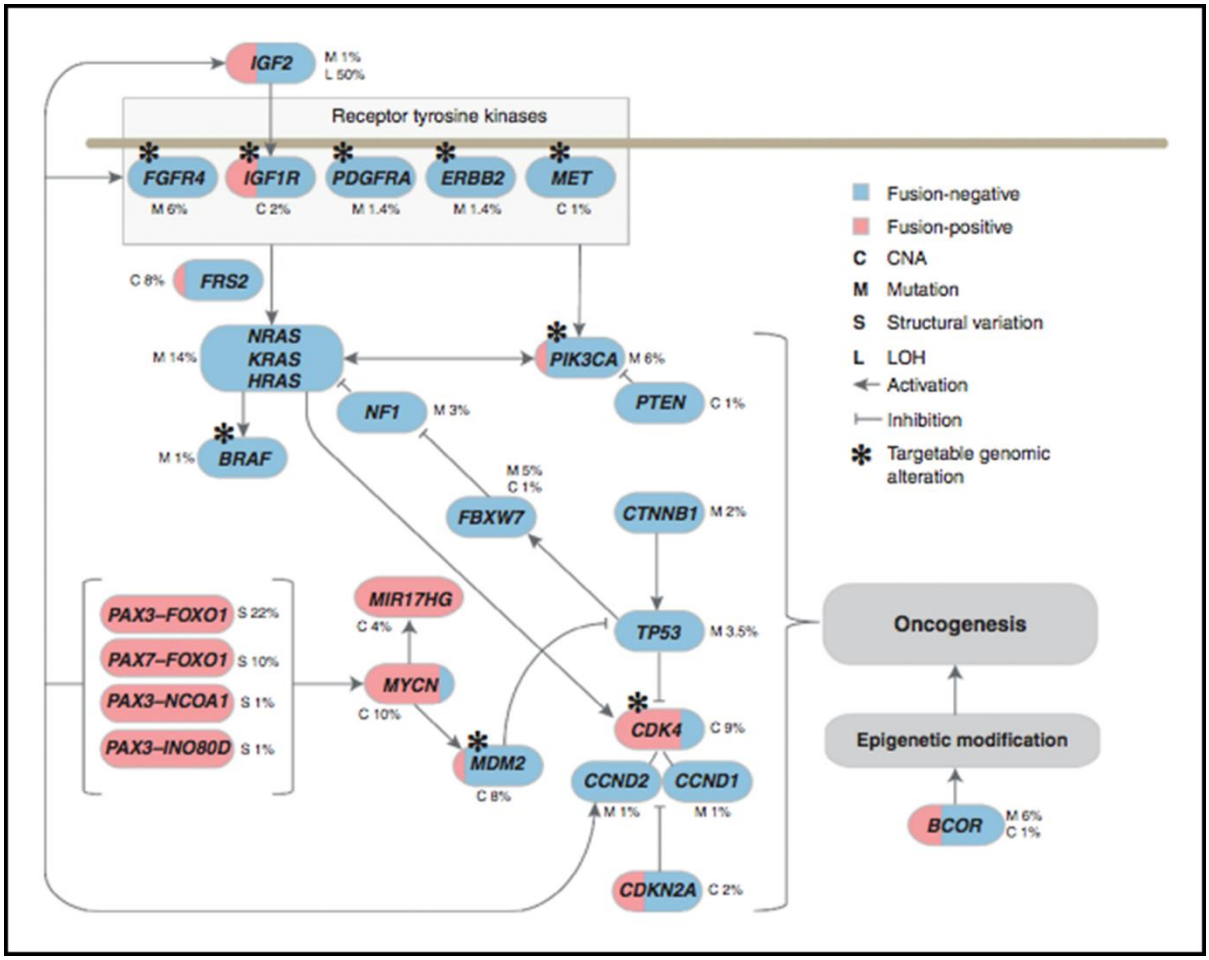

Fig. 1.2 Model of genetic alterations in RMS. *Genes coloured light red are found in fusion-positive tumours (ARMS) and genes coloured in blue are found in PAX gene fusion-negative tumours (ERMS). Alterations and their frequency in the population include mutations and small indels (M), copy number deletions and amplifications (C), or structural variations (S) that affect the gene. IGF2: insulin-like growth factor 2; FGFR4: fibroblast growth factor receptor 4; IGF1R: insulin-like growth factor 1 receptor; PDGFRA: platelet derived growth factor receptor alpha; ERBB2: epidermal growth factor receptor 2; MET: mesenchymal-epithelial transition factor; FRS2: fibroblast growth factor receptor substrate 2; NF1: neurofibromatosis type I; PIK3CA: catalytic component of the phosphoinositide-3 kinase complex; PTEN: phosphatase and tensin homolog; FBXW7: F-Box and WD repeat domain containing 7; MIR17HG: micro-RNA cluster miR-17-92; MDM2: mouse double minute 2 homolog; CDK4: cyclin-dependant kinase 4; BCOR: BCL-6 corepressor (taken from Shern et al. 2014).*

1.3.3 Molecular mechanisms underpinning RMS

Although the genetic features of ERMS and ARMS tumours are distinct, they share a common phenotype of a defective muscle differentiation program that contributes to oncogenesis. During myogenesis, pluripotent mesodermal precursor cells commit to a myoblast lineage, proliferate, differentiate, fuse into multinucleated myotubes and mature to form myofibers (Fig. 1.3). PAX3 and PAX7 expression drive pluripotent mesodermal precursor cells towards a myogenic program and muscle differentiation is regulated by sequential activation of

conserved basic helix–loop–helix (bHLH) transcription factors belonging to the myogenic regulatory factor (MRF) family (Buckingham & Relaix, 2007). This begins with expression of muscle specific factors Myf5 then MyoD, followed by the muscle differentiation factor, myogenin, and then finally Myf6 the muscle maturation factor is activated (Keller & Guttridge, 2013; Perry & Rudnick, 2000; Pownall, Gustafsson, & Emerson, 2002; Wang, 2012; Yu & Guttridge, 2018). MRFs work in concert with myocyte enhancer factor-2 (MEF2) family members, MEF2C and MEF2D, to stimulate transcription of muscle-specific structural genes including for example troponin 1 type 2 (*TNNI2*), myosin light chain phosphorylatable fast skeletal muscle (*MYLPF*), alpha-actinin-1 (*ACTN1*) and muscle creatine kinase gene (*MCK*) (Keller & Guttridge, 2013; Perry & Rudnick, 2000; Pownall et al., 2002; Wang, 2012). Among the MRFs, MyoD is considered the master regulator of the muscle-specific transcription program as its activity is sufficient to drive non-muscle cells, for example primary fibroblasts, towards a muscle lineage (Tapscott, 2005; Weintraub et al., 1989).

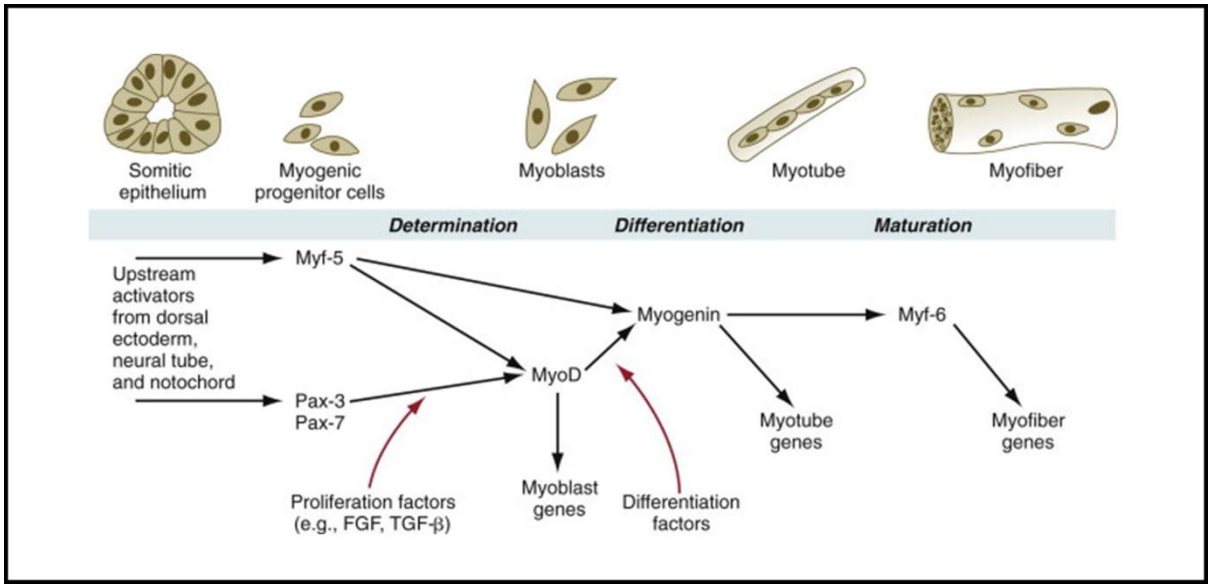

Fig. 1.3 Schematic representation of myogenesis *shows the sequence of expression of MRFs and other influences on the myogenic process. FGF: fibroblast growth factor; TGF-β: transforming growth factor-β (Taken from Carlson 2014).*

Although ARMS and ERMS cells express the myogenic marker MyoD, which is used as a diagnostic marker to identify the disease, its ability to complete muscle differentiation is impaired in these cells. Indeed, several lines of evidence suggest that it is the deregulation of MyoD transcriptional activity, and not its expression levels, that are likely to account for the block in differentiation observed in RMS (Keller & Guttridge, 2013). For example, in vitro

binding assays showed that although MyoD can bind to its cognate DNA sequences, it is unable to activate reporter genes containing the same binding sites (Tapscott, Thayer, & Weintraub, 1993). Interestingly, other studies have reported that the inability of RMS cells to differentiate into muscle cells may be due to the inappropriate binding of MyoD to target genes. Whole-exome and whole-transcriptome sequencing revealed a recurrent somatic mutation encoding p.Leu122Arg in MyoD in a subset of ERMS tumours. This caused MyoD to preferentially bind to *MYC* consensus sequences, thus switching cells to proliferate rather than differentiate (Kohsaka et al., 2014; Van Antwerp, Chen, Chang, & Prochownik, 1992). Moreover, gene profiling combined with chromatin immunoprecipitation-coupled high throughput sequencing (ChIP-seq) revealed that the differentiation defect in RMS cells relates more to the suppression of MyoD cofactors including MEF2C, runt-related transcription factor 1 (RUNX1), nuclear factor I C (NFIC) and jun dimerization protein 2 (JDP2). This was a significant finding as the increased expression of these cofactors in RMS was capable of restoring muscle differentiation in RMS cells (MacQuarrie et al., 2013). As described below, myogenesis has also been shown to be blocked in RMS through various signalling pathways and pathogenic modulators.

1.3.3.1 Signalling pathways

Numerous signalling pathways including nuclear factor-kappa B (NF-κB), yes-associated protein (YAP)/transcriptional coactivator with PDZ-binding motif (TAZ), Hippo, Notch, Wnt and MEK/ERK signalling have been implicated in rhabdomyosarcomagenesis and will be briefly described in this section.

The NF-κB is a transcription factor that can orchestrate a wide variety of complex biological responses including regulation of immune responses and inflammation as well as regulating muscle differentiation and homeostasis (Dolcet, Llobet, Pallares, & Matias-Guiu, 2005; Peterson, Bakkar, & Guttridge, 2011). NF-κB functions as a negative regulator of myogenic differentiation (Guttridge, Albanese, Reuther, Pestell, & Baldwin, 1999; Guttridge, Mayo, Madrid, Wang, & Baldwin, 2000). It is overexpressed in RMS and it suppresses differentiation through decreased expression of pro-differentiator miR-29 through ying yang 1 (YY1) and the polycomb repressor complex 2 (PRC2) (Wang et al., 2008). In ARMS cells with a PAX3/7–

FOXO1 translocation, NF-κB activity was also shown to inhibit myogenesis via activation of cyclin D1/CDK4 complexes, which sequester MyoD (Charytonowicz et al., 2012).

YAP and TAZ are two highly related transcriptional regulators (referred to as YAP/TAZ) that play key roles in cell proliferation and tissue growth. In muscle development, TAZ and YAP both promote myoblast proliferation in early muscle progenitor cells (Sun et al., 2017; Totaro, Panciera, & Piccolo, 2018). Inactivation of YAP/TAZ activity is required for muscle differentiation and is mediated by the Hippo pathway (Judson et al., 2012; Watt et al., 2010). The Hippo pathway regulates tissue growth and maintains homeostasis through a kinase cascade including mammalian Ste20-like kinases 1/2 (MST1/2) which is, in part, responsible for inactivating YAP/TAZ (Wackerhage et al., 2014). In RMS cells, YAP protein levels are elevated and in RMS tumours YAP nuclear staining is increased. Overexpression of YAP in activated satellite cells generates tumours similar to ERMS and knockdown of YAP in ERMS inhibits tumorigenesis (Tremblay et al., 2014). The PAX3–FOXO1 fusion in ARMS directly upregulates Ras association domain family member 4 (RASSF4) which associates with MST1 and inhibits its tumour suppressor function (Crose et al., 2014). Thus, YAP and the Hippo signalling pathways are implicated in the maintenance of pro-proliferative, anti-differentiation phenotypes in RMS (Svalina & Keller, 2014).

Notch signalling is an important regulator of myogenesis as Notch1 activation sustains myoblast proliferation and Notch3 activation inhibits myoblast fusion and differentiation (De Salvo et al., 2014). In RMS, Notch signalling is upregulated and cross talks with Hippo, Hedgehog, Wnt, and transforming growth factor-β (TGF-β) pathways (Conti et al., 2016). Not surprisingly, inhibition of the Notch pathway showed a significant decrease in RMS cell mobility and invasiveness in vitro (Roma et al., 2011). In ERMS, Notch1 signalling is activated and it drives tumourigenesis by upregulating the E-cadherin repressor, SNAIL1, and blocking MEF2C (Ignatius et al., 2017). Interestingly, when Notch was inhibited in ERMS, tumourigenesis was blocked in vivo but this was apparently not accompanied by terminal differentiation (Belyea et al., 2011). Notch3 is required in ARMS tumours as its depletion reduced the tumorigenic potential of RMS cells both in vitro and in vivo and resulted in differentiation as evidenced by formation of multinucleated myotubes expressing myosin heavy chain (MYH) (De Salvo et al., 2014; Raimondi et al., 2012).

Wnt signalling is one of the key cascades regulating development and stemness and has also been tightly associated with cancer (Zhan, Rindtorff, & Boutros, 2017). The development of skeletal muscle from immature precursors is mediated by Wnt signalling at various levels including cell proliferation, differentiation and homeostasis, in part, through the positive regulation of MRFs, Myf5 and MyoD (Chen, 2016; von Maltzahn et al., 2012; Münsterberg et al., 1995; Tajbakhsh et al., 1998). Although it has been thought that Wnt signalling contributes to RMS, this is not necessarily the case. Ragab et al. (2018) showed that while the Wnt pathway was maintained in RMS cell lines, transcriptional activation of its key target genes were consistently impaired. However, upon activation or inhibition of Wnt/β-catenin there were only moderate effects on proliferation, apoptosis or myodifferentiation of RMS cells. This suggests a subordinate role of the Wnt/β-catenin signalling pathway in RMS. On the other hand, Annavarapu et al. (2013) showed that in keeping with its function to promote myogenesis, activation of Wnt via its agonist Wnt3a decreased proliferation and induced myogenic differentiation in ARMS cells, suggesting that Wnt signalling in RMS functions as a tumour suppressor.

Although not necessarily a signalling mediator, DNA methyltransferase (DNMT) enzymes are responsible for de novo DNA methylation during DNA replication that also impinge on gene expression (Kim, Samaranayake, & Pradhan, 2009). DNMT3B is a specific family member that has been found to be upregulated in patient RMS tumours and cell lines compared to normal skeletal muscle (Megiorni et al., 2016). It appears to function as a negative regulator of myogenesis in RMS as knockdown of DNMT3B in ERMS cells promotes myogenic terminal differentiation by increasing the expression of MyoD, myogenin and MYH. DNMT3B silencing caused RMS cells to undergo a G_1 arrest by reducing expression of cyclin B1, cyclin D1 and cyclin E2, while increasing expression of p21 and p27 and reversed the oncogenic phenotype by decreasing clonogenic potential and migratory capacity. Inhibition of MEK/ERK signalling in RMS cells resulted in reduced DNMT3B protein, suggesting that DNMT3B functions downstream of MEK/ERK signalling (Megiorni et al., 2016).

1.3.3.2 Pathogenic modulators

PAX3/7–FOXO1 fusion proteins, enhancer of zeste homolog 2 (EZH2), MEF2 family of proteins, several miRNAs and the transcription factors TBX2 and TBX3 have been reported to be pathogenic modulators of RMS. These factors will be briefly introduced in this section, but due to their relevance to this study TBX2 and TBX3 will be described in more detail.

The PAX3/7–FOXO1 fusions, which are the hallmark feature of ARMS, also serve as inhibitors of myogenic differentiation of RMS cells. As described earlier, PAX3–FOXO1 promotes tumorigenesis via Hippo pathway suppression (Crose et al., 2014). PAX3–FOXO1 and PAX7–FOXO1 products can also prevent myogenic differentiation by suppressing the transcriptional activation of MyoD target genes, even while increasing MyoD expression (Calhabeu et al., 2013). P-cadherin, a direct target of PAX3–FOXO1 in ARMS cell lines, is expressed in muscle progenitor cells in vivo and its expression decreases once muscle progenitor cells begin to express MRFs (Thuault et al., 2013). It has been implicated in ARMS cell proliferation, transformation, migration and invasion (Christofori, 2003; Thuault et al., 2013). Indeed, P-cadherin expression levels increase in metastatic ARMS and this correlates with a downregulation of N- and M-cadherins. Another direct target of the PAX3–FOXO1 fusion protein is jumonji and AT-rich interaction domain containing 2 (JARID2) which encodes a protein that is known to recruit histone methylating complexes to their target genes. JARID2 expression has been associated with metastatic RMS and silencing JARID2 in ERMS and ARMS resulted in reduced cell proliferation and increased expression of myogenin and myosin light chain. JARID2 was shown to bind promoter regions of MRFs and alter methylation of histone H3 lysine 27 (H3K27). Through this mechanism, JARID2 maintains the undifferentiated myogenic phenotype of RMS (Walters et al., 2014).

The polycomb group proteins are epigenetic silencers of transcription that play key roles in differentiation by functioning within polycomb repressor complexes (Di Croce & Helin, 2013). PRC2 catalyses H3K27 trimethylation and contains several components including suppressor of zeste 12 homolog (SUZ12), embryonic ectoderm development (EED) and the catalytic subunit EZH2. In skeletal muscle progenitors, EZH2 represses muscle-specific gene expression and is downregulated during differentiation (Caretti et al., 2004; Ciarapica et al., 2009;

Marchesi et al., 2012). In ERMS cells, EZH2 directly binds muscle-specific gene promoters including *myogenin*, *MYH* and *MyoD*. Ablation of EZH2 in ERMS cells decreases the trimethylation of H3K27 and increases expression of myogenin, MYH and MyoD. In addition, MyoD binding to muscle specific promoters was increased, resulting in partial reversion of the tumour phenotype by the formation of myotubes in culture (Marchesi et al., 2012). In vivo studies have shown that ARMS tumour growth is impaired when EZH2 function is blocked, leading to tumour cell apoptosis (Ciarapica et al., 2009). Thus, reducing the activity of EZH2 has been proposed as a novel adjuvant strategy against high-risk ARMS (Ciarapica et al., 2014; Ramaglia et al., 2016).

The MEF2 family of proteins regulate many developmental programs including myogenesis (Potthoff & Olson, 2007). Both MEF2C and MEF2D regulate myogenesis by working in combination with MRFs (Molkentin et al., 1995; Penn et al., 2004; Potthoff & Olson, 2007). In RMS cell lines, while MRFs are present, MEF2D levels are downregulated and there is reduced association with promoters of the muscle specific genes *RNNI2*, leiomodin 2 (*LMOD2)*, desmin (*DES)* and *MCK* (Zhang, Truscott, & Davie, 2013). Similar to other myogenic regulators, re-expression of MEF2D in ARMS cells promotes their differentiation as determined by expression of MYH. This phenotype is associated with a reduction in proliferation, motility, and anchorage-independent growth in vitro, and strong inhibition of tumour growth in vivo (Zhang et al., 2013). Regulation of MEF2C in ARMS cells follows a similar pattern to MEF2D (Nishijo et al., 2009), and functionally, exogenous addition of MEF2C in ERMS promotes the expression of differentiation-specific genes and increases MyoD binding at sites of its target genes, suggesting that MEF2C might stabilize binding of MyoD or increase accessibility of these sites to MyoD (MacQuarrie et al., 2013). Activation of MEF2C during myogenesis is also maintained through alternative splicing which gives rise to the MEF2Cα1 and MEF2Cα2 isoforms. While MEF2Cα1 is ubiquitously expressed and lacks myogenic activity, MEF2Cα2 is required for efficient differentiation of human myoblast cells and RMS cells (Zhang, Zhu, & Davie, 2015). Exon α in *MEF2C* was found to be aberrantly alternatively spliced in RMS cells, with the ratio of α2/α1 highly downregulated in RMS cells compared with normal myoblasts. The switch between MEF2Cα1 to MEF2Cα2 is regulated by serine and arginine rich splicing factor (SRSF) protein kinase 3 (SRPK3), which itself is downregulated in RMS cells. Furthermore, the MEF2Cα1 isoform preferentially interacts with HDAC5, and as a complex

functions in transcriptional repression of myogenic genes. In contrast, addition of the MEF2Cα2 isoform inhibited recruitment of HDAC4 and HDAC5 to muscle-specific target promoters such as *CDKN1A* and *LMOD2*, leading to a block in both proliferation and anchorage-dependent growth and promoted differentiation in RMS cells (Zhang et al., 2015).

A group of miRNAs have been referred to as myomiRs (miR-1, -133a/b, -206) for their contribution to promoting skeletal muscle differentiation (Cieśla, Dulak, & Józkowicz, 2014; Ju et al., 2015; Novák et al., 2013; Romania et al., 2012). They subsequently have been shown to possess anti-cancer functions in numerous malignancies including RMS. Among the most studied in the context of myogenesis in RMS is miR-206 which increases during myogenesis and its levels are downregulated in RMS (MacQuarrie et al., 2012). Functionally, miR-206 promotes differentiation by targeting anti-differentiation mediators *PAX7*, *PAX3*, *NOTCH3*, and *CCND2* for degradation (Hanna et al., 2016). In addition, miR-206 directly targets the BAF53a subunit of the SWItch/Sucrose Non-Fermentable (SWI/SNF) nucleosome remodelling complex. BAF53a interferes with differentiation in myogenic cells and silencing BAF53a in RMS increases the expression of myogenic markers and inhibits proliferation and anchorage-independent growth (Taulli et al., 2014).

1.3.3.2.1 The T-box transcription factors TBX2 and TBX3

TBX2 and TBX3 are highly homologous members of the conserved T-box family of transcription factors that are dynamically expressed in many tissues and organs during early embryonic development and play highly specific and critical roles in diverse processes ranging from the specification of the primary germ layers to limb patterning and organogenesis (Bollag et al., 1994; Papaioannou, 2014; Sebé-Pedrós et al., 2013). Indeed, mutations in these factors are causally linked to severe developmental disorders (Packham & Brook, 2003; Papaioannou, 2014). For example, mutations leading to haploinsufficiency of TBX3 result in ulnar–mammary syndrome which is characterised by abnormalities of the forelimb and malformations of the apocrine gland, axillary hair, mammary glands, areola and dental structures, as well as defects in the heart, limbs, jaw and genitalia (Bamshad et al., 1997; Tada & Smith, 2001; Wilson & Conlon, 2002). Although there is no established disorder linked to TBX2 mutations, two studies have associated microdeletions on chromosome 17q23, which

affect both TBX2 and TBX4, with a yet to be named syndrome. Common features of this syndrome include developmental retardation, microcephaly, delayed postnatal growth and heart, limb, hand and foot abnormalities (Ballif et al., 2010; Nimmakayalu et al., 2011).

TBX2 and TBX3 are also expressed in various adult tissues but to date they have no known functions in these tissues (Bamshad et al., 1999; Campbell et al., 1995; Law et al., 1995). They have however been reported to be overexpressed in a number of carcinomas and sarcomas including breast, liver, bladder, ovarian, cervical, pancreatic and gastric cancer, melanoma and RMS where they have been shown to contribute directly to several oncogenic processes (Carreira, Liu, & Goding 2000; Han et al. 2013; Liu, Jiang, & Zhang 2010; Liu et al. 2010; Mahlamäki et al. 2002; Wang et al. 2012; Yu et al. 2015; Zhu et al. 2014; Vance et al. 2005; Dimova et al. 2009; Wansleben et al. 2014; Willmer et al. 2016; Miao et al. 2016). Indeed, as summarised in Fig. 1.4 and Fig. 1.5 and as described below, TBX2 and TBX3 can promote the bypass of senescence (irreversible/permanent exit from the cell cycle), proliferation, tumour formation, migration and invasion and are able to confer resistance to apoptotic cell death and anti-cancer drugs (Wansleben et al., 2014). Not surprisingly, TBX2 and TBX3 have been identified and biologically validated as novel drug-targets for the treatment of cancers that are addicted to their expression for cancer progression.

Senescence bypass

Cellular senescence is the irreversible exit from the cell cycle. All cells have a finite replicative life span after which they undergo replicative or cellular senescence. This process is established and maintained by at least two major tumour suppressor pathways namely the p53/p21 and $p16^{INK4a}$ and retinoblastoma (pRB) pathways. These pathways have been recognised as a formidable barrier to malignant tumorigenesis (Campisi, 2013). TBX2 and TBX3 have both been shown to bypass senescence and consequently immortalise mouse embryonic fibroblasts (MEFs) through a mechanism involving the repression of $p19^{ARF}$/$p14^{ARF}$ by either directly binding a T-element present in the initiator or by recruiting HDAC 1,2,3 and 5 to epigenetically silence the promoter (Brummelkamp et al., 2002; Carlson et al., 2001; Lingbeek, Jacobs, & van Lohuizen, 2002; Yarosh et al., 2008). TBX2 mediated senescence bypass was shown to also involve direct repression of p21, while TBX3 mediated senescence

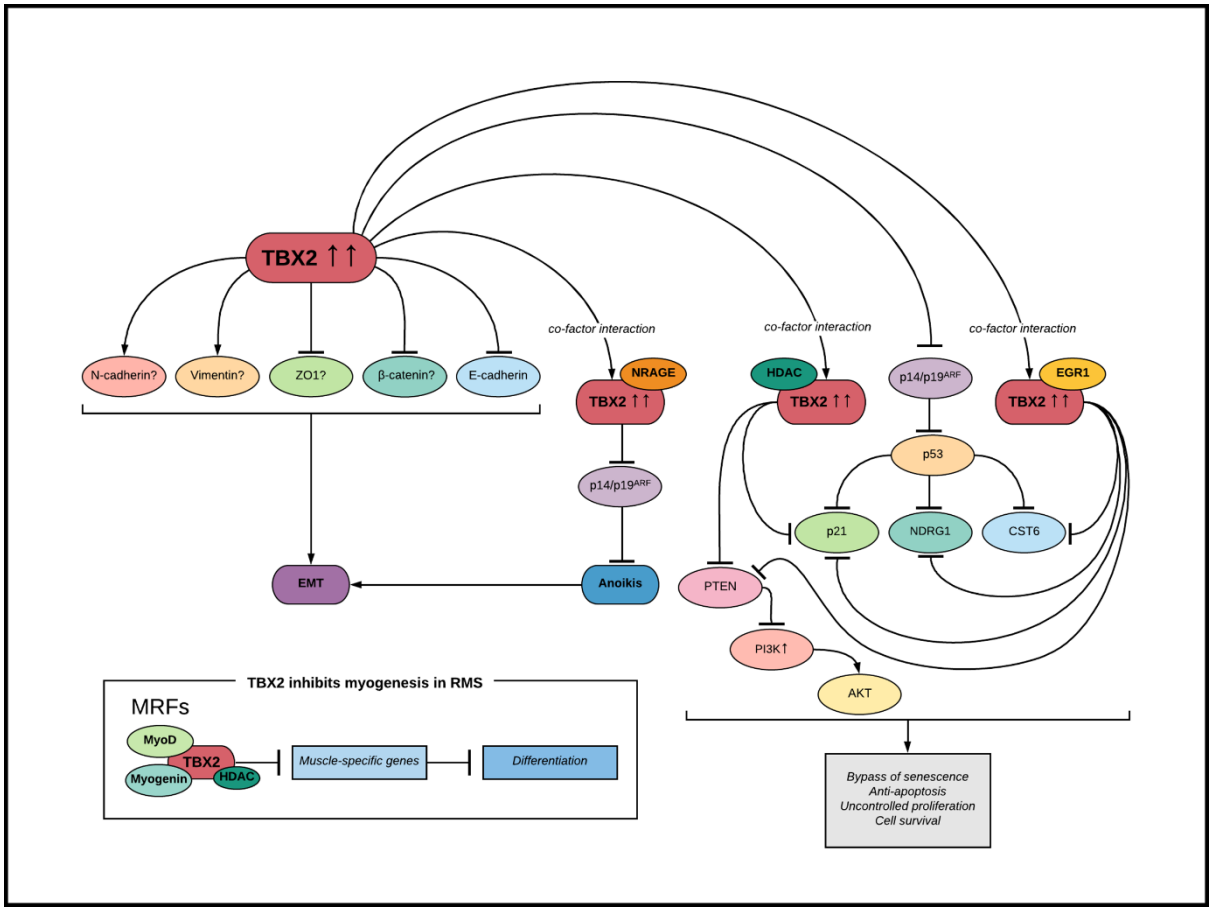

Fig. 1.4 TBX2 oncogenic roles mediated through its known co-factors and target genes. *ZO1: zonula occulens; EMT: epithelial-mesenchymal transition; NRAGE: neurotrophin receptor-interacting melanoma antigen; HDAC: histone deacetylase; PTEN: phosphatase and tensin homolog; PI3K/AKT: phosphatidylinositol 3-kinase/protein Kinase B; NDGR1: N-MYC down-regulated gene 1; EGR1: early growth response 1; CST6: cystatin 6; MRFs: myogenic regulatory factors (adapted from Wansleben et al. 2014; Zhu & Davie 2015).*

was shown to involve repression of $p16^{INK4\alpha}$ (Kumar et al., 2014; Prince et al., 2004). TBX2 repression of p21 has also been implicated as a mechanism of anti-senescence in both mouse and human melanoma cells (Peres et al., 2010; Vance et al., 2005).

Cell proliferation

TBX2 and TBX3 have been shown to promote proliferation in numerous cancer cells including melanoma, breast cancer, head and neck squamous carcinoma, papillary thyroid carcinoma, nasopharyngeal cancer and some sarcomas including RMS (Burgucu et al., 2012; D'Costa et al., 2014; Li et al., 2018; Lv et al., 2017; Vance et al., 2005; Wansleben et al., 2014; Willmer et al., 2016; Zhu et al., 2014). The molecular mechanism by which TBX2 does this was revealed

by the group of Paul Mullan (School of Medicine, Dentistry and Biomedical Sciences, Queen's University Belfast) in breast cancer cells. Indeed, TBX2 was shown to promote cell proliferation by interacting with and recruiting early growth response 1 (EGR1) to target and repress the tumour suppressor, N-MYC down-regulated gene 1 (*NDRG1*) promoter. In nasopharyngeal cancer cells TBX2 knockdown significantly inhibited proliferation which correlated with increased expression of p21 and the tumour suppressor phosphatase and tensin homolog (PTEN), a negative regulator of the phosphatidylinositol 3-kinase (PI3K)/ protein Kinase B (AKT) pro-survival pathway (Chalhoub & Baker, 2009; Lv et al., 2017).

TBX3 mRNA and protein were reported to show an inverse correlation with the tumour suppressor PTEN in head and neck squamous carcinoma cells and it was shown that TBX3 could promote proliferation by directly repressing PTEN by binding to a region within its promoter (Burgucu et al., 2012). Recently, the CDKI $p57^{KIP2}$ has been identified as a TBX3 target that mediates papillary thyroid carcinoma cell proliferation. Reduced expression of TBX3 resulted in increased $p57^{KIP2}$ levels, while knockdown of $p57^{KIP2}$ rescued the cell-cycle arrest phenotype. Mechanism investigation revealed that TBX3 directly binds to the *CDKN1C* promoter region and represses transcription of the protein product ($p57^{KIP2}$) through interaction with HDAC1 and HDAC2 (Li et al., 2018).

Tumour formation, migration and invasion

TBX2 has been shown to contribute to tumour migration and invasion through its ability to promote epithelial-mesenchymal transition (EMT). EMT is an important process during embryogenesis that allows primitive immotile epithelial cells to convert to mobile mesenchymal cells which has been implicated in cancer invasion and metastasis (Iwatsuki et al., 2010). Indeed, ectopic expression of TBX2 in normal breast epithelial cells resulted in decreased expression of the epithelial markers E-cadherin, β-catenin and zonula occulens (ZO1) and increased mesenchymal markers N-cadherin and vimentin. Furthermore, these cells had the increased ability to migrate and invade, while silencing TBX2 in metastatic breast cancer cells led to the opposite effect. Importantly, when metastatic breast cancer cells with silenced TBX2 were injected into the tail vein of nude mice, no pulmonary metastasis was

observed compared to the control mice (Wang et al., 2012). It has also been proposed that TBX2 can promote EMT through negatively regulating anoikis, a form of apoptosis that occurs

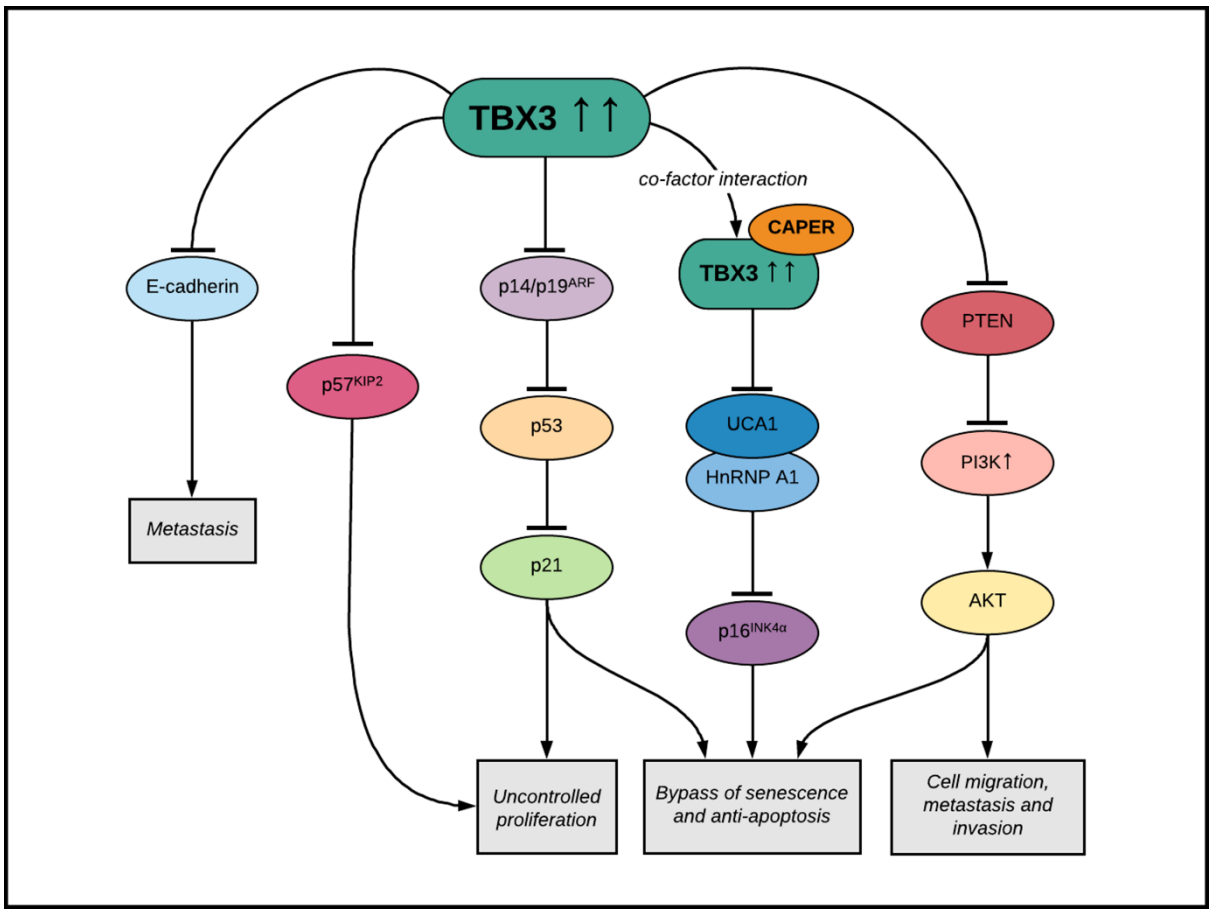

Fig. 1.5 Mechanisms by which TBX3 has been shown to promote the cancer phenotype. *CAPER: coactivator of AP1 and oestrogen receptor; UCA1: urothelial cancer associated 1; HnRNP A1: heterogeneous ribonucleoprotein A1; PI3K/AKT: phosphatidylinositol 3-kinase /protein Kinase B; PTEN: phosphatase and tensin homolog; AKT: protein kinase B (adapted from Wansleben et al. 2014).*

when anchorage-dependent cells become detached from the surrounding extracellular matrix and lose adherence to a substrate (Frisch, Schaller, & Cieply, 2013; Kumar et al., 2011). Moreover siRNA mediated knockdown of TBX2 in human nasopharyngeal cancer cells and prostate cancer cells upregulated E-cadherin and downregulated N-cadherin, vimentin and fibronectin (Du et al., 2017; Lv et al., 2017).

TBX3 has been implicated in tumour formation, migration and invasion. Indeed, elevated TBX3 mRNA levels showed a strong correlation with metastasis in breast cancer and silencing TBX3 with shRNA inhibited migration and tumour forming ability of breast cancer cells (Chen,

Lü, & Ji, 2009; Fillmore et al., 2010; Peres et al., 2010). The ectopic expression of TBX3 in radial growth phase non-malignant melanoma cells was shown to be sufficient to promote tumour forming ability and invasion of these cells and knockdown of TBX3 in vertical growth phase advanced melanoma cells inhibited migration and tumour formation (Peres et al. 2010; Peres & Prince 2013). Numerous studies have demonstrated that TBX3 promotes cell migration through its ability to repress E-cadherin (Du et al. 2014; Peres et al. 2010; Rodriguez et al. 2008; Boyd et al. 2013; Humtsoe et al. 2012).

Apoptosis resistance

Apoptosis (see section 1.8.1), a type of programmed cell death, is an evolutionarily conserved process that plays an essential role in organism development and tissue homeostasis. However, in pathological conditions, particularly cancer, cells lose their ability to undergo apoptosis induced death leading to uncontrolled proliferation (Mohammad et al., 2015). Indeed, TBX2 was shown to co-operate with EGR1 to repress the cysteine protease inhibitor, cystatin 6 (CST6) to inhibit apoptosis in breast cancer cells (D'Costa et al., 2014; Redmond et al., 2010). TBX3 has been shown to co-operate with MYC and the oncogene H-Ras^{v12} mutant to suppress apoptosis and facilitate transformation of primary MEFS. This was speculated to occur through the disruption of the pro-apoptotic p19^{ARF}-MDM2-p53-p21 pathway as ectopic expression of TBX3 significantly downregulated p19^{ARF}, p53 and p21 levels (Carlson et al. 2002). Furthermore, TBX3 was shown to promote cell proliferation of mammary epithelial cells (MECs) by repressing p19^{ARF} which was accompanied by the downregulation of p21 (Platonova et al., 2007).

TBX2 and TBX3 cancer drug resistance

Overexpression of TBX2 has been shown to confer drug resistance to cisplatin through a mechanism involving its ability to induce DNA repair by disrupting the double-stranded DNA damage pathway, ATM-Chk2-p53 in breast cancer cells (Davis et al. 2008; Wansleben 2013). A recent study corroborated these findings by showing that sensitivity to cisplatin and carboplatin treatment increased significantly when TBX2 expression was inhibited in serous carcinoma cells in vitro. Furthermore, patients with serous carcinoma tumours with low levels of TBX2 were more sensitive to platinum-drug treatment compared to tumours with high

levels of TBX2 (Tasaka et al., 2017). TBX3 has been implicated as a downstream target of the Wnt/β-catenin pathway in liver cancer. It was shown that the inhibition of TBX3 expression by siRNAs blocked β-catenin mediated cell survival and rendered hepatoblastoma cells sensitive to doxorubicin-induced apoptosis (Calvisi et al., 2007). Recently, knocking down TBX3 in colorectal cancer cells has been shown to sensitise them to cisplatin treatment (Aliwaini 2017).

TBX2 and TBX3 in RMS

There is mounting evidence provided by the groups of Judith Davie (Southern Illinois University School of Medicine) and Sharon Prince (University of Cape Town) that TBX2 and TBX3 may also be central to the pathology of RMS. The Davie laboratory has shown that TBX2 is expressed in primary myoblasts and is strongly downregulated in differentiated muscle cells. Importantly, they demonstrate that TBX2 is overexpressed in ARMS and ERMS cells and that it represses myogenesis by recruiting HDAC1 to the promoters of *MyoD* and *myogenin* inhibiting their expression and consequently their ability to upregulate their muscle specific target genes including *TNNI2*, myosin light chain, *MYLPF*, *ACTN1* and *p21*. TBX2 was shown to repress *p21* through recruitment of HDAC1 to the *p21* promoter and suppression of $p14^{ARF}$/$p19^{ARF}$ was also observed. Furthermore, they showed that the overexpression of TBX2 in normal myoblasts inhibits muscle differentiation and depletion of TBX2 in RMS cells by either siRNA or a dominant negative upregulated muscle-specific genes, decreased cell proliferation, inhibited clonal growth, reduced the migratory ability of cells in vitro and prevented tumour growth in vivo (Zhu et al., 2014). In another study these authors showed that TBX2 also binds to and directly represses the tumour suppressor PTEN by recruiting HDAC1 to its promoter in RMS cells (Zhu et al., 2016). Recently, EGR1 was identified as a tumour suppressor in RMS and it was shown that, similar to what was reported in breast cancer, TBX2 interacts with EGR1 and inhibits EGR1-dependant expression of p21, PTEN, NDGR1 and CST6. Indeed, overexpression of EGR1 was sufficient to rescue expression of these genes and induce apoptosis in RMS cells (Mohamad et al., 2018).

The ectopic overexpression of TBX3 in normal myoblasts has also been shown to inhibit muscle differentiation and research by Sharon Prince's group (University of Cape Town) has

shown that ERMS cells are addicted to TBX3 for their cancer phenotype (Carlson et al., 2002). Using TBX3 knockdown and TBX3 overexpression cell culture models, TBX3 was shown to be required for anchorage-independent growth, migration and in vivo tumour forming ability of ERMS cells (Sims, 2016; Willmer et al., 2016).

1.4 Current management of RMS

The current standard treatment for patients with RMS is multimodal therapy consisting of local control with surgery and/or radiation therapy in conjunction with multi-agent chemotherapy (Egas-Bejar & Huh, 2014). Surgical management of patients with RMS is site-specific and is only implemented if functionality is not compromised. Successful surgical removal is achieved with a minimum margin of 0.5cm (Leaphart & Rodeberg, 2007). Radiation therapy is often administered to patients with unresected tumours, residual disease after surgery, disease in regional lymph nodes and if the cancer has alveolar histology (Cecchetto et al., 2008; Eaton et al., 2013; Raney et al., 2010). The dose of radiation is dependent on the extent of the disease and is usually initiated between 6-12 weeks after the start of chemotherapy. Low-risk patients are treated with 36Gy which can be increased to 50.4Gy for higher-risk patients (Eaton et al., 2013).

In the early 70's, disease control for patients with localised or completely resected RMS (low-risk) was achieved with combinational chemotherapy including vincristine, dactinomycin (actinomycin D) and cyclophosphamide (VAC) administered for two years. However, this treatment regimen did not achieve the same results for patients with regional spreading, incomplete resection or metastasis, also referred to as intermediate- or high-risk patients (Pappo et al. 1995). Furthermore, these drugs are associated with debilitating side effects because they act non-specifically and induce cytotoxicity in normal cells. The mechanisms of action, side effects and chemical structures of the chemotherapeutic drugs discussed in this section can be found in Table 1.1.

The Intergroup Rhabdomyosarcoma Study Group (IRSG), a US and Canadian initiative, was formed in 1972 with the aim to systematically study current treatment regimens in children with RMS and to improve outcomes in higher-risk patients (Maurer et al., 1977). The first

study, IRS-1 conducted from 1972 to 1978, evaluated the addition of doxorubicin to VAC with radiation. However, the overall survival of patients was only 20% (Maurer et al., 1988). The IRS-II study (1978-1984) evaluated the use of a repetitive cycle of VAC compared to alternating cycles of VAC and vincristine, cyclophosphamide and doxorubicin. Although a complete remission rate of 53% was achieved for these patients, the overall survival was only 26% and no better than the standard VAC treatment (Maurer et al., 1993). The IRS-III study in 1984 examined the addition of cisplatin and etoposide to the IRS-II treatment regimens but failed to improve the survival of patients with metastatic disease with a 5-year overall survival rate of 27% (Crist et al., 1995). The final IRS-IV study that ran from 1991-1997 evaluated the addition of ifosfamide and etoposide to VAC. The results presented no significant improvement in patients with metastatic disease in comparison to prior studies with only 25% achieving 3-year event free survival and 39% with 3-year overall survival (Breneman et al., 2003). Nonetheless, it is important to note that the overall survival for patients with localised RMS improved from 55% to 71% in IRS-I to IRS-IV (Breneman et al., 2003; Maurer et al., 1988).

More recently, several studies and randomised trials have failed to improve the outcomes for intermediate- and high-risk RMS patients when treating them with VAC together with other chemotherapeutic agents, such as irinotecan and topotecan (Arndt et al., 2008, 2009; Malempati & Hawkins, 2012; Weiss et al., 2014). This is in agreement with Perkins et al. (2014) who stated: "despite improvements in survival in children with metastatic disease over the past four decades, the outcome in some diseases continues to be poor. This is especially true for bone and soft tissue sarcomas." While the introduction of IRS therapy during the 1970s and 1980s improved the treatment of RMS, there has since been a lack of significant improvement and VAC is still the standard treatment regimen for paediatric RMS patients (Elsebaie et al., 2018). With advances in understanding RMS biology and in an effort to find more effective and less toxic therapies, there are several targeted therapies that are being explored for the treatment of RMS which will be detailed in the next section.

Table 1.1 *The current chemotherapeutic drugs used to treat RMS with their mechanisms of action, main side effects and structures.*

Chemotherapeutic	Mechanism of action	Main side effects	Structure
Vincristine (Makin, 2014; Neidle, 2013)	**Mitotic inhibitor:** binds to tubulin dimers, inhibiting assembly of microtubule structures and arresting mitosis in metaphase.	Peripheral neuropathy, hyponatremia, constipation, hair loss	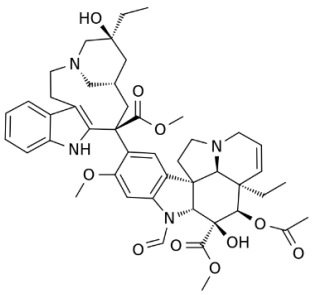
Dactinomycin (Silverman & Holladay, 2014)	**Actinomycin antibiotic:** inhibits transcription by binding DNA at the transcription initiation complex hence preventing RNA elongation by RNA polymerase.	Bone marrow suppression, fatigue, hair loss, mouth ulcers, loss of appetite	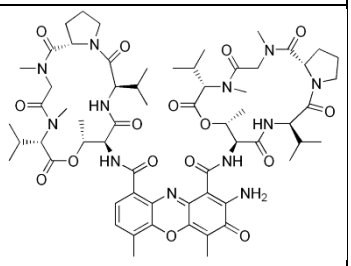
Cyclophosphamide (Silverman & Holladay, 2014; Smith & Williams, 2005)	**Nitrogen mustard alkylating agent:** attaches alkyl groups to guanine bases of DNA forming irreversible DNA crosslinks thus inducing DNA breaks and causing cell death.	Nausea, vomiting, bone marrow suppression, stomach ache, haemorrhagic cystitis, diarrhoea	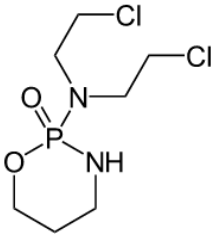
Doxorubicin (Brody, 2011; Silverman & Holladay, 2014; Smith & Williams, 2005)	**Anthracycline:** intercalates between DNA base pairs and binds to DNA associated enzymes such as topoisomerases leading to DNA damage and cell death.	Cardiotoxicity, bowel infection, eruptions of palms of hands or soles of feet, erythema (redness of skin), nausea and vomiting, pain at site of injection	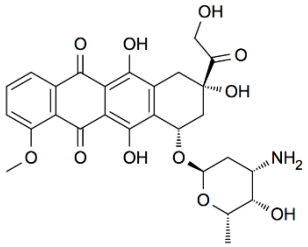
Cisplatin (Brody, 2011; Makin, 2014; Ummat et al., 2012)	**Platinum-based drug:** binds to guanine bases of DNA causing crosslinking that induces double stranded breaks and leads to cell death.	Nephrotoxicity, neurotoxicity, nausea and vomiting, hearing loss, bone marrow suppression, electrolyte disturbance	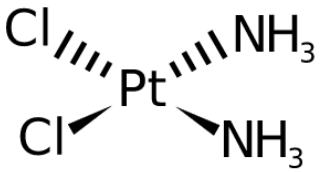

Etoposide (Brody, 2011; Makin, 2014; Smith & Williams, 2005)	**Topoisomerase inhibitor:** forms a ternary complex with DNA and the topoisomerase II enzyme (aids in DNA unwinding preventing torsional strain), inhibiting re-ligation of strands and causing DNA strand breaks and eventually cell death.	Low blood pressure, hair loss, pain or burning at intravenous site, constipation or diarrhoea, bone marrow suppression	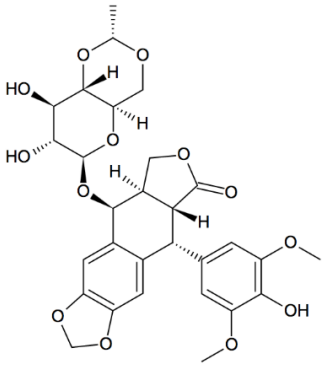
Ifosfamide (Brody, 2011; Makin, 2014; Smith & Williams, 2005)	**Nitrogen mustard alkylating agent:** attaches alkyl groups to guanine bases of DNA forming irreversible DNA crosslinks causing DNA damage which leads to cell death.	Haemorrhagic cystitis, renal tubular acidosis, salt-wasting nephropathy, central neurotoxicity, encephalopathy	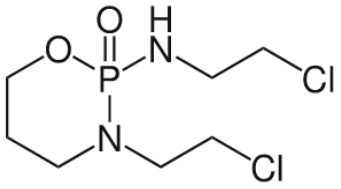
Irinotecan (Brody, 2011; Babu et al., 2012; Mathijssen et al., 2002; Smith & Williams, 2005)	**Topoisomerase inhibitor:** intercalates between DNA bases and binds to topoisomerase I, which interferes with its function causing DNA strand breaks and hence cell death.	Severe diarrhoea and extreme suppression of the immune system	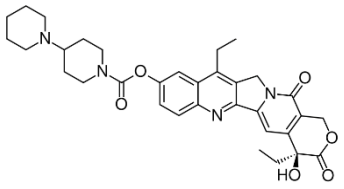
Topotecan (Brody, 2011; Marchand et al., 2006; Mathijssen et al., 2002; Smith & Williams, 2005)	**Topoisomerase inhibitor:** intercalates between DNA bases and interferes with the action of topoisomerase I causing DNA strand breaks, which lead to cell death.	Bone marrow suppression, diarrhoea, susceptibility to infection	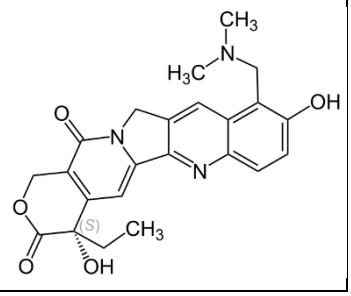

1.5 Targeted therapies for the treatment of RMS

The term 'targeted therapy' refers to a new generation of cancer drugs which are designed to interfere with a specific molecular target (typically a protein) that has a critical role in tumour growth or progression and therefore have fewer side effects than other types of cancer treatment (Sawyers, 2004). This has been made possible as our understanding of the molecular basis of various cancers improve and this section will highlight targeted therapies that are in preclinical and clinical trials for the treatment of RMS which are summarised in Fig. 1.6.

1.5.1 Receptor tyrosine kinase inhibitors

Receptor tyrosine kinases (RTKs) are a subclass of cell surface growth factor receptors with intrinsic, ligand-controlled tyrosine kinase activity. They regulate diverse cellular processes in normal cells such as proliferation, migration, metabolism, differentiation and survival. RTK activity in resting, normal cells is tightly controlled, however, RTKs become potent oncoproteins when they are mutated or structurally altered. Therefore, RTK inhibitors are rational targets for therapeutic intervention. Several RTK receptors have been implicated in RMS including IGF, FGF, ALK, vascular endothelial growth factor (VEGF), PDGF, epidermal growth factor (EGF) and MET receptors (Gschwind, Fischer, & Ullrich, 2004). This section will briefly describe drugs targeting these receptors for the treatment of RMS.

The IGF pathway has been implicated in the pathogenesis of bone and soft tissue sarcomas including RMS. Activation of the receptor by its ligand IGF1 and IGF2 triggers signalling cascades including the PI3K/AKT/mammalian target of rapamycin (mTOR) and Ras/Raf/mitogen-activated protein kinase (MAPK) signalling axes leading to cell survival, growth and proliferation (Maki, 2010; Pollak, 2008; Rikhof, de Jong et al., 2009). Elevated expression of IGF1R has been reported in RMS tumour samples and various RMS cell lines and it has been described as a target of the PAX3/7-FOXO1 fusion-protein in ARMS (Ayalon, Glaser, & Werner, 2001; El-Badry et al., 1990; Shapiro et al., 1994). Importantly, a mouse monoclonal antibody against IGF1R inhibited ERMS tumour growth in a xenograft model (Kalebic, Tsokos, & Helman, 1994). Furthermore, a phase II study of R1507, a recombinant human monoclonal antibody to IGF1R, revealed that while it was well tolerated in patients with recurrent or refractory RMS, osteosarcoma, synovial sarcoma and others, limited efficacy was observed (NCT00642941). Indeed, R1507 had an overall objective response rate of 2.5%, median progression-free survival of 5.7 weeks and median overall survival of 11 months (Pappo et al., 2014). Cixutumumab (IMC-A12), a fully human immunoglobulin G1 (IgG1) monoclonal antibody to IGF1R, was tested in a phase II trial and was also well tolerated in patients with previously treated advanced or metastatic RMS, leiomyosarcoma, adipocytic sarcoma, synovial sarcoma or Ewing's sarcoma. Indeed, it was associated with limited gastrointestinal adverse events, fatigue and hyperglycaemia. Cixutumumab was most

efficacious in adipocytic sarcoma with a 32% rate of progression-free survival compared to RMS with the lowest rate of progression-free survival of 12%. The results from this study suggest that cixutumumab may be a feasible and effective treatment for patients with adipocytic sarcoma (Schöffski et al., 2013). A phase II pilot study to evaluate cixutumumab in combination with intensive multi-agent chemotherapy including cyclophosphamide, dactinomycin, doxorubicin, etoposide, ifosfamide, irinotecan and vincristine has recently been completed, but analyses of the study results have not yet been published (NCT01055314). A small molecule ATP competitive inhibitor of IGF1R, BMS-754807, has shown promising activity as a single agent in RMS cell lines in vitro and a dose-escalation phase I trial showed that its safety and tolerability were feasible for daily treatment (Desai et al., 2010; Kolb et al., 2011). It is however worth noting that the maximum tolerated dose for BMS-754807 was not determined.

FGFR4 signalling is constitutively activated in fusion-positive and fusion-negative RMS, due to upregulation by PAX3/7-FOXO1 and a point mutation, respectively. This makes FGFR4 an attractive candidate for targeted therapy of RMS. Recent work demonstrated that the approved tyrosine kinase inhibitor ponatinib (AP24534) potently inhibited FGFR4 signalling in cell lines expressing either wild-type or mutant FGFR4. This drug also inhibited growth and induced apoptosis of RMS cell lines in vitro and inhibited tumour growth in xenografts of RMS cell lines expressing mutant FGFR4 (Li et al., 2013).

Aberrant expression of ALK has been implicated in the tumorigenesis of several cancer types including RMS. ALK activation triggers multiple downstream pathways involved in cell proliferation, survival and cell cycle progression including PI3K/AKT, MEK/ERK, and the janus kinase (JAK)/signal transducer and activator of transcription (STAT) /cyclin D2 pathways and is thus considered a therapeutic target of ALK-positive tumours (Chiarle et al., & Inghirami, 2008; Hallberg & Palmer, 2016). Pillay et al. (2002) reported that 23% of 99 RMS patient samples that they tested showed positive ALK expression with a higher prevalence in ARMS (45%) compared to ERMS (15%) samples. Crizotinib (PF-02341066) and ceritinib (LDK378) are first- and second-generation ALK inhibitors that are under investigation in clinical trials for the treatment of ALK-positive tumours. Crizotinib is associated with a more multi-kinase targeting profile inhibiting ALK and MET, which has also been implicated in the malignant progression

of RMS, where ceritinib is a ALK specific inhibitor (Megiorni et al., 2015; van Erp et al., 2017). A cross-tumoral phase II trial testing the anti-tumour activity of crizotinib on a variety of advanced tumours with alterations in ALK and/or MET pathways including ARMS patients has recently been completed (NCT01524926). Results indicated that while crizotinib is well tolerated, it does not display any meaningful activity as a single agent in patients with advanced metastatic ARMS (Schöffski et al., 2018). A phase I study recruiting paediatric malignancies with genetic alterations in ALK, including RMS, neuroblastoma, anaplastic large-cell lymphoma and inflammatory myofibroblastic tumour, is currently underway (NCT01742286). The purpose of the study is to determine the maximum tolerated dose and/or recommended dose of ceritinib for paediatric patients while also assessing safety, tolerability, pharmacokinetics and preliminary evidence of anti-tumour activity. Furthermore, a phase II study is also currently underway to assess the efficacy and safety of crizotinib in patients harbouring an alteration in ALK and/or MET and ARMS and ERMS patients with amplified ALK are also being recruited (NCT02034981).

Pazopanib (GW786034) is a selective multi-targeted RTK inhibitor that targets, among other receptors, VEGFRs, PDGFRs, and c-kit and it has been shown to block tumour growth and angiogenesis (Boehm et al., 2010). Pazopanib was the first molecular-targeted therapy approved for the treatment of advanced non-adipocytic soft tissue sarcoma and a phase II COG trial (NCT01956669) is currently underway to test the effects of pazopanib on, among other resistant and aggressive cancers, patients with relapsed or refractory RMS (van der Graaf et al., 2012).

Bevacizumab is a monoclonal antibody to all five isoforms of human VEGF and has been shown to decrease general tumour growth by inhibiting angiogenesis and has displayed promising activity in RMS xenograft models (Gerber et al., 2000; Presta et al., 1997). A phase II study which investigated the addition of bevacizumab to a standard chemotherapy backbone including ifosfamide, vincristine, actinomycin D and doxorubicin reported that the drug was well tolerated in paediatric metastatic RMS patients and it enhanced the overall response rate from 36% in patients receiving only chemotherapy to 54% (Chisholm et al., 2016).

The tyrosine kinase receptor EGFR, when phosphorylated, activates a variety of downstream effector molecules regulating cell proliferation and differentiation. Aberrant EGF cell signalling via the EGFR has been implicated in the development or progression of several human cancers including RMS (De Giovanni et al., 1996; Ganti et al., 2006; Gilbertson, 2005). Drugs that inhibit EGFR signalling may thus potentiate the effects of cytotoxic chemotherapy and radiation therapy (Ciardiello et al., 2000; Raben et al., 2005; Woodburn, 1999). Erlotinib, a highly potent oral inhibitor of EGFR, has been approved by the US Food and Drug Administration (FDA) for adults with recurrent non-small cell lung cancer and advanced pancreatic cancer (Cohen et al., 2005; Kelley & Ko, 2008; Moyer et al., 1997). In combination with the alkylating chemotherapy agent temozolomide, erlotinib was tested in phase I and pharmacokinetic studies involving patients with relapsed/recurrent/refractory paediatric solid tumours including RMS (Jakacki et al., 2008). The studies revealed favourable results for maximum tolerated dose, adverse effects, toxicity and preliminary anti-tumour activity and thus a phase II trial is currently recruiting patients to investigate the overall response rate to treatment (NCT02689336).

1.5.2 Cell cycle inhibitors

During the differentiation of myoblasts into myotubes, the cells exit the cell cycle which is mediated, in part, by the downregulation of cyclin D1 and a decrease in CDK4/CDK6 activity. RMS results from proliferating myoblast cells that fail to exit the cell cycle and RMS tumours frequently have amplification of CDK4 and genetic loss of the CDK4 and CDK6 inhibitor $p16^{Ink4a}$ (*CDKN2A*). Treatment of RMS cell lines with the CDK4/6 inhibitor palbociclib (PD-0332991) triggers a G_1 arrest and induces the expression of muscle-specific markers (Saab et al., 2006). A phase II trial is currently recruiting patients with advanced sarcomas, including RMS, with CDK4 overexpression to evaluate palbociclib second line treatment (NCT03242382). The MDM2 locus is also frequently amplified in RMS and MI-63, an inhibitor of the MDM2–p53 interaction, has been shown to decrease proliferation and increase apoptosis in RMS cell lines expressing wild-type p53 and it is currently in early phase I clinical trials (Canner et al., 2009).

1.5.3 Mammalian target of rapamycin (mTOR) inhibitors

In response to insulin and various endogenous growth factors, the protein kinase mTOR regulates cell growth, proliferation, protein synthesis and transcription via the PI3K/AKT pathway. The control of cell growth and proliferation by the PI3K/AKT/mTOR pathway is abnormally activated in many human tumours and alterations in the RTK/RAS/PI3K axis has been reported in 93% of RMS cases (Blay, 2011; Preuss et al., 2013; Zhu & Davie, 2015). The mTOR inhibitor rapamycin was shown to potently inhibit cell proliferation in RMS cell lines and induces p53-independent apoptosis (Dilling et al., 1994; Hosoi et al., 1999; Rini, 2008). Furthermore, RMS xenograft models treated with the mTOR inhibitor temsirolimus (CCI-779) showed significant suppression of mTOR signalling and tumour growth (Wan et al., 2006). A phase II trial of temsirolimus in children with high-grade glioma, neuroblastoma and RMS did not meet the primary objective efficacy threshold of an overall response to treatment, but disease stabilisation in 41% of glioma patients, 32% of neuroblastoma patients and only 6% of RMS patients was observed within 12 weeks of treatment (Geoerger et al., 2012). A phase II trial of bevacizumab or temsirolimus in combination with vinorelbine and cyclophosphamide for the treatment of patients with first relapse/disease progression RMS (NCT01222715) showed that the addition of temsirolimus was more efficacious than bevacizumab. Event-free survival was 50% for the bevacizumab treatment regimen and 65% for the temsirolimus treatment regimen and the rate of progressive disease was 26% and 9% respectively (Mascarenhas et al. 2014). A phase I trial of another mTOR inhibitor, everolimus, in paediatric patients with recurrent refractory solid tumours including RMS has been completed and a phase II study of everolimus is currently recruiting children and adolescents with refractory or relapsed RMS and other soft tissue sarcomas (NCT01216839).

1.5.4 RAF, MEK and PI3K Inhibitors

Ras isoforms are commonly mutated in fusion-negative RMS and thus Ras effectors including PI3K and BRAF are thus potential drug targets. Vemurafenib and dabrafenib are BRAF inhibitors and trametinib is a MEK inhibitor that have all gained FDA approval for the treatment of Ras-driven cancers, such as metastatic melanoma. Recent work has shown that the small-molecule inhibitors of MEK and PI3K, U0126 and PI103 respectively, have a

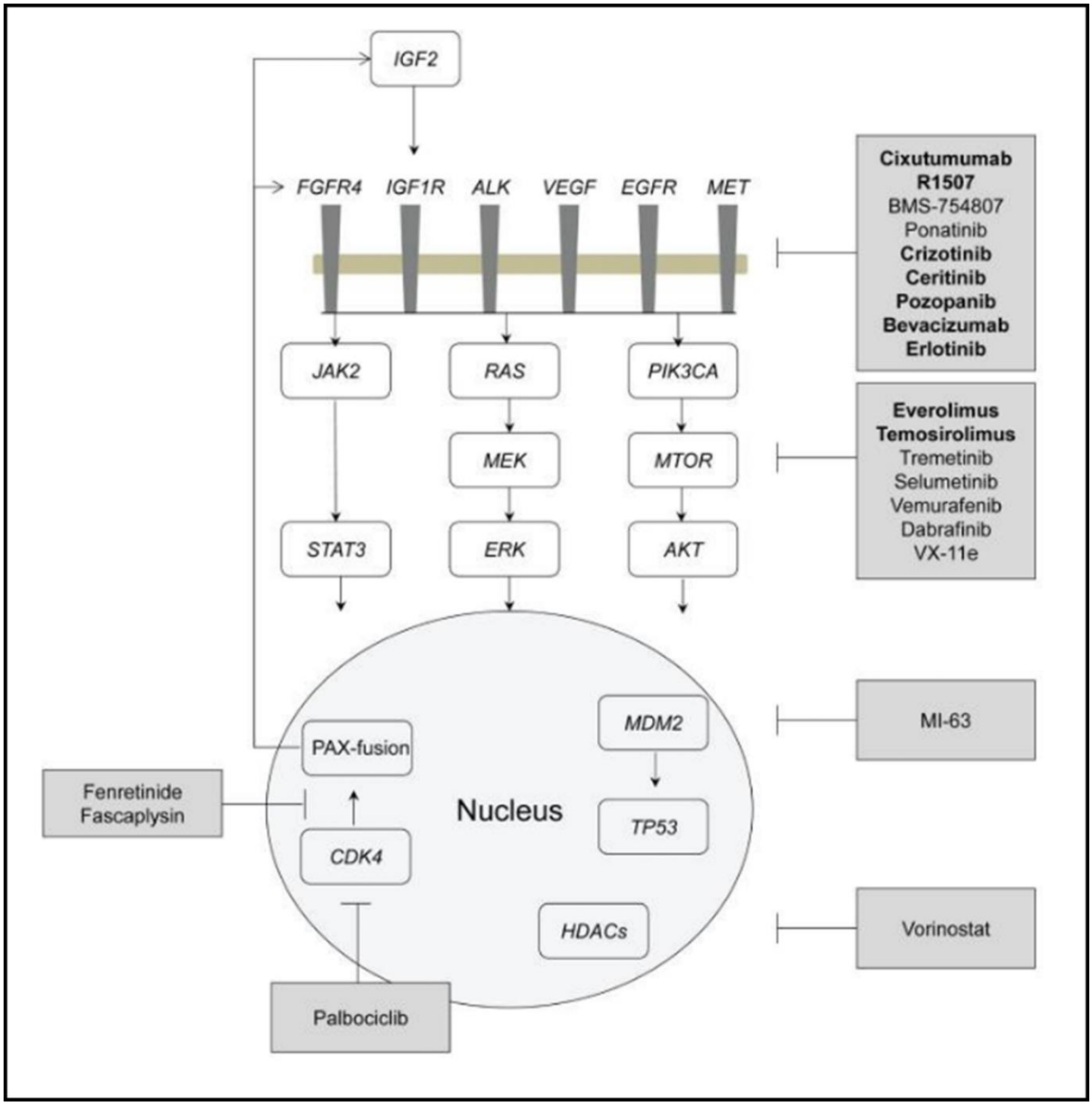

Fig. 1.6 Targeted therapies in preclinical and clinical trials for the treatment of RMS. *IGF2: insulin-like growth factor 2; FGFR4: fibroblast growth factor receptor 4; IGF1R: insulin-like growth factor 1 receptor; ALK: anaplastic lymphoma kinase; VEGF: vascular endothelial growth factor; EGFR: epidermal growth factor; MET: mesenchymal-epithelial transition factor; JAK2: janus kinase 3; STAT3: signal transducer and activator of transcription; PIK3CA: catalytic component of the phosphatidylinositol 3-kinase complex; MTOR: mammalian target of rapamycin; AKT: protein kinase B; CDK4: cyclin-dependent kinase 4; MDM2: mouse double minute 2 homolog; HDAC: histone deacetylase (taken from Shern, Yohe, & Khan 2015).*

synthetic lethal interaction in the fusion-negative ERMS cell line RD which harbours an activating mutation in *NRAS* (Guenther, Graab, & Fulda, 2013). Moreover, studies have shown that growth of RD cells is dependent on the RAS-RAF-MEK-ERK signalling pathway as the MEK inhibitor selumetinib (AZD244) and the ERK2 inhibitor VX-11e have been shown to inhibit proliferation in vitro (Z. Li et al., 2013).

Although targeted therapy is a rapidly developing field, it is still at its infancy with regards to therapies for RMS as there are currently no approved targeted therapies for the treatment of this cancer. This is, in part, because (I) there needs to be a better understanding of the molecular biology of RMS to identify better targets; (II) results from targeted therapies currently in clinical trials have not been that efficacious or only show efficacy when in combination with current chemotherapeutics; and (III) the drug discovery and development pipeline is an incredibly arduous and costly process. In light of the above, investigation into more effective and less toxic chemotherapeutic drugs is still a successful and growing field and this thesis therefore investigates palladium-based complexes as potential therapeutics for the treatment of RMS (discussed in section 1.7). Secondly, drug repurposing has become an attractive approach to fast-track the drug discovery pipeline and the current study explores combining drug repurposing (described in the next section) with a targeted approach.

1.6 Drug Repurposing

Despite a rapidly growing understanding of human disease and technological advances, translation of this into therapeutic applications has been limited (Ashburn & Thor, 2004; Scannell et al., 2012). This, in part, is due to the escalating costs, time and risk for de novo drug development (Pammolli, Magazzini, & Riccaboni, 2011; Waring et al., 2015). A recent approach to circumvent these issues is drug repurposing (also referred to as drug repositioning, reprofiling or re-tasking) which is a strategy to identify new applications for an existing drug for which it is not currently prescribed (Ashburn & Thor, 2004).

This approach is underpinned by the fact that common molecular pathways contribute to many different diseases and capitalises on the fact that drugs have already passed safety studies and there is information on their pharmacology, formulation, dose, and potential toxicity (Ashburn & Thor, 2004). This has important time and cost implications and Fig. 1.7 summarises the differences between de novo drug development and drug repurposing. For example, the time required to develop a new drug is estimated to take 10 to 17 years and to cost $2-3 billion, compared to 3 to 12 years and on average $300 million to repurpose a drug (Nosengo, 2016). Moreover, drug repurposing provides a better risk-versus-reward trade-off.

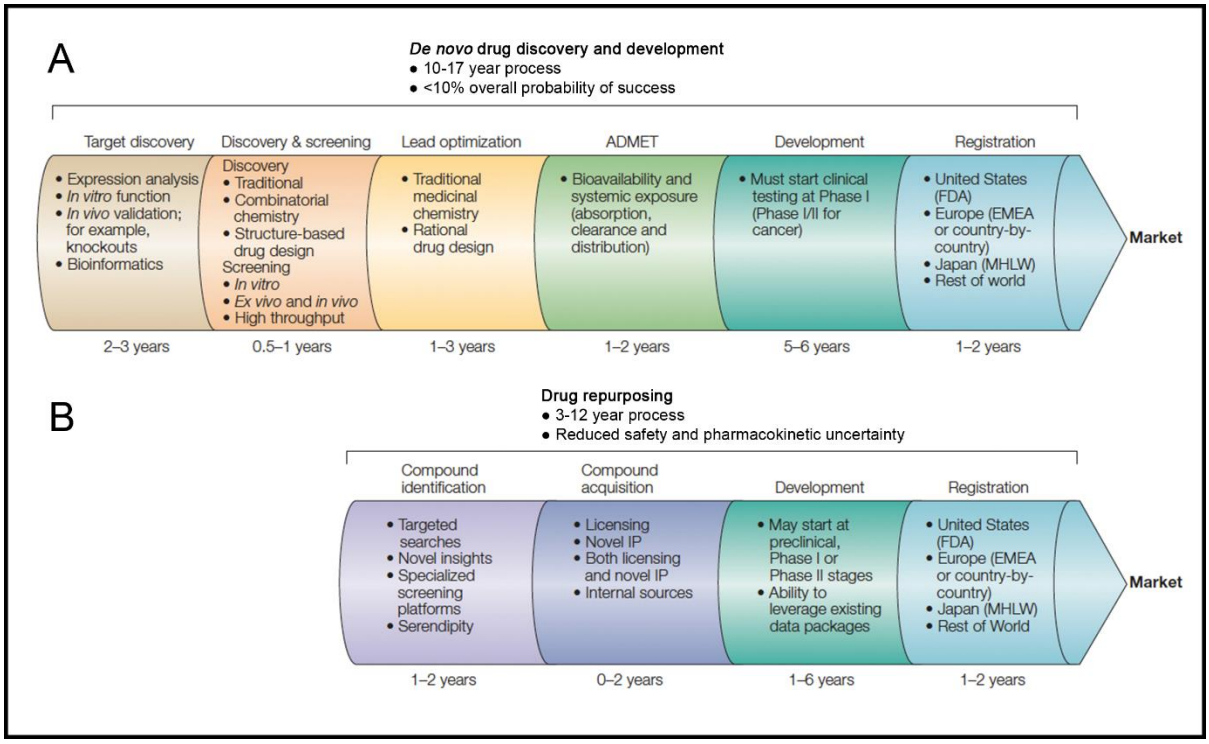

Fig. 1.7 A comparison between de novo drug discovery and development and drug repurposing. *ADMET: absorption, distribution, metabolism, excretion and toxicity; EMEA: European Medicines Agency; FDA: Food and Drug Administration; IP: intellectual property; MHLW: Ministry of Health, Labour and Welfare (adapted from Ashburn and Thor 2004).*

Indeed, the percentage of de novo candidates reaching approved status once human testing begins may be as low as 10%, but drug repurposing increases this approval rate to 40% (Ashburn & Thor, 2004; Pushpakom et al., 2018; Tobinick, 2009).

Historically, drug repurposing has mostly been serendipitous where an off-target or new on-target effect was identified, and the drug was taken forward for further validation and commercial exploitation. Recently, a more systematic approach involving the following three steps has been adopted before taking the candidate drug through the development pipeline: (I) identification of a drug for a given indication; (II) assessment of the effect of the drug in preclinical models; and (III) evaluation of drug efficacy in phase II clinical trials (assuming there is sufficient safety data from phase I studies undertaken as a part of the original indication). Computational and experimental approaches have been employed to identify the potential of a drug to be repurposed (Pushpakom et al., 2018). Computational approaches are largely data-driven and involve systematic analysis of data such as signature matching, genome-wide association studies, computational molecular docking, pathway and network mapping and

retrospective clinical analysis of electronic health records. Experimental approaches include binding assays to identify target interactions and phenotypic screening.

There have been many successful drug repurposing examples to date and Table 1.2 highlights several of them. However, with relevance to this thesis, it is important to note that there have been numerous success stories of drugs repurposed for their use as anti-cancer therapies. For example, metformin, a first-line medication for the treatment of type 2 diabetes was identified to exert possible anti-cancer activity in 2005 during a case-controlled study that included 11 876 type 2 diabetes patients (Evans et al., 2005). Consequently, multiple epidemiological studies have documented an association between metformin and reduced cancer incidence and mortality. There are 55 completed clinical trials (Phase I – III) to date that have examined the anti-cancer effect of metformin on a variety of cancer types including breast, colon, oesophageal, endometrial, head and neck and prostate cancer (Heckman-Stoddard et al., 2017). The underlying mechanism by which metformin has been shown to exerts its anti-cancer activity involves targeting the IGF and 5' adenosine monophosphate (AMP)-activated protein kinase (AMPK) signalling pathways (Dowling et al., 2007; Gallagher & LeRoith, 2010; Zi et al., 2018). Another example is the anti-fungal compound itraconazole which was identified as one of the most promising 'hits' in a drug screen designed to identify angiogenesis inhibitors in 2007 (Chong et al., 2007). Subsequently itraconazole has been shown to also mediate its anti-tumour activity through the inhibition of the Hedgehog pathway, induction of cell cycle arrest and auto-phagocytosis (Pounds et al., 2017). Several clinical trial studies have reported on the ability of itraconazole to increase drug efficacy and overcome drug resistance alone or in combination with other chemotherapeutics in several cancer types including, prostate, ovarian, breast, lung, pancreatic cancer and basal cell carcinoma (Antonarakis et al., 2013; Kim et al., 2014; Rudin et al., 2013; Tsubamoto, Sonoda, & Inoue, 2014; Tsubamoto et al., 2014). An example of a drug repurposed as a targeted anti-cancer therapy is all-trans retinoic acid (ATRA) for the treatment of acute promyelocytic leukaemia (APL) in 1987. ATRA is a compound used in medications that treat severe acne and was shown to bind to the unique APL fusion oncoprotein, promyelocytic leukaemia-retinoid X receptor-alpha (PML-RARA) and induce cellular differentiation. Although ATRA does not have anti-cancer properties when used on its own, in combination with current chemotherapeutics for APL it results in 90-100% complete remission in patients compared to

Table 1.2 Examples of successfully repurposed drugs (Adapted from Pushpakom et al. 2018)**.**

Drug name	Original Indication	New Indication	Date of Approval	Repurposing approach used
Zidovudine	Cancer	HIV/AIDS	1987	In vitro screening of compound libraries
Minoxidil	Hypertension	Hair loss	1988	Retrospective clinical analysis (identification of hair growth as an adverse effect)
Sildenafil	Angina	Erectile dysfunction	1998	Retrospective clinical analysis
Thalidomide	Morning sickness	Erythema nodosum leprosum and multiple myeloma	1998 and 2006	Off-label usage and pharmacological analysis
Celecoxib	Pain and inflammation	Familial adenomatous polyps	2000	Pharmacological analysis
Atomoxetine	Parkinson disease	ADHD	2002	Pharmacological analysis
Duloxetine	Depression	SUI	2004	Pharmacological analysis
Rituximab	Various cancers	Rheumatoid arthritis	2006	Retrospective clinical analysis (remission of coexisting rheumatoid arthritis in patients with non-Hodgkin lymphoma treated with rituximab)
Raloxifene	Osteoporosis	Breast cancer	2007	Retrospective clinical analysis
Fingolimod	Transplant rejection	MS	2010	Pharmacological and structural analysis146
Dapoxetine	Analgesia and depression	Premature ejaculation	2012	Pharmacological analysis
Topiramate	Epilepsy	Obesity	2012	Pharmacological analysis
Ketoconazole	Fungal infections	Cushing syndrome	2014	Pharmacological analysis
Aspirin	Analgesia	Colorectal cancer	2015	Retrospective clinical and pharmacological analysis

ADHD: attention deficit hyperactivity disorder; MS: multiple sclerosis: SUI: stress urinary incontinence

previous complete remission rates of 55-88% on an anthracycline-based chemotherapeutic regimen (McCulloch, Brown, & Iland, 2017).

1.7 Palladium-based compounds as chemotherapeutics and the DNA damage response

The use of transition metal complexes as potential therapeutics and in diagnostic medicine is of considerable importance. Platinum drugs, particularly cisplatin, are the mainstay of metal-based compounds in the treatment of cancer. However, due to dose-related adverse effects and multi-drug resistance associated with this line of therapy there has been an ongoing search for alternative metallic compounds with improved anti-cancer activity and distinct mechanisms of action (Ndagi, Mhlongo, & Soliman, 2017). In this regard, palladium-based complexes have been of particular interest for reasons including (I) their structural similarity to cisplatin (i.e. should exert anti-cancer activity) (II) reports of their superior cytotoxicity at much lower concentrations compared to cisplatin and (III) challenges of stabilising palladium-based complexes have been overcome.

In order to understand what can be expected from palladium-based compounds as anti-cancer agents, it is important to know how cisplatin exerts its anti-cancer activity. DNA is the primary target of cisplatin where its platinum ions covalently bind to guanine bases of DNA and form intra- and inter-strand crosslinks. These cisplatin-DNA adducts interfere with DNA replication and transcription, but the double stranded DNA breaks (DSBs) caused by the crosslinks between adjacent guanine residues are largely responsible for the cytotoxicity exerted by cisplatin (Cheung-Ong, Giaever, & Nislow, 2013; Lukas, Lukas, & Bartek, 2011; Woods & Turchi, 2013). This genotoxic stress triggers a canonical DSBs DNA damage response (DDR) pathway (Fig. 1.8) through activation of ataxia telangiectasia mutated (ATM) and ATM-Rad3-related (ATR). These master regulators drive the accumulation of the phosphorylated form of the histone variant H2AX, referred to as γH2AX, to the site of DNA damage. Detection of γH2AX is therefore considered a robust biomarker for detecting DSBs (Valdiglesias et al., 2013).

It facilitates the activation of checkpoint kinase 2 (Chk2) and the tumour suppressor p53, which has multi-functional roles in mediating several responses to DNA damage. These include cell cycle arrests and DNA repair or if the damage is too extensive it initiates programmed cell death (Zhou & Elledge, 2000). Mitogen-activated protein kinases (MAPKs) are also implicated in the DDR. Indeed, the p38/MAPK pathway has shown to play a key role

in cisplatin-induced cytotoxicity (Hernández Losa et al., 2003). In response to DSBs p38 is phosphorylated allowing for its nuclear localisation and the activation of its targets that induce cell cycle checkpoints and DNA repair. Phosphorylated p38 (p-p38) also targets and activates p53, thus amplifying the DDR (Wood et al., 2009). Ultimately the DSBs caused by cisplatin leads to cell cycle arrest and cell death by apoptosis (Basu & Krishnamurthy, 2010; Cohen & Lippard, 2001).

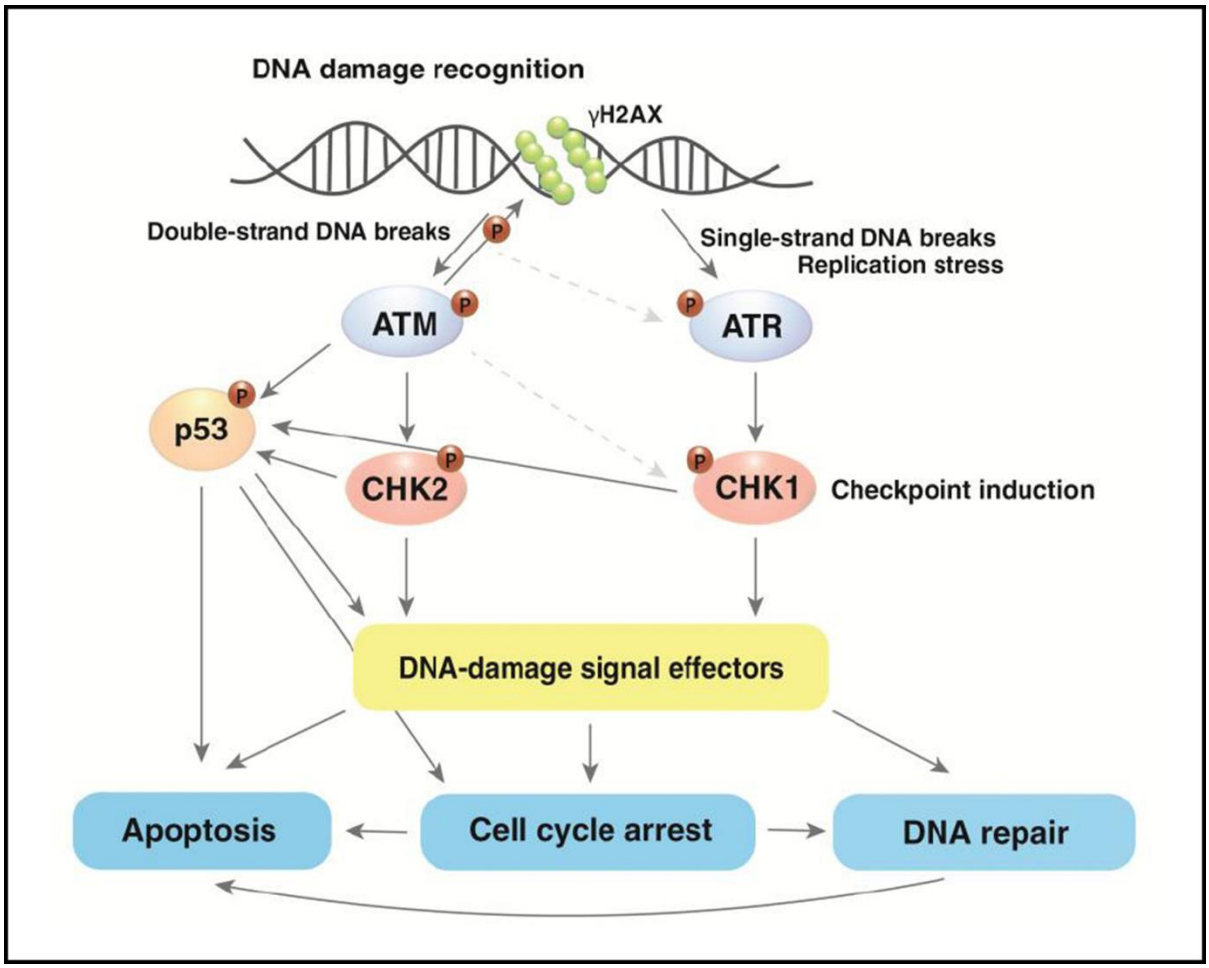

Fig. 1.8 The canonical DNA damage response pathway. *DNA damage is detected by sensors which transduce the signal through ATM for double-stranded DNA damage and ATR for single-stranded DNA damage. These master regulators activate checkpoint kinases CHK1 and CHK2 which activate cell cycle checkpoints and the tumour suppressor transcription factor p53 and other DNA damage signal effectors which mediate cell cycle arrests to enable DNA repair or cell death via apoptosis. ATM also phosphorylates histone H2AX forming histone variant γH2AX which amplifies the DNA damage signal. ATM is also able to activate the ATR pathway. ATM: ataxia telangiectasia-mutated; ATR: ataxia telangiectasia and Rad3-related protein; CHK1: checkpoint kinase 1; CHK2: checkpoint kinase 2; P: phosphorylation (Tšuiko et al., 2018).*

It has been suggested that based on the structural similarity between palladium and platinum ions, that palladium-based complexes may also induce their cytotoxic effects via a mechanism involving the induction of DNA damage (Mukherjee et al., 2011; Serrano et al., 2011; Ulukaya et al., 2013). Indeed, studies have shown that palladium-based compounds do induce DSBs and encouragingly, palladium-based compounds have been shown to exert a much greater degree of cytotoxicity in cancer cells compared to cisplatin. Furthermore, palladium-based compounds have also been reported to exert anti-cancer activity against cisplatin-resistant cells suggesting a different mechanism of action (Akdi et al., 2002; Jahromi et al., 2016; Kruszewski et al., 2003). For example, a series of water-soluble palladium-based complexes showed potent anti-cancer activity at IC_{50} concentrations much lower than that obtained for cisplatin in gastric cancer, oesophageal cancer, squamous cell carcinoma and hepatocellular carcinoma cell lines (Hadizadeh et al., 2014). Moreover, a chiral palladium N-heterocyclic carbene complex has recently been shown to exert potent cytotoxicity. The induction of DNA damage was measured by phosphorylation of H2AX in MCF-7 breast cancer cells and the palladium complex was shown to induce a significantly greater degree of phosphorylated H2AX compared to cisplatin at the same concentration (4uM) (Kumar et al., 2017). Tanaka et al. (2013) synthesised and tested a glycoconjugated palladium complex [PdCl2 (L)] against cisplatin-resistant gastric cell lines. This complex was shown to exert anti-cancer activity against these cisplatin-resistant gastric cancer cells through the induction of DSBs and apoptosis. Furthermore, PdCl2 (L) was able to significantly repress proliferation in a xenograft model. Fiuza et al. (2011) compared the anti-cancer activity of a dinuclear palladium-based complex, Pd(2) -Spm, to cisplatin in human breast cancer cell lines. Similar to cisplatin, Pd(2) -Spm was shown trigger DSBs indicated by increased levels of γH2AX, but in the presence of the PI3K inhibitor wortmannin, Pd(2) -Spm displayed a greater anti-proliferative effect compared to cisplatin. Furthermore, when co-administered, Pd(2) -Spm and cisplatin showed a synergistic effect. These results suggest distinct mechanisms of action for each of these complexes.

In a series of studies, the novel Pd(II) complex, PdCl(terpy)](sac)·$2H_2O$, showed promising anti-cancer activity against breast cancer, prostate cancer, cervical cancer, non-small cell lung cancer, neuroblastoma and glioma cell lines in vitro and in vivo. Importantly, IC_{50} values were significantly higher for noncancerous cells suggesting specificity and the compound exhibited

superior anti-cancer effects compared to cisplatin. In most cases the complex induced apoptosis and autophagy, however in non-small cell lung cancer cell lines the induction of necrosis was evident, with no induction of apoptosis. Furthermore, the complex was able to reduce the viability of cancer stem cells (Kacar et al., 2014; Ulukaya at al., 2011; Ulukaya et al., 2013). Lastly, AJ-5, a novel binuclear palladacycle complex with 1,2-bis(diphenylphosphino)ethane as co-ligand was identified in the Prince laboratory as a lead compound. Importantly, the concentration of AJ-5 required to kill aggressive and resistant breast cancer and melanoma cells was 50-fold less than that of cisplatin and AJ-5 displayed promising in vivo clearance of advanced melanoma (Aliwaini et al., 2013, 2015). This suggests that AJ-5 is more effective at killing melanoma and breast cancer cells than cisplatin and may present with fewer side effects. These studies suggest that palladium-based compounds are promising anti-cancer agents that may prove to be less toxic and more effective for the treatment of aggressive and resistant cancers.

1.8 Programmed cell death

Ultimately, the aim of cancer therapies is to induce cell death. There are several mechanisms by which cell death can occur which are generally divided into programmed cell death (PCD) and non-programmed cell death (Edinger & Thompson, 2004). PCD is an evolutionary conserved process that has drawn attention in anti-cancer treatments and, as depicted in Fig. 1.9**,** is divided into three main categories: type I PCD or apoptosis, type II PCD or autophagy, and type III PCD or programmed necrosis (Tan et al. 2014;). These three PCD pathways can be distinguished at morphological, biochemical and biomolecular levels (Galluzzi et al., 2007; Kroemer et al., 2009).

1.8.1 Type I PCD: apoptosis

Apoptosis was the first PCD mechanism to be identified. It has been extensively studied with characteristic morphological features including cell shrinkage, membrane blebbing, chromosome condensation and nuclear fragmentation (Ziegler 2004) (Fig. 1.9). It is a process that degrades cellular components by a group of cysteine proteases called caspases that are irreversibly activated through two distinct but convergent pathways namely, the intrinsic and the extrinsic pathways (Elmore, 2007).

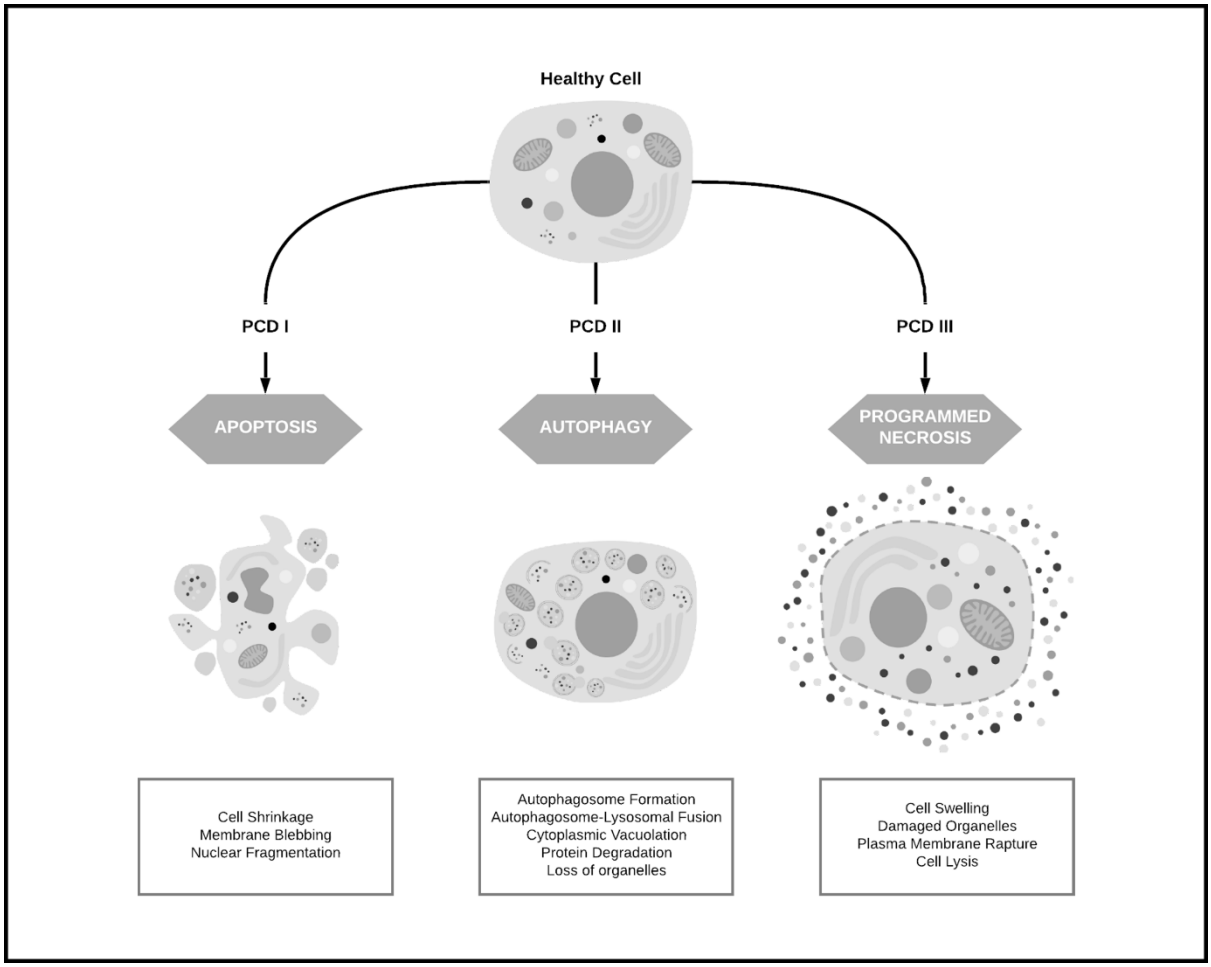

Fig. 1.9 Morphological features of apoptosis, autophagy and programmed necrosis. *This diagram highlights the distinguishing morphological features of type I (apoptosis), type II (autophagy) and type III (programmed necrosis) programmed cell death (PCD) (adapted from Tan et al. 2014).*

The intrinsic apoptotic pathway can be stimulated by the absence of growth factors and intracellular stresses, such as DNA damage, oxidative stress, calcium overload and endoplasmic reticulum stress. It is a mitochondria-centred cell death that is triggered by mitochondrial outer membrane permeabilization (MOMP) (Danial & Korsmeyer, 2004; Galluzzi et al., 2012). Activation of the pro-apoptotic proteins BAX and BAK which are members of the B-cell lymphoma 2 (BCL-2) family, results in MOMP. This causes the release of other pro-apoptotic proteins, including cytochrome c, from the mitochondrial intermembrane space into the cytosol (Eskes et al., 2000; Wei et al., 2000, 2001). Cytochrome c binds apoptotic protease activating factor 1 (APAF1) forming the apoptosome and activating caspase-9. Once active, caspase-9 can directly cleave and activate effector caspases-3 and -7 (Li et al., 1997; Srinivasula et al., 1998) (Fig. 1.10). Effector caspases mediate key cellular apoptotic events including cleavage of a key DNA repair protein poly (ADP-ribose) polymerase

(PARP), which serves as a useful biomarker of apoptosis (Oliver, 1998; Soldani & Scovassi, 2002). Through the activities of these caspases the characteristic morphological features of apoptosis, mentioned above, become evident (Shi, 2002; Woo et al., 1998).

The extrinsic apoptotic pathway is induced by extracellular stress signals that are sensed and propagated by specific transmembrane death receptors (Galluzzi et al., 2012). Binding of lethal ligands, such as the FAS ligand, to their death receptors initiates this apoptotic cascade. The FAS-associated death domain (FADD) protein adaptor associates with the cytosolic domain of the activated death receptor and initiates recruitment and activation of caspase-8. Together these components form the death-inducing signalling complex (DISC) which triggers autoproteolytic processing of the effector caspases (Wajant, 2002). Caspase-8 is a crucial trigger of the extrinsic apoptotic pathway and because it activates the effector caspases directly it is sufficient to induce apoptosis independently of MOMP (Fulda, 2009). However, the intrinsic and extrinsic pathways also have the ability to crosstalk at the level of caspase-8 leading to the intensification of the death signal via the mitochondria (Adams & Cory, 2007; Green, 2000; Wang & El-Deiry, 2003) (Fig. 1.10).

p53 plays a critical role in apoptosis by regulating the BCL-2 family of proteins (Riley et al., 2008). Apoptosis is modulated by these proteins through the release of intermembrane mitochondrial factors (Kluck et al., 1997). While the majority of these BCL-2 proteins are anti-apoptotic, such as BCL-2 and BCL-extra large (XL), a subset of them are classified as pro-apoptotic for example BAX and BAK (Brunelle & Letai, 2009; Ola, Nawaz, & Ahsan, 2011). p53 also acts in response to cellular stresses by inducing cell cycle arrests through activating the expression of the CDKI p21. This response leads to the activation of intrinsic and extrinsic apoptosis (Haupt et al., 2003).

1.8.2 Type II cell death: autophagy

Autophagy (see Fig. 1.11) is a tightly regulated fundamental catabolic process that maintains cellular homeostasis and promotes cell survival under conditions of stress (He & Klionsky, 2009; Levine, 2007). During autophagy, double-membraned vesicles known as autophagosomes engulf misfolded proteins, damaged organelles and superfluous cell

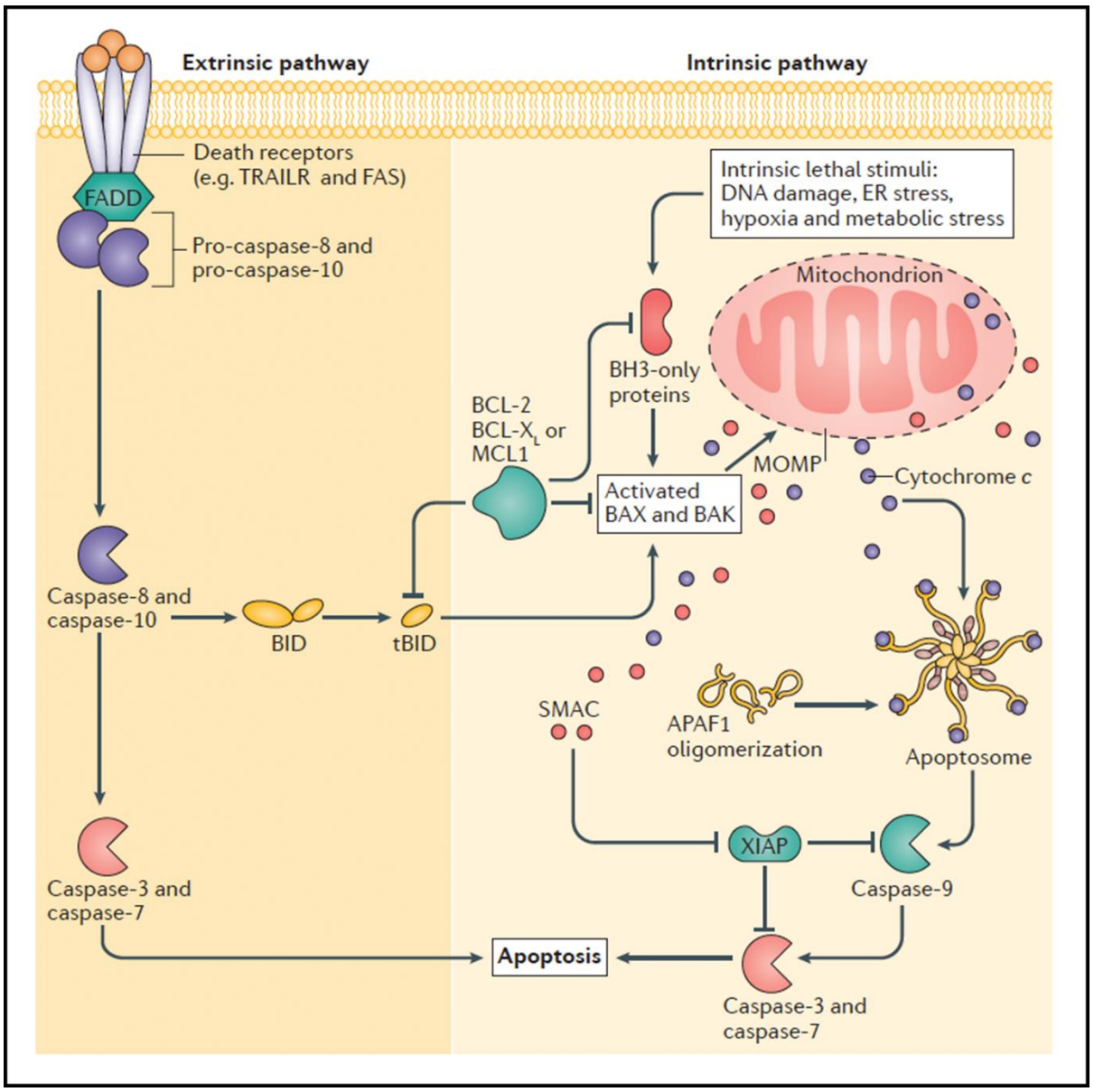

Fig. 1.10 Extrinsic and intrinsic apoptotic signalling pathways. Left panel: *In the extrinsic (death receptor) apoptotic pathway activates death receptors such as TRAILR and FAS, upon binding to their cognate ligand, can activate initiator caspases (caspase-8 and caspase-10) through dimerization mediated by adaptor proteins such as FADD. Active caspase-8 and caspase-10 then cleave and activate the effector caspase-3 and caspase-7 leading to apoptosis.* ***Right panel****: In the intrinsic (mitochondrial) pathway of apoptosis cell stresses engage BH3-only protein activation leading to BAX and BAK activity which triggers MOMP. Anti-apoptotic BCL-2 family proteins counteract this. Following MOMP, mitochondrial intermembrane space proteins such as SMAC and cytochrome c are released into the cytosol. Cytochrome c interacts with APAF1 which triggers apoptosome formation and activates caspase-9. Active caspase-9, in turn, activates caspase-3 and caspase-7 leading to apoptosis. Mitochondrial release of SMAC facilitates apoptosis by blocking the caspase inhibitor XIAP. Caspase-8 cleavage of the BH3-only protein BID enables crosstalk between the extrinsic and intrinsic apoptotic pathways. TRAILR: tumour necrosis factor (TNF)-related apoptosis-inducing ligand (TRAIL) receptor; FADD: FAS-associated death domain protein; MOMP: mitochondrial outer membrane permeabilization; BCL-2: B-cell lymphoma 2; BH3: BCL-2 homology domain 3; SMAC: second mitochondria-derived activator of caspases; APAF1: apoptotic protease activating factor 1; XIAP: X-*

linked inhibitor of apoptosis protein; BID: BH3-interacting death domain agonist; tBID: truncated BID; MCL1, myeloid cell leukaemia 1; ER: endoplasmic reticulum (taken from Ichim and Tait 2016).

contents that are targeted for degradation. Autophagolysosomes are formed when autophagosomes fuse with hydrolase containing lysosomes, after which the cargo is degraded into basic biomolecules and recycled back into the cell for reuse. The formation of the autophagosome is regulated by autophagy-related (ATG) proteins of which Beclin 1 and microtubule-associated protein 1A/1B-light chain 3 (LC3) are key components (Mizushima & Komatsu, 2011; Wirawan et al., 2012). Beclin 1, sequestered by BCL-2 under nutrient-rich conditions, is crucial for initiation of autophagosome formation and regulation of the autophagic process (Cao & Klionsky, 2007). LC3I, the cytosolic form of LC3, is conjugated to phosphatidylethanolamine (PE) forming the autophagosomal membrane bound form, LC3II. This conversion of LC3 is widely used to detect and monitor autophagy. Furthermore, LC3II is degraded in the autophagosomal lumen after lysosomal fusion and this turnover of LC3 is an indicator of autophagic flux (Mizushima & Yoshimori, 2007; Tanida, Ueno, & Kominami, 2008).

The induction of autophagy is tightly controlled by complex regulatory mechanisms involving diverse upstream input signals such as hormones, nutrients, growth factors, adenosine triphosphate (ATP) levels and intracellular Ca^{2+} concentrations. These signals converge on the mTOR (Dunlop & Tee, 2014; Jung et al., 2010). mTOR, which is activated by class I PI3Ks, negatively regulates autophagy under favourable, nutrient-rich conditions. However, in response to extra-or intra-cellular stress signals such as starvation, growth factor deprivation, pathogen infection and endoplasmic reticulum stress, mTOR is inhibited by class III PI3Ks and thus allows the induction of autophagy (Lu et al., 2008; Yap et al., 2008). For example, the metabolic sensor AMPK is activated under energy stress conditions i.e. low levels of intracellular ATP and represses mTOR thus triggering autophagy (Shackelford & Shaw, 2009). p53 can also positively mediate autophagy by activating AMPK and thus inhibiting mTOR. In addition, p53 can initiate autophagy via its other downstream targets such as insulin-like growth factor-binding protein 3 (IGFBP3), damage-regulated modulator of autophagy (DRAM) and pro-apoptotic proteins PUMA and BAX that also positively regulate autophagy (Sui et al., 2011).

There is substantial evidence to suggest that the roles of autophagy in cancer are double-faced and context-specific (White, 2012; White & DiPaola, 2009). Decreased expression of ATG proteins i.e. the inhibition of autophagy has been linked to the initiation and/or progression of cancer, while on the other hand, autophagy has been shown to support the survival of established tumours by providing extra energy (Eskelinen, 2011; Liang et al., 2006; Mathew, Karantza-Wadsworth, & White, 2007; Qu et al., 2003; Shintani & Klionsky, 2004; Yang et al., 2011). These results suggest that autophagy can function to either prevent or support tumourigenesis.

Autophagy is one of the most important mechanisms to tolerate cytotoxic stresses and thus the function of autophagy in cancer treatment is also complex. Autophagy can cause anti-cancer drug resistance and can enable tumour recurrence after long-term cytotoxic treatment, but extreme stress over a protracted period can also commit a cell to undergo autophagic cell death (Bhutia et al., 2013; Livesey, Tang, Zeh, & Lotze, 2009). Indeed, the inhibition of autophagy has been shown to be a successful approach to enhance therapeutic benefits in many experimental settings where autophagy has been shown as a drug resistance pro-survival mechanism (Amaravadi et al., 2007; Longo et al., 2008; Rao et al., 2012; Yang et al., 2010). In apoptosis-resistant cancer cells especially, the induction of autophagic death has been reported and shown to be a useful therapeutic approach. For example, several chemotherapeutic drugs including alkylating agents, actinomycin D and arsenic trioxide have been shown to trigger autophagic cell death in various cancer cells in vitro (Chen & Karantza, 2011). Whether the autophagic response to chemotherapy is an attempt to support cancer cell survival or the cause of death is context dependent (Fulda, 2012).

1.8.3 Type III cell death: regulated necrosis

Necrosis is often viewed as an accidental and unregulated cellular event characterised by swelling of organelles and cells, rupture of the plasma membrane and release of the intracellular contents. However, evidence now reveals that, like apoptosis, necrosis can be executed by regulated mechanisms which include necroptosis, parthanatos, ferroptosis or oxytosis, mitochondrial permeability transition (MPT)-dependent necrosis, pyroptosis and pyronecrosis, and NETosis or ETosis (Berghe et al., 2014; de Almagro & Vucic, 2015; Galluzzi

& Kroemer, 2008; Vandenabeele et al., 2010). Of these, necroptosis is the best characterised and it generally exhibits morphological features of necrosis (Galluzzi et al., 2017; Lorenzo Galluzzi & Kroemer, 2008; Vandenabeele et al., 2010).

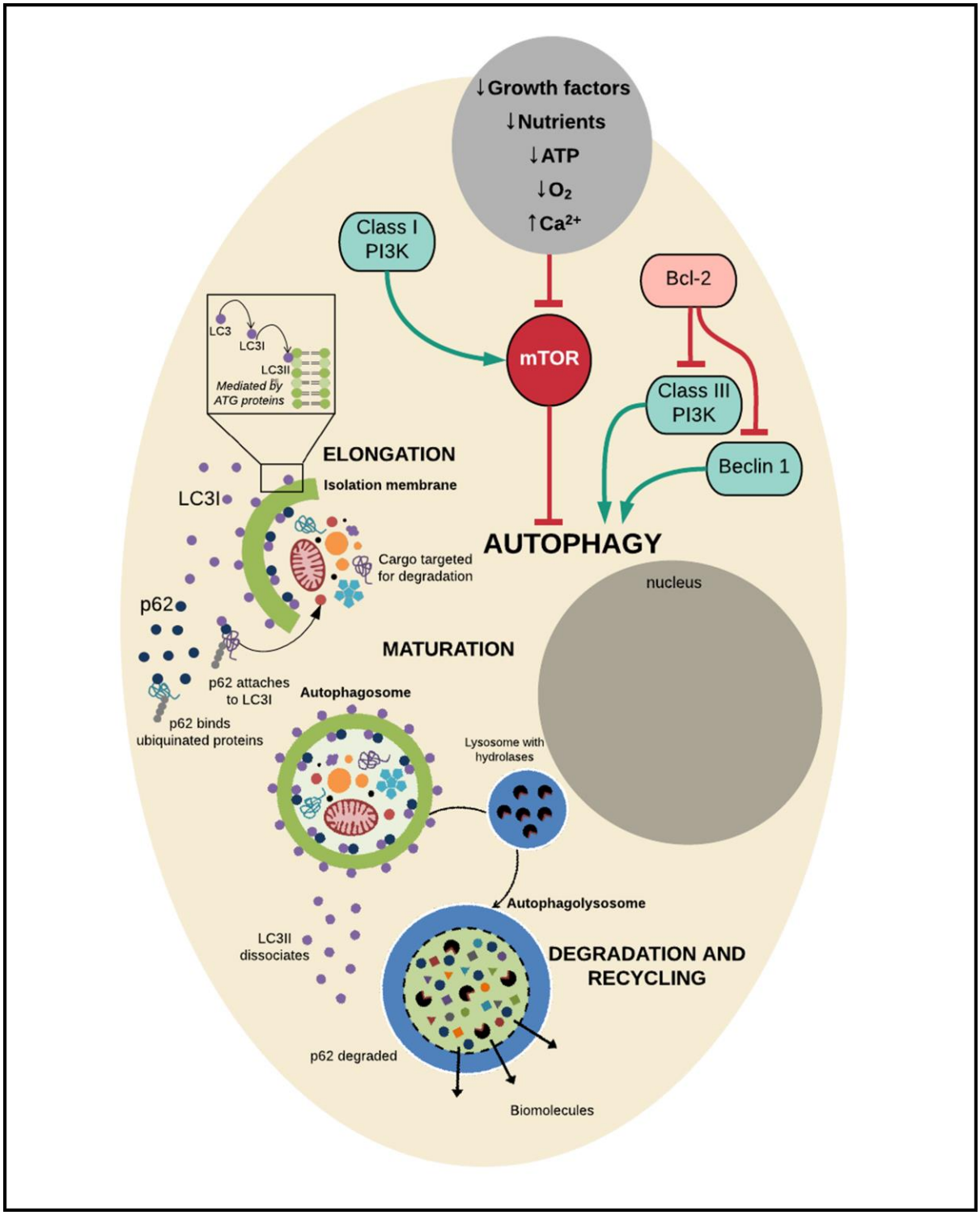

Fig. 1.11 Schematic representation of the key mediators involved in the autophagic process. *The negative regulator of autophagy, mTOR, is activated by class I PI3Ks and key promoters of autophagy are sequestered by Bcl-2 under normal conditions. Stress signals inhibit mTOR and cause Bcl-2 to*

release its inhibition thus activating autophagy. Beclin 1 plays a crucial role in autophagosome initiation and regulation of the autophagic process and cleaved and conjugated LC3I to PE (LC3II) is essential for autophagosomal membrane elongation. The autophagosome cargo protein p62 binds to ubiquitinated proteins and attaches to LC3I for selective autophagy. The mature autophagosome fuses with a hydrolase containing lysosome to from an autophagolysosome in which cargo is degraded and recycled back into the cytosol for reuse. LC3II dissociates from the mature autophagosome while p62 is degraded and recycled in the autophagolysosome. mTOR: mammalian target of rapamycin; PI3K: phosphoinositide 3-kinase; Bcl-2: B-cell lymphoma 2; LC3: microtubule-associated protein 1A/1B-light chain 3; PE: phosphatidylethanolamine.

The term 'necroptosis' was coined to describe a non-apoptotic mode of cell death that is induced by the ligation of various death receptors which are common to apoptosis signalling and include FAS, tumour necrosis factor (TNF) receptor 1 (TNFR1) and TNFR2, various Toll-like receptors and intracellular sensors such as DNA-dependent activator of interferon-regulatory factors (DAI) and protein kinase R (PKR) (Chan, Nailwal, & Moriwaki, 2019; Linkermann & Green, 2014; Zhou & Yuan, 2014). Of these, the TNFR signalling pathway is the most well characterised necroptotic programme (Fig. 1.12). Following binding of TNF, TNFR1 recruits receptor-interacting serine/threonine-protein kinase 1 (RIPK1), TNFR1 associated death domain (TRADD), cellular inhibitor of apoptosis protein (cIAP) 1 and cIAP2, and TNFR associated factor 2 (TRAF2) and TRAF5, which form complex I. cIAPs mediate Lys63 linked ubiquitylation of RIPK1, which enables the docking of TGFβ-activated kinase 1 (TAK1), TAK1 binding protein 2 (TAB2) and TAB3 and results in the activation of the inhibitor of nuclear factor-κB (NF-κB) kinase (IKK) complex. This complex, in turn, targets inhibitor of NF-κB-α (IκBα) for degradation, which liberates NF-κB, allowing it to translocate to the nucleus where it drives transcription of pro-survival genes as well as genes encoding negative-feedback proteins such as IκBα and interleukin17 (IL-17) receptor D (Fuchs et al., 2012; Karin & Ben-Neriah, 2000; Wertz et al., 2004; Wright et al., 2007). Two such pro-survival NF-κB target genes are those encoding zinc-finger protein A20 and FLICE-like inhibitory protein (FLIP). Whereas, A20 polyubiquitylates RIPK1 at Lys48 thereby marking it for proteasomal degradation, the deubiquitylating enzyme cylindromatosis (CYLD) eliminates Lys63-linked ubiquitin chains from RIPK1, leading to the dissociation of RIPK1 from complex I (Hitomi et al., 2008; Wright et al., 2007). When RIPK1 is deubiquitylated at Lys63 its function changes from promoting survival to promoting death through formation of the DISC (also known as complex IIa), which comprises RIPK1, RIPK3, TRADD, FADD, caspase-8 and FLIP (Berghe et al., 2014; Micheau & Tschopp, 2003). The DISC has a dual role: it facilitates the cleavage and

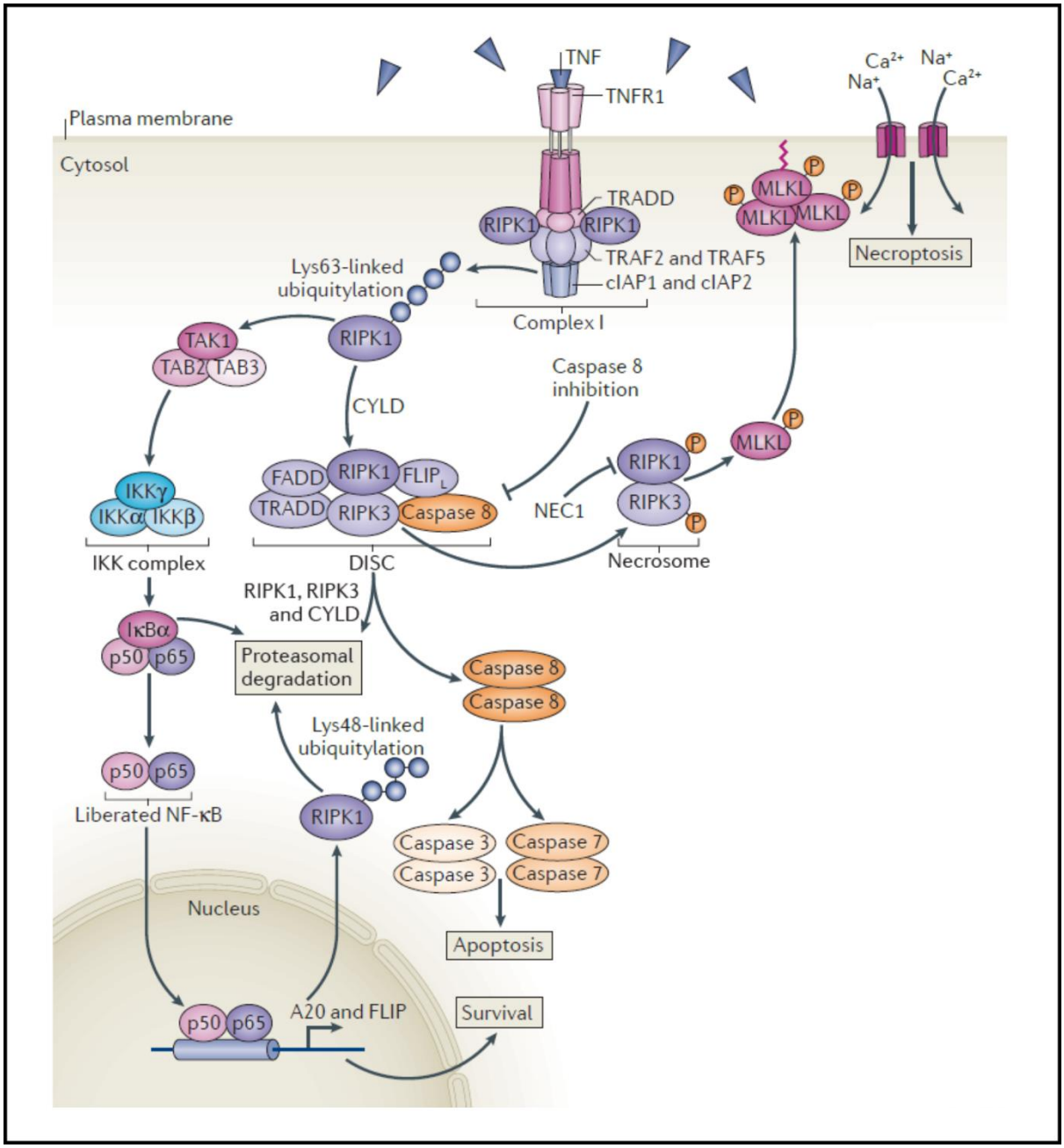

Fig. 1.12 TNF-mediated survival, apoptosis and necroptosis. *Ligation of TNFR1 results in the recruitment of RIPK1, TRADD, cIAP1 and cIAP2, and TRAF2 and TRAF5 to TNFR1 to form complex I. cIAP1 and cIAP2 mediate Lys63–linked ubiquitylation of RIPK1, which facilitates docking of TAK1 and its binding partners TAB2 and TAB3. The signal is then propagated to the IKK complex, which promotes the degradation of IκBα, the cytoplasmic inhibitor of canonical NF–κB. Once liberated from IκBα, NF–κB translocates to the nucleus, where it drives the transcription of pro-survival genes as well as feedback antagonists. These pro-survival NF–κB-target genes include those encoding A20 and FLIP, which promote the association of RIPK1 with cytoplasmic RIPK3, TRADD, FADD, caspase-8 and the NF–κB target FLIP to form the DISC. FLIPL can heterodimerize with caspase-8 and facilitate the cleavage and degradation of CYLD, RIPK1 and RIPK3. However, the DISC also causes homodimerization and catalytic activation of caspase-8, which activates caspase-3 and caspase-7 to induce apoptosis. When caspase-8 is deleted or inhibited, RIPK1 interacts with RIPK3, leading to the formation of the necrosome; this interaction can be inhibited by NEC1. RIPK3 recruits and phosphorylates mixed-lineage kinase domain-like protein (MLKL), leading to the formation of MLKL oligomers that translocate to the plasma membrane. Once at the plasma membrane, MLKL forms membrane disrupting pores, which*

regulate influx of both Na+ and Ca2+, resulting in membrane rupture. TNF: tumour necrosis factor; TNFR1: TNF receptor 1; RIPK1: receptor-interacting serine/threonine protein kinase 1; TRADD: TNFR1–associated death domain; cIAP1: cellular inhibitor of apoptosis protein 1; TRAF2: TNFR-associated factor 2; TAK1: transforming growth factor-β (TGFβ)-activated kinase 1; TAB2: TAK1–binding protein 2; IKK: inhibitor of nuclear factor-κB (NF-κB) kinase; FLIP: FLICE-like inhibitory protein; FADD: FAS-associated death domain protein; DISC: death-inducing signalling complex; FLIPL: FLIP long isoform; CYLD: cylindromatosis; NEC1: necrostatin-1; p: phosphorylation; MLKL: mixed-lineage kinase domain-like protein (adapted from Fuchs & Steller 2015).

degradation of CYLD, RIPK1 and RIPK3 to inhibit necroptosis; and it enables the homodimerization and catalytic activation of caspase-8 to stimulate apoptosis. The key function of complex IIa is to regulate necroptosis (Kaczmarek, Vandenabeele, & Krysko, 2013; Kaiser et al., 2013; Oberst et al., 2011). When caspase-8 is inactivated, RIPK1 associates with RIPK3, resulting in autophosphorylation, transphosphorylation and formation of the necrosome (Cho et al., 2009; He et al., 2009; Zhang et al., 2009). Necrostatin-1 targets the kinase domain of RIPK1 which inhibits its interaction with RIPK3. This prevents necroptosis but does not affect the pro-survival NF-κB pathway downstream of RIPK1 (Christofferson & Yuan, 2010; Degterev et al., 2005; Degterev & Yuan, 2008). Necroptosis is initiated when phosphorylated RIPK3 recruits and phosphorylates mixed lineage kinase domain-like protein (MLKL) which leads to the formation of MLKL oligomers that translocate to the plasma membrane, bind to phosphatidylinositol phosphates and form membrane disrupting pores (Sun et al. 2012; Xie et al. 2013; Dondelinger et al. 2014; Wang et al. 2014). The resulting perturbation of membrane integrity seems to induce influx of both Na^+ and Ca^{2+}, leading to a rise in osmotic pressure that causes membrane rupture and the release of immune-stimulating molecules (Cai et al., 2014; Xin Chen et al., 2014; Huayi Wang et al., 2014). It is important to note that necroptotic tumour cells efficiently elicit a cytotoxic CD8+ T-cell response, known to play a major role in the immune surveillance and elimination of cancer cells, against tumour grafts (Aaes et al., 2016; Fehres et al., 2014; Yatim et al., 2015).

1.9 Aims of this study

RMS, although a rare soft tissue sarcoma, contributes to a considerable loss of years of life in comparison to other cancers as it largely affects children and adolescents. Although localised RMS has a high rate of overall survival with current treatment regimens, there has been very limited improvement in the treatment of the metastatic form and the chemotherapeutic agents used are associated with debilitating side effects. There is therefore a need for new treatment options that can improve the outcomes of metastatic disease and that cause fewer adverse effects. This study set out to address these issues by adopting a two-pronged approach outlined in the aims and objectives below.

Aim 1*:*

Based on the promising data generated in the Prince laboratory on the novel palladium-based complex, AJ-5, against advanced melanoma and breast cancer cells, this study aimed to test the efficacy of AJ-5 against aggressive cancers of mesenchymal origin, specifically RMS. Therefore, to achieve this aim the objectives were:

1. To test the efficacy of AJ-5 in RMS and non-malignant cell lines
2. To investigate the DDR as a signalling cascade that mediates AJ-5 induced cytotoxicity
3. To investigate modes of AJ-5 induced cell death in RMS cells
4. To investigate the pharmacokinetic properties of AJ-5 in healthy nude mice
5. To test and compare the efficacy of the more water-soluble AJ-5 derivative, BTC2, in RMS and non-malignant cell lines

Aim 2:

With advances in understanding the molecular biology that drives rhabdomyosarcomagensis, the T-box transcriptions factors TBX2 and TBX3 are of particular interest as they have been identified as key drivers of RMS and have been validated as biological targets for therapeutic intervention. However, developing a targeted therapy is time-consuming and costly. Therefore, the aim of this aspect of the study was to adopt a drug repurposing strategy to

identify FDA-approved drugs that target TBX2 and/or TBX3. The objectives to achieve this aim were:

1. To design, run and analyse a cell-based high throughput immunofluorescence drug repurposing screen to identify already FDA-approved compounds that negatively regulate TBX2 and/or TBX3
2. To validate selected 'hits' identified in the drug screen for their effect on TBX2/3
3. To perform preliminary experiments to determine the mechanism(s) by which the 'hits' inhibit TBX2/3
4. To determine if 'hit' drugs decrease cancer cell viability through inhibiting TBX2/3
5. To determine if knockdown of TBX2/3 sensitises cells to selected 'hit' drugs

CHAPTER 2

Materials and Methods

2.1 Cell culture

RH30 human ARMS cells (kindly provided by Associate Professor Judith Davie, Southern Illinois University), AX-OH-1 human ARMS and FL-OH-1 human ERMS cells (kindly provided by Professor Stefan Bath, University of Cape Town) were cultured in Roswell Park Memorial Institute Medium (RPMI)-1640 (Sigma Aldrich, Missouri, USA). RD human ERMS cells (ATCC® CCL-136™), FG0 and DMB human skin fibroblasts (kindly provided by Associate Professor Denver Hendricks, University of Cape Town), mouse myoblast cells (ATCC® CRL-1772™**,** referred to as C2C12), human mesenchymal stem cells A10021501 (kindly provided by Professor Michael Pepper, University of Pretoria and confirmed to meet the criteria to be defined as mesenchymal stem cells as set out by the Mesenchymal and Tissue Stem Cell Committee of the International Society for Cellular Therapy (Dominici et al., 2006)), HT1080 human fibrosarcoma cells (ATCC® CCL-120™), SW1353 human chondrosarcoma cells (ATCC® HTB-94™), SW982 human synovial sarcoma cells (ATCC® HTB-93™), SW872 human liposarcoma (ATCC® HTB-92™) and MG-63 human osteosarcoma cells (kindly provided by Associate Professor Philippa Hulley, University of Oxford) were cultured in Dulbecco's Modified Eagle's Medium (DMEM) (Sigma Aldrich). All culture medium was supplemented with 10% heat-inactivated foetal bovine serum (FBS), 100U/mL penicillin and 100µg/mL streptomycin. Cells were maintained at 37°C in a 95% air and 5% CO_2 humidified incubator. Medium was replaced every 2 to 3 days and cells were routinely subjected to mycoplasma tests. Only mycoplasma free cells were used in experiments. Cell morphology was monitored using an Olympus CKX41 inverted microscope (MSAC Ltd, UK) and imaged with an EVOS™ XL AMEX1000 Core Imaging System (Thermo Fisher Scientific, Massachusetts, USA).

2.1.1 Stable cell lines

2.1.1.1 Inducible TBX2/3-FLAG 501mel cells

Monoclonal inducible stable human melanoma (501mel) cell lines expressing 3XFLAG-tagged TBX2 and 3XFLAG-tagged TBX3 were previously established in Professor Colin Goding's laboratory, Ludwig Institute for Cancer Research, University of Oxford using a tetracycline-controlled transcriptional activation (Tet-On) system combined with the piggyBAC (PB) transposase mediated genomic integration system (Schmidt, 2015). The cDNAs for TBX2 and TBX3 including the 3XFLAG peptide were cloned under control of the minimal promoter hCMV*-1 with an upstream tetracycline response element (TRE), not transcriptionally active alone. Administered doxycycline (D9891, Sigma-Aldrich, USA), a tetracycline derivative, binds to the constitutively expressed reverse tetracycline transactivator (rtTA) enabling its binding to the TRE, subsequently activating the expression of TBX2 and TBX3 (Fig. 2.1A). The PB transposase system was used to efficiently integrate the coding sequences of TBX2 and TBX3 with their minimal promoter into the genomic DNA. The above described sequences were inserted between inverted terminal repeat sequences (ITRs), recognised by the PB transposase. Upon recognition the PB transposase excises the sequence from the plasmid and mediates efficient integration into genomic DNA at TTAA sites (Fig. 2.1B). Inducible TBX2-FLAG 501mel monoclonal cell line 8 and 501mel inducible TBX3-FLAG monoclonal cell line 9 were selected to be used in this study and were maintained and cultured in RPMI medium as described earlier.

2.1.1.2 shTBX2 and shTBX3 501mel cell lines

Monoclonal stable melanoma (501mel) cell lines with shRNA mediated knockdown of TBX2 and TBX3 were previously established in our laboratory. shTBX2 clone 5 was used with corresponding shControl clone 8 and shTBX3 was used with corresponding shControl clone 3 (Peres et al., 2010). Cell lines were cultured in RPMI medium as described earlier.

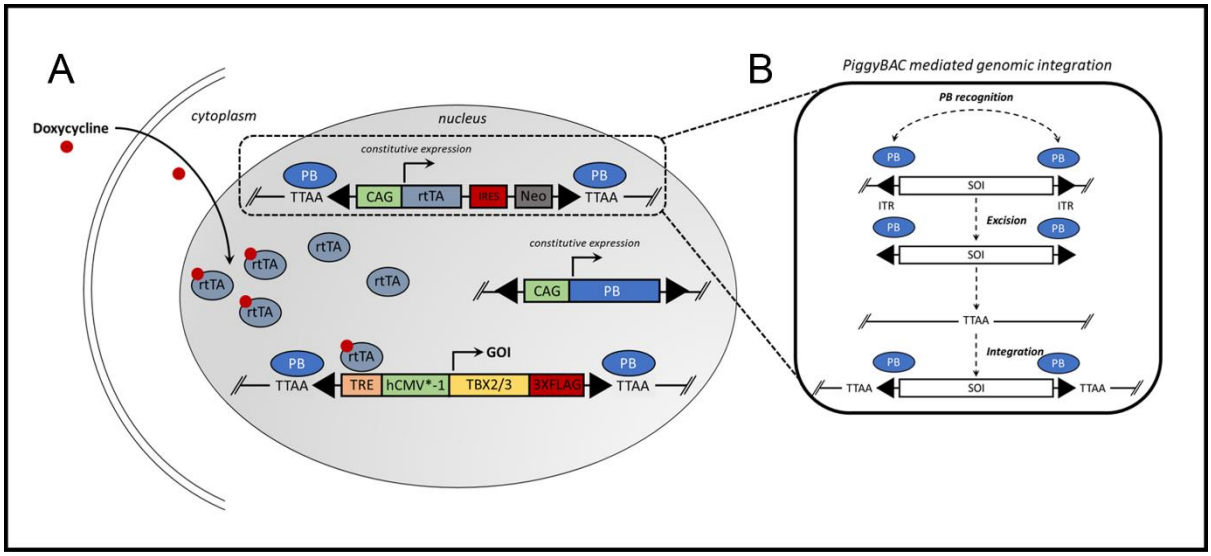

Fig. 2.1 The piggyBAC-Tet-On system used in this study. *Constructs for TBX2 and TBX3 flanked by ITRs were respectively co-transfected with an rtTA construct also flanked by ITRs and a PB construct. (A) Tet-on system. The GOI (TBX2/3-FLAG) is under the control of a minimal promoter which is transcriptionally inactive by itself. Doxycycline, a tetracycline derivative binds to constitutively expressed rtTA and the complex binds the TRE driving expression of the GOI. (B) piggyBAC mediated genomic integration. ITRs flanking the SOI are recognised by PB transposase, excised together with the SOI and integrated at accessible TTAA sites in the genome. ITRs: inverted terminal repeat sequence; rtTA: reverse tetracycline transactivator; PB: piggyBAC transposase; GOI: gene of interest; TRE: tetracycline response element; SOI: site of interest.*

2.1.1.3 Inducible CRISPR/Cas9 induced pluripotent stem cells (iPSCs)

iPSCs with a Tet-On CRISPR/Cas9 system (established and kindly provided for use by Professor Musa Mhlanga, University of Cape Town) were maintained as described earlier and cultured in feeder-free StemPro iPSC medium which included DMEM/F12, GlutaMAX™ supplement (10565042) supplemented with 2% StemPro™ hESC SFM (A1000701), 1.8% bovine serum albumin (BSA) (A1000801), 55mM 2-mercaptoethanol (21985023) and 10µg/mL FGF-Basic (AA 1-155) Recombinant Human Protein (PHG0264) all from Thermo Fisher (Massachusetts, USA).

2.1.2 Mycoplasma test

Cells were grown on a coverslip in a 35mm dish for a minimum of 24h in antibiotic-free medium. The cells were fixed in a 1:3 mixture of glacial acetic acid and methanol for 5s, briefly washed with water to remove the fixing solution and air-dried at room temperature (RT) for a couple of minutes. Once dried, 500µl 0.5µg/ml Hoechst (33342, Invitrogen, California, USA)

was applied for 7s to stain the DNA, followed by a brief wash with water to remove excess stain. The coverslip was mounted on a slide with mounting fluid (Appendix 7.1) and viewed with a Carl Zeiss Axioskop 2 MOT fluorescence microscope (Zeiss, Germany) using the ultraviolet (UV) channel. Mycoplasma negative cells stained positive with Hoechst only in the nucleus, while mycoplasma infected cells showed positive staining in both the nucleus and the cytoplasm. Staining in the latter is due to the DNA of the bacteria, which is not confined to the nucleus of the host cell.

2.2 Cell treatments

2.2.1 Palladacycle complexes

AJ-5 (MW: 1210.93g.mol^{-1}), synthesised as previously described (Aliwaini et al., 2013) and Bridged Tethered Complex 2 (BTC2) (MW: 1419.141g.mol^{-1}) synthesised as previously described (Blanckenberg, 2016) were dissolved in dimethyl sulfoxide (DMSO) (Sigma Aldrich, Missouri, USA) with several 10s intervals of heating at 90°C for AJ-5 and 65°C for BTC2 to give a 5mM drug stock which was stored at (RT) and used within 5 days. AJ-5 and BTC2 were diluted in cell culture medium to achieve the desired final concentration and a vehicle control (DMSO) of the same concentration was prepared simultaneously. Cells were treated at a confluency of 60%.

2.2.2 Chemical compounds and small molecule library

Mitomycin C (M4287, Sigma Aldrich, Missouri, USA) was used to inhibit proliferation during scratch motility assays at a concentration of 10µM administered after wound formation (Eccles, Box, & Court, 2005). Doxorubicin (z/26/0167, Teva Pharmaceutical Industries Ltd, Israel) was used as a positive control in Caspase-Glo experiments at a concentration of 0.5µM. Doxycycline (D9891, Sigma Aldrich, Missouri, USA) was used (20ng/mL - 200ng/mL and 2µg/mL) to induce expression of inducible TBX2-FLAG and inducibleTBX3-FLAG 501mel cell lines. The Pharmakon 1600 drug library (MicroSource Discovery Systems, Connecticut, USA), 1600 known drugs (10mM in DMSO) from US and International Pharma, was provided by the Target Discovery Institute, University of Oxford. All compounds within the Pharmakon 1600 collection have reached clinical evaluation and demonstrate biological activity against known

targets. Cells were treated with the library at a concentration of 10µM. The following small compounds were purchased for further validation and characterisation: niclosamide (N3510), tacrolimus (Y0001933), piroctone olamine (51872), pyrvinium pamoate (P0027) from Sigma Aldrich (Sigma Aldrich, Missouri, USA), and vardenafil hydrochloride (sc-220368, Santa Cruz Biotechnology, Texas, USA). For validation and characterisation experiments cells were treated with 10µM (except pyrvinium pamoate which was administered at 2.5µM) at 60% confluency for 24h.

2.2.3 Pathway inhibitors

Necrostatin-1 selectively targets the kinase activity of RIP1, a key mediator of necroptosis (A Degterev, Maki, & Yuan, 2013) and thus inhibition of necroptosis was achieved by 2h pre-treatment with 50µM necrostatin-1 (N9037, Sigma Aldrich, Missouri, USA) prior to the addition of AJ-5 for 48h. For western blotting experiments investigating autophagic flux, cells were treated for 2h post 24h IC_{50} AJ-5 treatment with 200nM bafilomycin A1 (B1793, Sigma Aldrich, Missouri, USA) which blocks the autophagy pathway by inhibiting fusion of autophagosomes with lysosomes (Mauvezin & Neufeld, 2015). For inhibition of ubiquitin mediated protein degradation through the S26 proteasome (Guo & Peng, 2013), cells were pre-treated with 5µM MG-132 (474790, Calbiochem (Merck), Massachusetts, USA) for 2h prior to the addition of drug (AJ-5/niclosamide/piroctone olamine/pyrvinium pamoate) for 24h.

2.3 Cell viability assays

Cell viability was measured using the 3-(4,5-dimethylthiazol-2-yl)-2,5-diphenyl-trazolium bromide (MTT) assay which is based on the ability of metabolically active cells to metabolise the yellow tetrazolium salt, MTT, to purple formazan crystals by mitochondrial succinate dehydrogenase (Riss et al., 2013). An MTT kit (Roche, Switzerland) was used according to the manufacturer's instructions or MTT (M2128, Sigma Aldrich, Missouri, USA) and solubilising reagents were made up in the lab (Appendix 7.2). Cells were seeded in 96-well plates and treated the next day at a confluency of 60%. For the palladacycle complexes, AJ-5 and BTC2, cells were treated with a range of 10 concentrations (0.1µM - 1.0µM) and vehicle (1.0µM DMSO). For niclosamide and pyrvinium pamoate cell viability assays cells were treated with

2µM, 4µM, 6µM, 8µM, 10µM of drug and 10µM vehicle (DMSO) and for piroctone olamine cells were treated with 4µM, 8µM, 12µM, 16µM, 20µM of drug and 20µM vehicle (DMSO). After treatment, 10µl of MTT reagent was added to each well and left to incubate for 4h followed by overnight incubation with 100µl solubilising reagent after which absorbance was measured at 585nm using a spectrophotometer (RT-2100C Microplate Reader, China). Wells with medium and drug only (no cells) were used as a blank. Mean cell viability for each treatment condition was calculated as a percentage of the mean vehicle control. At least three independent experiments in quadruplicate were performed.

2.3.1 Determination of half maximal inhibitory concentration (IC_{50})

IC_{50} concentrations were determined using cell viability assays after 48h of drug treatment. A dose-response curve was fitted using GraphPad Prism version 6.0 (GraphPad Software, California, USA) from which the IC_{50} concentration was calculated or in some cases predicted. All in vitro experiments with AJ-5 and BTC2 used the IC_{50} concentration for treatment with many experiments including a lower concentration.

2.3.1.1 Selectivity Index (SI)

To determine if a drug displays differential activity against cancer cells and normal cells an SI was determined using the following equation:

$$SI = \frac{IC_{50}\ normal\ cell\ line}{IC_{50}\ \ cancer\ cell\ line}$$

An SI of < 2 indicates general toxicity of the drug and is considered unfavourable where an SI ≥ 2 is favourable and suggests that the drug has selective cytotoxicity towards cancer cells. The higher the SI, the more selective the drug towards cancer cells (Badisa et al., 2009; Koch et al., 2005).

2.4 Clonogenic assays

Cells were seeded and treated at 60% confluency the following day with IC_{50}, ½ IC_{50}, ¼ IC_{50} and vehicle. After 24h, 800-4000 cells were seeded in 35mm dishes in drug-free medium.

Formation of colonies were monitored, medium changed when necessary and after 7-21 days cells were fixed with 3:1 methanol: acetic acid and stained with crystal violet (Sigma Aldrich, Missouri, USA) (Appendix 7.3). Dishes were imaged and percentage colony area was determined using ImageJ v1.50i (Schneider, Rasband, & Eliceiri, 2012) and the plugin ColonyArea (Guzmán et al., 2014). Colony area was determined for each drug concentration as a percentage of vehicle treated control.

2.5 Scratch Motility Assay

Cells were seeded in 6-well plates and treated with IC_{50} AJ 5 and vehicle for 24h. Cells were collected, counted and replated to achieve 100% confluency in a 24-well plate. The following day a sterile 2µL pipette tip was used to make a vertical scratch in the cell monolayer of each well and the cells treated with 10µM mitomycin C to inhibit proliferation. Cells were imaged at 0, 3, 6, 9, 12 and 24h post-wound formation and ImageJ v1.50i (Schindelin et al., 2012) was used to calculate the area of the scratch. The total areas migrated was determined by subtracting the area for a specific time point from the area measured at 0h.

2.6 Western blot analyses

Cells were lysed at 4°C in 2X boiling blue solution (Appendix 7.4) by either resuspension of the cell pellet or scraping of cells (volume used depended on pellet size or cell confluency to adjust for equal protein loading) followed by boiling at 100°C for 10min. Equal amounts of protein were loaded and PageRuler™ Prestained Protein Ladder, 10 to 180kDa (Thermo Fisher Scientific, Massachusetts, USA) or Color Prestained Protein Standard, Broad Range (11 - 245kDa) (New England BioLabs, Massachusetts, USA) was used for accurate protein sizing (Appendix 7.5). Protein samples were resolved by 6-15% sodium dodecyl sulphate-polyacrylamide gel electrophoresis (SDS-PAGE) and transferred to Hybond ECL membranes (Amersham, UK). All SDS-PAGE reagent recipes can be found in Appendix 7.6. The membranes were blocked for 1h at RT with 1X phosphate-buffered saline (PBS) (Appendix 7.7) or 1X tris-buffered saline (TBS) (Appendix 7.8) containing 0.1% Tween 20 and 5% non-fat dry or fat-free milk followed by primary antibody incubation in appropriate buffer (according to the datasheet or optimised in the laboratory) overnight at 4°C with shaking. After primary antibody incubation, membranes were washed with 1XPBS/TBS 0.1% Tween 20 and

incubated with goat anti-rabbit, goat anti-mouse (Bio-Rad Laboratories, California, USA) or donkey anti-goat (Santa Cruz Biotechnology, Texas, USA) horseradish peroxidase (HRP)-conjugated secondary antibodies for 1h at RT. Membranes were washed again with 1XPBS/TBS 0.1% Tween 20 and reactive proteins were visualised by enhanced chemiluminescence using SuperSignal West Pico Chemiluminescent Substrate Kit (Thermo Fisher Scientific, Massachusetts, USA) or WesternBright ECL HRP Substrate Kit (Advansta, California, USA). Densitometry readings were obtained using ImageJ v1.50i (Schneider et al., 2012) and protein expression levels were represented as a ratio of protein of interest/p38 loading control normalised to the vehicle treated control sample if appropriate. All blots are representative of at least two independent repeats. The following primary antibodies, diluted 1:1000 unless otherwise stated, were used in this study: rabbit polyclonal antibodies to phospho-histone H2A.X (Ser139) (#2577), phospho-chk2 (Thr68) (#221), phospho-p38 MAPK (Thr180/Tyr182) (#9211), cleaved caspase-3 (Asp175) (#9661), PARP (#9542), caspase-9 (#9502), LC3B (#2775), p38 MAPK (#9212) (1:5000), rabbit monoclonal antibody to cleaved caspase-7 (Asp198) (D6H1) (#8438), phospho-RIP3 (Ser227) (D6W2T) (#93654), phospho-MLKL (Ser358) (D6H3V) (#91689), mouse monoclonal antibodies to phospho-ATM (Ser1981)(D6H9) (#5883), Cyclin B1 (V152) (#4135), Caspase-8 (1C12) (#9746), SQSTM1/p62 (D5L7G) (#88588) (1800) from Cell Signaling Technology (Massachusetts, USA); mouse monoclonal antibody to p53 (DO-1) (sc-126), rabbit polyclonal antibodies to p21 (C-19) (sc-397) (1:500), cyclin A (H-432) (sc-751) (1:500), cyclin B1 (H-433)(sc-752), PARP-1 (H-250) (sc-7150) (1:500), goat polyclonal antibody to TBX2 (sc-17880) from Santa Cruz Biotechnology (Texas, USA); mouse monoclonal antibody to FLAG® M2 (F1804), rabbit polyclonal antibody to p38 MAP kinase (M0800) (1:5000) from Sigma-Aldrich (Missouri, USA); and rabbit polyclonal antibody to TBX3 (ab99302) (Abcam, UK).

2.7 Immunofluorescence

Cells were plated on glass coverslips and post treatment they were fixed with 4% paraformaldehyde (Appendix 7.9) for 15min at RT or ice-cold 100% methanol at -20°C for 5min followed by 1XPBS washes and blocking and permeabilization with 0.2% Triton-X-100 (Sigma Aldrich, USA) and 5% BSA in 1XPBS for 30min at RT. Slides were incubated with primary antibody in blocking buffer overnight at 4°C (except the FLAG antibody which was incubated

for 1h at RT). Rabbit polyclonal antibodies to phospho-histone H2A.X (#2577) (1:500), LC3B (#2775) (1:200) (Cell Signaling Technology, Massachusetts, USA), TBX3 (ab99302, Abcam, USA) (1:100), and mouse monoclonal antibody to FLAG® M2 (F1804) (1:500) (Sigma Aldrich, Missouri, USA) were used in this study. After 1XPBS washes coverslips were incubated with the appropriate secondary antibody diluted 1:1000 in blocking buffer for 1h at RT in the dark. The secondary antibodies used included donkey anti-rabbit Cy3, donkey anti-rabbit, donkey anti-mouse and donkey anti-goat Alexa Fluor® 488 (Jackson ImmunoResearch Laboratories Inc. Pennsylvania, USA or Thermo Fisher Scientific, Massachusetts, USA). A secondary-antibody-only control was always included in the experiment. Nuclei of cells were stained with Hoechst (33342, Invitrogen, California, USA) or 4',6-diamidino-2-phenylindole (DAPI) (Thermo Fisher Scientific, Massachusetts, USA) either simultaneously with secondary antibody incubation (1:1000) or afterwards for 10min at RT in the dark. After 1XPBS washes, coverslips were mounted using Mowiol mounting medium. Cells were imaged with a LSM 510, 710 or 880 confocal microscopes (Zeiss, Germany) using a Plan-Apochromat 63x/1.40 Oil DIC objective. In most cases, multiple z layers were acquired with 1µm step width, images were processed using ZEN 2012 imaging software (Zeiss, Germany) and maximum intensity projections were generated. For quantification, mean fluorescence was measured from at least 20 fields of view (FOV) per treatment condition and pooled from three independent repeats.

2.8 Flow cytometry

2.8.1 Cell cycle analyses

Cells were treated for 24h and 48h at 60% confluency with IC_{50} AJ-5 or vehicle, trypsinised, washed with 1XPBS, counted and permeabilised in 70% EtOH at -20°C overnight. Cells were pelleted and treated with 50µg/mL RNase (Fermentas, Massachusetts, USA) in 1XPBS at 37°C for 15min then stained with the DNA intercalating dye propidium iodide (PI) (Appendix 7.10) to a final concentration of $1X10^6$ cells/mL in a FACS tube. A minimum of 50 000 cells/sample were subjected to analysis using a Becton Dickinson FACSCalibur flow cytometer (Becton Dickinson, New Jersey, USA) with a 488nm coherent laser. The data were acquired using CellQuest Pro version 5.2.1. software (Becton Dickinson, New Jersey, USA) and the analyses were done using ModFit version 2.0. software (Verity Software House Inc, Maine, USA). The

proportion of cells in each phase of the cell cycle are identified based on their PI fluorescence, a measure of DNA content. Dividing cells in the G_2/M phase of the cell cycle have double the amount of DNA than cells in G_1 and thus the PI fluorescence of cells will be twice as high. Cells in S phase show fluorescence intensity somewhere in between G_1 and G_2/M phase cells and dead cells with damaged and lost DNA show sub-G_1 PI fluorescence (Darzynkiewicz, 2010).

2.8.2 Measurement of apoptosis: Annexin V-FITC assay

In apoptotic cells, phospholipid phosphatidylserine (PS) is translocated from the inner to the outer surface of the plasma membrane serving as a recognition signal for phagocytes. Annexin V is a calcium-dependent phospholipid-binding protein with high affinity for PS and thus binds to the membrane surface of apoptotic cells. Annexin V-FITC thus serves as a probe for flow cytometric analysis of cells undergoing apoptosis. Double staining with PI is used for identification of early and late apoptotic cells as PS translocation precedes the loss of membrane integrity. Therefore, viable cells with intact membranes exclude PI, whereas the membranes of dead and damaged cells are permeable to PI. Accordingly, cells that are considered viable are both Annexin V-FITC and PI negative, while cells that are in early apoptosis are Annexin V-FITC positive and PI negative, cells that are in late apoptosis are both Annexin V-FITC and PI positive and cells that are only PI positive are considered to be undergoing necrosis (which can include programmed necrosis) (van Engeland, Nieland, Ramaekers, Schutte, & Reutelingsperger, 1998; Vermes, Haanen, Steffens-Nakken, & Reutellingsperger, 1995).

After treatment cells were collected by trypsinisation (including all floaters), washed with 1XPBS and counted. The FITC Annexin V/Dead Cell Apoptosis kit (V13242, Thermo Fisher Scientific, Massachusetts, USA) was used according to the manufacturer's instructions. Briefly, pelleted cells were resuspended in binding buffer to a cell density of $1x10^6$ cells/mL and double stained with PI and Annexin V for 15min in the dark in a FACS tube. A negative control of unstained cells and positive controls of cells treated with 3% formaldehyde (F8775, Sigma Aldrich, Missouri, USA) for 30min on ice and stained with either PI or Annexin-V were used to gate the flow cytometer for viable, early apoptotic, late apoptotic and necrotic cell populations. A minimum of 20 000 cells/sample were subjected to analysis using a Becton

Dickinson FACSCalibur flow cytometer (Becton Dickinson, New Jersey, USA) and data were acquired and analysed using CellQuest Pro version 5.2.1. software (Becton Dickinson, New Jersey, USA).

2.9 Caspase activity assays

Cells were treated for 24h at 60% confluency with IC_{50} AJ-5, vehicle, or 0.5µM Doxorubicin (IC_{50} determined in RD and RH30 cells after 3 independent MTT assays in quadruplicate), a well-known apoptotic inducer (Wei et al., 2015). Cells were trypsinised, washed and counted and caspase-8, -9, -3/7 activity was measured using Caspase-Glo® 8, 9 and 3/7 assay kits (Promega, Wisconsin, USA) respectively according to the manufacturer's instructions. Briefly, the appropriate Caspase-Glo® cell lysis and proluminogenic caspase-specific substrate containing reagent was added to cells in suspension in a 96-well format. In the presence of the caspases of interest (3/7, 8 or 9) the proluminogenic substrate would be cleaved resulting in a luminescent signal. The signal generated is proportional to the amount of caspase activity present. Luminescence was measured 45min after incubation with Caspase Glo® reagent using a Luminoscan Ascent luminometer (Thermo LabSystems Inc, Massachusetts, USA). Luminescence signal for treated samples were normalised to vehicle treated samples to express a fold change increase in caspase activity.

2.10 Supravital staining with acridine orange

Acridine orange is a fluorescent dye that readily enters cells, stains DNA and RNA and accumulates in vesicles. It emits green fluorescence when bound to double stranded DNA (dsDNA), but in acidic compartments, the acridine orange dye molecules become protonated, sequestered and trapped in the vesicles and the dye emits red fluorescence and thus acridine orange is used as an acidic vesicle tracer to identify lysosomes, endosomes and autophagosomes (Millot et al., 1997; Pierzyńska-Mach, Janowski, & Dobrucki, 2014). Cells were seeded on glass coverslips and treated for 24h with IC_{50} AJ-5 or vehicle and then stained with 2µg/mL acridine orange (Michrome No. 714, Edward Gurr Ltd., UK), which was added directly to the medium, for 15min at RT in the dark. Coverslips were mounted on glass slides and visualised and imaged as described for immunofluorescence (Millot et al., 1997).

2.11 Single cell autophagosome flux analyses

The autophagy steady state variables were measured in RD cells treated with IC_{50} AJ-5 for 48h. The autophagosome flux was calculated from the rate of autophagosome accumulation as previously described (du Toit at al., 2018). Briefly, this was determined after the complete inhibition of fusion between autophagosomes and lysosomes using 400nM bafilomycin A1 (B0025, LKT Laboratories Inc, Minnesota, USA).

Cells were transfected with a GFP-LC3 construct using Lipofectamine 3000 (L3000001, Thermo Fisher Scientific) according to the manufacturer's instructions and maintained for two days in order to achieve high levels of GFP-LC3 expression. Thereafter, cells were harvested by trypsinisation and seeded into an 8-chamber cover slip-based dish (155411 Nunc™ Lab-Tek™, Thermo Fisher Scientific) to achieve 60% confluency after which they were treated with IC_{50} AJ-5 for 48h.

Autophagosome, autolysosome and lysosome pool size were assessed by supplementing the culture media with 25nM LysoTracker Red (L7528, Thermo Fisher Scientific, Massachusetts, USA) 2h prior to image acquisition. An LSM 780 confocal with ELYRA S.1 Superresolution platform (Carl Zeiss, Germany) was used for image acquisition. The 8-chamber dish was placed in a heated chamber maintained at 5% CO_2 that encased the microscope objective. An LCI Plan-Apochromat 63x/1.4 Oil DIC M27 objective was used and samples excited with an Argon multiline laser 25mW at 488nm and 514nm with appropriate beam splitters and GaAsP detector 32+2 PMT. Multiple z layers were acquired with 1µm step width. Laser power and electron gain were set to achieve an optimal signal to noise ratio without causing photo-toxicity. Images were processed using ZEN 2011 imaging software (Carl Zeiss, Germany) and the maximum intensity projections were exported to Fiji software (Schindelin et al., 2012) for further analysis (du Toit et al., 2018).

2.12 Pharmacokinetics studies of AJ-5 in healthy mice

All studies and procedures were conducted with prior approval of the Animal Ethics Committee of the University of Cape Town (Protocol 012/049) in accordance with the South African National Standard (SANS 10386:008) for the Care and Use of Animals for Scientific

Purposes (SABS Standards Division, 2015), and guidelines from the Department of Health (Department of Health, 2015).

Pharmacokinetic parameters of AJ-5 were determined after intravenous (IV), intraperitoneal (IP) and oral (PO) dosing in MF1 nude mice randomly divided into groups. AJ-5 was prepared in the respective formulations immediately prior to dosing. For the IV group, the compound was made up in a mixture of 10% DMSO and 90% of an IV mixture, which consisted of 60% propylene glycol, 10% ethanol and 30% polyethylene glycol. For the PO group, AJ-5 was dissolved in DMSO and a hydroxypropylmethylcellulose solution (0.5% in water) containing 0.2% Tween 80 in a ratio of 1:9. For the IP group, AJ-5 was dissolved in 10% DMSO and 90% 1XPBS. Mice were permitted access to food and water ad libitum. AJ-5 was administered (100µL) by oral gavage at a dose of 20mg/kg (n=3), intravenously into the penile dorsal vein at a dose of 2mg/kg (n=2) and intraperitoneally at a dose of 2mg/kg (n=3).

Blood samples (20µL/sample) were collected by tail tip bleeding in lithium Heparin tubes at predetermined time-points to evaluate the kinetic profile over 24h. Samples were stored at -80°C until analysis. Blood samples together with calibration standards and quality controls were quantified using ICP-MS. All results reported are for palladium (Pd). Pharmacokinetic parameters of the AJ-5 complex were determined using non-compartmental analysis in PK Solutions 2.0 (Summit Research Systems, Montrose CO, USA).

2.13 TBX2/3 rescue experiments

2.13.1 Transient TBX2/3 overexpression in ARMS (RH30) cells

RH30 cells were fast forward transfected using Lipofectamine® 3000 Transfection Reagent (L3000008, Thermo Fisher Scientific, Massachusetts, USA) with a p3XFLAG-CMV vector with either a mouse expression construct for Tbx2, mouse expression construct for Tbx3, or an empty control (kindly provided by Professor Colin Goding, University of Oxford). For MTT cell viability assays cells were seeded in 96-well plates and transfected with 50ng FLAG-mtbx2 and 100ng FLAG-mtbx3 and for western blot analyses cells were seeded in 24-well plates and transfected with 250ng FLAG-mtbx2 and 500ng FLAG-mtbx3 with equal amounts of control FLAG-empty vector for each experiment. For the fast forward transfection protocol cells were

seeded and immediately transfected. Briefly, for an individual transfection reaction 0.3µL or 1.5µL Lipofectamine® 3000 Reagent was diluted in 5µL or 25µL serum-free medium for a 96-well or 24-well reaction respectively. DNA was diluted in a separate tube with the same volume of serum-free medium and P3000™ Reagent (2µL/µg DNA) was added and mixed well. The contents of the diluted DNA tube were added to the diluted Lipofectamine® 3000 Reagent tube (1:1 ratio), gently mixed and left to incubate for 5min at RT. The transfection reagent/DNA complex was then added in a dropwise manner to the freshly seeded cells. Cells were treated the following day with IC_{50} AJ-5 or vehicle (added to transfection reagent containing medium) for 24h and MTT and western blot analyses were performed as described earlier.

2.13.2 Proof of Concept: TBX2/3 rescue using inducible TBX2/3-FLAG 501mel cells.

Inducible TBX2-FLAG 501mel cells and TBX3-FLAG cells were seeded in 96-well and 6-well plates and treated the following day at 60% confluency with 10µM niclosamide, 10µM piroctone olamine, 2.5µM pyrvinium pamoate or vehicle for 24h. After 12h of drug treatment, 100ng/mL and 200ng/mL doxycycline was as added to the drug-containing medium of the TBX2-FLAG cells and the TBX3-FLAG cells to induce TBX2/3 expression respectively and 12h later MTT assays (96-well plate) and western blot (6-well plate) analyses were performed as described earlier.

2.14 Quantitative real-time PCR (qRT-PCR)

Inducible CRISPR/Cas9 iPSCs were seeded in a 24-well plate and treated 3 days later at 60% confluency with 20ng/mL and 2µg/mL doxycycline for 24h to induce Cas9 expression. Tacrolimus, piroctone olamine and vehicle were added to the medium of the cells to achieve a final concentration of 10µM and left for 24h after which total RNA was extracted using Direct-zol™ RNA MiniPrep Plus (Zymo Research, California, USA) according to the manufacture's instructions. The quality and concentration of RNA was determined by spectrophotometry using a NanoDrop® ND-1000 spectrophotometer (Agilent Technologies, California, USA). Samples with an A260/A280 ratio of ≥ 1.8 and A260/A230 ratio of approximately 2 were reverse transcribed using the ImProm-II™ Reverse Transcription System (A3800, Promega, Wisconsin, USA) according to the manufacturer's instructions. Briefly,

100ng of RNA was combined with 0.5µg of Oligo(dT)$_{15}$ primer made up to a final volume of 5µL with nuclease-free water and denatured at 70°C for 5min, chilled on ice and combined with reverse transcription reaction mix (5X ImProm-II™ Reaction Buffer, 3mM $MgCl_2$, 0.5mM dNTP mix, 10U RNasin® Ribonuclease Inhibitor and 1µl of ImProm-II™ Reverse Transcriptase to a final volume of 20µL). The annealing of the primers to the template RNA occurred at 25°C for 5min, the reactions were incubated at 42°C for 1h for the reverse transcription of the template, followed by 15min incubation at 70°C to inactivate the reverse transcriptase. qRT-PCR was conducted with the KAPA SYBR® FAST qPCR Master Mix (2X) Kit (KR0389, Massachusetts, USA) according to the manufacturer's instructions. Briefly, each PCR resection contained 2.6µL nuclease-free water, 5µL KAPA SYBR FAST qPCR Master Mix (2X), 1µL BSA (2.5µg/µL) and 0.4µL of combined forward and reverse primers (10µM stock) per 9µL reaction. Primers specific to Cas9 (Forward-5'-GCGATCAGATTTTCCAGCCG-3', Reverse-5'-ACATGATCAAGTTCCGGGGC-3') were kindly provided by Professor Musa Mhlanga, University of Cape Town and primers specific to β-actin (Forward-5'-CGGCATCGTCACCAACTG-3', Reverse-5'-AAC ATGATCTGGGTCATCTTCTC-3') were custom designed and ordered (Integrated DNA Technologies, Iowa, USA) and used as an internal control to correct for sample-to-sample variations. PCR reactions were made up as master mixes and aliquoted into glass capillaries with the addition of 1µL of cDNA per capillary to give a final reaction volume of 10µL. LightCycler 3.0 (Roche, Switzerland) PCR cycle parameters were: denaturation for 3min at 95°C, annealing and amplification for 40 cycles for 10s at 95°C, 20s at 55°C and 1s at 72°C, melting for 15s at 65°C and cooling for 30s at 40°C. Each DNA sample was quantified in duplicate and a negative control without cDNA template was run with every assay to assess the overall specificity and monitor for contamination. Melting curve analyses were carried out to ensure product specificity and data was analysed using the $2^{-\Delta\Delta Ct}$ method. Relative Cas9 mRNA expression levels were normalised to B-actin expression levels and data was represented as a fold change of Cas9 mRNA expression in Tet-On CRISPR/Cas9 iPSCs induced with doxycycline and treated with drug or vehicle relative to uninduced and untreated Tet-On CRISPR/Cas9 iPSCs.

2.15 Small molecule library screen

Inducible TBX2-FLAG 501mel cells were harvested, counted and resuspended in FBS-free medium at a density of $1X10^6$ cells/mL. CellTracker™ Orange (34551, Thermo Fisher Scientific, Massachusetts, USA) (1:1000) was added and cells were incubated for 45min at 37°C, spun and resuspended in 1mL FBS-free medium and incubated for another 30min at 37°C. Cells were spun, resuspended in normal medium, and counted. A total of $6x10^6$ stained inducible TBX2-FLAG 501mel cells were mixed with $6X10^6$ inducible TBX3-FLAG 501mel cells and 80µL containing 800 cells (~400 from each population) were seeded in 30X (5 drug library plates, 3 timepoints done in technical duplicates) 384-well clear-bottom plates (781097, Greiner Bio-One, Austria) using an automated Perkin Elmer FlexDrop™ PLUS (PerkinElmer, Massachusetts, USA). Plates were incubated as per normal culture conditions. From this point all liquid handling steps of the drug screen protocol were performed with a Perkin Elmer JANUS® Automated Workstation equipped with a 384-well Modular Dispense Technology™ (PerkinElmer, Massachusetts, USA) unless otherwise stated. Once the cells adhered (day after seeding), medium was removed and fresh medium containing 20ng/mL doxycycline was added (75µL per well) and cells were incubated for 24h. A LABCYTE Echo® 550 (Agilent Technologies, California, USA) was used to transfer 640nL of drug from the Pharmakon 1600 drug library (5X 384-well source plates each with 320 compounds at a concentration of 10mM) to intermediate 384-well plates to achieve a final concentration of 160µM in 40µL medium. 5µL of drug (160µM) from the intermediate drug library plates were transferred to the 384-well cell culture plates (75µL medium) to achieve a final concentration of 10µM in 80µL. Pharmakon compounds were dispensed in columns 3-22, row A-P and vehicle (DMSO) control was dispensed in column 2 and 23, row A-P for each 384-well plate. After 4h, 12h and 24h medium was removed and wells were washed 3X with 1XPBS, followed by fixation with 4% paraformaldehyde for 15min at RT after which plates were washed 3X with 1XPBS again and stored at 4°C until immunofluorescence processing. Cells were blocked and permeabilised with 1XPBS containing 5% BSA and 0.2% Triton-X-100 for 20min at RT and then incubated with mouse monoclonal anti-FLAG M2 (1:500) (Sigma Aldrich, Missouri, USA) for 1h at RT in blocking buffer. Wells were washed 3X with 1XPBS and incubated with Alexa Fluor® 488 secondary antibody and DAPI (1:1000) for 1hr at RT in the dark. Wells were washed 3X with 1XPBS and imaged with an IN Cell Analyzer 6000 (GE Healthcare Life Sciences, Illinois,

USA) using the 20x 0.75NA air objective, on line cell counting to 1000 cells/well (up to 16 fields of view). And the following channel settings: UV DAPI: 75ms, confocal 0.99AU; FITC: 2500ms, confocal 1.23AU; and dsRED: 100ms, open aperture.

2.15.1 Screen analyses

2.15.1.1 Automated parameter extraction from images

A customised parameter extraction protocol was developed using IN Cell Developer Toolbox v1.6.2 (GE Healthcare Life Sciences, Illinois, USA) for automated image analyses. Briefly, this protocol segmented nuclei of cells (UV channel), separated the TBX2-FLAG (CellTracker Orange stained cells) and TBX3-FLAG cell populations (dsRED channel) for independent analyses and measured whole cell, nuclear, cytoplasmic, eroded nuclear and nuclear collar FITC fluorescence intensity (FITC channel). Other numerical descriptions of cellular morphology unrelated to TBX2/3 protein levels and subcellular localisation were also extracted and calculated during the automated image analyses protocol which are described in Table 4.1. in Chapter 4. This automated analyses protocol is detailed in the results section 4.4.

2.15.1.2 z-score 'hit' identification

Mean nuclear, eroded nuclear and nuclear collar FITC Fluorescence intensity measurements representing TBX2/3 protein levels in defined areas of the cell were used for analyses to identify 'hit' compounds. Mean nuclear FITC fluorescence was used as the end-point parameter for total protein levels as TBX2/3 localise to the nucleus and the end-point parameter used to indicate subcellular localisation was calculated as follows:

$$Nuclear/Cytoplasmic\ Ratio = \frac{Mean\ eroded\ nuclear\ FITC\ fluorescence}{Mean\ nuclear\ collar\ FITC\ fluorescence}$$

A mean nuclear/cytoplasmic ratio >1 indicates nuclear localisation and a ratio <1 indicates cytoplasmic localisation. The parameter for total protein levels and the parameter for subcellular localisation for each drug treated well where normalised to their respective

averaged vehicle control parameter. This was done on a plate-to-plate basis to account for plate-to-plate variation in assay performance. The normalised parameter measurements for the technical repeats were averaged as an R^2 correlation > 0.8 and a Pearson's correlation > 0.9 were calculated for each duplicate. To identify 'hit' compounds a z-score was calculated for each normalised parameter for each drug treatment. A z-score assumes that the data is normally distributed and is a measure of the number of standard deviations below or above the population mean that a data point is and was calculated as follows:

$$z\text{-}score_i = \frac{(S_i - mean(S_{plate}))}{Std(S_{plate})}$$

$z\text{-}score_i$ is the z-score determined for the i^{th} sample (S_i) by dividing the difference between S_i and the sample mean of the plate (S_{plate}) by the standard deviation of the plate. z-scores ≥ 2 or ≤ 2 (i.e. 2 standard deviations above or below the sample mean) are considered 'hits' that are worth taking forward for validation (Goktug, Chai, & Chen, 2013; Zhang, 2011). These 'hits' were filtered by a cell count threshold of at least 25 cells/FOV. Our study aimed to identify FDA-approved drugs that negatively regulate TBX2 and/or TBX3 (i.e. reduced nuclear fluorescence levels and nuclear/cytoplasmic ratios of <1) and thus we were interested in z-scores ≤ 2 (i.e. 2 standard deviations below the sample mean).

2.15.1.3 HC StratoMineR analyses

HC StratoMineR is a web-based tool for rapid analyses of high-content datasets (Omta et al., 2016). Using extracted and calculated parameters from our image analyses we used the decision supportive HC StratoMineR platform that guides users through a high-content data analysis workflow to mine our multiparametric screen data. The multiparametric data was analysed separately for each assay timepoint (4, 12 and 24h) and at each timepoint independent analyses were conducted for TBX2-FLAG and TBX3-FLAG cell populations. The analysis workflow was conducted on a plate and replicate level to account for variation in assay performance. Each parameter was normalised against the sample mean for that parameter and where there was significantly skewed distribution ($p<0.0001$) the parameter data was transformed to achieve a normal distribution. To prevent bias towards a parameter

that has a larger range, the data was scaled using the robust z-score method. Data reduction was then performed using the principal component analysis based on a correlation matrix. Parameters were reduced to factors and the number of factors included for further analyses were selected using the Elbow method (3 factors were suggested for all our analyses). The loadings of each parameter within a factor were used to calculate factor scores for every sample well and control well which were used to identify significant outlier samples ('hits') different from the vehicle control. The Manhattan distance of all the vectors to the vehicle control was calculated which reduced data for each well (drug treatment) to just one distance score which is the measure of the phenotypic effect of the drug on the cells in that well. The Manhattan distances are then transferred to p-values by using a Poisson probability distribution with the Lambda of the sample distribution. Statistically significant hits were then identified based on our p-value cut-off of $p<1x10^{4}$.

2.16 Statistical analyses

All data were obtained from at least three independent experiments (unless otherwise stated) with error bars representing standard error of the mean (SEM). Data were analysed using GraphPad Prism version 6.0 (GraphPad Software) and a parametric unpaired t-test was performed. Significance was accepted at *p<0.05, **p<0.01 and ***p<0.001.

CHAPTER 3

The anti-cancer activity of novel palladacycle complexes in rhabdomyosarcoma cells

3.1 Introduction

RMS is an aggressive sarcoma that largely affects children and adolescents. Since the 1970s, disease control for patients with localised or completely resected RMS has been achieved with combinational chemotherapy most commonly using the VAC regimen (Hosoi, 2016). However, this treatment regimen has had limited success for patients with regional spreading, incomplete resection or metastasis and these drugs are associated with debilitating side effects (Pappo et al. 1995). Therefore, there is a need for continued collaborative efforts to find more effective treatments with fewer side effects. As described in the literature review, palladium-based complexes may prove to be less toxic and more effective for the treatment of aggressive cancers. Recently, AJ-5, a novel binuclear palladacycle complex with 1,2-bis(diphenylphosphino)ethane as co-ligand was shown to exert potent anti-tumour activity in advanced melanoma and breast cancer cells with very promising in vivo clearance of advanced melanoma (Aliwaini et al. 2013, 2015). In the present study we therefore explored the anti-cancer activity of AJ-5 in RMS and other sarcoma subtypes. We show here for the first time that AJ-5 displays potent and selective cytotoxicity at sub-micromolar concentrations (≤ 0.2μM) against ARMS and ERMS cells and inhibits their ability to survive, proliferate and migrate. We show that AJ-5 induces DSBs which triggers the canonical DSBs ATM/Chk2 pathway as well as the p38/MAPK stress signalling pathway leading to a G_1 cell cycle arrest, reduction in autophagic flux, induction of apoptosis as well as an increase in necroptotic cell death markers. AJ-5 also shows efficacy in a range of sarcoma subtypes and displays a promising pharmacokinetic profile in healthy mice. Furthermore, the more water-soluble derivative of AJ-5, BTC2 was shown to display comparable anti-cancer activity in RMS. This study therefore provides evidence that AJ-5 and BTC2 have promising therapeutic potential for the treatment of RMS and a range of other sarcoma subtypes.

3.2 AJ-5 shows potent and selective cytotoxicity against RMS cells

Here we investigated the anti-tumour effects of the binuclear palladacycle complex, AJ-5 (Fig. 3.1A), in RMS cells. To this end, MTT assays were performed on ARMS (RH30 and AX-OH-1 cell lines) and ERMS (RD and FL-OH-1 cell lines) cells treated with a range of AJ-5 concentrations (0.1-1.0μM) for 48h. IC_{50} concentrations of ≤ 0.2μM were obtained for all cell lines (Fig. 3.1B). Light microscopy images of RMS cells treated for 24h and 48h with their respective IC_{50} concentrations show the impact of AJ-5 on cell viability and morphology (Fig. 3.1B). To determine the selectivity of AJ-5 for RMS cells, IC_{50} values were determined in non-malignant fibroblasts (FG0 and DMB) and mouse myoblasts (C2C12). Results show that AJ-5 is less cytotoxic in the non-malignant cells with a selectivity index (SI) of > 2 in all cases (Fig. 3.1C and D). Interestingly, there is growing evidence that mesenchymal stem cells are the cell of origin for specific sarcoma types including RMS (Hettmer & Wagers, 2010; Rodriguez, Rubio, & Menendez, 2012), and compared to the other non-malignant cells tested, the mesenchymal stem cells (A100021501) were the most sensitive to AJ-5 (Fig. 3.1C and D).

3.3 AJ-5 inhibits the ability of RMS cells to survive, proliferate and migrate.

To explore the potential impact of AJ-5 on the long-term fate of RMS cells, clonogenic assays were performed (Galluzzi et al., 2009). Fig. 3.2A shows representative images and quantification of colonies formed over 7-21 days after 24h of AJ-5 treatment. It is evident that AJ-5 significantly inhibits the ability of RMS cells to survive and proliferate. Indeed, for all except one RMS cell line tested, there was a significant decrease in colony area at ¼ IC_{50} treatment and only a few or no RMS cell colonies formed at IC_{50} concentrations. Importantly, the ability of the non-malignant C2C12 myoblasts to survive and proliferate was not significantly hindered after 24h of 0.3μM AJ-5 (Fig. 3.2B). This is at least 1.5 times higher than the IC_{50} values obtained for the RMS cells. To further explore the anti-cancer activity of AJ-5, RMS cells were exposed for 24h to IC_{50} concentrations of the drug and scratch motility assays were performed. Fig. 3.2C shows that AJ-5 reduced the migratory ability of all RMS cells tested. Taken together, this data suggests that AJ-5 inhibits the ability of RMS cells to survive, proliferate and migrate.

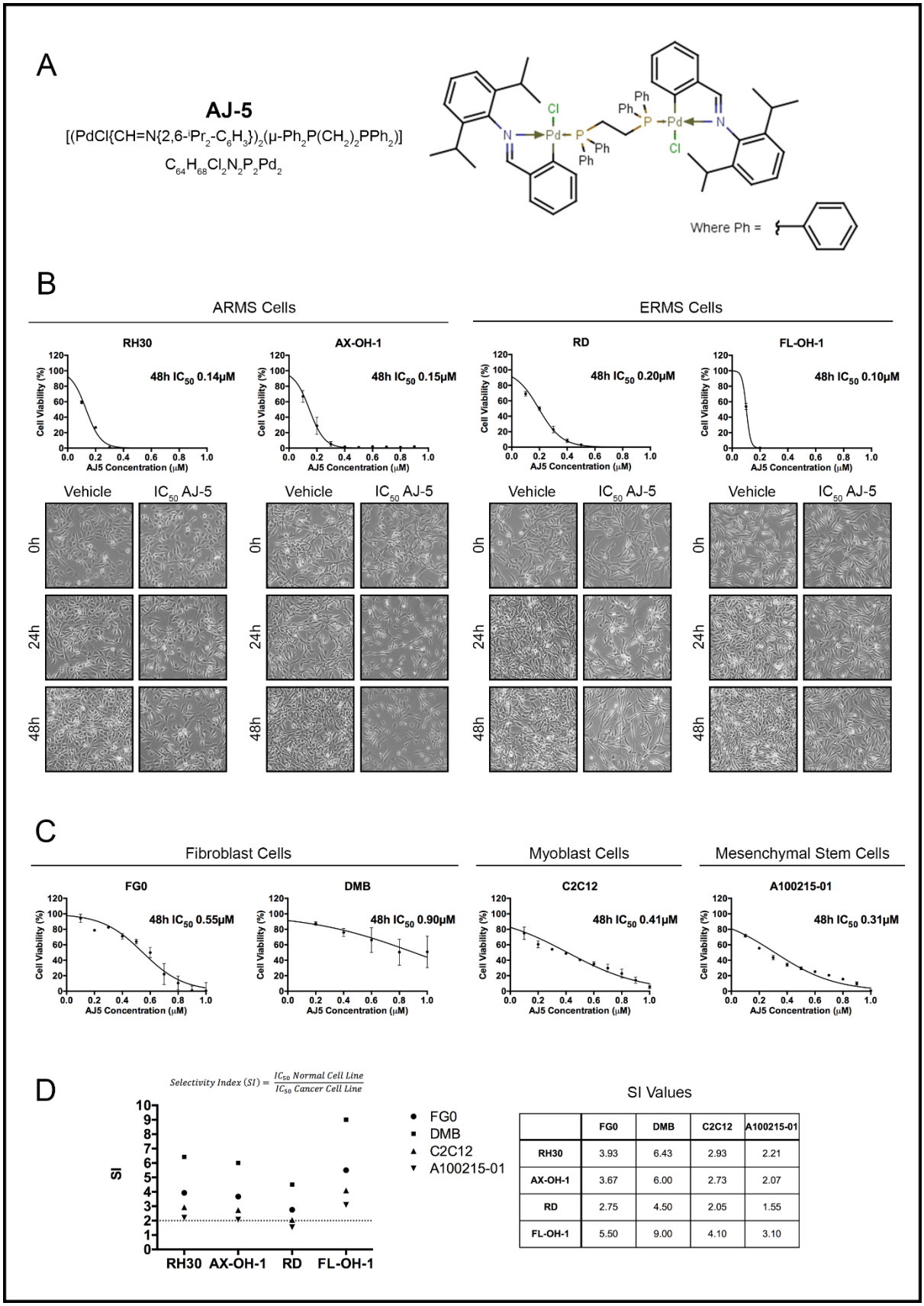

	FG0	DMB	C2C12	A100215-01
RH30	3.93	6.43	2.93	2.21
AX-OH-1	3.67	6.00	2.73	2.07
RD	2.75	4.50	2.05	1.55
FL-OH-1	5.50	9.00	4.10	3.10

Fig. 3.1 AJ-5 shows potent and selective cytotoxicity against ARMS and ERMS cells. *(A) Structure and molecular formula of AJ-5 (B) MTT cell viability assays of ARMS cell lines, RH30 and AX-OH-1, and ERMS cell lines, RD and FL-OH-1, treated with a range of AJ-5 concentrations (0.1μM – 1.0μM) or vehicle for*

48h. Graphs show mean cell viability as a percentage of vehicle control ± SEM for each concentration of AJ-5 determined from three independent experiments performed in quadruplicate. A curve was fitted to determine the IC_{50} concentration of AJ-5 for each cell line. Below are representative light microscopy images (200X; EVOS XL AMEX1000 Core Imaging System) of ARMS and ERMS cell lines treated with their respective IC_{50} concentrations of AJ-5 or vehicle for 24 and 48h. (C) MTT cell viability assays of non-malignant human fibroblast cell lines, FG0 and DMB, mouse myoblast cell line, C2C12, and mesenchymal stem cell line, A10021501, treated with AJ-5 and IC_{50} concentrations determined as described in (B) above. (C) Selectivity indices (SIs) were determined for each RMS cell line by dividing the IC_{50} of each non-malignant cell line by the IC_{50} of each RMS cell line.

To further explore the mechanisms by which AJ-5 exerts its cytotoxicity the ARMS cell line RH30 and the ERMS cell line RD were used for further characterisation.

3.4 AJ-5 activates the DNA damage and p38/MAPK pathways in RMS cells.

γH2AX is a robust marker of DSBs (Valdiglesias et al., 2013) and western blotting and immunocytochemistry revealed a dose dependent increase in levels of γH2AX (Fig. 3.3A) and an accumulation of distinct γH2AX foci in the nuclei of AJ-5 treated cells (Fig. 3.3B) respectively. Furthermore, AJ-5 treatment led to increased levels of phosphorylated ATM and its downstream target Chk2 as well as phosphorylated p38 (Fig. 3.3C). AJ-5 thus activated the canonical DSB and p38/MAPK stress signalling pathways. Both of these pathways converge on p53 which ordinarily plays an important role in transcriptionally activating the cyclin dependant kinase p21 (Sionov & Haupt, 1999). However, both the RMS cell lines used in this study harbour p53 mutations that result in high levels of inactive p53 (Felix et al., 1992). Importantly, p21 levels increased at the IC_{50} concentrations of AJ-5 and this response was particularly pronounced after 24h of treatment (Fig. 3.3C). These results suggest that p21 levels increase in a p53-independent manner.

3.5 AJ-5 triggers a G_1 cell cycle arrest and induces apoptosis and necrosis

To investigate the effect of AJ-5 on cell cycle progression, FACS analyses were performed on RMS cells treated with drug for 24h and 48h. Results show that AJ-5 induces a G_1 cell cycle arrest in both cell lines at the expense of the S phase (Fig. 3.4A). This correlated with a decrease in levels of cyclin A and cyclin B which are required for progression through the S and G_2/M phases respectively (Karimian, Ahmadi, & Yousefi, 2016) (Fig. 3.4B). The sub-G_1

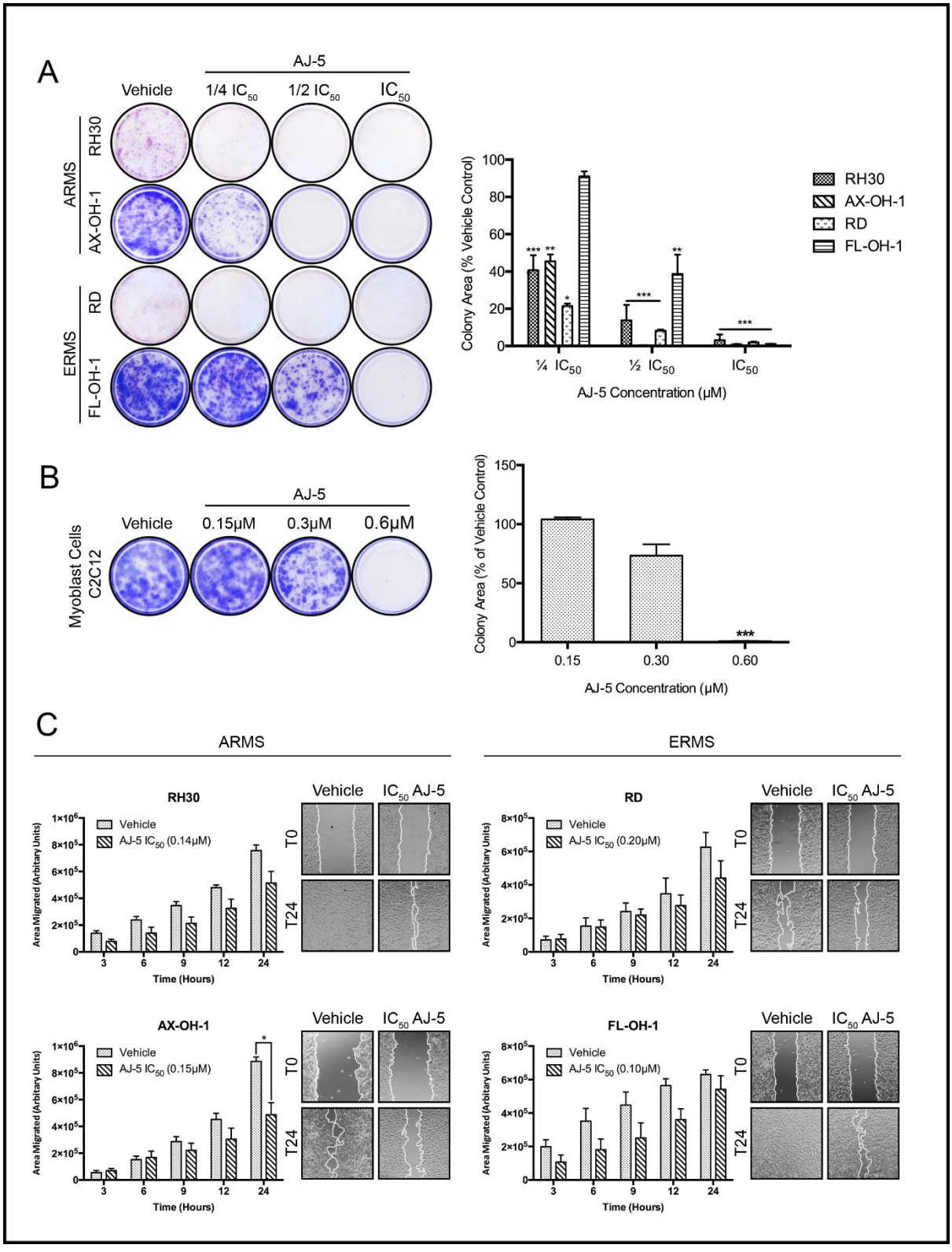

Fig. 3.2 AJ-5 inhibits the ability of RMS cells to survive, proliferate and migrate. *Representative images and quantification of clonogenic assays of ERMS and ARMS cells treated with vehicle, ¼ IC_{50}, ½ IC_{50} or IC_{50} concentrations of AJ-5 for 24h and then replated at low densities in drug-free medium and left for 7-21 days for colonies to form. Colonies were stained with crystal violet and images from three independent repeats were quantified using the ImageJ plugin ColonyArea. The graph represents the mean colony area ± SEM of each treatment condition as a percentage of the vehicle control. (B) The same as (A) above for the non-malignant mouse myoblast cell line C2C12, but treated with vehicle,*

*0.15µM, 0.3µM or 0.6µM AJ-5. (C) Representative images (200X; EVOS XL AMEX1000 Core Imaging System) and quantification of scratch motility assays of ERMS and ARMS cells pre-treated with IC_{50} concentrations of AJ-5 or vehicle for 24h and then replated at 100% confluency in drug-free medium. After cell adherence, a sterile 2µL pipette tip was used to make a linear wound in the cell monolayer and cells were treated with 10µg/mL mitomycin C to inhibit proliferation. Cells were imaged at 0, 3, 6, 9, 12 and 24h post wound formation. Total area migrated was calculated by subtracting the wound area at each timepoint from the wound area at time 0h which is represented in the graphs as mean area migrated ± SEM pooled from three independent repeats. Data was analysed using GraphPad Prism 6.0 and a parametric unpaired t-test was performed, where *p<0.05, **p<0.01, ***p<0.001.*

peaks seen in Fig. 3.4A suggested that AJ-5 treatment leads to cell death. Indeed, Annexin V-FITC assays confirm that AJ-5 induces apoptotic and necrotic cell death (Fig. 3.4C).

3.6 AJ-5 triggers the intrinsic and extrinsic apoptosis pathways in RMS cells.

To confirm that AJ-5-induces apoptosis, RD and RH30 cells were treated with AJ-5 and biological, molecular and biochemical markers of apoptosis were investigated by light microscopy, western blotting and enzymatic Caspase-Glo assays respectively. The results show that AJ-5 induced characteristic features of apoptosis including membrane blebbing and cell shrinkage (Fig. 3.5A). In addition, AJ-5 treatment led to increased levels and activity of cleaved caspase-8 and caspase-9, the effectors of the extrinsic and intrinsic pathways respectively (Fig. 3.5B and C). This correlated with increased levels of the active (cleaved) forms of the executioner caspases-3/7 and their substrate PARP (Fig. 3.5B and C) (Oliver, 1998; Soldani & Scovassi, 2002). Interestingly, we observed an ~20kDa band above the 18kDa active cleaved caspase-8 fragment. A similar band has also been reported by other researchers and it has been suggested that it represents an intermediate product of procaspase-8 processing (Hoffmann et al., 2009; Wang et al., 2012). Importantly, caspases-8 and -9 were more robustly activated in RD cells treated with AJ-5 than those treated with IC_{50} doxorubicin, a drug commonly used in the treatment of RMS and used as a positive control in apoptosis assays (Fig. 3.5C). Together these results show that AJ-5 induces cell death in RMS cells, in part, through the extrinsic and intrinsic apoptotic pathways.

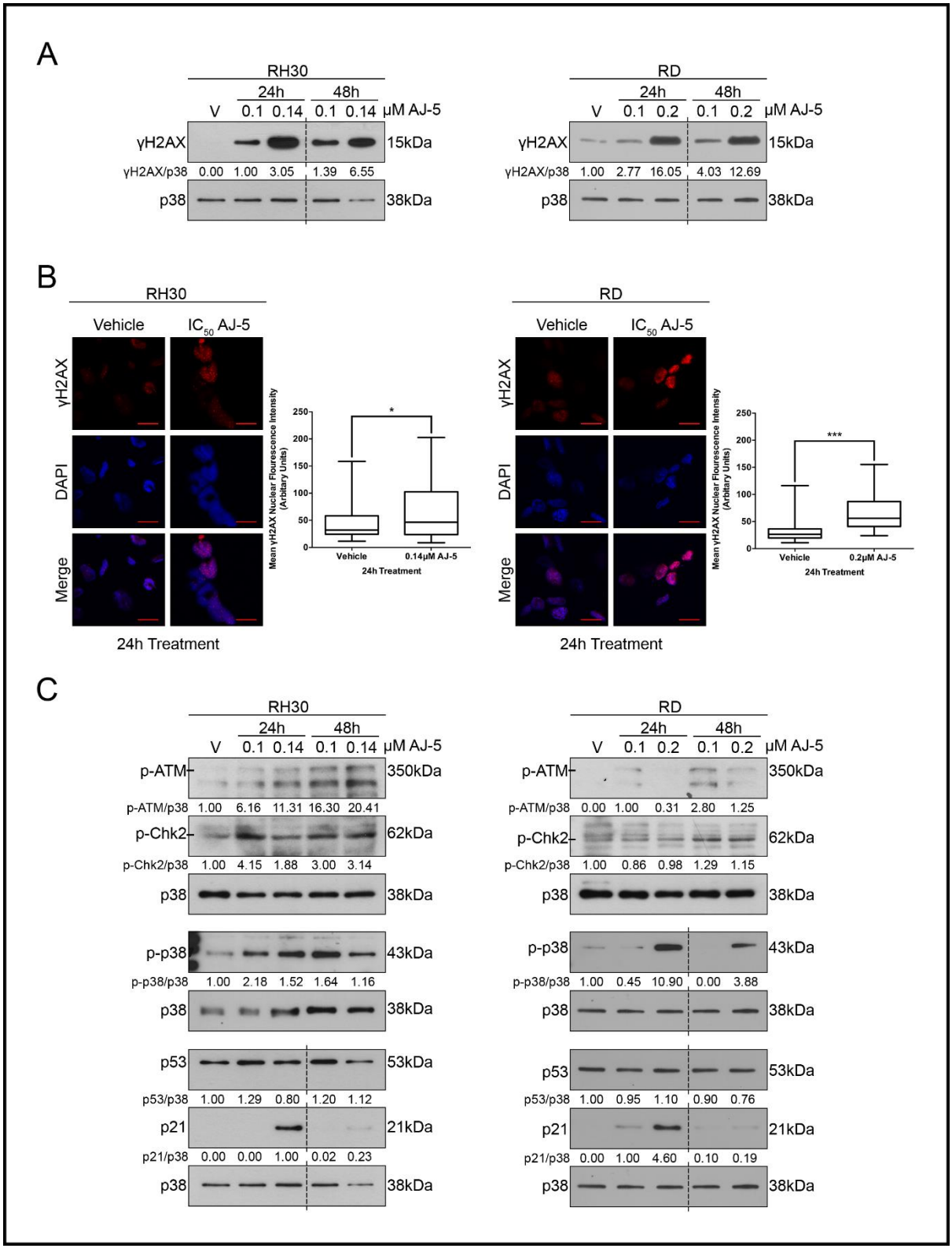

Fig. 3.3 AJ-5 activates the DNA damage and the p38/MAPK pathways. *γH2AX protein levels detected by western blotting in RH30 (ARMS) and RD (ERMS) cells treated with vehicle (V), 0.1μM or IC_{50} AJ-5 for 24 and 48h. p38 was used as a loading control. Densitometry readings were obtained using ImageJ and protein expression levels are represented as a ratio of protein of interest/p38 normalised to the vehicle control sample (where possible). Blots are representative of at least two independent repeats (B) Representative confocal immunofluorescence maximum intensity projection images (630X; Carl Zeiss LSM 510) of RH30 and RD cells treated with IC_{50} AJ-5 or vehicle for 24h and γH2AX detected with*

*a fluorophore conjugated Cy3 secondary antibody. Nuclei of cells were stained with DAPI. Scale bar is 20µm. Box plots represent quantification of γH2AX levels per treatment condition as mean nuclear Cy3 fluorescence from 20 fields of view from three independent repeats. Data was analysed using GraphPad Prism 6.0 and a parametric unpaired t-test was performed, where *p<0.05, **p<0.01, ***p<0.001. (C) Western blot analyses with antibodies to key DNA damage and stress signalling pathway proteins: p-ATM, p-Chk2, p-p38, p53 and p21. RH30 and RD cells were treated with AJ-5 and protein expression quantified as described above in (A). Broken lines in western blots shown in this figure indicate where lanes not relevant were removed.*

3.7 AJ-5 induces markers of necroptosis in RMS cells

Fig. 3.4C showed that AJ-5 triggers necrosis in RMS cells and therefore we explored the possibility that it may induce necroptosis, the regulated form of necrosis. Indeed, AJ-5 treatment of RD and RH30 cells led to increased levels of phosphorylated RIP3, a critical component of the necrosome, as well as increased levels of phosphorylated MLKL, a downstream target of the necrosome (Fig. 3.6A). Importantly, Fig. 3.6B shows that when RMS cells were treated with AJ-5 in the presence of necrostatin-1, an inhibitor of the necroptotic pathway, cell viability increased significantly. These results suggest that the cell death induced by AJ-5 possibly involves necroptosis. Consistent with this possibility, Annexin V-FITC assays (Fig. 3.6C) reveal that when cells were treated with AJ-5 in the presence of necrostatin-1 there was an almost complete shift of the necrotic cell population to viable cells with no change in the apoptotic population. These results imply that AJ-5 induced cell death in ERMS and ARMS cells not only involves apoptosis, but also possibly involves necroptosis.

3.8 AJ-5 induces several markers of autophagy in RMS cells

We next investigated whether AJ-5 induced autophagy because large vacuolar structures and acidic vesicles were observed in RMS cells treated with this drug (Fig. 3.7A). To this end, western blotting and immunocytochemistry were performed with an antibody to LC3. Fig. 3.7B shows that LC3II (the autophagosomal membrane bound form of LC3) was induced in both RMS cell lines in a time and dose dependant manner. Furthermore, Fig. 3.7C shows distinct puncta, presumed to represent LC3II aggregates conjugated to autophagosomal membranes, in RD and RH30 cells from as early as 6h after AJ-5 treatment.

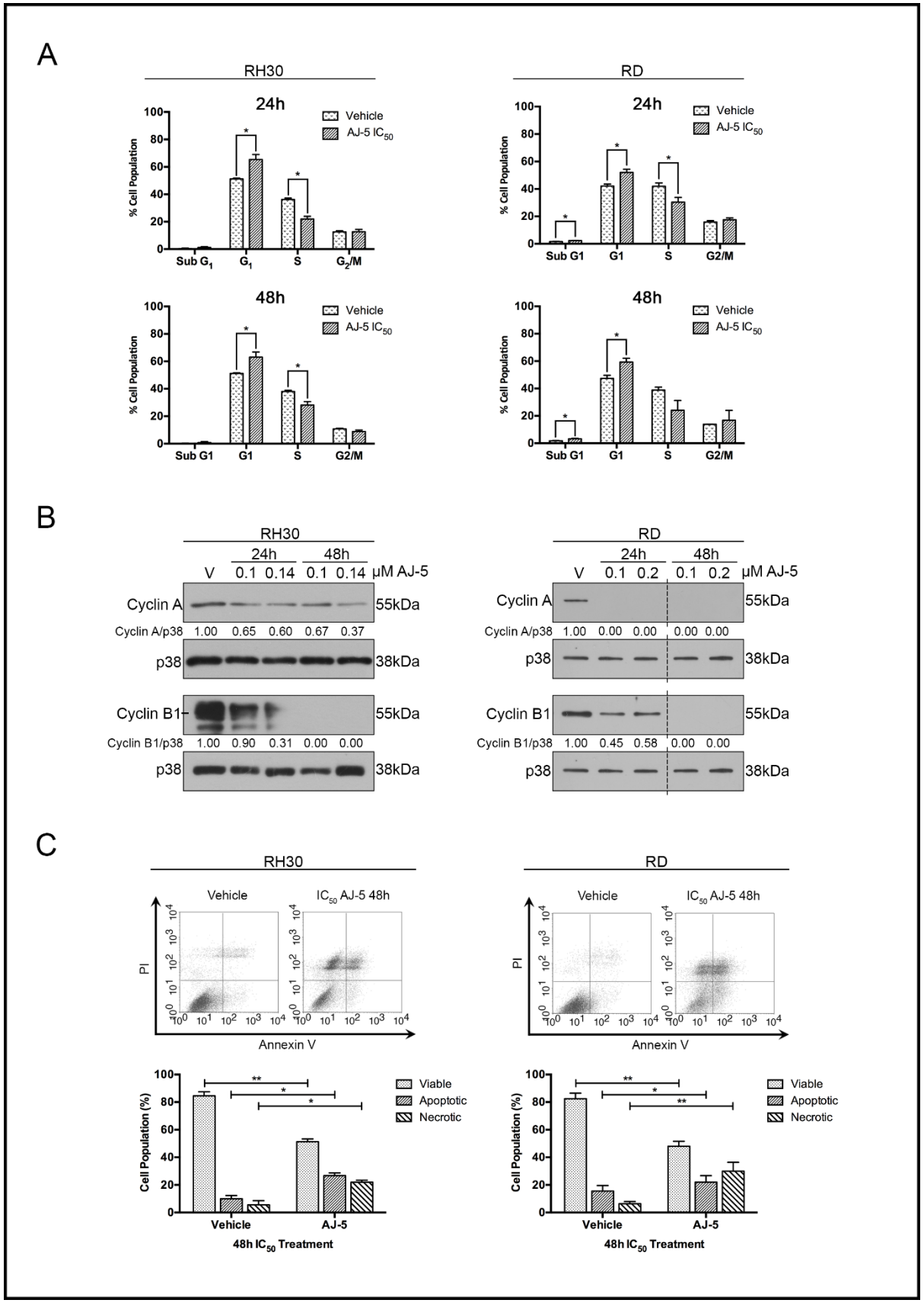

Fig. 3.4 AJ-5 triggers a G1 cell cycle arrest and induces apoptotic and necrotic cell death in RH30 and RD cells. *Flow cytometry analyses of cells treated with vehicle or IC_{50} AJ-5 for 24 and 48h. Graphs represent the mean proportion of cells ± SEM at each phase of the cell cycle pooled from three*

*independent repeats. (B) Western blot analyses of protein harvested from cells treated as indicated and incubated with antibodies against cell cycle markers cyclin A and cyclin B1. p38 was used as a loading control. Densitometry readings were obtained using ImageJ and protein expression levels are represented as a ratio of protein of interest/p38 normalised to the vehicle control sample. Blots are representative of at least two independent repeats. Broken lines indicate where lanes not relevant were removed. (C) Flow cytometric analyses of cells treated with vehicle or IC_{50} AJ-5 and stained with Annexin V-FITC and PI. Graphs represent the mean ± SEM percentage of viable (lower left hand quadrant), apoptotic (lower right hand quadrant + upper right hand quadrant) and necrotic (upper left hand quadrant) cells from three independent experiments. For (A) and (C) data were analysed using GraphPad Prism 6.0 and a parametric unpaired t-test was performed, where *p<0.05, **p<0.01, ***p<0.001.*

3.9 AJ-5 reduces autophagic flux in RD and RH30 cells

The detection of LC3II alone does not distinguish between autophagy induction and cessation in the downstream steps of autophagy. We therefore next determined the impact of AJ-5 treatment on autophagic flux by measuring the levels of p62, a receptor of polyubiquitinated proteins. The rationale for this is based on observations that upon autophagy induction, p62 is incorporated within an autophagosome and degraded within an autolysosome (Pankiv et al., 2007). The turnover of p62 is therefore considered an indicator of autophagic flux. Interestingly, Fig. 3.8A shows that whereas AJ-5 appears to reduce autophagic flux in RH30 cells, it increases autophagic flux in RD cells. To confirm the above data, levels of LC3II were determined by western blotting in the presence and absence of bafilomycin A1 which blocks the autophagy pathway by inhibiting fusion of autophagosomes with lysosomes (Mauvezin & Neufeld, 2015). An accumulation of LC3II in the presence of this inhibitor is therefore considered evidence of autophagic flux. Consistent with our p62 data in RH30 cells, AJ-5 treatment followed by bafilomycin A1 exposure led to decreased levels of LC3II (Fig. 3.8B). Interestingly, contrary to our p62 data in RD cells, in the presence of bafilomycin A1, AJ-5 treatment led to a negligible change in LC3II compared with vehicle treated cells (Fig. 3.8B). We therefore further investigated the impact of AJ-5 on autophagic flux in the RD cell line by performing single cell autophagosome flux analyses. Our results reveal that RD cells are characterised by a predominant autolysosomal pool (*nA*=83 autolysosomes/cell), with only a very minor pool of autophagosomes and lysosomes per cell (Fig. 3.8C). Moreover, the cells are characterised by a basal autophagosome flux *J* of 6.3 autophagosomes/hour/cell. Upon AJ-5 treatment, however, both autolysosome pool size as well as autophagosome flux significantly decreased. This suggests that AJ-5 negatively impacts the rate of autophagosome

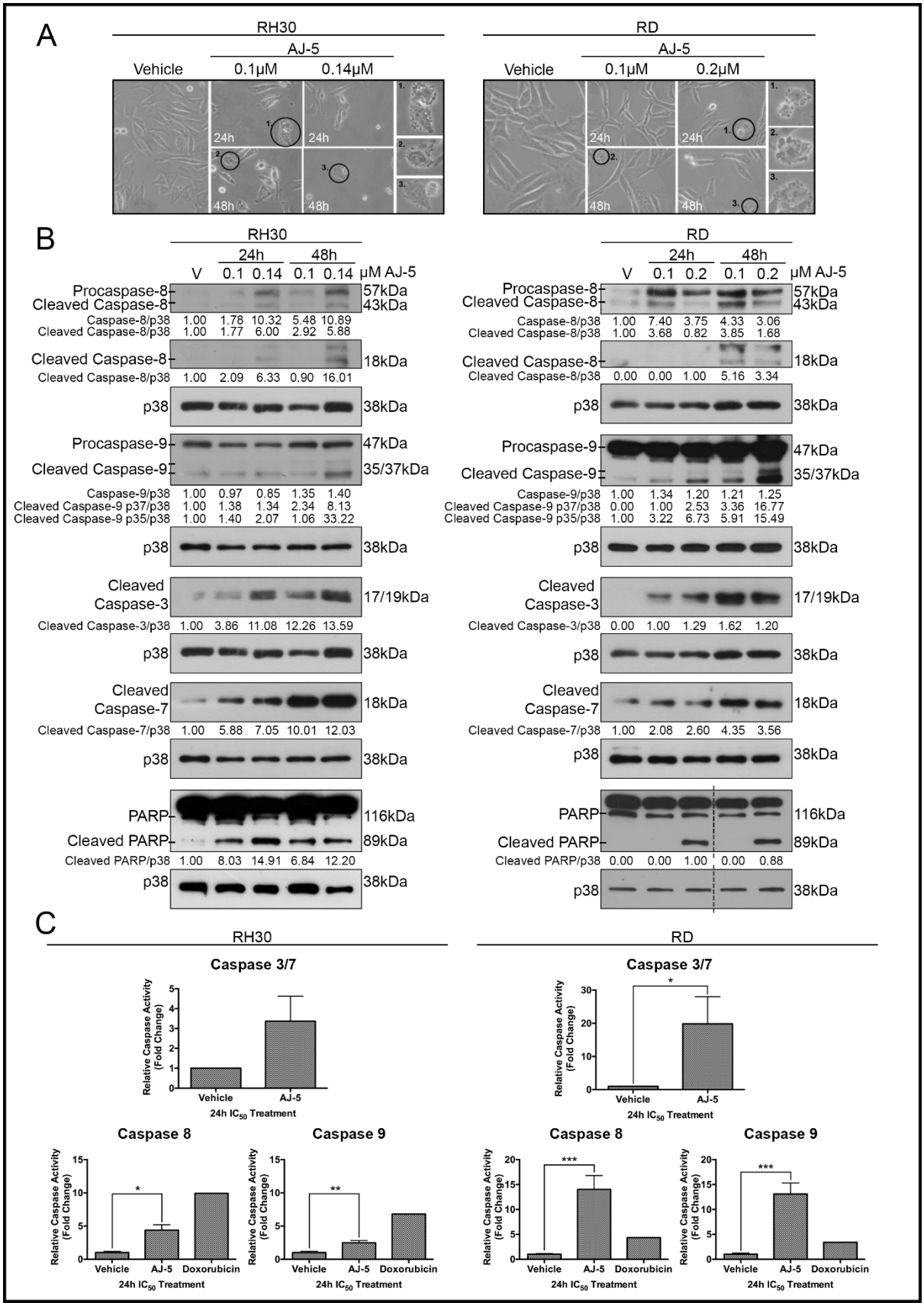

Fig. 3.5 AJ-5 triggers the intrinsic and extrinsic apoptosis pathways in RMS cells. *Representative light microscopy images (200X; EVOS XL AMEX1000 Core Imaging System) showing the morphology of RH30 and RD cells treated with vehicle, 0.1μM or IC_{50} AJ-5 for 24 and 48h. Numbered circles correspond to*

*magnified images on the right which highlight characteristic apoptotic morphology including membrane blebbing and cell shrinkage. (B) Western blot analyses of protein harvested from cells treated as in (A) and incubated with antibodies as indicated. p38 was used as a loading control and densitometry readings were obtained using ImageJ. Protein expression levels are represented as a ratio of protein of interest/p38 normalised to vehicle control samples (where possible). Blots are representative of at least two independent repeats. Broken lines indicate where lanes not relevant were removed. (C) Caspase-Glo assays showing the enzymatic activity of caspase-3/7, caspase-8 and caspase-9 for cells treated with vehicle or IC_{50} AJ-5. Doxorubicin was included as a positive control for caspase-8 and -9 assays at the IC_{50} concentration (0.5μM) established in the cell lines tested. Graphs represent the mean fold change of caspase activity ± SEM pooled from three independent repeats. Data was analysed using GraphPad Prism 6.0 and a parametric unpaired t-test was performed, where *p<0.05, **p<0.01, ***p<0.001.*

synthesis which supports the data showing that in the presence of bafilomycin A1, AJ-5 treatment does not lead to LC3II accumulation (Fig. 3.8B). Together these data suggest that AJ-5 reduces autophagic flux in RH30 and RD cells.

3.10 AJ-5 can regulate TBX2 and TBX3 in RMS cells.

The T-box transcription factors TBX2 and TBX3 have been implicated in rhabdomyosarcomagenesis (Sims, 2016; Willmer et al., 2016; Zhu et al., 2014) and due to their relevance in this thesis, the ability of AJ-5 to regulate these oncogenic proteins was of interest. Therefore, levels of TBX2 and TBX3 were detected in RD and RH30 cells after AJ-5 treatment (Fig. 3.9A). In the RH30 cell line TBX2 and TBX3 levels were convincingly reduced at all concentrations and timepoints tested. However, the same trend was not observed in the RD cell line where TBX2 levels increased after AJ-5 treatment and TBX3 levels initially increased after 24h and then drastically decreased after 48h of treatment. The increase in TBX2 levels can possibly be explained by the fact that TBX2 has been shown to be upregulated in response to the DNA damaging agent cisplatin and contributes to DNA repair and subsequent cisplatin-resistance (Wansleben et al., 2013). This response could be cell-type specific and thus it was not observed in the RH30 cell line. The initial increase in TBX3 levels in the RD cell line could be associated with an initial drug resistance response which is then overridden by longer exposure to AJ-5. Another explanation for the drop in TBX3 levels at the 48h timepoint, when TBX2 levels have increased significantly, is the ability of TBX2 to suppress its homologue TBX3 which has been previously shown in the Prince laboratory (unpublished).

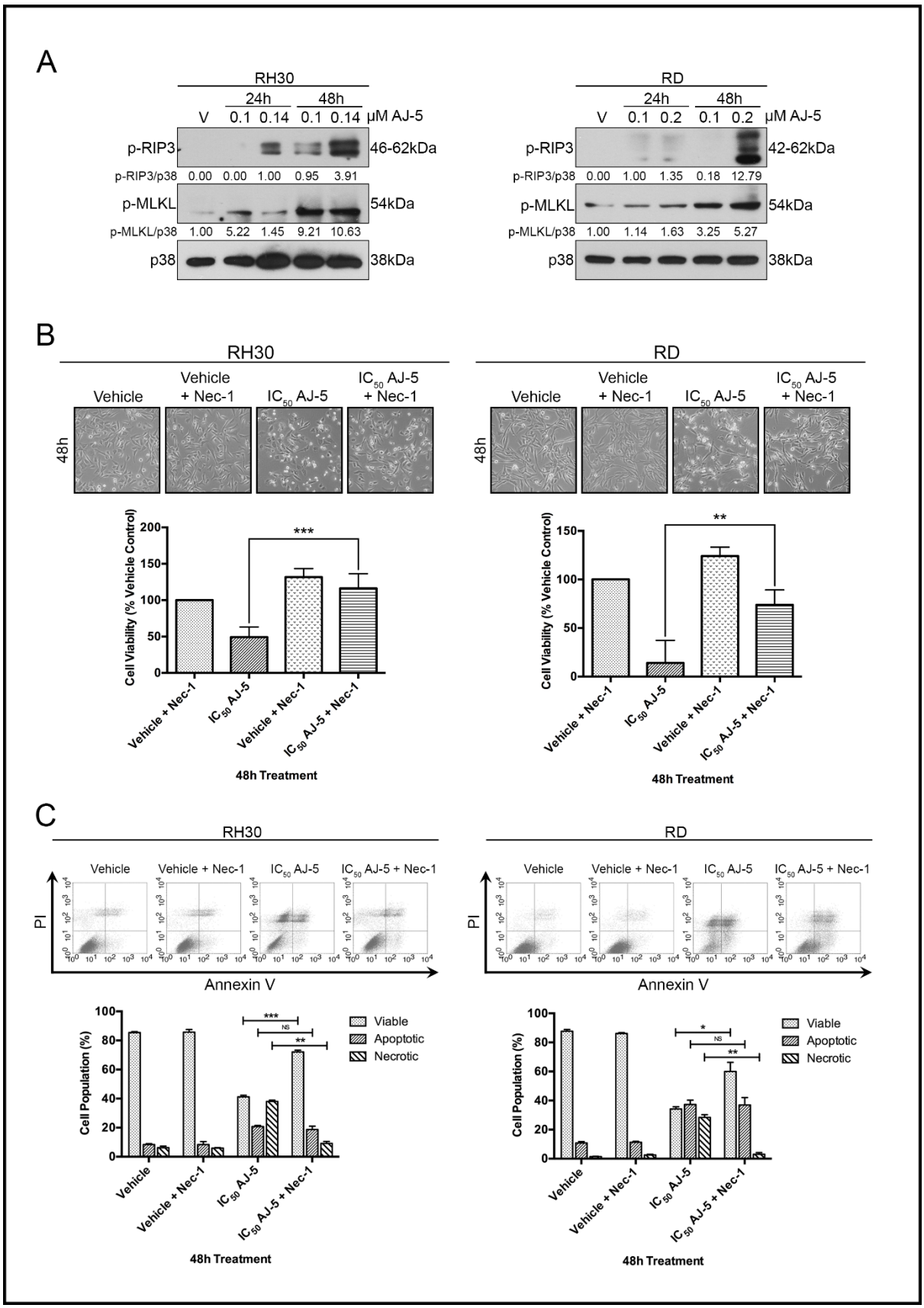

Fig. 3.6 Cell death induced by AJ-5 in RMS cells involves necroptosis. *Western blot analyses showing levels of p-RIP3 and p-MLKL and the loading control, p38, in RH30 and RD cells treated with vehicle (V), 0.1μM or IC_{50} AJ-5 for 24 and 48h. Densitometry readings were obtained using ImageJ and protein*

*expression levels are represented as a ratio of protein of interest/loading control normalised to a control sample. Blots are representative of at least two independent repeats. (B) Representative light microscopy images (200X; EVOS XL AMEX1000 Core Imaging System) and MTT assays showing cell viability of RH30 and RD cells pre-treated with 50µM necrostatin-1 for 2 hours followed by the addition of IC_{50} AJ-5 for 48h. Graphs show mean cell viability as a percentage of vehicle control ± SEM determined from three independent experiments performed in quadruplicate. (C) Flow cytometric analyses of cells treated with vehicle or IC_{50} AJ-5 in the presence of absence of necrostation-1 as described in (A) above and stained with Annexin V-FITC and PI. Graphs represent the mean ± SEM percentage of viable (lower left hand quadrant), apoptotic (lower right hand quadrant + upper right hand quadrant) and necrotic (upper left hand quadrant) cells from three independent experiments. For (B) and (C) data were analysed using GraphPad Prism 6.0 and a parametric unpaired t-test was performed, where *p<0.05, **p<0.01, ***p<0.001.*

Given that AJ-5 was so effective at downregulating TBX2 and TBX3 in the ARMS RH30 cell line, this cell line was used to investigate the possible mechanism(s) by which AJ-5 negatively regulates TBX2/3. It was hypothesised that AJ-5 may be targeting TBX2/3 proteins for degradation though the proteasome. Therefore, RH30 cells were pre-treated with the 26S proteasome inhibitor MG-132 prior to drug treatment followed by western blotting (Fig. 3.9B). Consistent with previous results (Fig. 3.9A), in the absence of MG-132, AJ-5 was very effective at downregulating TBX2/3 levels. Importantly, this effect was rescued in the presence of MG-132. This suggests that AJ-5 is targeting TBX2 and TBX3 through ubiquitination for degradation through the 26S proteasome in RH30 cells.

The next set of experiments were performed to determine whether AJ-5 exhibits anti-cancer activity through negatively regulating TBX2/3 in RH30 cells. Briefly, RH30 cells were transfected with FLAG-mtbx2, FLAG-mtbx3 or FLAG-EMPTY vector DNA and then treated with AJ-5 for 24h after which MTT cell viability assays were performed. Western blots for RH30 cells shown in Fig. 3.9C confirm that AJ-5 downregulated TBX2/3 levels in the FLAG-EMPTY cells and that cells transfected with FLAG-mtbx2 and FLAG-mtbx3 showed overexpression of TBX2 and TBX3 respectively. The MTT assays (Fig. 3.9C) show that while AJ-5 significantly impacts cell viability in the FLAG-EMPTY RH30 cells, overexpression of TBX2 or TBX3 did not significantly rescue this effect. This suggests, that although AJ-5 is very effective at downregulating TBX2 and TBX3 in RH30 cells, this ability is not one of the main mechanisms by which AJ-5 mediates its anti-cancer activity.

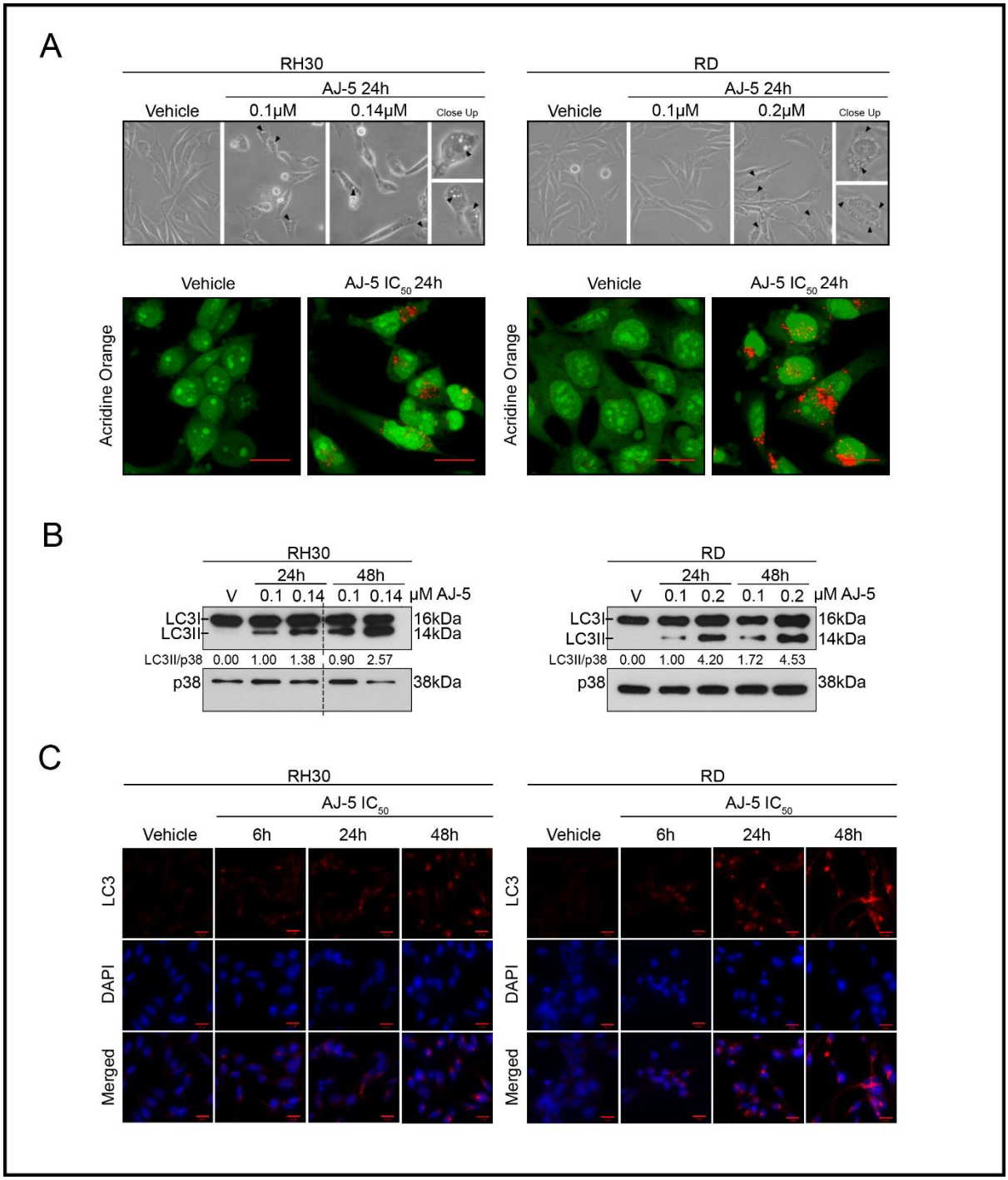

Fig. 3.7 AJ-5 induces several markers of autophagy in RMS cells. *(A) Representative light microscopy (200X; EVOS XL AMEX1000 Core Imaging System) and maximum intensity projection fluorescence images showing vacuolar structures and acidic vesicles respectively in RH30 and RD cells treated as indicated for 24h. Black arrow heads indicate vacuolar structures. Scale bar is 20μm. (B) Western blotting showing LC3I and LC3II protein levels in RH30 and RD cells treated with vehicle (V), 0.1μM or IC_{50} AJ-5 for 24 and 48h. p38 Was used as a loading control and densitometry readings were obtained using ImageJ. Protein expression levels are represented as a ratio of protein of interest/loading control normalised to a control sample. Blots are representative of at least two independent repeats. (C) Representative maximum intensity projection confocal immunofluorescence images (630X; Zeiss LSM 510; scale bar is 20μm) from three independent repeats of RH30 and RD cells treated with IC_{50} AJ-5 or vehicle for 6, 24 and 48h and incubated with LC3 primary antibody, fluorophore conjugated Cy3 secondary antibody and nuclei were stained with DAPI.*

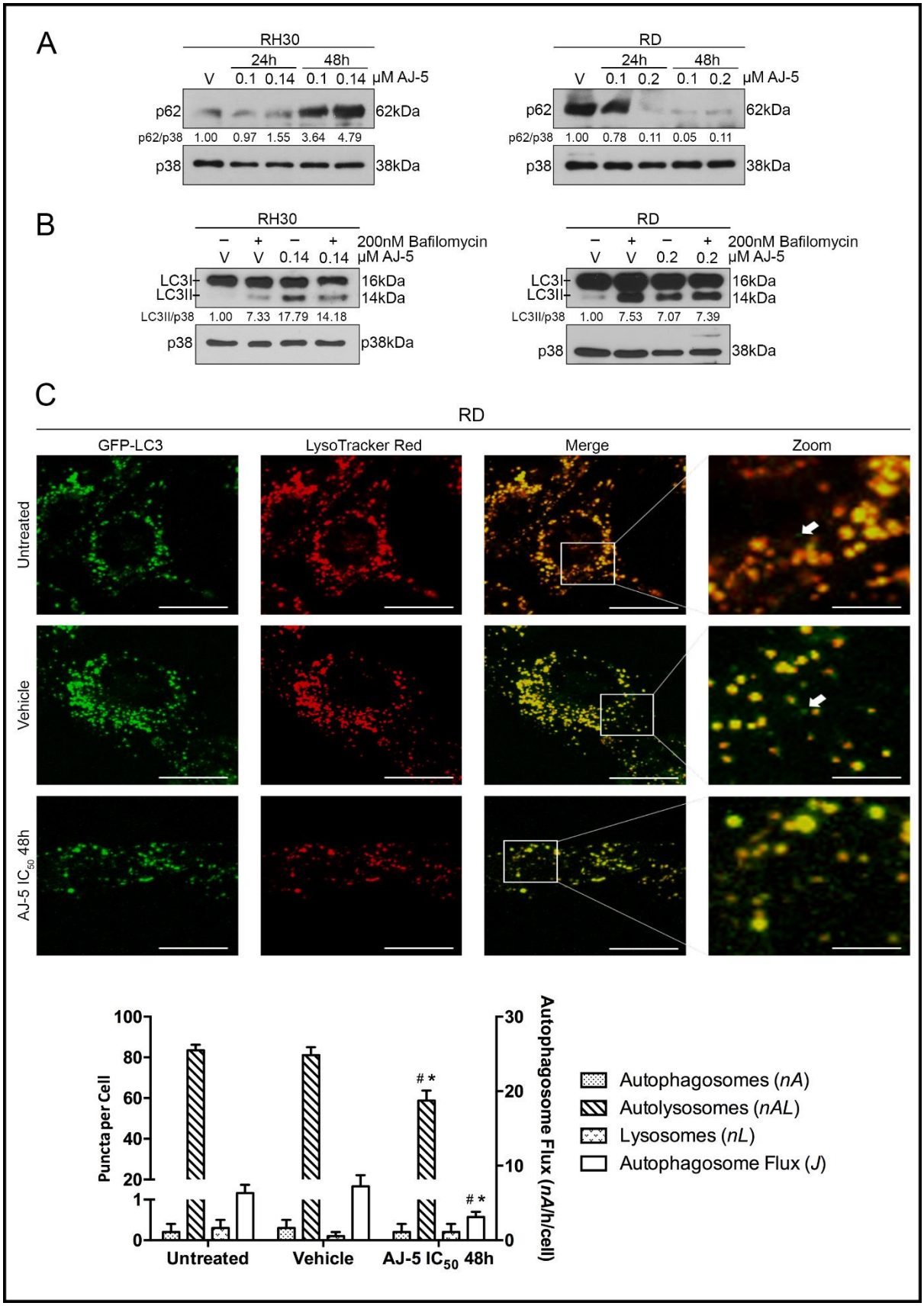

Fig. 3.8 AJ-5 reduces autophagic flux in RD and RH30 cells. *Western blotting of p62 protein levels in RH30 and RD cells treated with vehicle (V), 0.1μM or IC_{50} AJ-5 for 24 and 48h. (B) Western blotting showing LC3I and LC3II protein levels in RH30 and RD cells treated with vehicle (V) or IC_{50} AJ-5 for 24h*

*followed by 2 hours of treatment with 200nM bafilomycin A1. For western blots, p38 was used as a loading control and densitometry readings were obtained using ImageJ. Protein expression levels are represented as a ratio of protein of interest/p38 normalised to vehicle control sample. Blots are representative of at least two independent repeats. (C) Representative single cell fluorescence maximum intensity projection micrographs (630X; Carl Zeiss LSM 780; scale bar is 20µm) and pool size quantification of autophagy pathway intermediates: autophagosomes (GFP-LC3, nA) (indicated with white arrows in the merged image), autolysosomes (LysoTracker Red, nAL) and lysosomes (merged, nL). Autophagosome flux J was calculated. Data were analysed using GraphPad Prism 6.0 and a parametric unpaired t-test was performed, where *p<0.05, **p<0.01, ***p<0.001, # compared to untreated control and * compared to vehicle control.*

3.11 AJ-5 is cytotoxic in a range of sarcoma subtypes

To investigate if the therapeutic potential of AJ-5 could be extended to other sarcoma subtypes, chondrosarcoma (SW1353), liposarcoma (SW872), synovial sarcoma (SW982), fibrosarcoma (HT1080) and osteosarcoma (MG-63) cells were treated with the drug as described earlier and MTT assays were performed. Our results show that an IC_{50} of < 0.3µM was obtained for all the sarcoma cell lines tested (Fig. 3.10A) and a favourable SI of > 2 was achieved when calculated relative to the combined IC_{50} values for the normal fibroblasts (FG0 and DMB) (Fig. 3.10B). However, a sub-optimal SI between 1 and 1.5 was obtained when the IC_{50} values for the sarcoma cells were expressed relative to the mesenchymal stem cells (A10021501). This raises the interesting possibility that AJ-5 may be effective against the cells of origin of these sarcoma subtypes which may be of therapeutic benefit. Furthermore, clonogenic assays reveal that as little as a ¼ IC_{50} concentration of AJ-5 significantly reduced the ability of cells of all sarcoma subtypes to survive and proliferate (Fig. 3.10C). AJ-5 therefore shows potent selective cytotoxicity against a number of diverse sarcoma subtypes and may therefore have broad therapeutic potential.

3.12 Pharmacokinetic (PK) profile of AJ-5 in healthy mice

Given its importance to the drug discovery process, we next tested the in vivo PK profile of AJ-5 in whole blood of MF1 mice following a single dose of 2mg/kg IV, 2mg/kg IP or 20mg/kg PO for a period of 24h. The blood concentration-time curve of AJ-5 over a 24h period and the calculated PK parameters are shown in Fig. 3.11 and Table 3.1. For IV administration, AJ-5 illustrated a long half-life (>10h), which is most likely due to the low clearance (9.2 mL/min/kg) and a high volume of distribution (8.8L/kg). The exposure of AJ-5 following the IP dose of

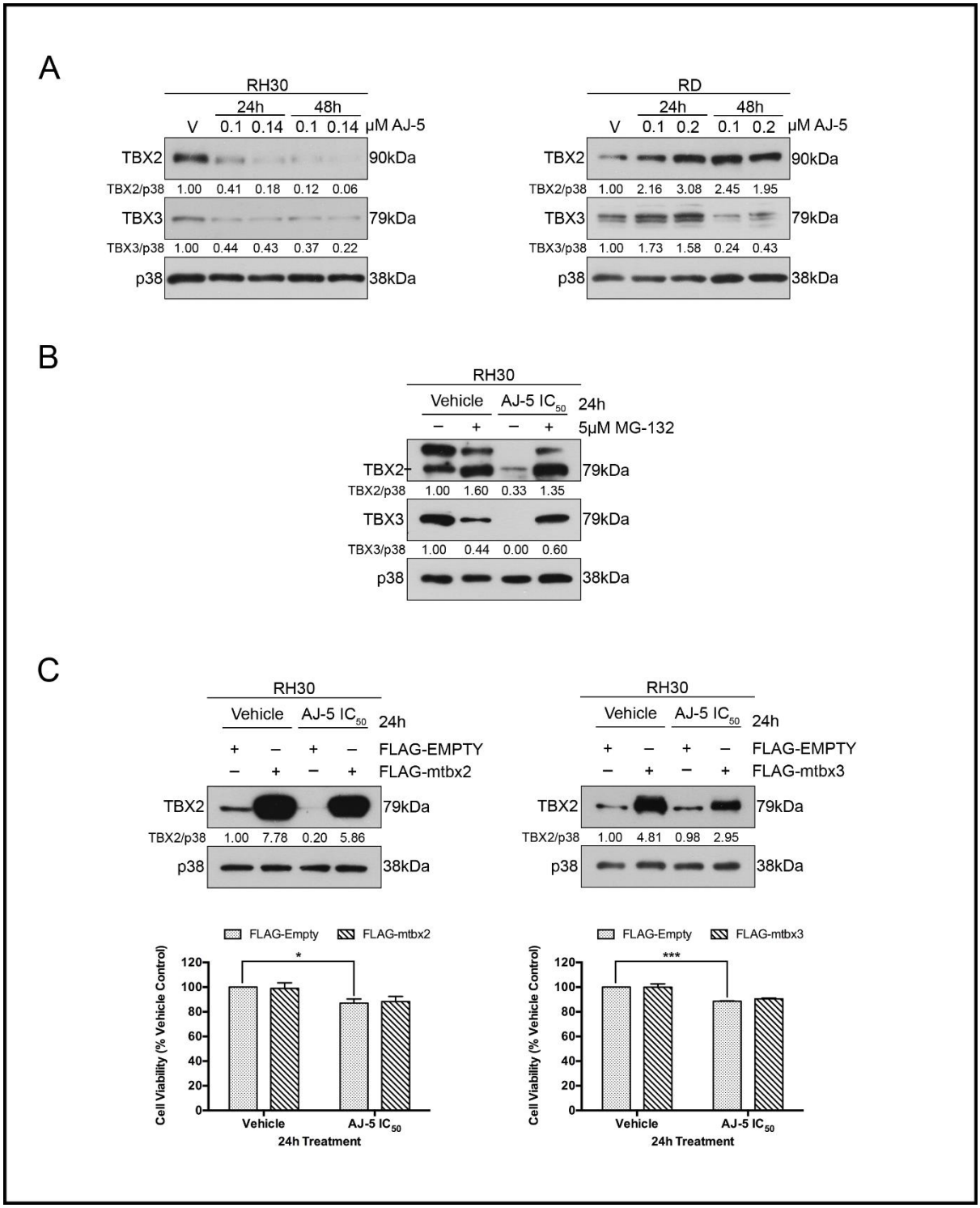

Fig. 3.9 AJ-5 can regulate TBX2 and TBX3 in RMS cells. *(A) Western blotting of TBX2 and TBX3 protein levels in RH30 and RD cells treated with vehicle (V), 0.1μM or IC_{50} AJ-5 for 24 and 48h. (B) TBX2 and TBX3 levels in RH30 cells pre-treated with 5μM MG-132 prior to the addition of IC_{50} AJ-5 or vehicle for 24h. (C) RH30 cells were fast forward transfected with 250ng FLAG-mtbx2, 500ng FLAG-mtbx3 or the equivalent amount of FLAG-EMPTY vector DNA and then treated the following day with IC_{50} AJ-5 or vehicle for 24h. TBX2 and TBX3 antibodies were used to detect protein levels by western blotting and cell viability was measured using MTT assays. For all western blots p38 was used as a loading control. Densitometry readings were obtained using ImageJ and protein expression levels are represented as a*

ratio of protein of interest/p38 normalised to the vehicle control sample (where possible). Blots are representative of at least two independent repeats.

2mg/kg was 8-fold higher compared to the PO dose of 20mg/kg with an area under the curve (AUC) of 88min.µM/L and 11min.µM/L respectively. The data obtained for the IP group in healthy mice correlated well with our previously observed in vivo efficacy of AJ-5 in advanced melanoma (Aliwaini et al., 2013).

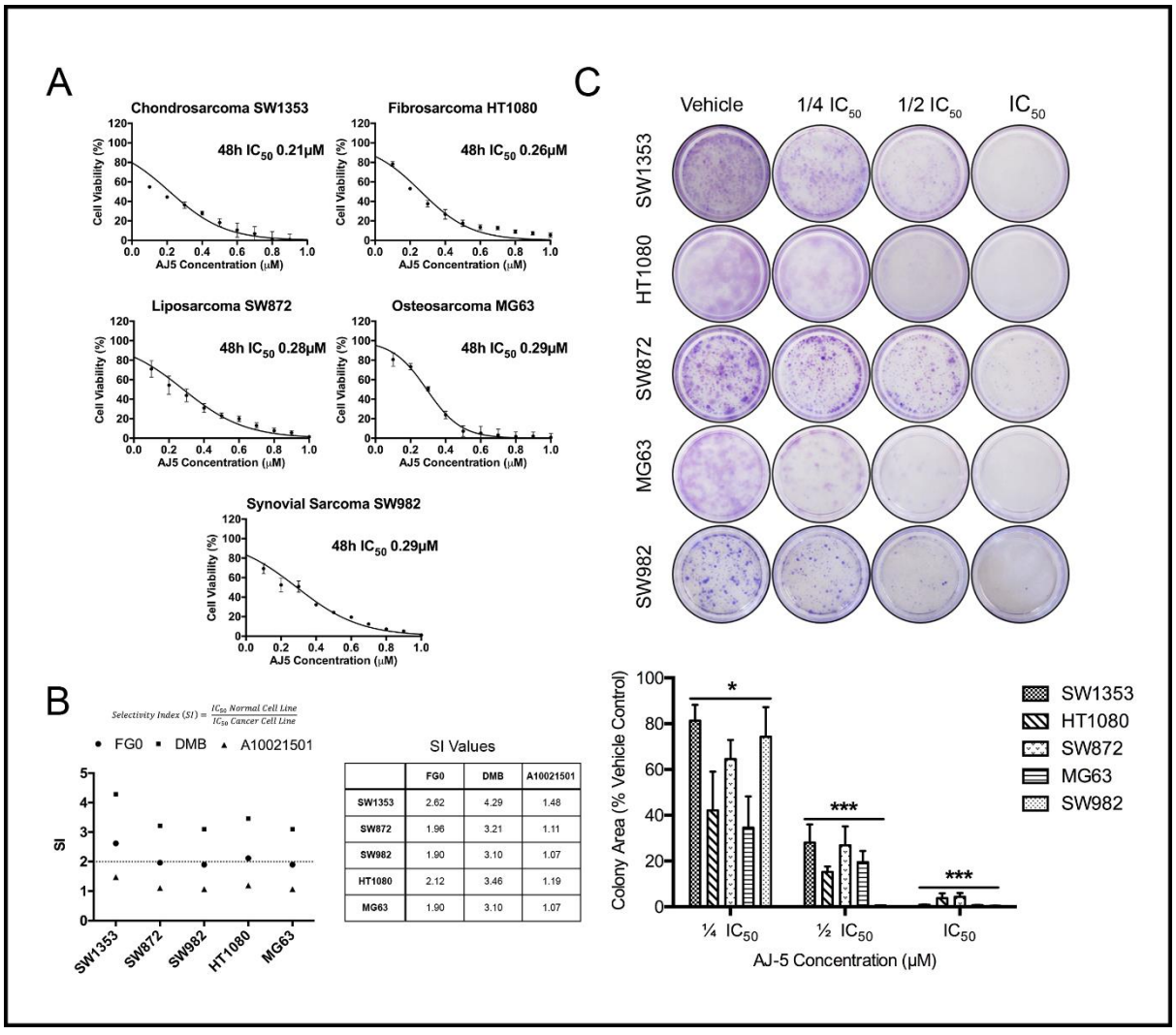

Fig. 3.10 AJ-5 is cytotoxic in a range of sarcoma subtypes. *MTT cell viability assays of chondrosarcoma (SW1353), fibrosarcoma (HT1080), liposarcoma (SW872), osteosarcoma (MG63) and synovial sarcoma (SW982) cells treated with a range of AJ-5 concentrations (0.1µM – 1.0µM) or vehicle for 48h. Graphs show mean cell viability as a percentage of vehicle control ± SEM for each concentration of AJ-5 determined from three independent experiments performed in quadruplicate. A curve was fitted to determine the IC50 concentration of AJ-5 for each cell line. (B) Selectivity indices (SIs) were determined for each cell line by dividing the IC50 of each non-malignant cell line (Figure 1C) including normal fibroblast cell lines (FG0 and DMB) and mesenchymal stem cell line (A10021501) by the IC50 of each sarcoma cell line. (C) Representative images (top panel) and quantification (lower panel) of clonogenic assays of sarcoma cell lines treated with vehicle, ¼ IC50, ½ IC50 or IC50 concentrations of AJ-5 for 24h*

*and then replated at low densities in drug-free medium and left for 7-21 days for colonies to form. Colonies were stained with crystal violet and images from three independent repeats were quantified using the ImageJ plugin ColonyArea. The graph represents the mean colony area ± SEM of each treatment condition as a percentage of the vehicle control. Data was analysed using GraphPad Prism 6.0 and a parametric unpaired t-test was performed, where *p<0.05, **p<0.01, ***p<0.001.*

3.13 Bridged Tethered Complex 2 (BTC2)

Although AJ-5 has displayed potent anti-cancer activity against advanced breast cancer and melanoma (Aliwaini et al. 2015, 2013) and, as shown in this study, AJ-5 is also efficacious against aggressive sarcomas, the drug-like properties of AJ-5 can however be improved. In this regard, Professor Selwyn Mapolie (Stellenbosch University) and his research group, who synthesised AJ-5, have been developing palladacycle complexes with more desirable drug-like properties, specifically solubility in aqueous solutions. Upon screening more-water soluble derivatives of AJ-5 that display comparable or more potent anti-cancer activity, BTC2 was discovered. The structure of BTC2 (Fig. 3.12A) is the same as AJ-5, but with the addition of two polyethylene glycol-type tethers that increase its water solubility. Indeed the solubility of BTC2 is 1.38mg/mL in 15% DMSO in water compared to the solubility of AJ-5 which was reported to be 0.735mg/mL in 43% DMSO in water (Blanckenberg, 2016).

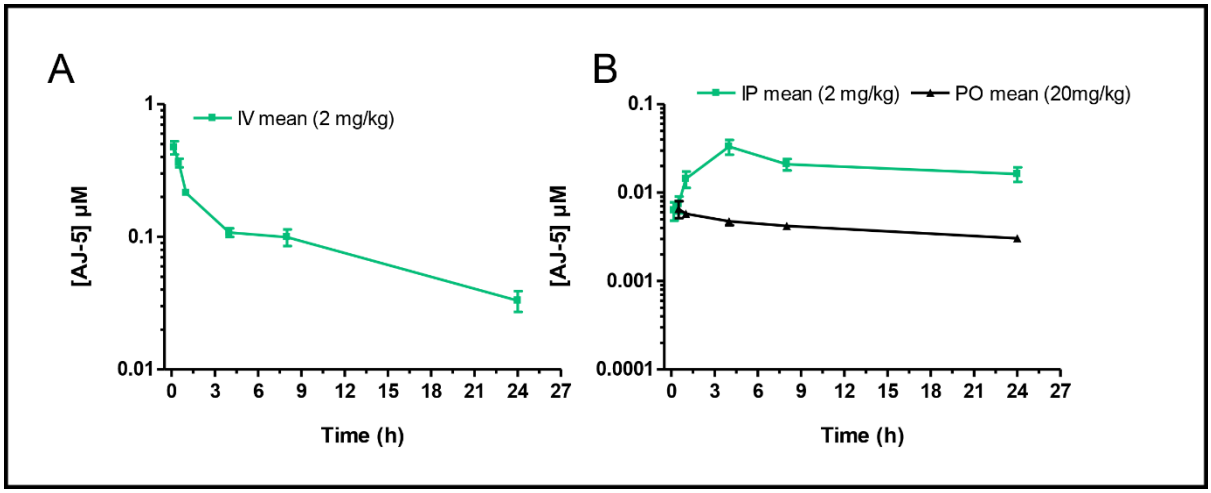

Fig. 3.11 Whole blood concentrations of AJ-5 over 24h in healthy mice. *A single dose of (A) 2mg/kg intravenous (IV) (n=3), (B) 2mg/kg intraperitoneal (IP) (n=3) or 20mg/kg oral (PO) (n=2) administration of AJ-5 in healthy MF1 mice.*

Table 3.1 *Pharmacokinetic parameters of AJ-5 obtained from whole blood of healthy MF1 mice following a single dose of intravenous (IV), intraperitoneal (IP) or oral (PO) administration of AJ-5 for 24h.*

PK parameters	IV at 2mg/kg (n=3)	IP at 2mg/kg (n=3)	PO at 20mg/kg (n=2)
C_{max} (µM)	ND	0.03 ± 0.01	0.006 ± 0.007
T_{max} (h)	ND	4.0 ± 0.00	0.8 ± 0.3
$t_{1/2}$ (h)	11.2 ± 4.8	ND	ND
CL (mL/min/kg)	9.2 ± 0.6	ND	ND
Vd (L/kg)	8.8 ± 3.3	ND	ND
$AUC_{0-\infty}$ (min.µmol/L)	179 ± 12	88 ± 67	11 ± 2
BA (%)	ND	49 ± 38	1 ± 0.1

C_{max} = maximum concentration observed; T_{max} = time at maximum concentration observed; $t_{1/2}$ = half-life i.e. time for concentration of drug to decrease by half; CL = drug clearance; Vd = volume of distribution; $AUC_{0-\infty}$ = total area under the concentration-time curve i.e. drug exposure; BA = bioavailability i.e. fraction of administered drug that reached the s; ND = not determined.

To compare the efficacy of BTC2 to AJ-5, MTT cell viability assays were performed on ARMS (RH30 and AX-OH-1) and ERMS (RD and FL-OH-1) cell lines treated with a range of BTC2 concentrations (Fig. 3.12B). IC_{50} values of ≤ 0.16µM were determined for all RMS cells lines tested which is comparable to what was observed for AJ-5 (Fig. 3.1B). Light microscopy images of BTC2 treated cells show a decrease in cell density and viability compared to vehicle treated control cells after 0, 12 and 24h (Fig. 3.12B). MTT assays were also performed on non-malignant cell lines including fibroblasts (FG0 and DMB), myoblasts (C2C12) and mesenchymal stem cells (A10021501) (Fig. 3.12C). This was done to determine the selectivity of BTC2 towards cancer cells by calculating SI values (Fig. 3.12D). BTC2 was at least 2.2 times and up to 4.3 times more selective towards RMS cells than the non-malignant cell lines tested which is comparable to the SI values determined for AJ-5 (Fig. 3.1D).

The long-term fate of RMS cells after BTC2 treatment was determined using clonogenic assays. Fig. 3.13A shows representative images and quantification of colonies formed over 7-21 days after 24h of pretreatment with BTC2. It is evident that BTC2, comparable to AJ-5 (Fig. 3.2A), significantly inhibited the ability of RMS cells to survive and proliferate,

especially the ERMS cell lines RD and FL-OH-1 which show a dramatic reduction in colony area after as little as ¼ IC_{50} treatment. There was negligible colony formation for all RMS cell lines at IC_{50} concentrations of treatment. Importantly, the ability of the non-malignant C2C12 myoblasts to survive and proliferate after 0.15µM BTC2 treatment, although not significant (p=0.46), was much more than what was observed for the RMS cell lines at the same or lower concentrations of BTC2 where negligible colonies formed (Fig. 3.13B). Again, this result was similar to what was observed for AJ-5 treated C2C12 cells (Fig. 3.2B).

3.14 Discussion

RMS is the most common soft tissue sarcoma found in children and adolescents and while the current treatment for localised tumours results in a high overall survival rate, the chemotherapeutic agents used are associated with debilitating adverse effects (Breneman et al., 2003; Makin, 2014; Malempati & Hawkins, 2012; Stevens, 2005; Wang, 2012). Moreover, more than 15% of patients present with metastatic disease and there has been limited improvement in the treatment of patients with recurrent and metastatic disease (Dasgupta & Rodeberg, 2012; McDowell et al., 2010; Oberlin et al., 2008; Perkins, Shinohara, DeWees, & Frangoul, 2014; Shern et al., 2014). The current study provides several lines of evidence that the binuclear palladacycle AJ-5 and its more water-soluble derivative, BTC2, may be promising chemotherapeutics to treat ARMS and ERMS as well as a range of other sarcoma subtypes. Furthermore, we provide novel and interesting mechanisms by which AJ-5 functions (Fig. 3.14).

Platinum compounds such as cisplatin have been used successfully as anti-tumour agents but they have been associated with severe toxicity and tumour drug resistance (Holohan et al., 2013). Palladium compounds have been proposed as more effective alternatives because they appear to be more active at lower concentrations with less severe side-effects (Jahromi et al., 2016; Johnstone, Suntharalingam, & Lippard, 2016). Cisplatin is occasionally used to treat RMS (Egas-Bejar & Huh, 2014) and was reported to have an IC_{50} of >0.5µM after 4-5 days of treatment in a range of RMS cell lines including RD and RH30 cells (Cocker et al., 2001; Cocker, Pinkerton, & Kelland, 2000). Our study shows that after only 2 days of AJ-5 treatment, IC_{50} values of ≤ 0.2µM were obtained in the RD and RH30 cells.

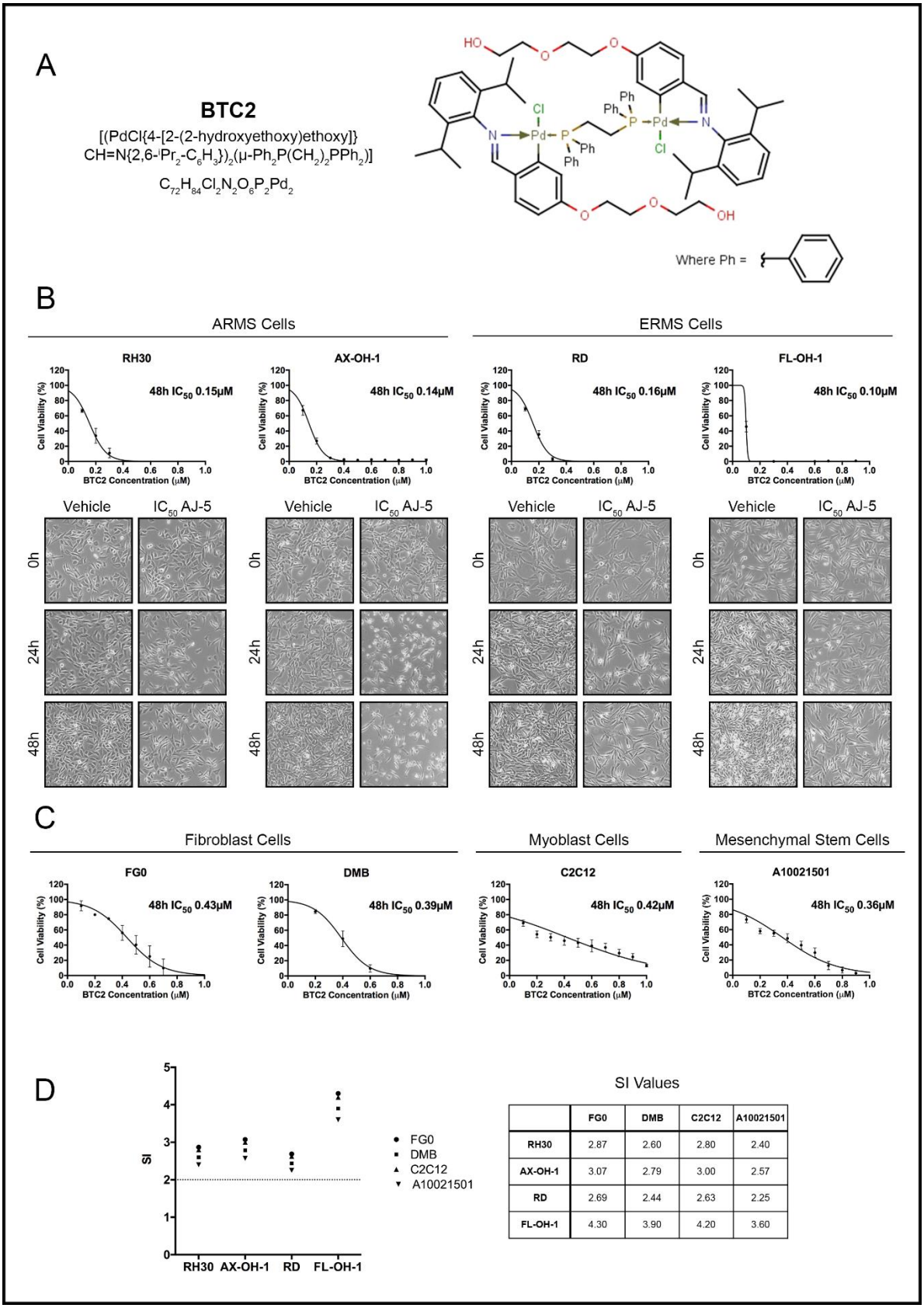

	FG0	DMB	C2C12	A10021501
RH30	2.87	2.60	2.80	2.40
AX-OH-1	3.07	2.79	3.00	2.57
RD	2.69	2.44	2.63	2.25
FL-OH-1	4.30	3.90	4.20	3.60

Fig. 3.12 BTC2 shows potent and selective cytotoxicity against ARMS and ERMS cells. *(A) Structure and molecular formula of BTC2 (B) MTT cell viability assays of ARMS cell lines, RH30 and AX-OH-1, and ERMS cell lines, RD and FL-OH-1, treated with a range of BTC2 concentrations (0.1μM – 1.0μM) or vehicle for 48h. Graphs show mean cell viability as a percentage of vehicle control ± SEM for each*

concentration of BTC2 determined from three independent experiments performed in quadruplicate. A curve was fitted to determine the IC_{50} concentration of BTC2 for each cell line. Below are representative light microscopy images (200X; EVOS XL AMEX1000 Core Imaging System) of ARMS and ERMS cell lines treated with their respective IC_{50} concentrations of BTC2 or vehicle for 24 and 48h. (C) MTT cell viability assays of non-malignant human fibroblast cell lines, FG0 and DMB, mouse myoblast cell line, C2C12, and mesenchymal stem cell line, A10021501, treated with BTC2 and IC_{50} concentrations determined as described in (B) above. (C) Selectivity indices (SIs) were determined for each RMS cell line by dividing the IC_{50} of each non-malignant cell line by the IC_{50} of each RMS cell line.

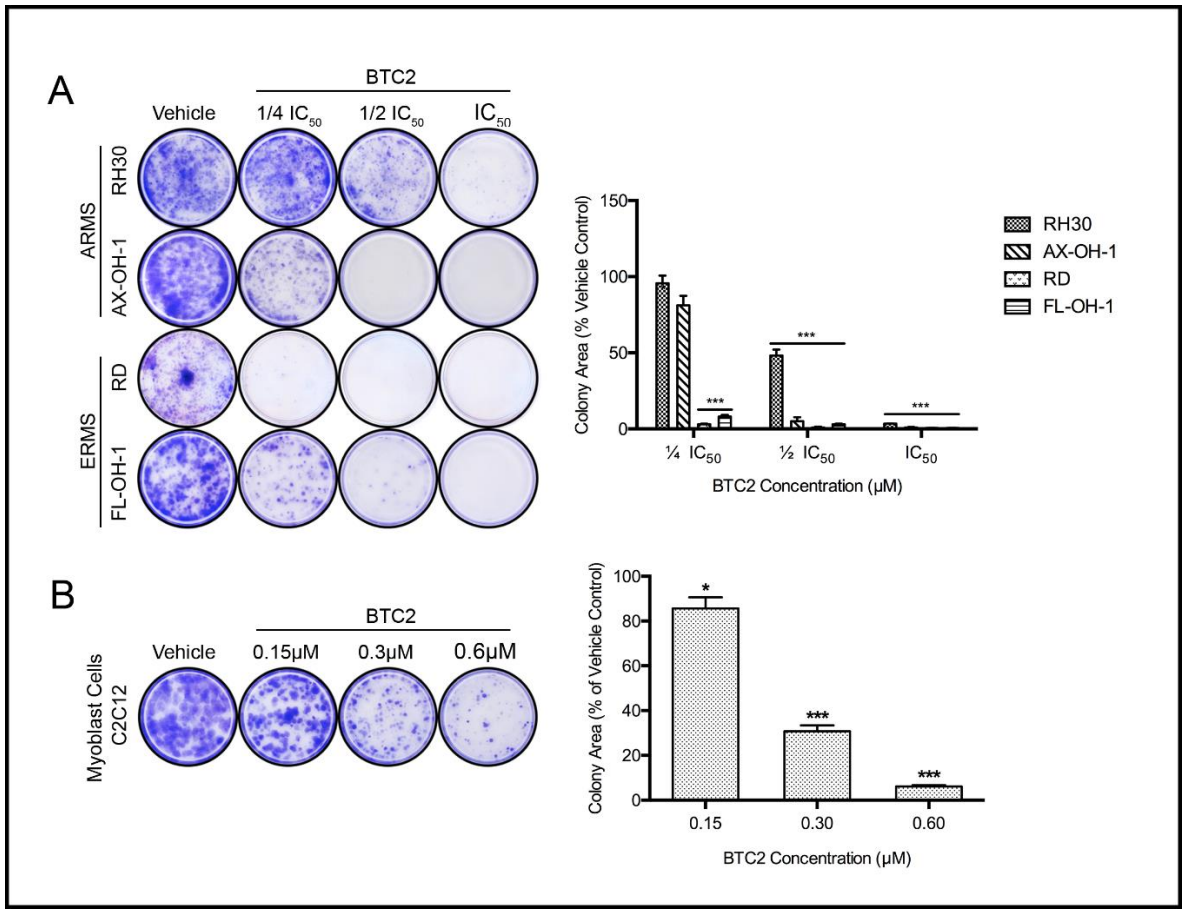

Fig. 3.13 BTC2 inhibits the ability of RMS cells to survive and proliferate. *(A) Representative images and quantification of clonogenic assays of ERMS and ARMS cells treated with vehicle, ¼ IC50, ½ IC50 or IC50 concentrations of BTC2 for 24h and then replated at low densities in drug-free medium and left for 7-21 days for colonies to form. Colonies were stained with crystal violet and images from three independent repeats were quantified using the ImageJ plugin ColonyArea. The graph represents the mean colony area ± SEM of each treatment condition as a percentage of the vehicle control. (B) The same as (A) above for the non-malignant mouse myoblast cell line C2C12, but treated with vehicle, 0.15μM, 0.3μM or 0.6μM AJ-5. Data was analysed using GraphPad Prism 6.0 and a parametric unpaired t-test was performed, where *p<0.05, **p<0.01, ***p<0.001.*

This suggests that AJ-5 displays more potent anti-cancer activity at much lower concentrations over a shorter period than cisplatin in these RMS cells. Furthermore, we show that AJ-5 displays a selectivity index of ≥ 2 which suggests that it has specificity for RMS cells

(Badisa et al., 2009; Koch et al., 2005). Indeed, whereas AJ-5 treated RMS cells were unable to form any colonies, mouse myoblasts treated with 1.5 to 3 times higher concentrations formed colonies with areas comparable to that obtained for vehicle treated cells (Fig. 3.2A and B). Furthermore, mesenchymal stem cells from different sources are thought to represent the target cell of origin for a variety of human sarcomas (Rodriguez et al., 2012) and our cell viability assays (Fig. 3.1C and D) show that the A100021501 mesenchymal stem cells were the most sensitive non-malignant cell line to AJ-5 treatment. This suggests that AJ-5 may have the ability to selectively target the sarcoma-initiating cell which could prove to be advantageous and more efficacious than current therapies. Taken together these findings support evidence that, compared to platinum compounds, palladium complexes display superior anti-cancer activity and that they may associate with fewer side effects.

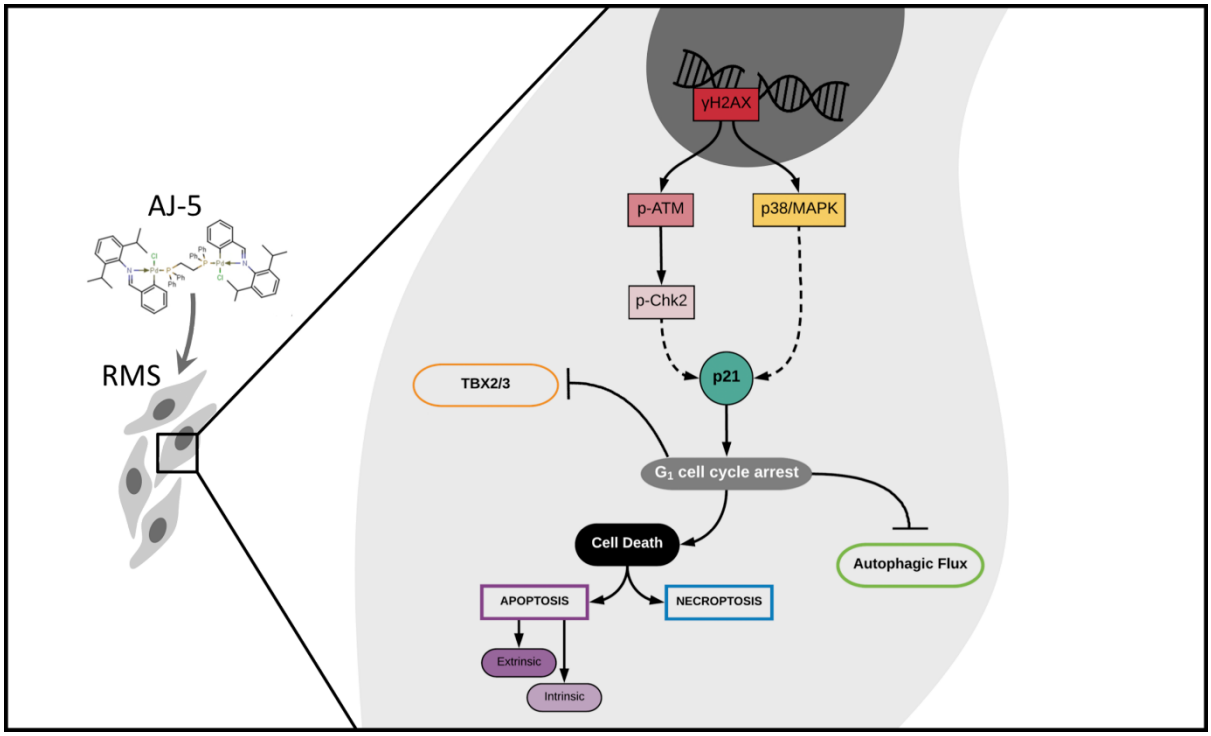

Fig. 3.14 Proposed model for AJ-5 in RMS. *At low concentrations (≤ 0.2μM) in ARMS and ERMS cells AJ-5 induces DSBs leading to increased levels of γH2AX and activation of both the canonical DSBs pathway (ATM/Chk2) and the p38/MAPK stress signalling pathway. This results in a p21 induced G_1 cell cycle arrest followed by the activation of the extrinsic and intrinsic apoptotic pathways, an increase in necroptosis markers and a reduction in autophagic flux. Furthermore, AJ-5 can inhibit TBX2 and TBX3 levels, but this is context dependent.*

This study suggests that AJ-5 mediates its cytotoxicity through the induction of DSBs and activation of the canonical DDR pathway as well as the p38/MAPK pathway (Fig. 3.3). This

mechanism has been characterised before in AJ-5 treated melanoma and breast cancer cells. The p38/MAPK pathway, specifically, was shown to mediate AJ-5 cytotoxicity where chemical (SB203580) and biological (siRNA) inhibition of the p38/MAPK pathway attenuated AJ-5 anti-cancer activity in melanoma cells (Aliwaini et al. 2013, 2015). It is thus not surprising that the same pathways are activated in RMS, however, to validate the role of the p38/MAPK pathway in AJ-5 mediated anti-cancer activity in RMS cells, p38/MAPK pathway inhibition and the effect of cell viability and cell death would need to be investigated. Although, this was attempted several times with siRNA and SB203580, successful inhibition was not achieved. Therefore, future work on this project would readdress these experiments.

While tumours initially respond to proapoptotic therapies, they frequently acquire the ability to bypass the apoptotic pathway and develop drug resistance leading to tumour recurrence (Ricci & Zong, 2006; Sachet, Liang, & Oehler, 2017). It is thus predicted that drugs that can trigger alternative or multiple PCD pathways such as autophagy (PCD type II) and programmed necrosis (PCD type III) would be more efficacious (Viola et al., 2012). The annexin V-FITC assays in Fig. 3.4C reveal that AJ-5 induces not only a significant apoptotic population, but also a significant cell population which could represent necrosis, programmed necrosis (necroptosis) and/or secondary necrosis which occurs when there is insufficient clearance of apoptotic cells (Sachet et al., 2017; Silva, 2010).

Necroptosis has generated a lot of interest for its potential therapeutic benefit (Su et al., 2016). It is underpinned by a molecular mechanism distinct from apoptosis and it is anticipated that cancer cells that acquire dysfunctional apoptotic pathways and/or resist apoptotic induction may be more sensitive to drugs that induce necroptosis (Krysko et al., 2017). Indeed, Han et al. (2007) showed that the naturally occurring small molecule compound, Shikonin, was able to circumvent apoptotic cancer drug resistance by the induction of necroptosis in MCF-7 breast cancer cells that overexpress mediators of drug resistance including the drug transporter P-glycoprotein and anti-apoptotic proteins BCL-2 and BCL-XL. In addition, the induction of necroptosis led to the reduction of caspase-8 deficient colorectal tumours that are refractory to current pro-apoptotic chemotherapeutic approaches (He et al., 2017). Furthermore, necroptotic cells have been associated with an efficient anti-tumour immunity because they release damage-associated molecular patterns,

induce maturation of dendritic cells and produce interferon-γ by T cells (Aaes et al., 2016; Krysko et al., 2017; Meng et al., 2016). To the best of our knowledge, while there is some evidence that the cisplatin derivative oxaliplatin and a novel platinum(II)-terpyridine complex can induce apoptotic and necroptotic cell death, this study is the first to suggest that a palladium-based compound can potentially induce necroptosis (Wu et al. 2015; Suntharalingam et al. 2013). Indeed, AJ-5 treatment causes an increase in key components of the necroptotic pathway including p-RIP3 and p-MLKL (Fig. 3.6A). Although, inhibition of necroptosis with necrostatin-1 was able to rescue the necrotic population of cells (Fig. 3.6C), this is not sufficient to conclusively confirm that AJ-5 does indeed induce necroptosis as it has been shown that necrostatin-1 inhibition cannot distinguish between programmed necrosis (necroptosis) and/or secondary necrosis. Therefore, although this data is exciting, annexin V-FITC assays of AJ-5 treated RMS cells in the presence of necrostatin-1 and the pan-caspase inhibitor Z-VAD-fmk will need to be performed.

Here we show for the first time that AJ-5 reduces autophagic flux in both ARMS and ERMS cells. This is an important finding because autophagy has been reported to promote cell survival and chemotherapeutic drug resistance in a number of sarcomas, including RMS, and thus autophagy has been identified as a drug target to treat sarcomas (Min et al., 2017; Ricci & Zong, 2006; Viola et al., 2012). For example, the autophagy inhibitor, chloroquine, enhanced RMS cell death induced by ciclopirox olamine, bortezomib and 17-DMAG and stimulation of autophagy by rapamycin prevented this (Peron, Bonvini, & Rosolen, 2012; Zhou et al., 2014). Consistent with our findings, palladium nanoparticles have recently been shown to block autophagic flux in Hela cells as shown by increased LC3II/I ratios, reduced degradation of p62 and autophagosome accumulation (Zhang et al., 2018). It is important to note that AJ-5 induces autophagy PCD in melanoma and breast cancer cells (Aliwaini et al. 2015, 2013) which suggests that the effect of palladium complexes on autophagy may be cancer type specific.

An important aspect in early stages of drug discovery and development is ensuring the lead-compound exhibits drug-like properties (Kerns & Di, 2008). In collaboration with the inorganic chemistry group headed by Professor Selwyn Mapolie (University of Stellenbosch), the AJ-5 derivative with superior water solubility, BTC2, was identified. Indeed, the average IC_{50} across

the 4 RMS cells test is 0.15µM for AJ-5 and 0.14µM for BTC2 (Fig. 3.1B and Fig. 3.12B). Furthermore, the average SI (calculated from all RMS and non-malignant cell lines tested) is 3.91 for AJ-5 and 3.00 for BTC2 (Fig. 3.1D and Fig. 3.12D). This suggests that the anti-cancer activity of AJ-5 and BTC2 is the same, however, although both drugs have a favourable average SI > 2, BTC2 does appear to be slightly less specific to cancer cells than AJ-5. Nonetheless, BTC2 exhibits more desirable solubility properties and should thus be taken forward for further in vitro and in vivo drug characterisation.

In conclusion, we show that AJ-5 and BTC2 may be promising chemotherapeutics to treat ARMS and ERMS because they display potent and selective cytotoxicity at sub-micromolar concentrations. Furthermore, AJ-5 inhibits the ability of RMS cells to survive, proliferate and migrate and is effective against a range of aggressive sarcoma subtypes. Importantly, AJ-5 induces apoptosis, increases markers of necroptosis, reduces autophagic flux and displays a favourable pharmacokinetic and safety profile.

CHAPTER 4

A target-based drug repurposing strategy to identify FDA-approved drugs that negatively regulate oncogenic TBX2 and TBX3

4.1 Introduction

There is a growing appreciation for the need to understand the molecular underpinnings of RMS with the aim of identifying, in part, novel targets to develop highly specific and effective treatments with negligible adverse effects (Ciavarella et al., 2010). In this regard, the highly homologous T-box transcription factors TBX2 and TBX3 are potentially interesting. TBX2 and TBX3 overexpression has been implicated in a wide range of malignancies and they have been biologically validated as druggable targets for the treatment of several cancers including melanoma, breast cancer and RMS (Wansleben et al. 2014; Willmer et al. 2016; Zhu et al. 2014; Peres & Prince 2013; Prince et al. 2004; Davis et al. 2008; Sims 2016). However, targeting transcription factors is notoriously challenging because unlike enzymes they do not have catalytic activity and deep binding pockets to which small molecule inhibitors can be designed and their predominant nuclear localisation makes them less accessible to therapeutic agents (Dang et al., 2017; Redell & Tweardy, 2006; Yeh, Toniolo, & Frank, 2013). This challenge is further exacerbated by the length of time and costs associated with de novo drug development. This study therefore adopts a novel strategy to circumvent these challenges by combining a targeted approach to TBX2/3 using drug repurposing. In this regard, a high throughput cell-based immunofluorescence screen was conducted to identify FDA-approved drugs that could negatively regulate TBX2 and/or TBX3 protein levels and nuclear localisation. Engineered cells expressing inducible exogenous FLAG-tagged TBX2 or TBX3 using a Tet-On system were screened with the Pharmakon 1600 drug library. 'Hits' were identified by z-scores. Amongst these were niclosamide, piroctone olamine and pyrvinium pamoate which were validated to be potent inhibitors of both TBX2 and TBX3 in ERMS and

ARMS and were shown to display anti-cancer activity in these sarcomas. These drugs have the potential to be repurposed for the treatment of TBX2/3 driven cancers either as single agents or in combination with currently used chemotherapeutics.

4.2 High-throughput screen: cell culture model development

To identify drugs that downregulate TBX2/TBX3 levels and/or that block their nuclear localisation and thus prevent them from regulating their target genes a high throughput screen that employed immunofluorescence as readout was performed. Due to a lack of reliable and high-grade antibodies against TBX2 and TBX3 for immunofluorescence, this study used a tetracycline-on (Tet-On) system that enabled the inducible expression of 3XFLAG-tagged TBX2 or 3XFLAG-tagged TBX3 in the 501mel human melanoma cell line. A further advantage of this system is that it enables control of the levels of TBX2/3 expression depending on the concentration of doxycycline, a tetracycline derivative, and thus avoids pleiotropic effects. In addition, the Prince laboratory had already confirmed key oncogenic roles for TBX2 and TBX3 in the 501mel cells and the inducible cell lines were already established in the laboratory of our collaborator, Prof Goding, and it was anticipated that any drugs that impact TBX2/3 levels and nuclear localisation in these cells would do the same in other TBX2/3 driven cancers such as RMS. Immunofluorescence and western blotting show the dose dependent expression and nuclear localisation of TBX2-FLAG and TBX3-FLAG (Fig. 4.1A and B). Importantly, the immunofluorescence images reveal that all cells stained positively with the FLAG antibody and western blots show that antibodies to FLAG and TBX2/3 gave similar results. To reduce the time and cost of conducting two separate screens, a TBX2-FLAG expressing cell population was pre-stained with CellTracker and co-cultured with a TBX3-FLAG cell population which enabled the TBX2-FLAG and TBX3-FLAG cell populations to be distinguished from one another in a single screen (Fig. 4.1C). To ensure that the cell culture model was as biologically relevant as possible, FLAG-TBX2/3 were induced using 20ng/mL doxycycline i.e. the lowest concentration capable of inducing detectable levels of TBX2/3.

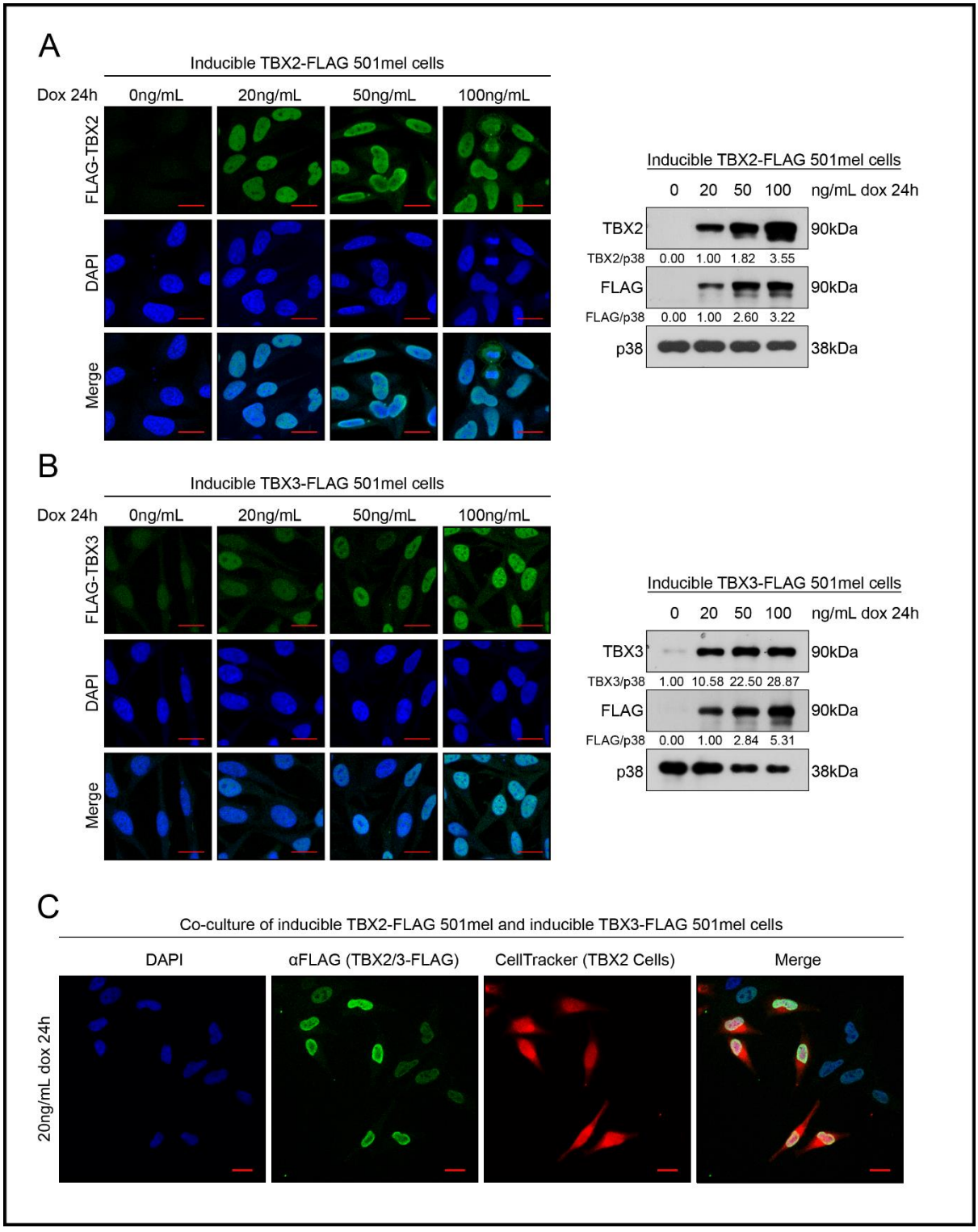

Fig. 4.1 Tet-On inducible cell culture model used in the high throughput screen. *(A, B) 501mel cell lines expressing an inducible FLAG-tagged TBX2/3 treated with a range of doxycycline (dox) concentrations. Representative confocal immunofluorescence maximum intensity projection images (630X; Carl Zeiss LSM 880) and western blotting of (A) FLAG-TBX2 and (B) FLAG-TBX3. For immunofluorescence a FLAG primary antibody and Alexa Fluor 488 secondary antibody was used and nuclei were stained with DAPI (scale bar is 20µm) and for western blotting, antibodies used were as indicated and p38 was included as a loading control. Densitometry readings were obtained using ImageJ and protein expression levels are represented as a ratio of protein of interest/p38 normalised to the vehicle control sample. (C) Representative confocal immunofluorescence images (200X, 2X*

zoom; Carl Zeiss LSM 710) of co-culture of TBX2-FLAG cells pre-stained with CellTracker (DeepRed) and TBX3-FLAG cells treated with 20ng/mL dox for 24h and processed for immunofluorescence as described above.

4.3 High-throughput screen: experimental design

Co-cultures of 501mel TBX2-FLAG cells (pre-stained with CellTracker Orange) and TBX3-FLAG cells were seeded in 384-well glass bottom plates (Fig. 4.2A) and TBX2/3-FLAG expression was induced the following day (Fig. 4.2B). The MicroSource Pharmakon 1600 library was prepared and drugs were added to the cells to achieve a final concentration of 10µM with DMSO used as a vehicle control (Fig. 4.2C). Ideally, compounds that negatively regulate TBX2/3 levels and nuclear localisation should have been included as positive controls. However, despite screening a range of compounds previously reported capable of this, none of them provided a large enough dynamic range in which 'hits' could be robustly identified (Z-factor and SSDM calculations). Cells were treated for 4, 12 and 24h and each plate was run in technical duplicates (5 library source plates, three timepoints in duplicate = 30 plates) (Fig. 4.2D). After treatment timepoints cells were fixed with 4% paraformaldehyde and processed for immunofluorescence with a FLAG primary antibody and Alexa Fluor 488 secondary antibody and nuclei were counterstained with DAPI (Fig. 4.2E). Plates were imaged, data stored and analysed on an IN Cell Analyzer 6000 (Fig. 4.2F).

4.4 High-throughput screen: image analyses for parameter extraction

The IN Cell Developer Toolbox was used to design a customised parameter extraction protocol. For each field of view the IN Cell Analyzer 6000 captured a composite image derived from three channels (Fig. 4.3A). The UV channel was used to identify DAPI stained nuclei and determined the population of cells that were taken for further analyses (Fig. 4.3B). This channel was also used for additional measurements (not required for our experimental design and intended analyses, but maybe of use at a later stage. See relevance in section 4.9) including cell count, nuclear area, nuclear form factor and length/width ratio, nuclear integrity as measured by fluorescence intensity and its standard deviation (Table 4.1). The dsRed channel was used to detect the CellTracker Orange stained TBX2-FLAG cell population (Fig. 4.3C) and the TBX2-FLAG and TBX3-FLAG cell populations were then analysed independently for their FLAG expression in the FITC channel (Fig. 4.3D). Nuclear FITC

fluorescence was measured using the DAPI mask and cytoplasmic FITC fluorescence was determined by subtracting nuclear fluorescence from whole cell fluorescence. To determine subcellular localisation nuclear FITC fluorescence was divided by cytoplasmic FITC fluorescence where a ratio of >1 indicates nuclear localisation and <1 indicates cytoplasmic localisation. The latter was also determined by measuring an eroded FITC nucleus which represents nuclear expression and a FITC nuclear collar which represents cytoplasmic expression followed by the same ratio calculation. Extracted and calculated parameters are described in Table 4.1.

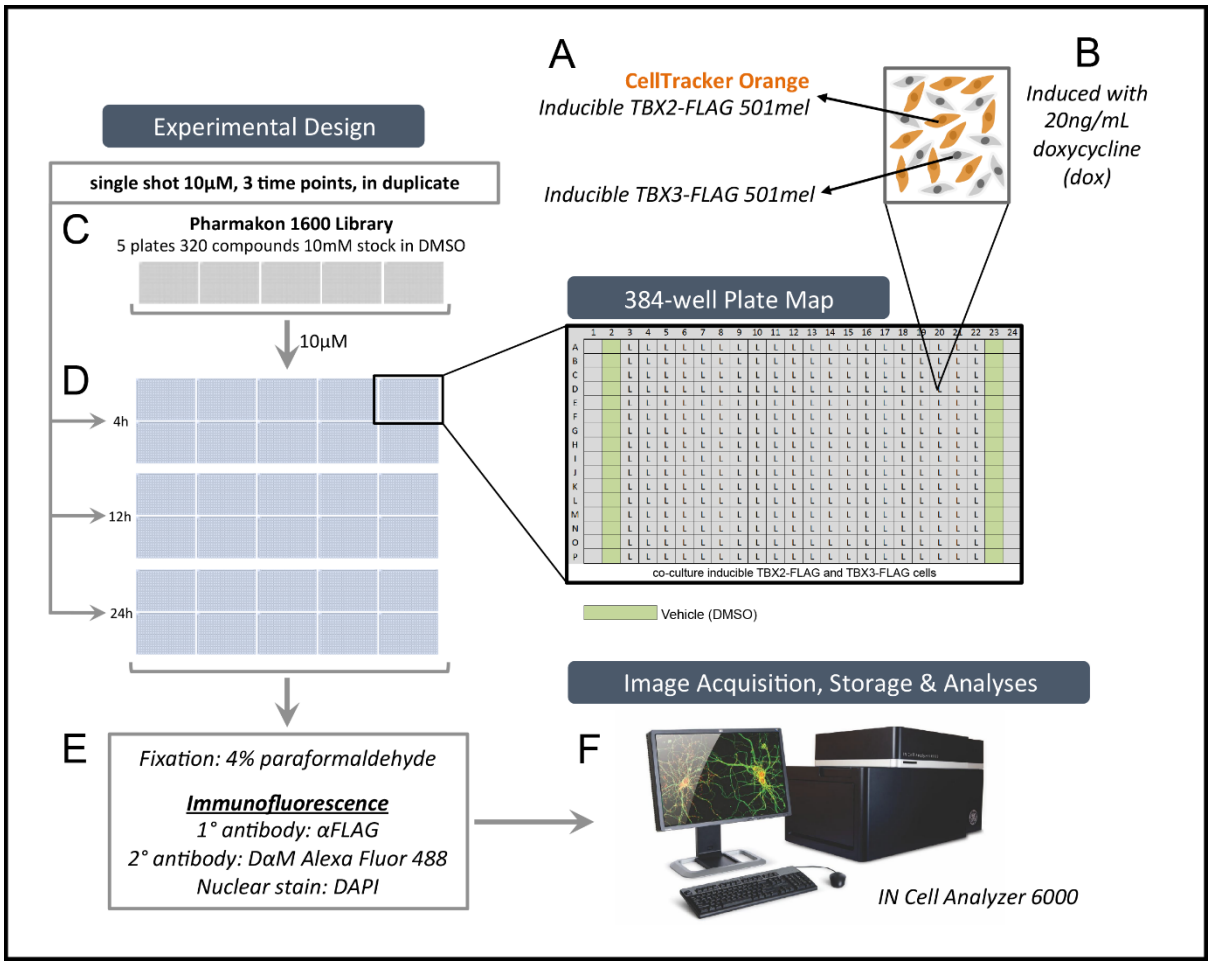

Fig. 4.2 Schematic of high throughput screen experimental design. *(A) Co-culture of inducible TBX2-FLAG 501mel and inducible TBX3-FLAG 501mel cells seeded in 384-well plates. (B) Cells were induced the following day with 20ng/mL doxycycline (dox). (C) The MicroSource Pharmakon 1600 drug library (5 library plates consisting of 320 compounds each) was added to cells to achieve a final concentration of 10µM and DMSO (10µM) was used as the vehicle negative control (green wells on 384-well plate map). (D) Cells were treated for 4, 12 and 24h and each library plate for each timepoint was run in technical duplicates. (E) Cells were fixed with 4% paraformaldehyde and processed for immunofluorescence. (F) Plates were imaged using an IN Cell Analyzer 6000 line scanning confocal high-content imager.*

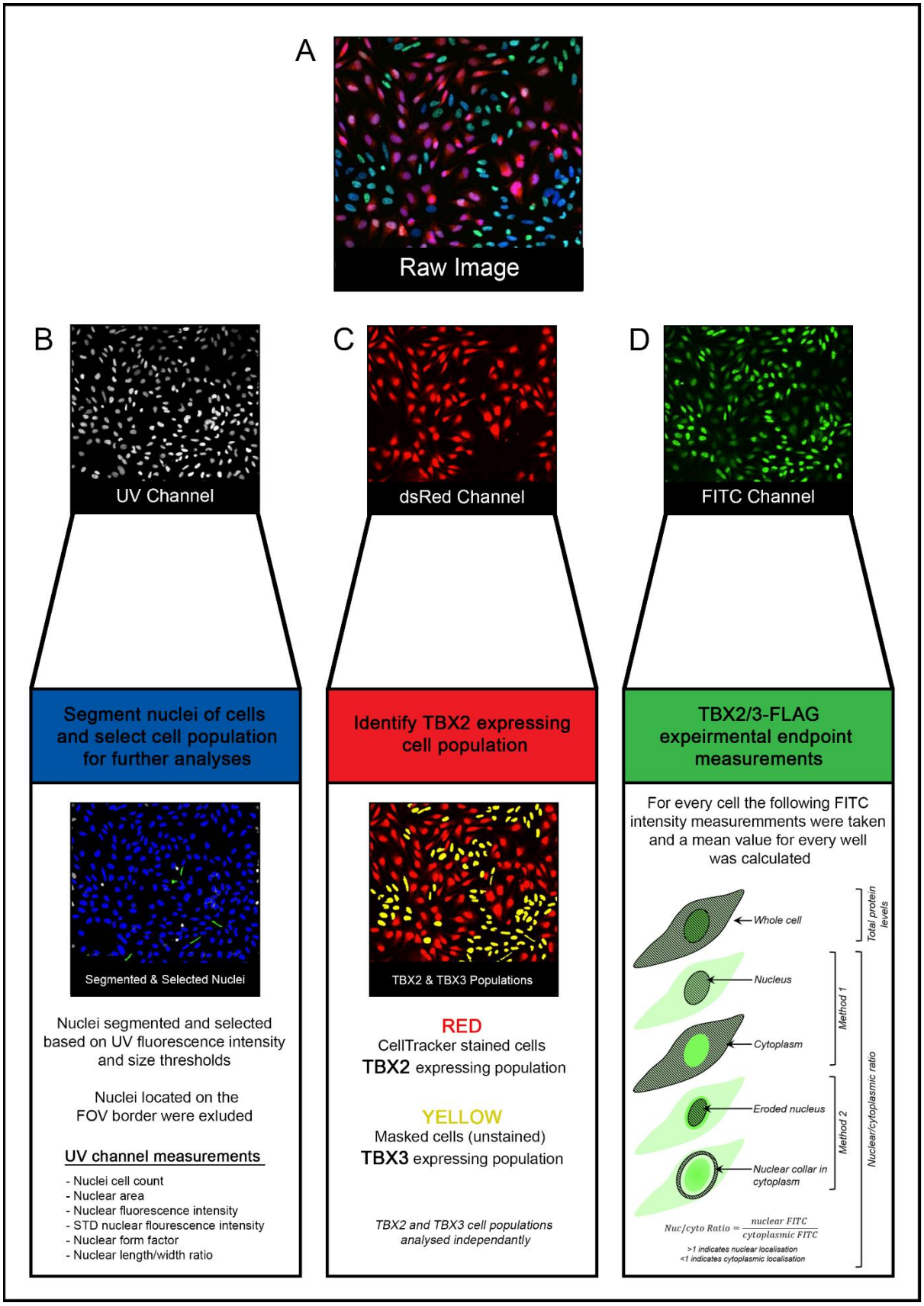

Fig. 4.3 IN Cell Developer Toolbox customised parameter extraction protocol. *(A) Raw merged image (UV, FITC and dsRed fluorescence channels). (B) The DAPI channel was used to segment the nuclei, select the cell population within the FOV for further analyses and additional nuclear measurements*

were taken as indicated. (C) The dsRed channel was used to separate the TBX2-FLAG (CellTracker stained cells) and TBX3-FLAG cell populations (yellow masked cells excluded from the TBX2 population and green masked cells selected as the TBX3 population). The two identified populations were then analysed independently. (D) The FITC channel represented TBX2/3-FLAG expression levels. Nuclear FITC fluorescence was measured using the DAPI mask. Cytoplasmic FITC fluorescence was determined by subtracting nuclear fluorescence from whole cell fluorescence. Additional measurements were taken for another method of determining nuclear/cytoplasmic localisation which included an eroded FITC nuclear measurement representing nuclear expression as well as a nuclear collar measurement representing cytoplasmic expression. The mean measurement for each parameter per well were used for analyses.

Table 4.1 *Details of extracted and calculated parameters.*

Extracted/Calculated Parameters	Description
CountDividebyFOV	Online cell counting to 1000 cells or maximum of 16 field of views (FOVs) imaged per well. Nuclei count (DAPI)/FOV gives an indication of cell number
AreaNuc	Area of nucleus from DAPI stain
MeanIntNuc	Mean DAPI intensity nucleus
DxANuc	MeanIntNuc multiplied by AreaNuc
FormFactorNuc	Nucleus shape scored by roundness (DAPI stain). Round = 1 which indicates cell death
NuclearAreaFactor	Nuclear area factor is AreaNuc/FormFactorNuc. It is used as an early indicator of cell death
STDIntNuc	Standard deviation of nuclear intensity DAPI (MeanIntNuc) indicates if there is apoptosis i.e. nuclear fragmentation
LengthWidthRatioNuc	Length/width ratio determined from DAPI stain
MeanInt FITCCell	Mean FITC (TBX2/3-FLAG) intensity of whole cell
MeanInt FITCNuc	Mean FITC (TBX2/3-FLAG) intensity of nucleus
MeanInt FITCCyto	Mean FITC (TBX2/3-FLAG) intensity of cytoplasm (MeanIntFITCNuc subtracted from Mean FITCCell)
RatioNucCytoFITC	Ratio of MeanIntFITCNuc divided by MeanIntFITCCyto. Indicates localization of FLAG-TBX2/3: >1 = nucleus and < 1 = cytoplasm
RatioNucCytoFITCCellsCollar	Ratio of mean erroded nuclear FITC divided by mean cytoplasmic collar FITC. Indicates localization of FLAG-TBX2/3: >1 = nucleus and < 1 = cytoplasm

4.5 'Hit' identification

'Hit' drugs were identified using a z-score cut-off of ≤ 2 and a cell count threshold of at least 25 cells per field of view (Goktug et al., 2013; Zhang, 2011). Briefly, z-scores were calculated

by measuring the number of standard deviations below or above the population mean for each of the following two experimental end-point parameters: (I) downregulation of TBX2/3 protein levels represented by reduced whole cell FITC fluorescence intensity and (II) cytoplasmic localisation represented by nuclear/cytoplasmic FITC fluorescence intensity ratios of <1. The cell count threshold was important because it enabled identification of drugs that could be further characterised for the mechanism by which they inhibit TBX2/3 levels and nuclear localisation. It is important to note though that drugs excluded from our 'hit' selection criteria can always be investigated at a later stage for their anti-cancer activity.

Fig. 4.4A and B show scatter plots of 'hits' identified to downregulate total TBX2 and TBX3 protein levels respectively at 4, 12 and 24h drug treatment timepoints. According to the 'hit' selection criteria, 19 Pharmakon compounds were identified to significantly downregulate TBX2 levels, 6 to significantly downregulate TBX3 levels and 7 that significantly downregulated both TBX2 and TBX3 levels (Fig. 4.4C). Scatter plots depicted in Fig. 4.5A and B show 'hits' identified based on their ability to block TBX2 and TBX3 nuclear localisation at the treatment timepoints tested. Of interest were drugs that specifically prevent TBX2/3 from entering the nucleus i.e. that resulted in more TBX2/3 protein being localised to the cytoplasm. Consequently, 'hits' that were also identified to downregulate TBX2/3 levels were excluded from Fig. 4.5C. Based on this, 16 compounds were identified for TBX2, 16 for TBX3 and 17 that impacted TBX2 and TBX3 nuclear localisation. When the raw immunofluorescence images for all the 'hits' listed in Fig. 4.4C and Fig. 4.5C were extracted (Appendix 7.11) and carefully inspected the 'hits' that downregulated TBX2/3 levels were visually more convincing and therefore only 'hits' from this group were taken forward for validation. Furthermore, some of the 'hits' shown in Fig. 4.4C are known to reduce global protein levels and therefore provided confidence in the data generated. These included protein synthesis inhibitors (indicated in green) and DNA damaging agents (indicated in purple). In addition, several current chemotherapeutic agents (indicated in blue) such as epirubicin hydrochloride, dactinomycin, daunorubicin and doxorubicin were identified which suggests that anti-cancer drugs currently in use are functioning, in part, through targeting TBX2/3 levels (Livshits, Rao, and Smith 2014). The current study was interested in compounds that are not currently approved to treat cancer and based on preliminary literature searches the following 'hits' were selected for validation and characterisation: (I) the TBX2 'hits', niclosamide and vardenafil hydrochloride

(Fig. 4.11A and B); (II) the TBX3 'hits', piroctone olamine and pyrvinium pamoate (Fig. 4.12A and B); and (III) the TBX2 and TBX3 'hit', tacrolimus (Fig. 4.13).

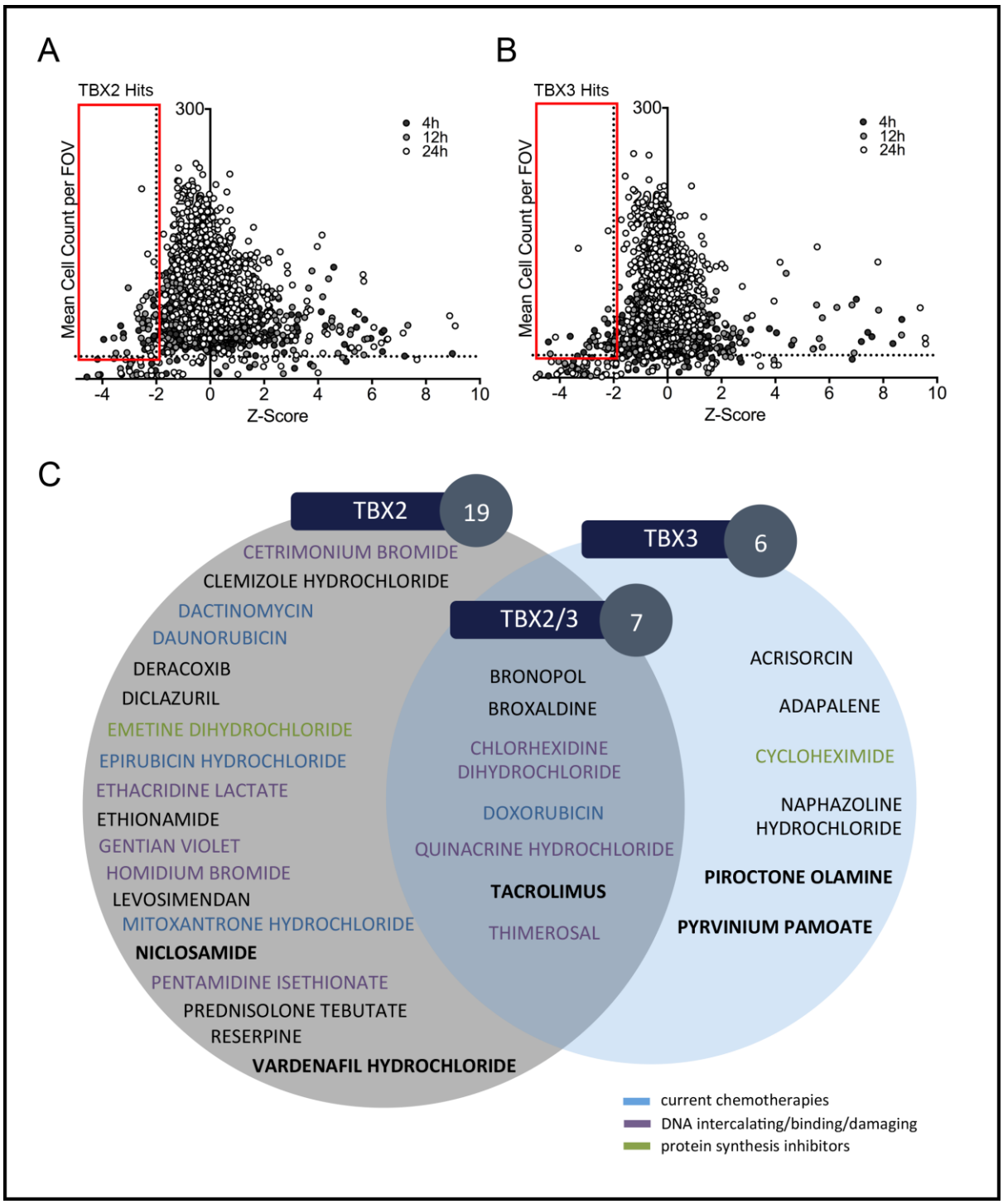

Fig. 4.4 z-score identification of 'hit' FDA-approved drugs that downregulate TBX2 and/or TBX3 protein levels. *z-score scatterplots of (A) TBX2-FLAG and (B) TBX3-FLAG expressing cells after 24h of doxycycline induction (20ng/mL) followed by Pharmakon drug library treatment (10μM) for 4, 12 and 24h. z-scores were calculated from normalised mean TBX2/3-FLAG nuclear fluorescence data (z=(x-μ)/σ, where x= well (drug) mean nuclear TBX2/3-FLAG fluorescence intensity value, μ=population (384-well plate) mean TBX2/3-FLAG fluorescence intensity value and σ= population standard*

deviation). It was assumed that the data was normally distributed and calculations were determined from two technical duplicates. A z-score cut-off of <-2 (i.e. more than 2 standard deviations below the population mean) and a cell count cut-off of > 25 cells per FOV were used to select 'hit' compounds (red box on graphs) that downregulate TBX2 and or TBX3. (C) Venn diagram showing the 'hit' compounds identified in (A) and (B) above where 19, 6 and 7 compounds were identified to downregulate TBX2, TBX3 and both TBX2 and TBX3 total protein levels respectively. Compound names in blue represent already existing chemotherapeutics, purple represent DNA intercalating/binding and/or damaging agents and green are known protein synthesis inhibitors. Bolded compounds were taken further for validation.

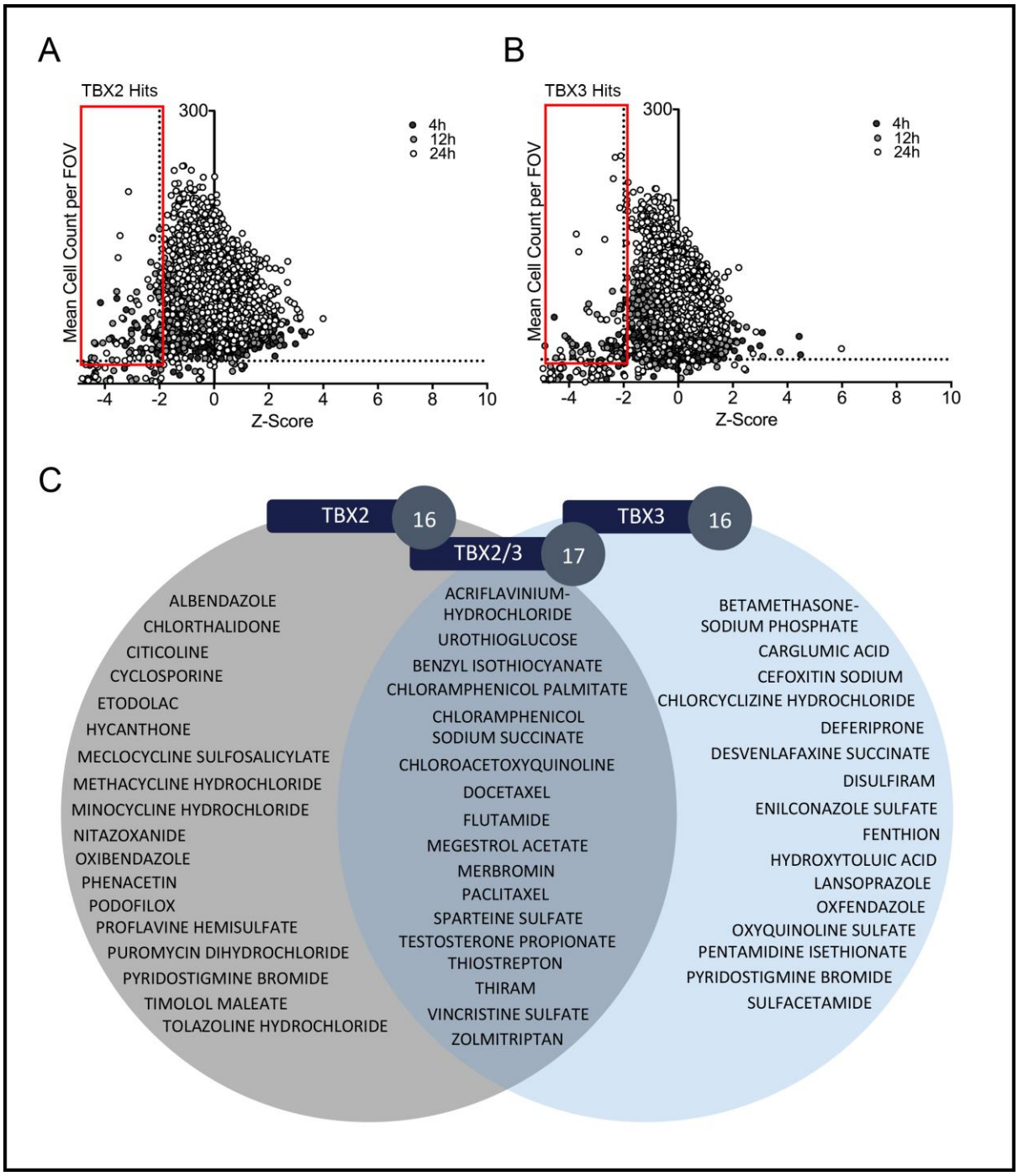

Fig. 4.5 z-score identification of 'hit' FDA-approved drugs that localise TBX2 and/or TBX3 proteins to the cytoplasm. *z-score scatterplots of (A) TBX2-FLAG and (B) TBX3-FLAG expressing cells after 24h of*

doxycycline induction (20ng/mL) followed by Pharmakon drug library treatment (10µM) for 4, 12 and 24h. z-scores were calculated from normalised mean TBX2/3-FLAG nuclear/cytoplasmic ratios determined from mean eroded αFLAG nuclear fluorescence divided by mean cytoplasmic collar αFLAG fluorescence (z=(x-µ)/σ, where x= well (drug) mean TBX2/3-FLAG nuclear/cytoplasmic ratio, µ=population (384-well plate) mean nuclear/cytoplasmic ratio and σ= population standard deviation). It was assumed that the data was normally distributed, and calculations were determined from two technical duplicates. A z-score cut-off of <-2 (i.e. more than 2 standard deviations below the population mean) and a cell count cut-off of > 25 cells per FOV were used to select 'hit' compounds (red box on graphs) that localise TBX2 and or TBX3 proteins to the cytoplasm. (C) Venn diagram showing the 'hit' compounds identified in (A) and (B) above (excluding compounds already identified in Fig. 12) where 16, 16 and 17 compounds were identified to localise TBX2, TBX3 or both TBX2 and TBX3 proteins to the cytoplasm respectively.

4.6 Selected 'hits'

4.6.1 Vardenafil hydrochloride

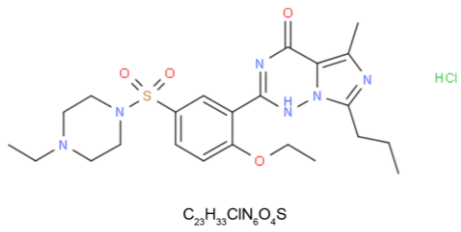

Fig. 4.6 Structure and molecular formula of vardenafil hydrochloride *(ChemSpider ID: 8318471).*

Vardenafil hydrochloride (commonly used brand names: Levitra® and Staxyn™) (Fig. 4.6) is a selective inhibitor of cyclic guanosine monophosphate (cGMP)-specific phosphodiesterase type 5 (PDE5). It was approved by the FDA in 2003 as an oral therapy for the treatment of erectile dysfunction. The drug was initially available as 2.5, 5, 10 and 20mg oral tablets and in 2010 a 10mg oral disintegrating tablet was approved. Based on its efficacy and side effects, the dosage prescribed was one tablet 60min before sexual activity and at least 24h apart. The most common side effects reported for vardenafil hydrochloride include headache, flushing, stuffy or runny nose, indigestion, upset stomach or dizziness. These side effects usually go away after a few hours (Bayer Pharmaceuticals Corporation, 2007; FDA, 2018).

4.6.2 Niclosamide

Niclosamide (commonly used brand names: Niclocide® and Yomesan®) (Fig. 4.7) is an anthelmintic indicted for the treatment of tapeworm and intestinal fluke infections such as *Taenia saginata* (beef tapeworm), *Taenia solium* (pork tapeworm), *Diphyllobothrium latum* (fish tapeworm) and *Fasciolopsis buski* (large intestinal fluke) and it is also used as a molluscicide in the control of schistosomiasis. Niclosamide is believed to kill worms upon

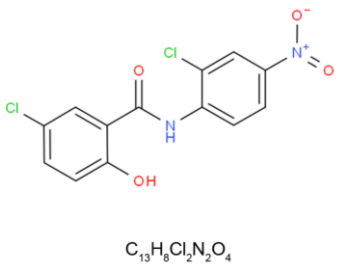

Fig. 4.7 Structure and molecular formula of niclosamide *(ChemSpider ID: 4322).*

contact by uncoupling of oxidative phosphorylation or stimulation of ATPase activity. It was approved in 1982 as a 500mg chewable oral tablet and is administered as a single dose of 1 tablet for children under 2 years, 2 tablets for children 2-6 years and 4 tablets for adults and children from 6 years upwards. Side effects include disturbances of the gastro-intestinal tract such as nausea, retching and abdominal pain. Niclosamide is on a long list of FDA drugs that have been discontinued not because they are not safe or efficacious but for reasons including that they are no longer marketed (Bayer Pharmaceuticals Corporation, 1988; FDA, 2018). This can result from, for example, a brand-name manufacturer losing interest in a product because of generic competition. It is however important to note that such dormant FDA-approved drugs can be remarketed.

4.6.3 Piroctone olamine

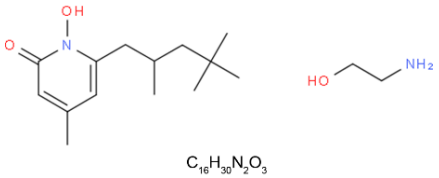

Fig. 4.8 Structure and molecular formula of piroctone olamine *(ChemSpider ID: 45574).*

Piroctone olamine (commonly used brand name: Octopirox®) (Fig. 4.8) is an antifungal agent found in anti-dandruff shampoos used to treat seborrheic dermatitis and dry scalp. It was first approved for addition to the United States Pharmacopeia (USP) in 2008, after the FDA sought additional safety and effectiveness data in 2004. Piroctone olamine as an ingredient is permitted up to 1% in rinse-off solutions (i.e. shampoo). Since its use in the 1970s (prior to approval) no known adverse effects or significant health effects have been observed. Piroctone olamine is not regulated as a medicine and formulations can be bought from supermarkets and pharmacies (Klug & Kreiling, 2004; The United States Pharmacopeial Convention, 2008).

4.6.4 Pyrvinium pamoate

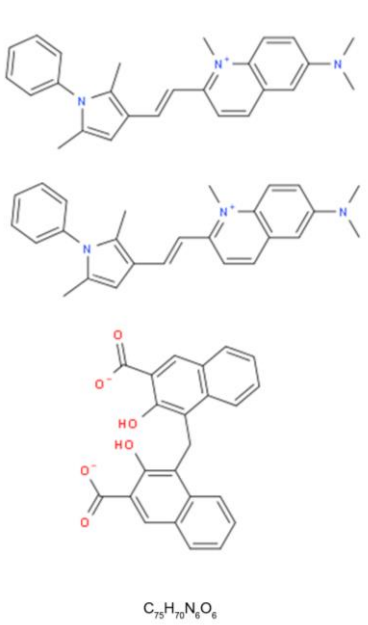

Fig. 4.9 Structure and molecular formula of pyrvinium pamoate *(ChemSpider ID: 10152945).*

Pyrvinium pamoate (commonly used brand names: Povan® and Vanquin®) (Fig. 4.9) is an anthelmintic used to treat enterobiasis caused by *Enterobius vermicularis* (pinworm). It is believed to interfere with glucose uptake by pinworms. Pyrvinium pamoate was approved by the FDA in 1982 as a 50mg/5mL oral suspension and a 50mg oral tablet. Pyrvinium pamoate has been approved as a single dose of 5mg/kg for adults and adolescents but can go up to 350mg as a single dose for adults regardless of weight. This single dosage is repeated after two to three weeks if necessary. Reported side effects of pyrvinium pamoate include diarrhoea, nausea and vomiting, stomach cramps, skin rash and increased sensitivity of skin to sunlight. As for niclosamide, pyrvinium pamoate is on the list of FDA drugs that have been discontinued not because they are not safe or efficacious (FDA, 2018; T. C. Smith, Kinkel, Gryczko, & Goulet, 1976; Turner & Johnson, 1962).

4.6.5 Tacrolimus

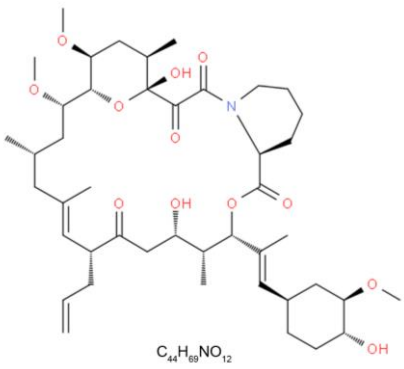

Fig. 4.10 Structure and molecular formula of tacrolimus *(ChemSpider ID: 393220).*

Tacrolimus is also known as fujimycin and FK506 (commonly used brand names: Prograf®, Advagraf® and Astagraf XL®) (Fig. 4.10). It is an immunosuppressive agent, specifically a calcineurin inhibitor, that is used for the prophylaxis of organ rejection after allogenic organ transplant. It was first approved by the FDA in 1994 for use in liver transplant which has been extended to include kidney, heart, small bowel, pancreas, lung, trachea, skin, cornea and limb transplants. Its indication now also includes the use of topical treatment for severe atopic

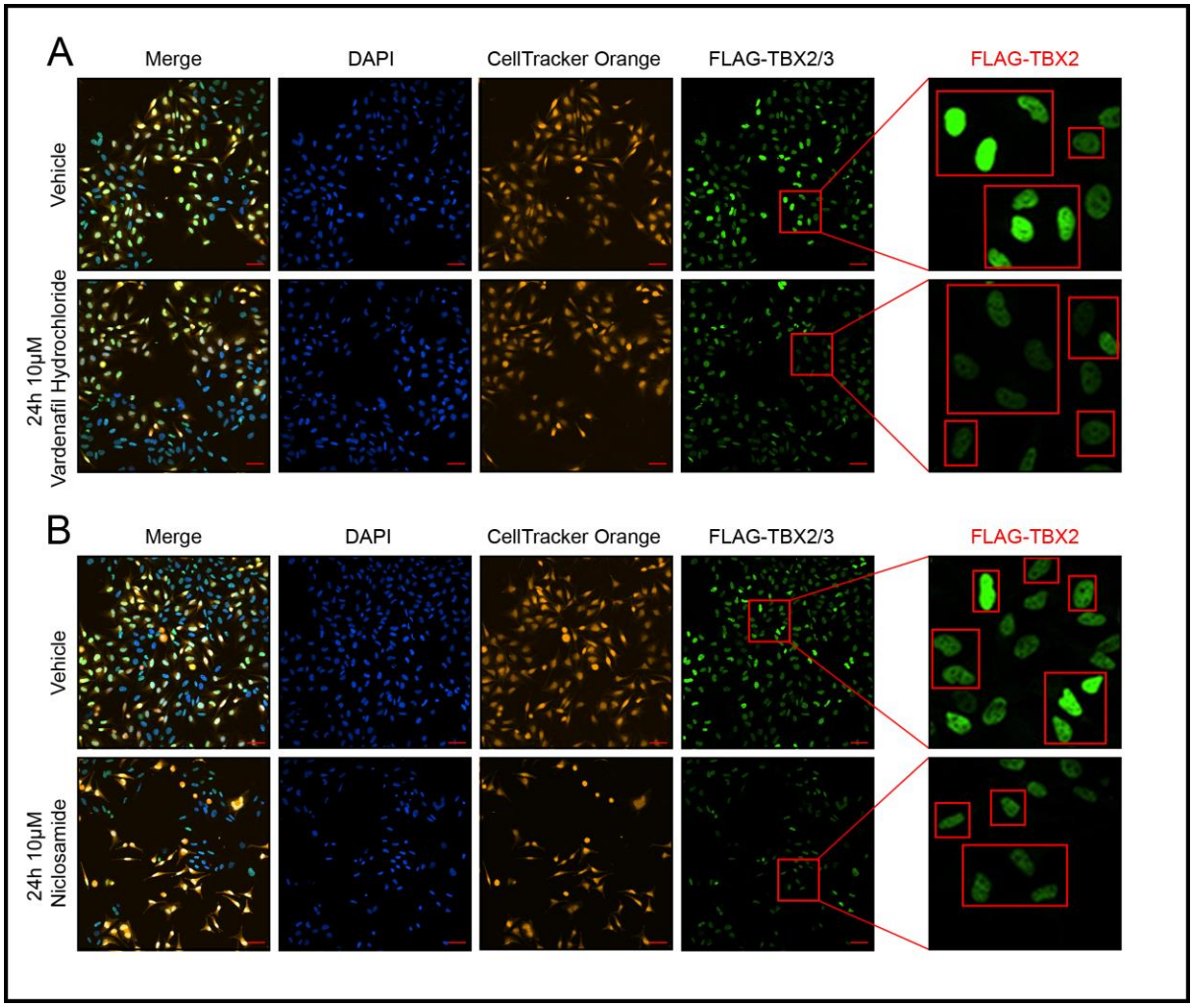

Fig. 4.11 High throughput screen immunofluorescence images of selected 'hit' FDA-approved drugs that downregulate TBX2 protein levels. *Representative IN Cell Analyzer 6000 images of inducible TBX2-FLAG 501mel and inducible TBX3-FLAG 501mel co-cultured cells treated for 24h with 20ng/mL doxycycline followed by 10μM (A) vardenafil hydrochloride and (B) niclosamide or vehicle for 24h. The TBX2-FLAG population was pre-stained with CellTracker Orange and a FLAG antibody with an Alexa Fluor 488 conjugated secondary antibody was used to detect FLAG-tagged TBX2 and TBX3. Nuclei were stained with DAPI. The scale bar is 60μm. Close up images in the far right panel show TBX2-FLAG expressing cells in red outlined boxes (identified from CellTracker Orange staining) with unboxed cells expressing TBX3-FLAG.*

have been approved by the FDA: highest dosage of 5mg for oral and extended release capsules, 1mg oral suspension, 5mg/mL solution for intravenous administration and a topical ointment with highest tacrolimus content of 0.1%. The highest oral capsule dose of tacrolimus administered is 0.2mg/kg/day for both adult and paediatric patients. Intravenous administration is reserved for patients who cannot tolerate capsules orally. The most common side effects of tacrolimus in patients receiving transplants include infection, tremors, high blood pressure, kidney problems, constipation, diarrhoea, headache, stomach pain,

dermatitis, trouble sleeping, nausea, swelling of the hands, ankles or legs, weakness, pain, high levels of phosphate, potassium or fat in the blood and anaemia (Astellas Pharma, 2012; FDA, 2018).

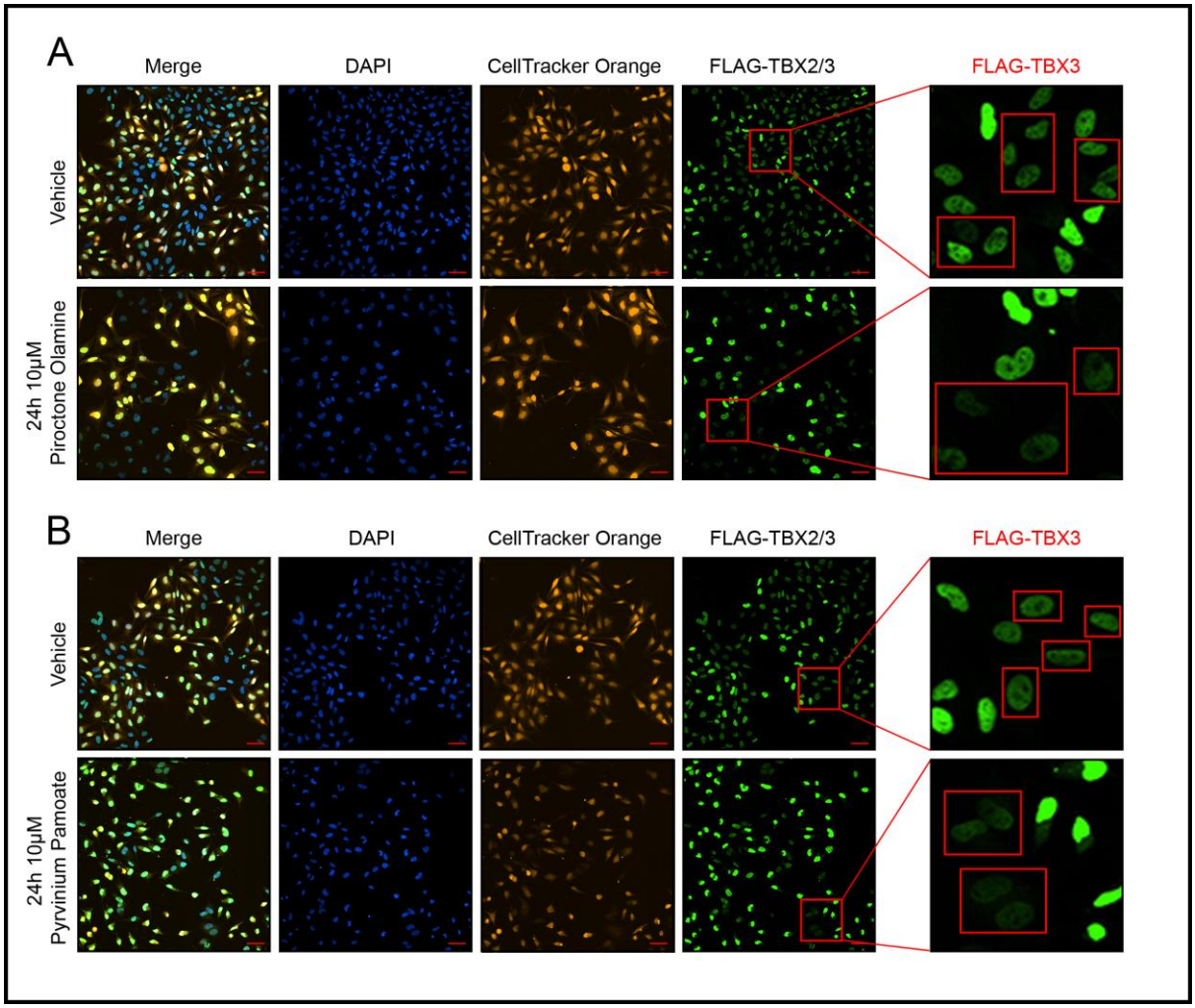

Fig. 4.12 High throughput screen immunofluorescence images of selected 'hit' FDA-approved drugs that downregulate TBX3 protein levels. *Representative IN Cell Analyzer 6000 images of inducible TBX2-FLAG 501mel and inducible TBX3-FLAG 501mel co-cultured cells treated for 24h with 20ng/mL doxycycline followed by 10μM (A) pyrvinium pamoate and (B) piroctone olamine or vehicle for 24h. The TBX2-FLAG population was pre-stained with CellTracker Orange and a FLAG antibody with an Alexa Fluor 488 conjugated secondary antibody was used to detect FLAG-tagged TBX2 and TBX3. Nuclei were stained with DAPI. The scale bar is 60μm. Close up images in the far-right panel show TBX3-FLAG expressing cells in red outlined boxes with unboxed cells expressing TBX2-FLAG (identified from CellTracker Orange staining).*

4.7 Validation of selected 'hits'

In the drug screen described earlier, niclosamide, vardenafil hydrochloride, piroctone olamine, pyrvinium pamoate and tacrolimus were used at 10μM and the

immunofluorescence results show that their inhibitory effects on TBX2/3 levels was most effective at the 24h timepoint. The selected 'hit' drugs were therefore tested under these conditions and all the drugs, but pyrvinium pamoate, were successfully validated (Fig. 4.14A and Fig. 4.15A). Indeed, quantification of nuclear TBX2/3-FLAG fluorescence intensity shows that niclosamide, vardenafil hydrochloride and tacrolimus significantly downregulated ($p<0.001$) nuclear TBX2-FLAG (Fig. 4.14B) and piroctone olamine and tacrolimus significantly downregulated ($p<0.001$) nuclear TBX3-FLAG (Fig. 4.15B) levels. Interestingly, in the validation experiments 10μM of pyrvinium pamoate almost completely killed the cells and therefore the cells were treated with 2.5μM of this drug which did not result in a significant decrease of TBX3-FLAG (Fig. 4.15).

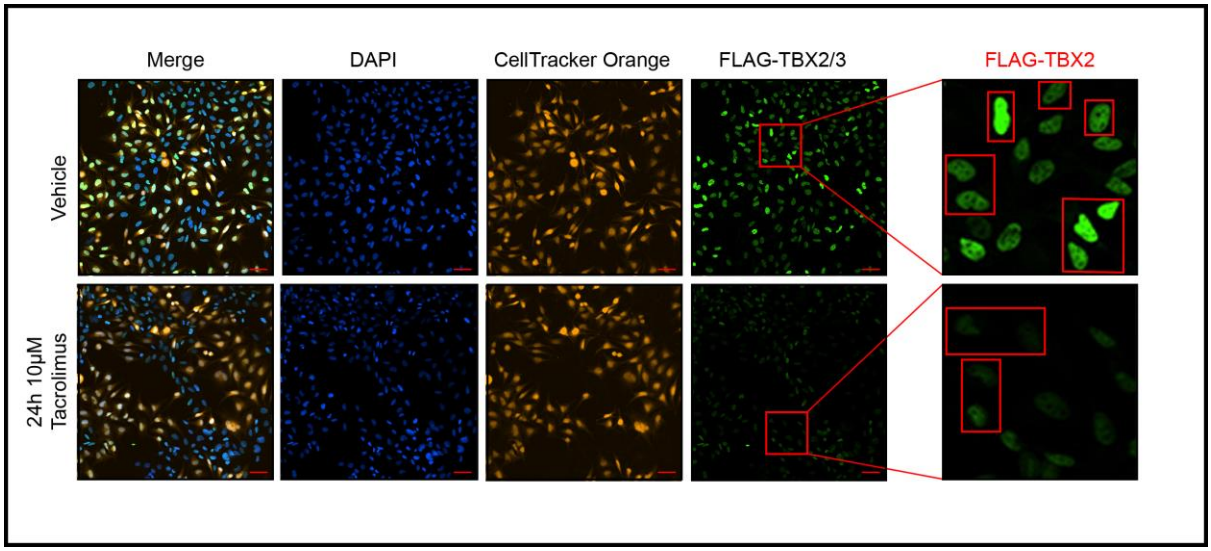

Fig. 4.13 High throughput screen immunofluorescence images of selected 'hit' FDA-approved drug tacrolimus that downregulates TBX2 and TBX3 protein levels. *Representative IN Cell Analyzer 6000 images of inducible TBX2-FLAG 501mel and inducible TBX3-FLAG 501mel co-cultured cells treated for 24h with 20ng/mL doxycycline followed by 10μM tacrolimus or vehicle for 24h. The TBX2-FLAG population was pre-stained with CellTracker Orange and a FLAG antibody with an Alexa Fluor 488 conjugated secondary antibody was used to detect FLAG-tagged TBX2 and TBX3. Nuclei were stained with DAPI. The scale bar is 60μm. Close up images in the far-right panel show TBX2-FLAG expressing cells (identified from CellTracker Orange staining) in red outlined boxes with unboxed cells expressing TBX3-FLAG.*

The inducible TBX2/3-FLAG 501mel cells were treated with the selected 'hit' drugs under conditions described above and the inhibitory effects of the drugs on TBX2/3 levels were further validated by western blotting with a FLAG-antibody. Consistent with the immunofluorescence data for TBX2-FLAG (Fig. 4.14), treatment with vardenafil hydrochloride,

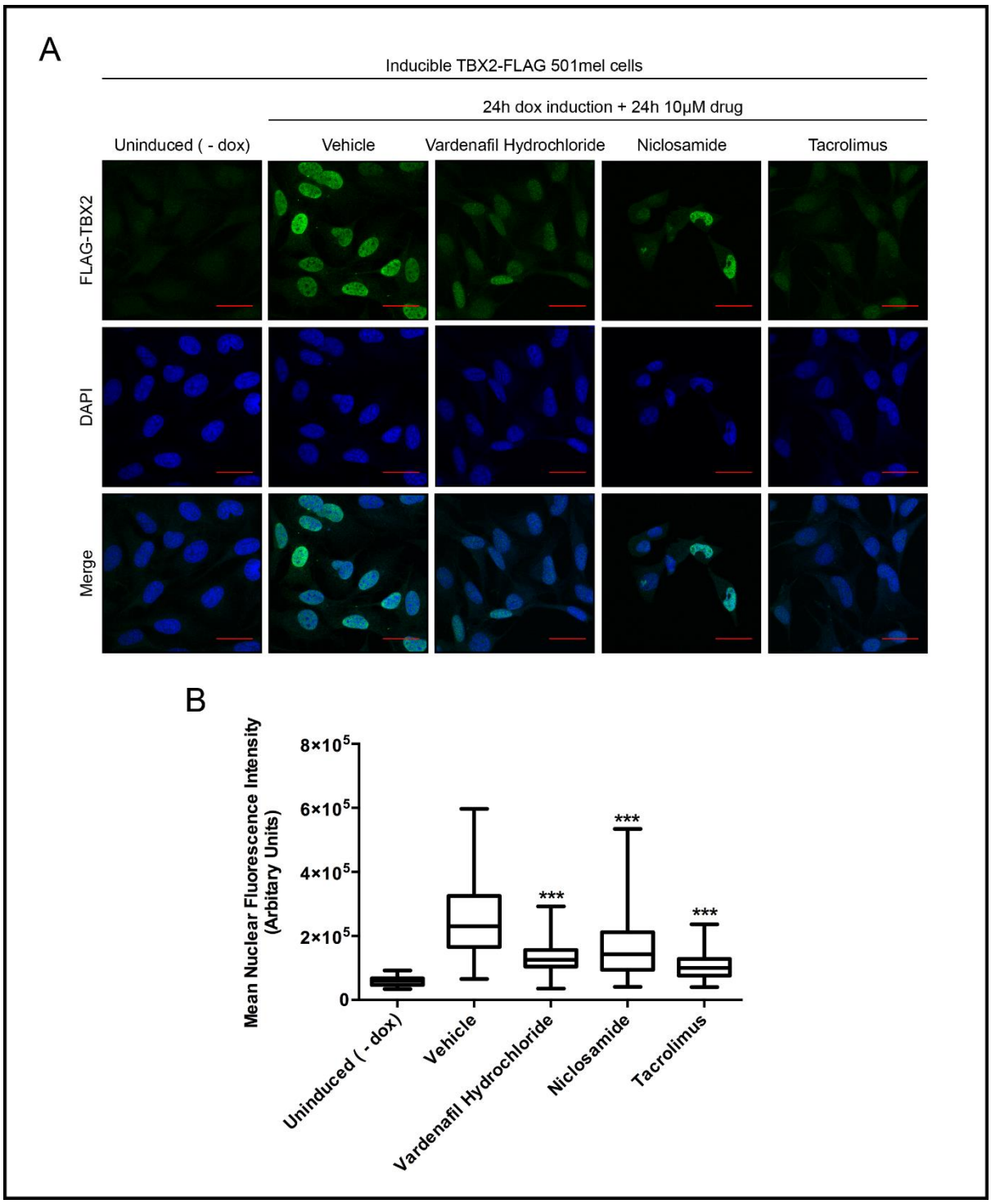

Fig. 4.14 Validation of selected 'hit' compounds identified to downregulate TBX2 protein levels. *(A) Representative confocal immunofluorescence maximum intensity projection images (630X; Carl Zeiss LSM 880) of inducible TBX2-FLAG 501mel cells induced with doxycycline (dox) for 24h followed by 10μM drug or vehicle treatment for 24h. Ectopic TBX2-FLAG was detected with a FLAG antibody and an Alexa Fluor 488 conjugated secondary antibody. Nuclei of cells were stained with DAPI. Scale bar is 20μm. (B) Box plots represent quantification of TBX2-FLAG levels per treatment condition as mean nuclear Alexa Fluor 488 fluorescence from 20 fields of view pooled from three independent repeats. Data was analysed using GraphPad Prism 6.0 and a parametric unpaired t-test was performed where, *p<0.05, **p<0.01, ***p<0.001.*

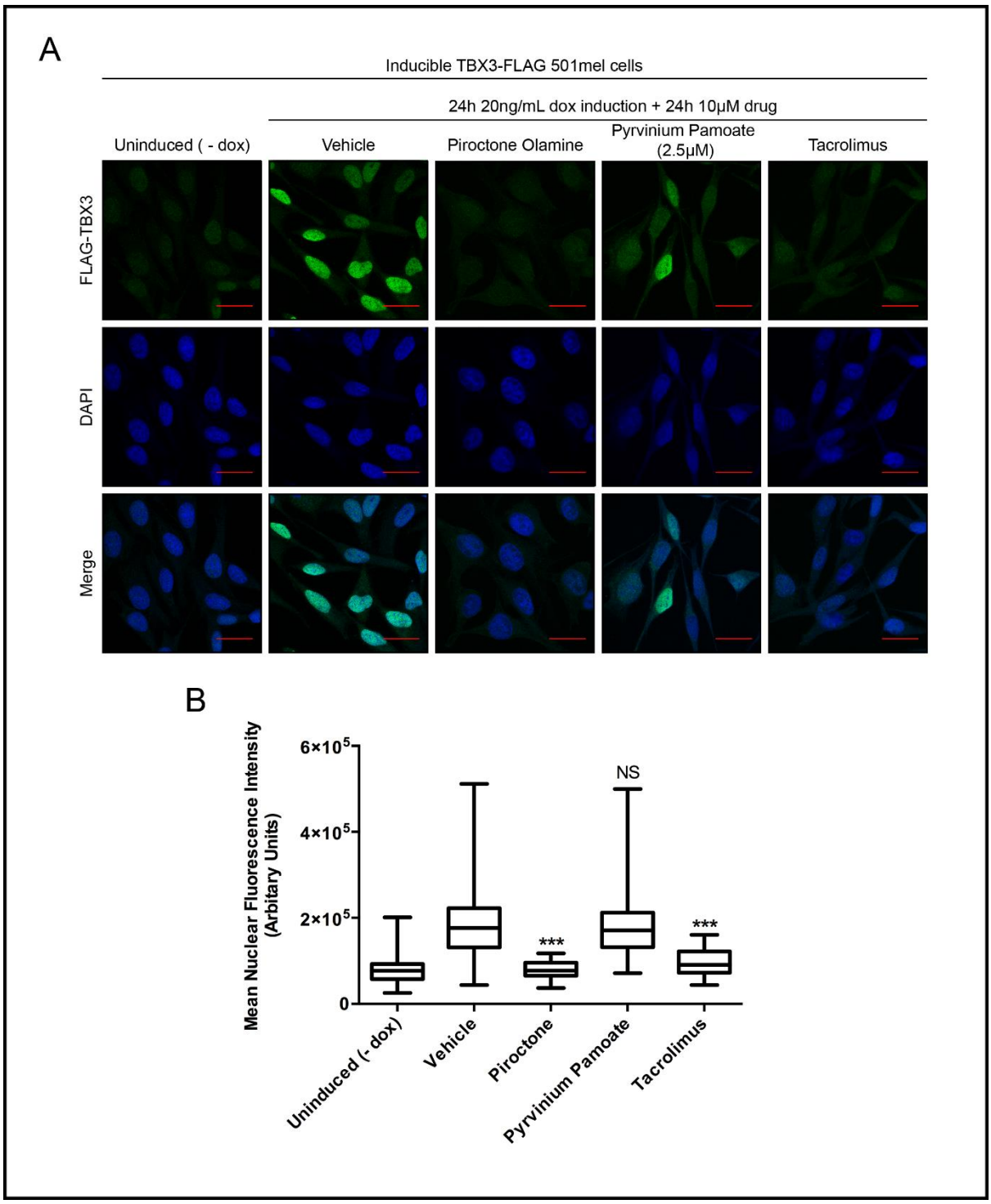

Fig. 4.15 Validation of selected 'hit' compounds identified to downregulate TBX3 protein levels. *(A) Representative confocal immunofluorescence maximum intensity projection images (630X; Carl Zeiss LSM 880) of inducible TBX3-FLAG 501mel cells induced with doxycycline (dox) for 24h followed by 10μM drug (2.5μM for pyrvinium pamoate due to cell sensitivity) or vehicle treatment for 24h. Ectopic TBX3-FLAG was detected with a FLAG antibody and an Alexa Fluor 488 conjugated secondary antibody. Nuclei of cells were stained with DAPI. Scale bar is 20μm. (B) Box plots represent quantification of TBX3-FLAG levels per treatment condition as mean nuclear Alexa Fluor 488 fluorescence from 20 fields of view pooled from three independent repeats. Data was analysed using GraphPad Prism 6.0 and a parametric unpaired t-test was performed where, *p<0.05, **p<0.01, ***p<0.001, NS = not significant.*

tacrolimus and niclosamide resulted in a dramatic decrease in TBX2-FLAG levels (Fig. 4.16A). Also similar to the immunofluorescence results for TBX3-FLAG (Fig. 4.15), piroctone olamine and tacrolimus treatment was effective at decreasing TBX3-FLAG levels and cells treated with 2.5µM pyrvinium pamoate had only a modest downregulation of TBX3-FLAG levels (Fig. 4.16B).

To test the effect of the selected 'hits' on endogenous TBX2 and TBX3 levels, the parental 501mel cells were treated with 10µM of niclosamide, vardenafil hydrochloride, piroctone olamine and tacrolimus and 2.5µM pyrvinium pamoate for 24h and western blotting was performed using antibodies specific to TBX2 and TBX3 (Fig. 4.16C). Interestingly, the western blots probed with an antibody to TBX2 reveal that while niclosamide was able to effectively downregulate endogenous TBX2, vardenafil hydrochloride and tacrolimus were not. The western blots probed for endogenous TBX3 on the other hand showed that piroctone olamine and pyrvinium pamoate were able to effectively downregulate TBX3 but, as was the case for TBX2, tacrolimus had no effect on TBX3. Quite unexpectedly, piroctone olamine and pyrvinium pamoate, the TBX3 'hit' drugs, were also able to inhibit endogenous TBX2 protein levels and niclosamide, the TBX2 'hit' drug, was able to inhibit endogenous TBX3 protein levels. This can possibly be explained by the fact that these drugs were identified as 'hits' for their ability to downregulate ectopic TBX2/3 i.e. posttranscriptional mechanisms, but in an endogenous setting, niclosamide may be able to transcriptionally downregulate TBX3 and piroctone olamine and pyrvinium pamoate may be able to transcriptionally downregulate TBX2.

It was hypothesised that failure to reproduce the inhibitory effect of tacrolimus and vardenafil hydrochloride on endogenous TBX2/3 levels was due to these 'hit' drugs interfering with the Tet-On system and therefore resulting in artefactual positive results in the screen and initial validation experiments in the inducible cell lines. To test this, induced pluripotent stem cells (iPSCs) engineered to express Cas9 using the Tet-On system (kindly provided by Professor Musa Mhlanga, University of Cape Town), were induced with 20ng/mL (same concentration as used for the inducible TBX2/3-FLAG 501mel cells) and 2µg/mL (concentration used by the Mhlanga lab) for 24h and treated with 10µM tacrolimus or 10µM piroctone olamine (included as a negative control) or vehicle for 24h. RNA was extracted and qRT-PCR was performed with

primers specific to Cas9. As hypothesised, tacrolimus but not piroctone olamine, was able to convincingly reduce Cas9 levels. This shows that tacrolimus, and possibly vardenafil hydrochloride, does indeed reduce TBX2/3 levels by blocking the Tet-On system rather than acting directly on these proteins. It is, for example, possible that these drugs prevent doxycycline from activating the Tet-On system and consequently the expression of TBX2/3-FLAG (Fig. 4.17).

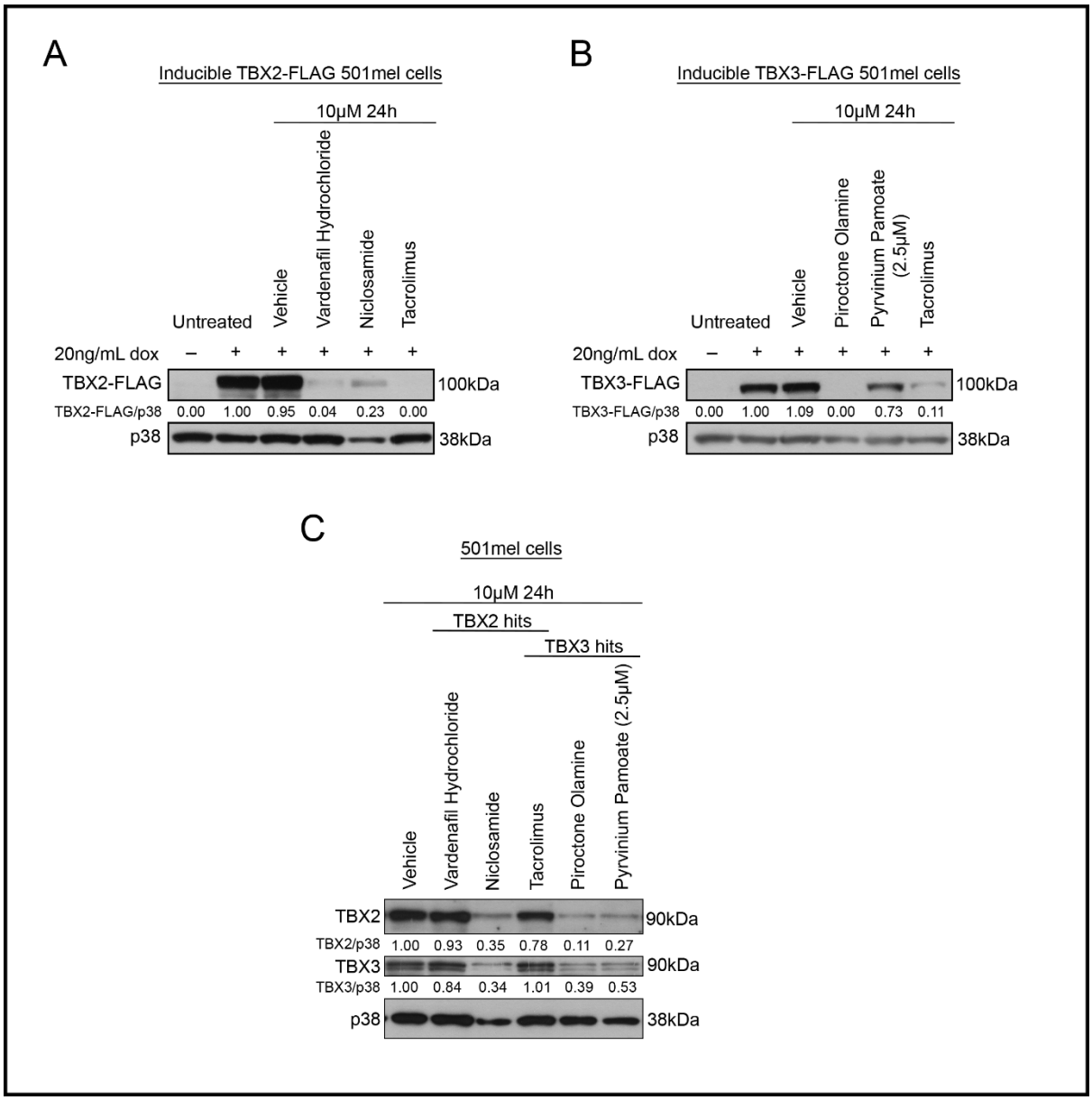

Fig. 4.16 Ectopic and endogenous validation of selected 'hit' compounds identified to downregulate TBX2 and/or TBX3 protein levels. *Ectopic TBX2 (A) and TBX3 (B) protein levels detected by western blotting using a FLAG antibody in inducible TBX2-FLAG 501mel and inducible TBX3-FLAG 501mel cells respectively induced with doxycycline (dox) for 24h followed by 10μM drug (2.5μM for pyrvinium pamoate due to cell sensitivity) or vehicle treatment for 24h. (C) Endogenous TBX2 and TBX3 levels in 501mel parental cell lines following 24h treatment with 10μM drug or vehicle determined by western*

blotting using antibodies to TBX2 and TBX3. (D) Western blot analyses of TBX2 and TBX3 protein levels in 501mel cells pre-treated with 5μM MG-132 prior to the addition of 10μM drug or vehicle for 24h. For all western blots p38 was used as a loading control. Densitometry readings were obtained using ImageJ and protein expression levels are represented as a ratio of protein of interest/p38 normalised to the vehicle control sample (where possible). Blots are representative of at least two independent repeats.

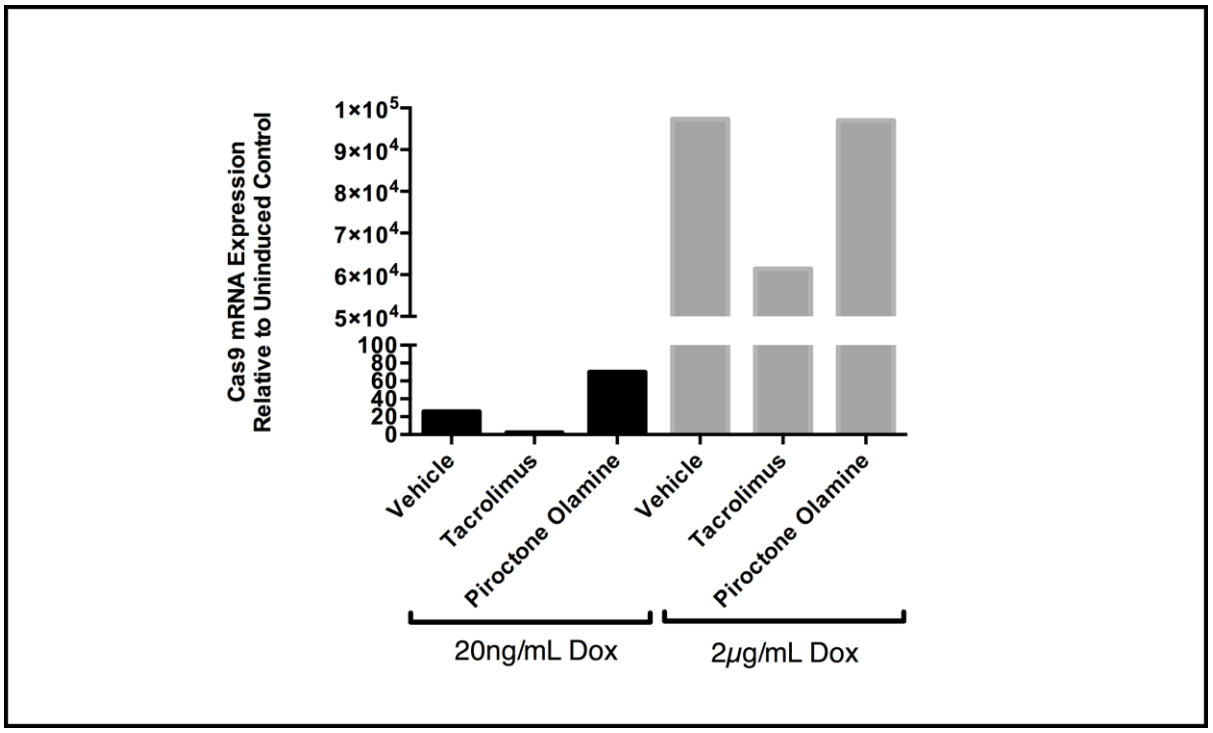

Fig. 4.17 The effect of tacrolimus on another Tet-On inducible system. *Quantitative RT-PCR performed on reverse transcribed RNA extracted from Tet-On inducible Cas9 stem cells induced with 20ng/mL or 2μg/mL doxycycline (dox) for 24h followed by treatment with 10μM tacrolimus, piroctone olamine and vehicle for 24h. Primers specific to Cas9 were used, mRNA levels were normalised to β-actin and expressed relative to the uninduced control.*

4.8 Posttranscriptional regulation of TBX2/3

Niclosamide, piroctone olamine and pyrvinium pamoate were successfully validated to downregulate endogenous levels of TBX2 and TBX3 in 501mel cells (Fig. 4.16C) and therefore, they were taken forward for further characterising. To explore the mechanism(s) by which these drugs impact TBX2/3 protein levels the possibility was considered that it may involve targeting them for degradation through the proteasome. To test this, 501mel cells were pre-treated with the 26S proteasome inhibitor MG-132 prior to drug treatment followed by western blotting (Fig. 4.18). Consistent with previous results (Fig. 4.16C), in the absence of MG-132, niclosamide, piroctone olamine and pyrvinium pamoate downregulated TBX2 levels. Importantly, this effect was rescued i.e. TBX2 levels increased in the presence of MG-132. This

suggests that these drugs are targeting TBX2 through ubiquitination for degradation through the 26S proteasome. It is worth noting that MG-132 also increased TBX2 levels in vehicle treated cells which suggests that basal levels of TBX2 are also regulated by the 26S proteasome. In keeping with previous results (Fig. 4.16C), TBX3 levels were downregulated by niclosamide, piroctone olamine and pyrvinium pamoate treatment in the absence of MG-132. Interestingly, in the presence of MG-132, the levels of TBX3 remained unchanged when treated with niclosamide and decreased further when treated with piroctone olamine and pyrvinium pamoate. MG-132 also decreased TBX3 levels in vehicle treated cells. Together these results suggest that basal levels of TBX3 as well as the impact of these drugs on TBX3 levels are not regulated by the 26S proteasome. A possible explanation for the decrease of TBX3 in the presence of MG-132 may relate to previous findings in the Prince laboratory that TBX2 is capable of transcriptionally repressing TBX3 (unpublished data). Indeed, the high levels of TBX2 in the presence of MG-132 correlates with decreased levels of TBX3.

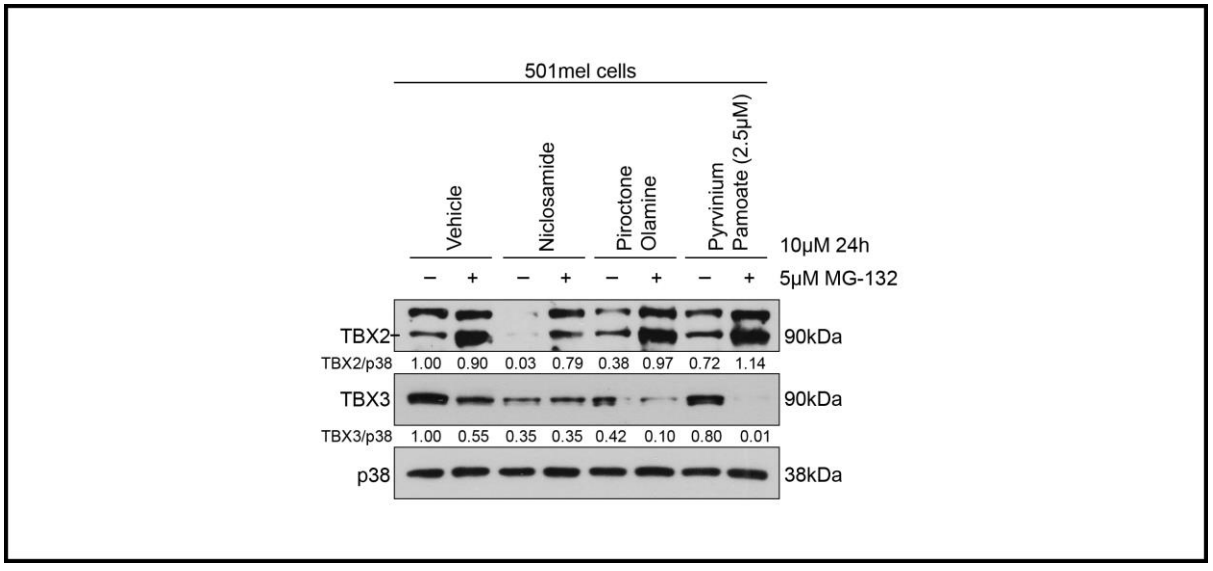

Fig. 4.18 Niclosamide, piroctone olamine and pyrvinium pamoate regulation of TBX2 and TBX3. *501mel cells pre-treated with 5μM MG-132 prior to the addition of vehicle, 10μM niclosamide, 10μM piroctone olamine or 2.5μM pyrvinium pamoate for 24h followed by western blotting with antibodies to TBX2 and TBX3. p38 was used as a loading control. Densitometry readings were obtained using ImageJ and protein expression levels are represented as a ratio of protein of interest/p38 normalised to the vehicle control sample. Blots are representative of at least two independent repeats.*

4.8.1 The effect of drug-induced TBX2/3 inhibition on cell viability

The next set of experiments were performed to determine whether niclosamide, piroctone olamine and pyrvinium pamoate exhibit anti-cancer activity through negatively regulating

TBX2/3. Briefly, the inducible TBX2/3-FLAG 501mel cells were treated with vehicle or drug for 12h and then dox was added to induce TBX2/3 for another 12h after which MTT cell viability assays were performed. As a control for these experiments, western blots were performed to confirm that the drugs tested did indeed inhibit TBX2/3 levels and that dox induced TBX2/3 levels (Fig. 4.19A and B). It is important to point out that niclosamide was very effective at reducing both endogenous (-dox) and inducible (+dox) TBX2 and TBX3 levels. The MTT assays for TBX2/3-FLAG 501mel cells (Fig. 4.19A and B) show that while niclosamide, piroctone olamine and pyrvinium pamoate treatment significantly reduces cell viability, induction of TBX2 or TBX3 did not significantly rescue this effect. However, albeit not statistically significant, induction of TBX2 or TBX3 in cells treated with pyrvinium pamoate showed a trend towards increased cell viability. It is important to note that dox on its own significantly reduced cell viability which may mask any ability of ectopic TBX2/3 to rescue the cytotoxic/anti-cancer effect of these drugs. Furthermore, future experiments to elucidate the functional significance of the inhibition of TBX2/3 by niclosamide, piroctone olamine and pyrvinium pamoate on cancer cells should include senescence, proliferation and migration assays.

4.8.2 Effect of further depletion of TBX2/3 by shRNA on sensitivity to drug treatment

The next set of experiments were performed to determine if further depletion of TBX2/3 by shRNA would sensitise 501mel cells to treatment with niclosamide, piroctone olamine or pyrvinium pamoate. Briefly, shControl 501mel and shTBX2/3 501mel cells (already available in the Prince laboratory; Peres et al., 2010) were treated with the drugs for 24h as previously described and cell viability assays were performed. Western blots in Fig. 4.20A and B confirm that TBX2 and TBX3 levels were indeed knocked down in the shTBX2/3 cells used. As expected, niclosamide and pyrvinium pamoate significantly reduced the viability of all cells tested (Fig. 4.20). The reason why piroctone olamine did not significantly reduce cell viability as previously observed (Fig. 4.19A and B) is not clear. Importantly, whereas knocking down TBX2 further sensitised 501mel cells to niclosamide (Fig. 4.20A), knocking down TBX3 had the opposite effect (Fig. 4.20B). It is tempting to speculate that the latter effect may relate to the knockdown of TBX3 levels leading to an increase in TBX2 levels causing cells to become more resistant to niclosamide treatment. The rationale for this is that the Prince laboratory has

reported that TBX2 is a powerful pro-proliferative factor in 501mel cells (Peres et al., 2010) and that TBX3 is able to repress TBX2 (Li et al., 2014). Knocking down TBX2 or TBX3 had no significant effect on the ability of piroctone olamine and pyrvinium pamoate to inhibit cell viability. It is however worth noting that, while not statistically significant, the shTBX3 cells do appear to be more sensitive to these two drugs. Future experiments should examine the levels of TBX2 and TBX3 in the cells following drug treatment and should test the effect of niclosamide, piroctone olamine or pyrvinium pamoate on 501mel cell proliferation and migration.

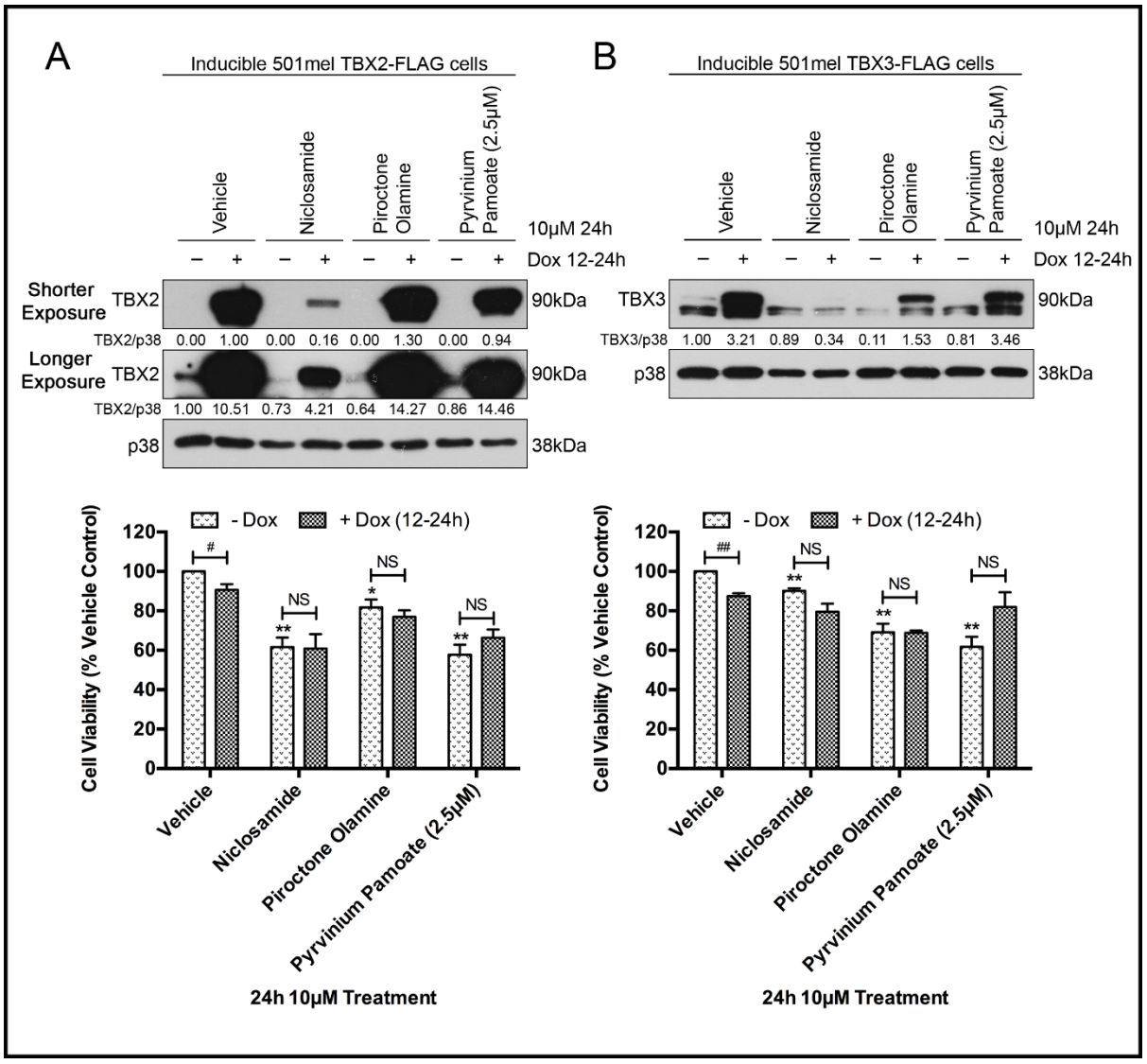

Fig. 4.19 Proof-of-concept: effect of drug-induced TBX2/3 inhibition on cell viability. *Inducible TBX2-FLAG 501mel cells (A) and inducible TBX3-FLAG 501mel cells (B) were treated with 10μM drug (2.5μM pyrvinium pamoate) or vehicle for 24h. After 12h of drug treatment 100ng/mL and 200ng/mL doxycycline (dox) was added to the drug-containing medium of the TBX2-FLAG and TBX3-FLAG cells to induce TBX2/3 expression respectively. TBX2 and TBX3 antibodies were used to detect protein levels by*

*western blotting and cell viability was measured using MTT assays. For western blots p38 was used as a loading control. Densitometry readings were obtained using ImageJ and protein expression levels are represented as a ratio of protein of interest/p38 normalised to the vehicle control sample (where appropriate). Blots are representative of at least two independent repeats. Graphs show mean cell viability as a percentage of vehicle control ± SEM for each concentration of drug determined from three independent experiments performed in quadruplicate. Data was analysed using GraphPad Prism 6.0 and a parametric unpaired t-test was performed where, *p<0.05, **p<0.01, ***p<0.001, NS = not significant.*

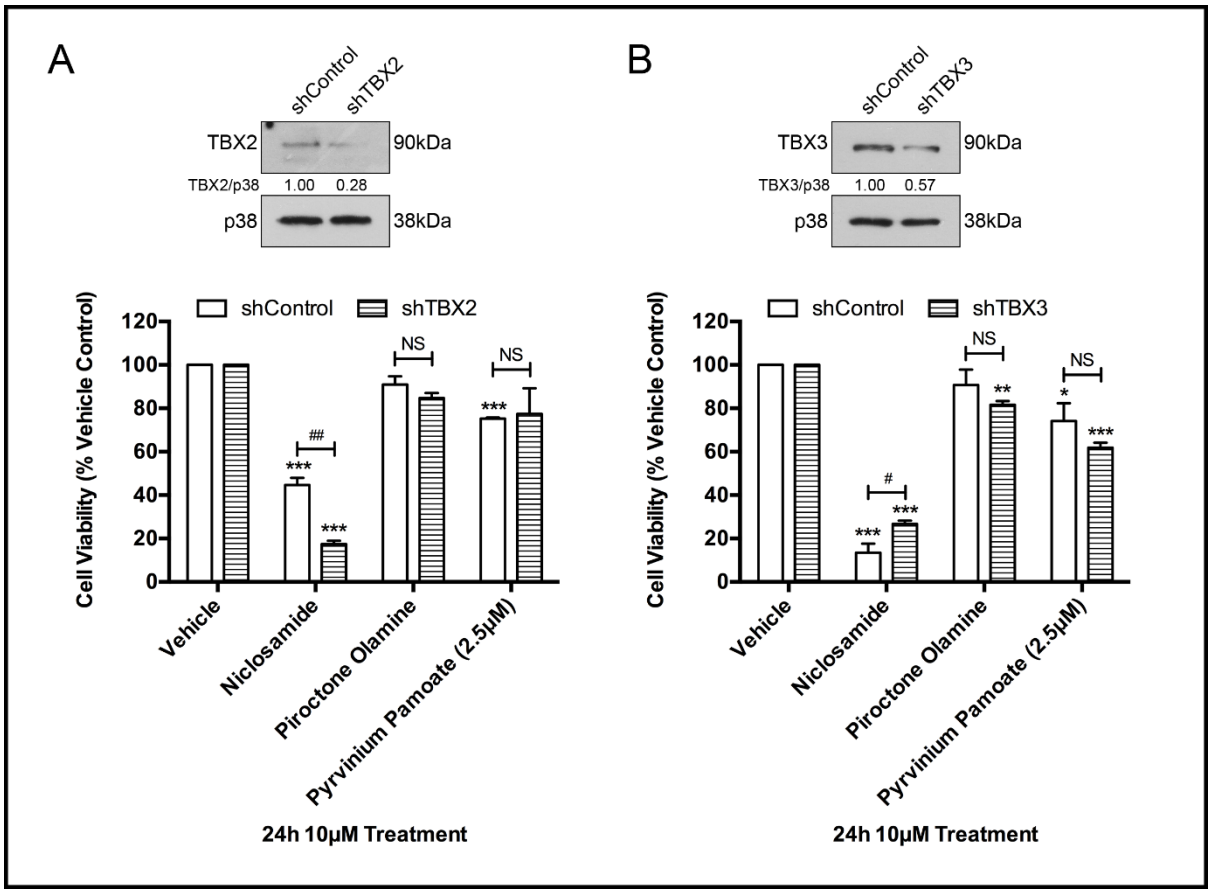

Fig. 4.20 Proof-of-concept: effect of further depletion of TBX2/3 by shRNA on sensitivity to drug treatments. *Levels of TBX2 in 501mel shTBX2 and shControl stable cell lines using western blotting with an antibody to TBX2 and cell viability MTT assays on the cell lines treated with 10μM drug (2.5μM pyrvinium pamoate) or vehicle for 24h. Graphs show mean cell viability as a percentage of vehicle control ± SEM for each concentration of drug determined from three independent experiments performed in quadruplicate. (B) Levels of TBX3 in 501mel shTBX3 and shControl stable cell lines using western blotting with an antibody to TBX3 and cell viability MTT assays on the cell lines as described in (A). For western blots p38 was used as a loading control. Densitometry readings were obtained using ImageJ and protein expression levels are represented as a ratio of protein of interest/p38 normalised to the vehicle control sample. Blots are representative of at least two independent repeats. Cell viability data was analysed using GraphPad Prism 6.0 and a parametric unpaired t-test was performed. '*' represents significant difference between vehicle and drug treated cells and '#' represents significant difference between shControl and shTBX2/3 cell lines, where */#p<0.05, **/##p<0.01, ***/###p<0.001, NS = not significant.*

4.8.3 The effect of selected 'hit' drugs on RMS cells

The drug screen was conducted using the inducible TBX2/3-FLAG 501mel cell lines and therefore the validation and preliminary proof-of-concept experiments, described above, were performed in the 501mel cells. It was however hypothesised that the anti-cancer activity of the 'hit' drugs may extrapolate to other TBX2/3 driven cancers including RMS. To test this, ARMS (RH30) and ERMS (RD) cells were treated with 10µM of niclosamide, 10µM piroctone olamine, 2.5µM pyrvinium pamoate or vehicle for 24h and levels of TBX2 and TBX3 were detected using western blotting. All three drugs convincingly downregulated TBX2 in ARMS and both TBX2 and TBX3 in the ERMS cells (Fig. 4.21A). Of the three drugs tested, only pyrvinium pamoate decreased TBX3 levels in the RH30 cell line. Together these findings suggest that niclosamide, piroctone olamine and pyrvinium pamoate also inhibit TBX2 levels in ARMS and ERMS cells and inhibit TBX3 levels in ERMS cells.

To investigate the anti-cancer activity of niclosamide, piroctone olamine and pyrvinium pamoate in RMS cells, cell viability assays were performed with a range of drug concentrations and IC_{50} values were calculated where possible. As shown in Fig. 4.21B, the RH30 and RD cells were most sensitive to pyrvinium pamoate with IC_{50} values of 7.10µM and 3.30µM respectively, followed by niclosamide with IC_{50} values of 11.06µM and 6.79µM respectively. In both RH30 and RD cells, piroctone olamine had an initial impact on cell viability but as the concentration of the drug increased this effect seemed to plateau. Light microscopy images show that niclosamide and pyrvinium pamoate treatment of RH30 and RD cells resulted in cell shrinkage and rounding indicative of cell death (Fig. 4.21C). Interestingly, piroctone olamine and pyrvinium pamoate treatment caused flattening and enlargement of both RH30 and RD cells typical of a senescent phenotype (Fig. 4.21C). Future experiments should confirm this possibility because it may reveal that these drugs can be used as pro-senescence therapy by a mechanism involving their ability to inhibit TBX2/3. This would be particularly exciting given the well described anti-senescence activity of TBX2 and TBX3 (Brummelkamp et al., 2002; Carlson et al., 2001; Lingbeek, Jacobs, & van Lohuizen, 2002; Yarosh et al., 2008). Lastly, it is interesting to note that compared to the RH30 cells, the RD cells are more sensitive to niclosamide and pyrvinium pamoate. This may relate to these drugs inhibiting both TBX2 and TBX3 in the RD cells, but only TBX2 in the RH30 cells.

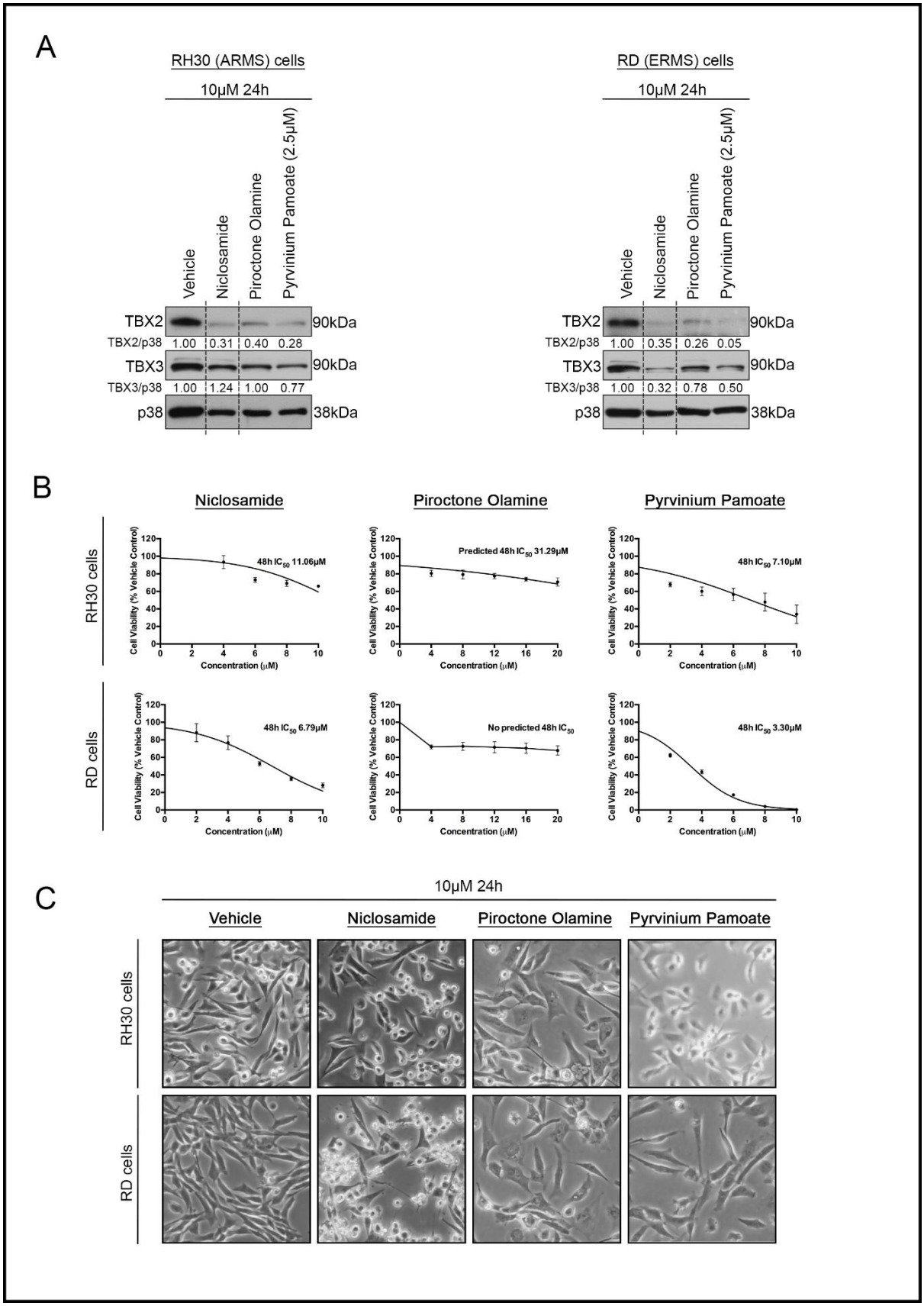

Fig. 4.21 The effect of selected 'hit' drugs on TBX2 and TBX3 levels in ERMS and ARMS cell lines. *Western blotting showing levels of TBX2 and TBX3 in ARMS (RH30 cell line) and ERMS (RD cell line) cells after 24h of 10μM drug (2.5μM pyrvinium pamoate) or vehicle treatment. p38 was used as a*

*loading control. Densitometry readings were obtained using ImageJ and protein expression levels are represented as a ratio of protein of interest/p38 normalised to the vehicle control sample. Blots are representative of at least two independent repeats. Broken lines in western blots show where lanes not relevant were removed. (B) MTT cell viability assays of RH30 and RD cells treated with a range of selected 'hit' drug concentrations and vehicle as indicated for 48h. Graphs show mean cell viability as a percentage of vehicle control ± SEM for each concentration of drug determined from three independent experiments performed in quadruplicate. Data was analysed using GraphPad Prism 6.0 and a parametric unpaired t-test was performed, where *p<0.05, **p<0.01, ***p<0.001, NS = not significant. (C) Representative light microscopy images (200X; EVOS XL AMEX1000 Core Imaging System) of RD and RH30 after 24h of 10μM drug (2.5μM pyrvinium pamoate) or vehicle treatment.*

4.9 HC StratoMineR Analyses

While niclosamide, piroctone olamine and pyrvinium pamoate were successfully identified and validated through z-score analyses, there was concern about the false positives that were identified (i.e. drugs that interact with the Tet-On system such as vardenafil hydrochloride and tacrolimus). Therefore, HC StratoMineR, a more powerful and sophisticated analysis tool was employed with the aim of instilling more confidence in the 'hit' lists. HC StratoMineR is a user-friendly web-based tool that has the power to mine multiparametric numerical datasets. This was made possible because while this study was primarily interested in 2 experimental end-point measurements viz TBX2/3-FLAG protein levels and subcellular localisation, there were 11 other potentially useful parameters that were also extracted/calculated during image analyses and hence the 13 parameters could be analysed by HC StratoMineR (Table 4.1).

HC StratoMineR analyses were performed for each Pharmakon drug library treatment timepoint tested (4, 12 and 24h) for TBX2-FLAG and TBX3-FLAG expressing cells (6 analyses in total). Key HC StratoMineR outputs included polar plots (Fig. 4.22A - Fig. 4.27A), 'hit' selection plots (Fig. 4.22B - Fig. 4.27B), and ranked 'hit' lists (Table 4.2 - Table 4.7). It is important to note that the p-values in the tables were filtered to only include drugs that downregulate TBX2/3 protein levels or block nuclear localisation but the original unfiltered ranked 'hit' lists can be found in Appendix 7.12. Furthermore, a cell count threshold of ≥ 25 cells per field of view was also applied.

Of the results obtained it is reassuring to note that HC StratoMineR analyses did not identify vardenafil hydrochloride as a 'hit' and it ranked tacrolimus as only the 16th 'hit' for TBX3 after 12h of treatment. This suggests that the HC StratoMineR analyses tool does indeed have the

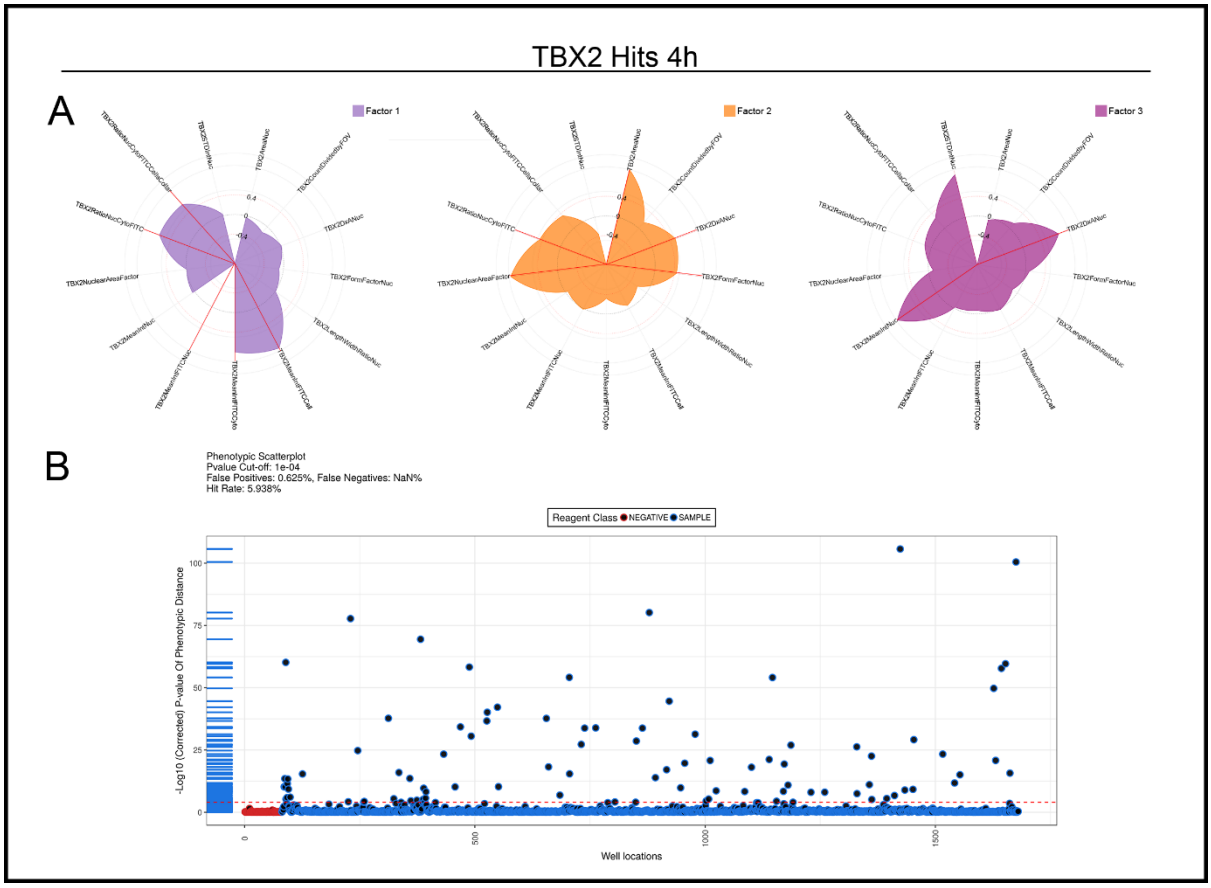

Fig. 4.22 HC StratoMineR analyses of TBX2-FLAG cells after 4h of drug library treatment. *(A) Polar plots representing 13 original parameters reduced into 3 factors. The polar angles represent the parameter names and the radius represents the factor loading of the parameter. A significant contribution is considered if >0.4 or <-0.4 and is indicated with a red line. (B) Phenotypic distance 'hit' selection plot calculated from factor scores transformed to p-values with a cut-off of p<1x10^{-4} (dotted red line).*

Table 4.2 *TBX2 4h 'hits' (filtered: Factor 1 <-2, Factor 2 <0, count >25). A 'hit' also detected as a TBX3 'hit' at this timepoint is indicated with an asterisk.*

	Comound	p-value	Distance Score	Factor 1	Factor 2	Factor 3
1	GENTIAN VIOLET	5.14E-59	8.06	-3.75	-7.24	1.62
2	DAUNORUBICIN*	6.99E-41	9.63	-2.68	-1.06	-9.04
3	DOXORUBICIN*	1.62E-34	7.07	-2.28	-1.24	-6.58
4	THIMEROSAL	1.08E-27	5.73	-2.03	-5.68	0.44
5	QUINACRINE HYDROCHLORIDE	5.25E-11	4.09	-3.17	-1.44	2.53
6	EPIRUBICIN HYDROCHLORIDE	2.36E-09	4.36	-2.11	-0.04	-3.79
7	EMETINE DIHYDROCHLORIDE	1.28E-07	3.55	-2.54	-2.78	0.55
8	DACTINOMYCIN	8.27E-07	3.32	-2.60	-1.16	-1.37

capacity to exclude or lower the 'hit' rank of possible false positive. Importantly, piroctone olamine was ranked 4th by HC StratoMineR analyses for its impact on TBX3 after 24h treatment which instils confidence in this drug as a 'hit' (Table 4.7). The information obtained for pyrvinium pamoate and niclosamide by HC StratoMineR analyses were however not

consistent with that obtained for the z-score analyses. Indeed, whereas HC StratoMineR analyses did not identify pyrvinium pamoate as a 'hit' and ranked niclosamide as a low TBX3 'hit' after 12h of treatment (Table 4.6), z-score analyses identified pyrvinium pamoate as a TBX3 'hit' and niclosamide as a TBX2 'hit' at the 24h timepoint. Niclosamide and pyrvinium pamoate were however validated to downregulate endogenous levels of both TBX2 and TBX3 (Fig. 4.16C) which suggests that it may be important to combine both analyses when deciding on 'hits.'

Interestingly, doxorubicin was identified as a 'hit' in the z-score analyses (Fig. 4.4C) and was the top ranked HC StratoMineR 'hit' for almost all time-points tested for TBX2 and TBX3 (Table 4.2 - Table 4.7 and Appendix 7.14). Since the aim of this study was to identify new anti-cancer drugs, doxorubicin was not validated and characterised because it is already used as an effective chemotherapeutic to treat acute lymphoblastic leukaemia, acute myeloblastic leukaemia, Wilms' tumour, neuroblastoma, soft tissue and bone sarcomas (including RMS), breast carcinoma, ovarian carcinoma, transitional cell bladder carcinoma, thyroid carcinoma, gastric carcinoma, Hodgkin's disease, malignant lymphoma and bronchogenic carcinoma (Bedford Laboratories, 2012; FDA, 2018). Together, the results do however suggest that TBX2 and TBX3 may be important targets of current efficacious chemotherapeutics which provides further evidence for them as novel therapeutic targets.

4.10 Discussion

Rhabdomyosarcoma presents a serious therapeutic challenge and a major strategy for developing new therapeutics is to target key molecular features of this cancer. In this regard, the transcription factors TBX2 and TBX3 are particularly interesting because they have been biologically validated as drug targets for several cancer types including rhabdomyosarcoma (Zhu et al. 2014; Sims 2016; Wansleben et al. 2014). Targeting transcription factors is, however, notoriously challenging because they do not have deep binding pockets to which small molecule inhibitors can be designed and their predominant nuclear localisation makes them less accessible to therapeutic agents (Dang et al., 2017; Redell & Tweardy, 2006; Yeh et al., 2013). Furthermore, the drug discovery and development pipeline is extremely arduous, expensive and risky and therefore repurposing of drugs for anti-cancer therapy has become

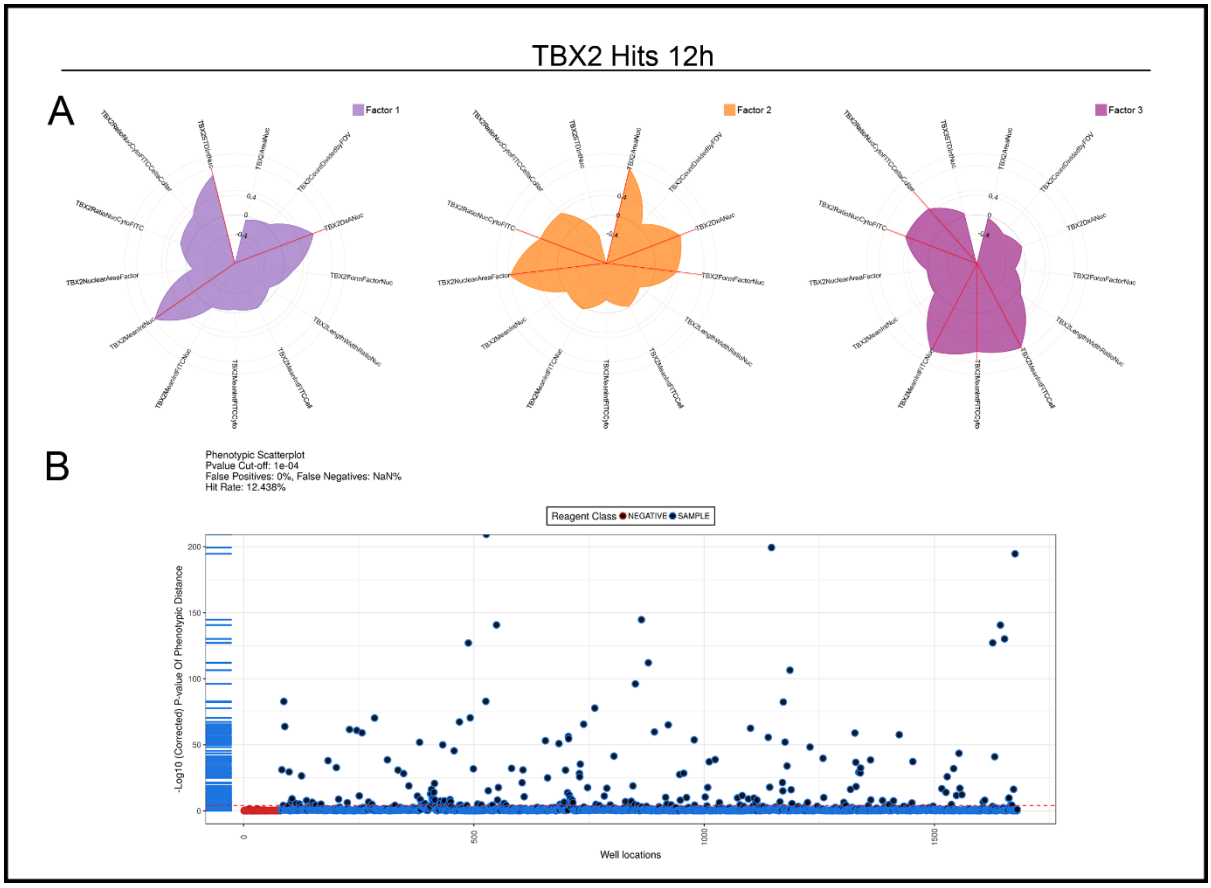

Fig. 4.23 HC StratoMineR analyses of TBX2-FLAG cells after 12h of drug library treatment. *(A) Polar plots representing 13 original parameters reduced into 3 factors. The polar angles represent the parameter names and the radius represents the factor loading of the parameter. A significant contribution is considered if >0.4 or <-0.4 and is indicated with a red line. (B) Phenotypic distance 'hit' selection plot calculated from factor scores transformed to p-values with a cut-off of p<1x10^{-4} (dotted red line).*

a popular cost and time effective alternative (Pammolli et al., 2011; Waring et al., 2015). This study therefore adopted a novel strategy by combining a targeted approach with drug repurposing. To this end, a high throughput cell-based immunofluorescence screen was conducted to identify FDA-approved drugs that could negatively regulate TBX2 and/or TBX3 protein levels and nuclear localisation. Metastatic melanoma cells (501mel), previously shown to be addicted to TBX2 and TBX3 for their cancer phenotype (Peres et al., 2010), were engineered to express inducible exogenous FLAG-tagged TBX2 or TBX3 using a Tet-On system and were screened with the Pharmakon 1600 drug library at 4, 12 and 24h timepoints. The rationale for using melanoma cells was two-fold. Firstly, the screen was done in collaboration with Professor Goding's laboratory (Ludwig Institute for Cancer Research, University of Oxford) who has a shared interest with the Prince laboratory in melanoma and based on the costs involved we could only screen one cancer type. Secondly, we hypothesised that any

Table 4.3 *TBX2 12h 'hits' (filtered: Factor 2 <0, Factor 3 <-2, count >25). A 'hit' also detected as a TBX3 'hit' at this timepoint is indicated with an asterisk.*

Ranking	Comound	p-value	Distance Score	Factor 1	Factor 2	Factor 3
1	DOXORUBICIN*	1.90E-145	10.99	-6.80	-2.52	-8.62
2	MITOXANTRONE HYDROCHLORIDE*	4.16E-42	6.22	-4.57	-2.15	-4.14
3	EPIRUBICIN HYDROCHLORIDE	1.69E-39	5.62	-1.69	-2.08	-5.26
4	CETRIMONIUM BROMIDE	5.39E-38	6.11	-4.28	-2.99	-2.75
5	CYTARABINE*	1.74E-32	5.39	4.96	-1.76	-2.17
6	ANCITABINE HYDROCHLORIDE*	1.56E-26	4.68	3.55	-1.42	-2.94
7	ETHIONAMIDE*	2.08E-21	4.04	-0.23	-1.77	-3.55
8	TRIFLURIDINE	2.73E-18	3.76	2.94	-0.99	-2.15
9	ETHACRYNIC ACID*	5.21E-17	3.75	0.06	-0.38	-3.45
10	CHLORTHALIDONE	1.01E-14	3.57	-0.52	-0.75	-3.19
11	CHLORPROMAZINE	9.28E-14	3.36	-0.73	-0.97	-2.90
12	ESTRONE	1.76E-13	3.26	-0.38	-0.94	-2.89
13	TIMOLOL MALEATE	2.55E-10	2.98	-0.74	-1.36	-2.35
14	CHLORPROPAMIDE	9.45E-10	3.21	-0.18	-0.86	-2.88
15	CHLORZOXAZONE	6.18E-09	3.02	-0.21	-0.98	-2.60
16	TOLAZOLINE HYDROCHLORIDE	6.25E-09	2.84	-0.02	-1.23	-2.40
17	BROXALDINE*	2.91E-08	3.73	0.04	-2.06	-3.06
18	FAMOTIDINE	2.93E-08	2.93	-0.48	-0.96	-2.45
19	PAMABROM	2.38E-07	2.60	-0.74	-1.18	-2.13
20	TOLBUTAMIDE	6.02E-07	2.61	-0.59	-1.03	-2.09
21	TRIAMTERENE	3.03E-06	2.55	-0.46	-0.17	-2.15
22	ETODOLAC	3.16E-06	2.51	-0.39	-1.22	-2.02
23	FLUTAMIDE	4.50E-06	2.52	0.09	-0.75	-2.23
24	ETHAMBUTOL HYDROCHLORIDE	8.06E-06	2.54	-0.29	-0.26	-2.15
25	CHLORAMPHENICOL SODIUM SUCCINATE	5.78E-05	2.45	0.18	-1.40	-2.19
26	DIXANTHOGEN	6.16E-05	2.51	-0.62	-1.05	-2.14

'hits' identified in the melanoma screen will also be relevant for other TBX2/3 driven cancers including rhabdomyosarcoma. Indeed, niclosamide, piroctone olamine and pyrvinium pamoate were identified and validated as 'hits' and were shown to display anti-cancer activity in RMS and therefore have the potential to be repurposed for the treatment of TBX2/3 driven cancers including RMS.

While the notion of drug repurposing as a rapid, cost effective approach to identifying anti-cancer therapies is still a fledgling field, there are already exciting success stories as outlined in section 1.6. This study provides new data to support a growing body of evidence that niclosamide, piroctone olamine and pyrvinium pamoate may also be good candidate drugs to repurpose for anti-cancer therapies. Indeed, this study shows that these drugs reduced melanoma, ARMS and ERMS cell viability (Fig. 4.19 and Fig. 4.21B). Furthermore, in vitro studies have revealed that niclosamide treatment of several cancers including breast, colon,

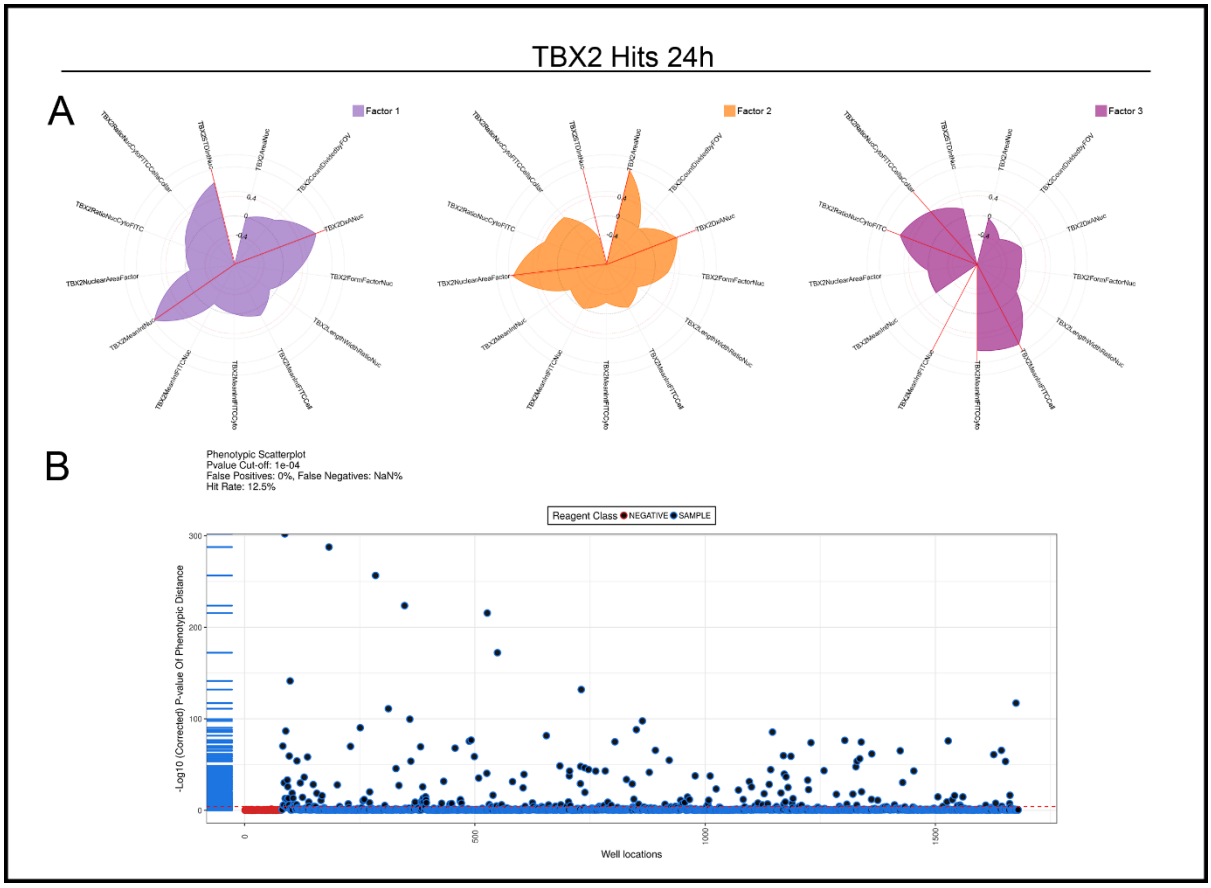

Fig. 4.24 HC StratoMineR analyses of TBX2-FLAG cells after 24h of drug library treatment. *(A) Polar plots representing 13 original parameters reduced into 3 factors. The polar angles represent the parameter names and the radius represents the factor loading of the parameter. A significant contribution is considered if >0.4 or <-0.4 and is indicated with a red line. (B) Phenotypic distance 'hit' selection plot calculated from factor scores transformed to p-values with a cut-off of $p<1x10^{-4}$ (dotted red line).*

ovarian, prostate, lung, glioblastoma and osteosarcoma results in the inhibition of cell migration, invasion, proliferation and the induction of apoptosis (King et al., 2015; Osada et al., 2011; Satoh et al., 2016; Wieland et al., 2013; Arend et al., 2014; Chen et al., 2009; Li et al., 2013; Liu et al., 2014; Lu et al., 2011). In addition, in vivo studies show that oral administration of niclosamide is efficacious with no observed toxicity (King et al., 2015; Osada et al., 2011; Satoh et al., 2016; Wieland et al., 2013). Pyrvinium pamoate has shown anti-cancer activity in colon, pancreatic, breast, bladder and prostate cancer as well as some haematological malignancies including lymphoma and myeloma and intraperitoneal administration of pyrvinium pamoate has been efficacious against several of these cancers (Basu, Reyes-Múgica, & Rebbaa, 2013; Esumi et al., 2004; Guo et al., 2016; Harada et al., 2012; Li et al., 2014; Yu et al., 2008; Deng et al. 2013; Thorne et al. 2010; Xu et al. 2013). Lastly, one study has reported that piroctone olamine significantly decreases the cell viability of myeloma

Table 4.4 *TBX2 24h 'hits' (filtered: Factor 1 <0, Factor 3 <-2, count >25). A 'hit' also detected as a TBX3 'hit' at this timepoint is indicated with an asterisk.*

Ranking	Comound	p-value	Distance Score	Factor 1	Factor 2	Factor 3
1	DOXORUBICIN*	2.18E-98	10.24	-3.39	-5.35	-8.47
2	IRINOTECAN HYDROCHLORIDE	5.91E-91	8.11	-1.16	7.94	-2.12
3	ANCITABINE HYDROCHLORIDE	1.41E-76	7.56	-1.22	6.95	-2.83
4	ETOPOSIDE	6.37E-71	7.45	-1.51	6.92	-2.71
5	MELPHALAN*	4.85E-60	6.49	-2.22	6.03	-2.05
6	CYTARABINE	2.07E-59	7.18	-1.04	6.82	-2.49
7	METHOTREXATE(+/-)	7.33E-37	5.29	-2.14	3.99	-3.02
8	SPARTEINE SULFATE	2.39E-26	4.54	-1.83	0.48	-4.00
9	EPIRUBICIN HYDROCHLORIDE	4.76E-24	6.24	-2.32	-3.03	-5.47
10	ENILCONAZOLE SULFATE	1.81E-15	3.73	-1.79	-0.02	-3.16
11	MEGESTROL ACETATE	8.55E-14	3.49	-1.36	-0.20	-2.88
12	CHLORAMPHENICOL SODIUM SUCCINATE	1.08E-13	3.77	-1.62	-0.01	-3.24
13	ZOLMITRIPTAN	1.25E-13	3.57	-1.44	0.01	-2.96
14	TESTOSTERONE PROPIONATE	5.62E-10	3.44	-1.62	-0.34	-2.85
15	CHLORAMPHENICOL PALMITATE	1.05E-09	3.30	-1.66	0.17	-2.75
16	EPINEPHRINE BITARTRATE	1.06E-06	2.72	-1.02	-0.83	-2.23
17	alpha-TOCHOPHEROL	1.28E-05	2.92	-0.88	-0.14	-2.49
18	LIOTHYRONINE	6.28E-05	2.52	-0.98	0.48	-2.12

and lymphoma cell lines and induces apoptosis. Furthermore, combination therapy of daily oral piroctone olamine and the currently used myeloma therapeutic lenalidomide was shown to have a significant additive effect in an in vivo myeloma model. Importantly, no side effects were observed for piroctone olamine (Kim et al., 2011; Song et al., 2011). Although niclosamide, piroctone olamine and pyrvinium pamoate are not currently approved to treat cancer, they exhibit anti-cancer properties with the ability to selectively target several oncogenic pathways.

This study shows that niclosamide, piroctone olamine and pyrvinium pamoate downregulate TBX2 and TBX3 in 501mel melanoma cells and RD ERMS cells (Fig. 4.16C and Fig. 4.21A) and downregulate TBX2 in RH30 ARMS cells with negligible effects on TBX3 levels (Fig. 4.21A). Understanding the mechanism(s) by which these drugs exert their anti-cancer activity may provide insight into how they are downregulating TBX2/3. This is important because it will shed light on versatile ways of targeting TBX2 and TBX3 in cancer therapies. In this regard it is worth noting that there is evidence to suggest that niclosamide, piroctone olamine and pyrvinium pamoate selectively target several oncogenic pathways with the Wnt/β-catenin pathway being a common target. It is tempting to speculate that the ability of these drugs to inhibit TBX2 and TBX3 may be through their inhibition of the Wnt signalling pathway because

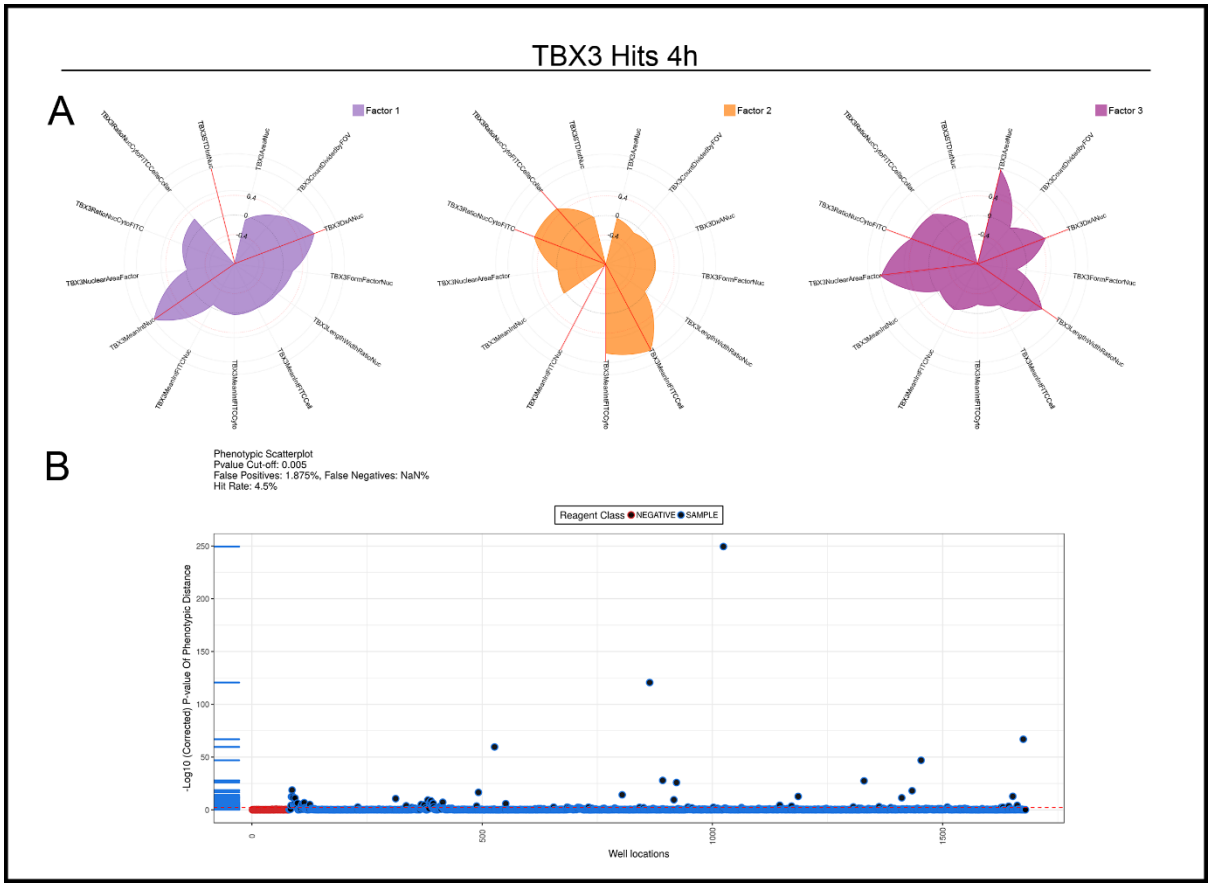

Fig. 4.25 HC StratoMineR analyses of TBX3-FLAG cells after 4h of drug library treatment. *(A) Polar plots representing 13 original parameters reduced into 3 factors. The polar angles represent the parameter names and the radius represents the factor loading of the parameter. A significant contribution is considered if >0.4 or <-0.4 and is indicated with a red line. (B) Phenotypic distance 'hit' selection plot calculated from factor scores transformed to p-values with a cut-off of $p<1x10^{-4}$ (dotted red line).*

it has been previously reported to regulate TBX2 in pancreatic and prostate cancer and TBX3 in liver cancer. Indeed, Chen et al. (2008) showed that the inhibition of β-catenin in pancreatic cancer cells reduced the expression of TBX2 and Nandana et al. (2017) showed that Wnt signalling is an essential mediator of TBX2 in prostate cancer metastasis and that blocking the pathway through neutralising antibodies or a Wnt antagonist blocked TBX2-induced invasion in prostate cancer cells. On the other hand, Renard et al. (2007) identified TBX3 as a downstream target gene activated by the Wnt/β-catenin signalling pathway in liver cancer. Importantly, the authors show that siRNA mediated inhibition of TBX3 impaired β-catenin mediated cell survival and rendered cells sensitive to doxorubicin-induced apoptosis. It is worthy to note that based on the cell culture model used for the drug screen, the 'hits' identified in the current study were identified to repress TBX2/3 posttranscriptionally and indeed niclosamide, piroctone olamine and pyrvinium pamoate were shown to target TBX2

Table 4.5 *TBX3 4h 'hits' (filtered: Factor 2 <-2, Factor 3 <0, count >25). A 'hit' also detected as a TBX2 'hit' at this timepoint is indicated with an asterisk.*

Ranking	Comound	p-value	Distance Score	Factor 1	Factor 2	Factor 3
1	DOXORUBICIN*	2.47E-121	13.26	-4.52	-8.78	-8.83
2	DAUNORUBICIN*	2.56E-60	13.31	-1.31	-9.15	-9.47
3	PROFLAVINE HEMISULFATE	8.31E-19	6.01	-0.16	-4.32	-4.73
4	MITOXANTRONE HYDROCHLORIDE	5.96E-15	5.49	-3.62	-2.84	-2.94
5	ZOLMITRIPTAN	1.31E-13	5.03	-1.58	-3.16	-3.19
6	BRONOPOL	1.60E-13	5.34	-3.39	-3.03	-3.48
7	BROXALDINE	4.14E-12	4.72	0.91	-3.59	-3.40
8	SULFADIMETHOXINE	7.22E-12	4.98	-1.66	-3.08	-3.16
9	TESTOSTERONE PROPIONATE	3.37E-09	4.36	-2.40	-2.37	-2.36
10	ETHIONAMIDE	6.69E-08	4.61	-1.64	-2.90	-2.97
11	MITOMYCIN	1.48E-07	3.78	-0.86	-2.33	-2.41
12	CHLORCYCLIZINE HYDROCHLORIDE	5.26E-07	4.08	-2.23	-2.13	-2.18
13	MEDRYSONE	1.10E-06	3.72	-1.24	-2.18	-2.31
14	CHLORHEXIDINE DIHYDROCHLORIDE	1.16E-06	3.91	-2.23	-2.09	-2.04
15	alpha-TOCHOPHEROL	6.11E-06	3.37	-0.71	-2.08	-2.13
16	DOCETAXEL	6.22E-06	3.80	-1.48	-2.22	-2.31
17	NIKETHAMIDE	9.80E-06	3.75	-1.64	-2.13	-2.20
18	MEGESTROL ACETATE	1.12E-05	3.81	-1.79	-2.15	-2.20
19	MECLOFENAMATE SODIUM	1.63E-05	3.49	-1.10	-2.13	-2.14
20	SULFACHLORPYRIDAZINE	2.85E-05	3.37	-1.17	-2.03	-2.03
21	LIOTHYRONINE	3.12E-05	3.51	-0.83	-2.15	-2.18
22	CHLORPROPAMIDE	3.30E-04	3.54	-0.41	-2.40	-2.40
23	ACRIFLAVINIUM HYDROCHLORIDE	1.04E-03	5.19	0.15	-3.78	-4.09
24	TOLONIUM CHLORIDE	3.07E-03	2.74	-0.82	-2.16	-2.17
25	CHLORPROMAZINE	4.63E-03	4.20	-0.95	-2.75	-2.89

for degradation by the proteasome 26S (Fig. 4.18) which begs the question as to whether this posttranslational mechanism could possibly be mediated by the Wnt/β-catenin pathway. However, there is no evidence of the Wnt/β-catenin pathway ubiquitinating targets for degradation and thus, maybe an alternative pathway is responsible for this. On the other hand, TBX3 levels were not rescued in the presence of MG-132 after treatment with the three drugs (Fig. 4.18) suggesting that if the Wnt/β-catenin pathway is regulating TBX3 it might be doing so on a transcriptional level. Future studies will therefore have to investigate if the Wnt/β-catenin pathway is involved and, if so, how it achieves this downregulation of TBX2/3. Taken together, it would thus appear that there is a link between the Wnt/β-catenin pathway and TBX2/3 and that any drug that inhibits this pathway may negatively impact TBX2/3 driven cancers. While the Wnt/β-catenin pathway has a controversial role in RMS, the regulation of TBX2/3 by this pathway in this cancer should be explored further.

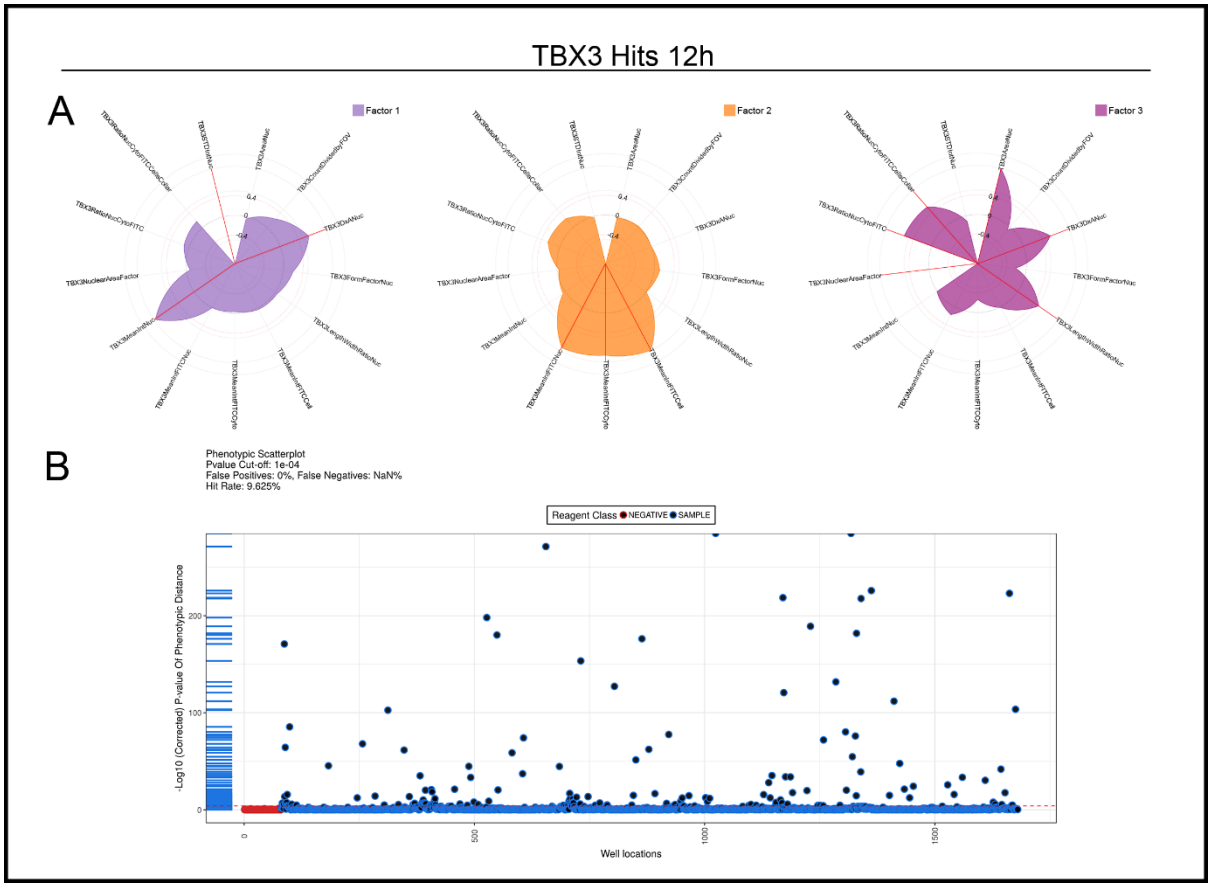

Fig. 4.26 HC StratoMineR analyses of TBX3-FLAG cells after 12h of drug library treatment. *(A) Polar plots representing 13 original parameters reduced into 3 factors. The polar angles represent the parameter names and the radius represents the factor loading of the parameter. A significant contribution is considered if >0.4 or <-0.4 and is indicated with a red line. (B) Phenotypic distance 'hit' selection plot calculated from factor scores transformed to p-values with a cut-off of $p<1x10^{-4}$ (dotted red line).*

In addition to the Wnt/β-catenin pathway, niclosamide, piroctone olamine and pyrvinium pamoate have also been reported to target other oncogenic pathways. For example, niclosamide is able to inhibit Notch, NF-κB and JAK/STAT and pyrvinium pamoate can target Hedgehog, Hippo and PI3K-dependant pathways (Lu et al. 2011; Osada et al. 2011; Sack et al. 2011; Arend et al. 2014; Zhao et al. 2016; Chen et al. 2009; Suliman et al. 2016; Wieland et al. 2013; Wang et al. 2009; Ren et al. 2010; Liu et al. 2014, 2015; Tomitsuka, Kita, and Esumi 2012; Harada et al. 2012; Yu et al. 2008; Deng et al. 2013; Thorne et al. 2010; Xu et al. 2013; Li et al. 2014; Basu, Reyes-Múgica, & Rebbaa 2013; Carrella et al. 2016; Xiao et al. 2016). While there is no evidence that the Hedgehog, Hippo, Notch, NF-κB and JAK/STAT pathways are regulators of TBX2/3, the PI3K pathway has been shown to regulate both TBX2 and TBX3 in melanoma cells. Indeed, inhibition of the PI3K pathway with specific PI3K inhibitors (LY294002 and GDC0941) downregulated TBX2 and TBX3 mRNA and protein levels and this was shown

Table 4.6 *TBX3 12h 'hits' (filtered: Factor 2 <-2, Factor 3 <0, count >25). A 'hit' also detected as a TBX2 'hit' at this timepoint is indicated with an asterisk.*

Ranking	Comound	p-value	Distance Score	Factor 1	Factor 2	Factor 3
1	DOXORUBICIN*	5.87E-177	10.59	-3.08	-3.20	-9.64
2	MITOXANTRONE HYDROCHLORIDE*	6.23E-128	8.78	-4.34	-5.98	-4.86
3	BROXALDINE*	1.22E-112	10.10	-4.01	-7.16	-5.98
4	PROSCILLARIDIN	9.40E-77	6.84	-4.33	-4.93	-2.98
5	POTASSIUM p-AMINOBENZOATE	1.01E-72	7.00	-4.21	-5.03	-3.42
6	THIMEROSAL	1.29E-34	5.17	-4.00	-3.69	-0.90
7	LANATOSIDE C	3.58E-34	5.70	-2.86	-4.39	-2.33
8	HOMIDIUM BROMIDE	4.32E-31	4.87	-0.72	-4.39	-2.30
9	ANCITABINE HYDROCHLORIDE*	2.09E-26	4.48	-0.01	-2.84	-3.60
10	CHLORHEXIDINE DIHYDROCHLORIDE	6.96E-21	3.93	-1.64	-2.99	-1.97
11	ETHACRYNIC ACID*	3.87E-19	4.85	-0.55	-2.17	-4.18
12	THIOTHIXENE	1.32E-17	3.65	-1.11	-2.21	-2.54
13	SULFADIMETHOXINE	1.82E-16	3.66	-1.08	-3.07	-1.73
14	ETHACRIDINE LACTATE	1.38E-15	3.62	0.11	-3.57	-1.26
15	ZOLMITRIPTAN	2.75E-14	3.40	-0.59	-2.57	-2.20
16	TACROLIMUS	3.65E-13	3.56	-1.32	-3.42	-0.63
17	ETHIONAMIDE*	3.62E-12	3.65	-0.68	-2.20	-2.73
18	CYTARABINE*	1.02E-08	3.62	0.32	-2.28	-2.68
19	DOCETAXEL	3.12E-08	2.68	-1.05	-2.29	-1.00
20	NICLOSAMIDE	8.69E-08	2.66	0.44	-2.80	-0.55
21	ETOPOSIDE	1.38E-07	2.79	-0.53	-2.67	-0.79
22	SULFACHLORPYRIDAZINE	7.00E-07	2.44	-0.08	-2.14	-1.29
23	FLUBENDAZOLE	3.22E-06	2.88	-1.20	-2.00	-1.63
24	ESTRIOL	7.06E-06	3.09	-0.36	-2.36	-1.95

to be mediated through PAX3 expression (Schmidt, 2015). Furthermore, TBX3 has been shown to be regulated by AKT3 and AKT1 (key mediators of PI3K signalling) through posttranslational phosphorylation resulting in stabilisation and nuclear localisation in melanoma and fibrosarcoma cells respectively (Cooper, 2016; Peres, Mowla, & Prince, 2015). This suggests that pyrvinium pamoate may potentially be downregulating TBX2 and TBX3 through the PI3K pathway. Niclosamide, piroctone olamine and pyrvinium may regulate TBX2/3 through the other mentioned (e.g. Hippo, Hedgehog, Notch) pathways or yet to be identified pathways. This is exciting as it could possibly reveal potential pathways that may be positively regulating TBX2/3.

Importantly, the Notch, Hippo and PI3K pathways have also been implicated in the underlying mechanisms of RMS i.e. in the dysregulation of terminal muscle differentiation (Yu & Guttridge 2018). Therefore, niclosamide, piroctone olamine and pyrvinium pamoate may be exerting anti-cancer activity in RMS cells by inducing cell differentiation. This is exciting because while some evidence points towards the potential of differentiation therapy for RMS,

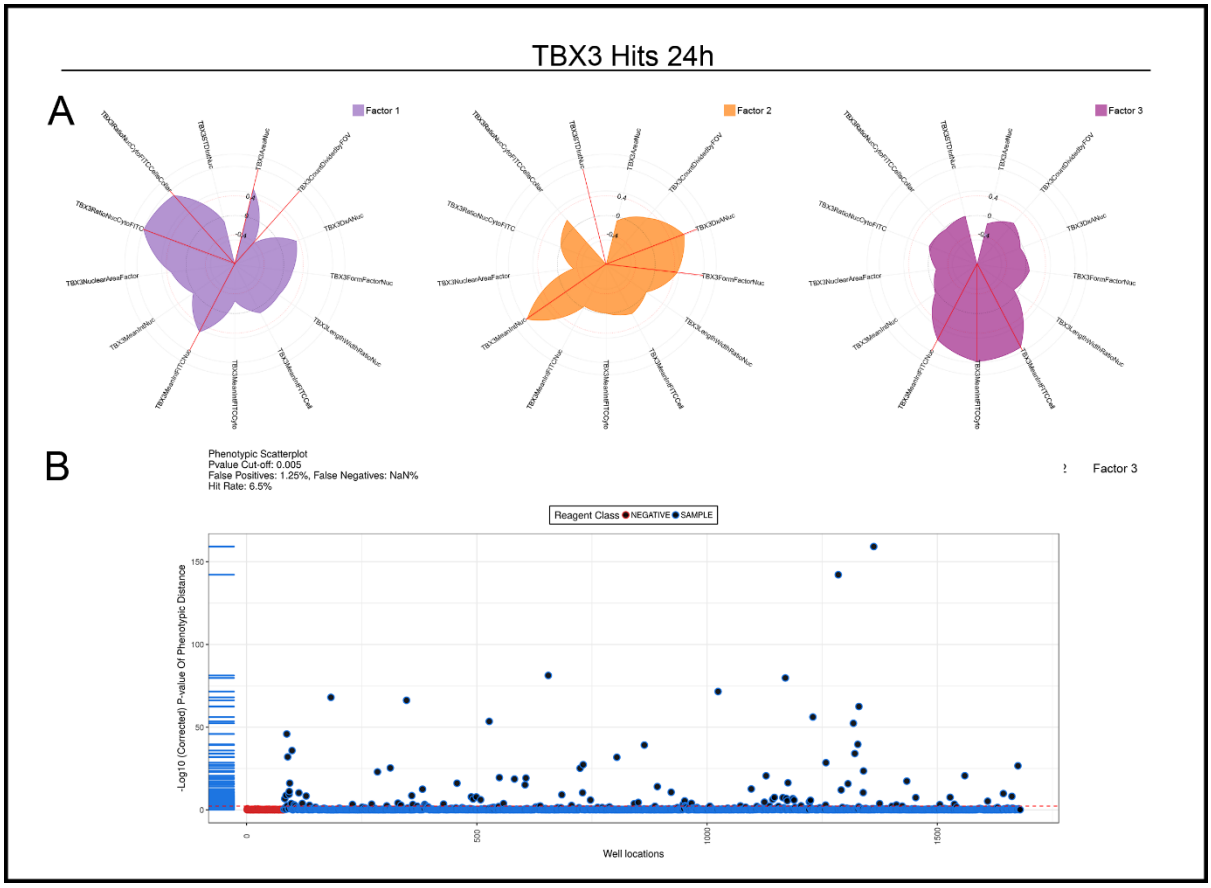

Fig. 4.27 HC StratoMineR analyses of TBX3-FLAG cells after 24h of drug library treatment. *(A) Polar plots representing 13 original parameters reduced into 3 factors. The polar angles represent the parameter names and the radius represents the factor loading of the parameter. A significant contribution is considered if >0.4 or <-0.4 and is indicated with a red line. (B) Phenotypic distance 'hit' selection plot calculated from factor scores transformed to p-values with a cut-off of p<1x10^{-4} (dotted red line).*

Table 4.7 *TBX3 24h 'hits' (filtered: Factor 1 <0, Factor 3 <-2, count >25). A 'hit' also detected as a TBX2 'hit' at this timepoint is indicated with an asterisk.*

Ranking	Comound	p-value	Distance Score	Factor 1	Factor 2	Factor 3
1	DOXORUBICIN*	6.52E-40	8.98	-1.78	-8.75	-2.09
2	NAPHAZOLINE HYDROCHLORIDE	6.79E-26	6.86	-2.74	-5.56	-3.35
3	MYCOPHENOLATE MOFETIL	8.92E-13	4.76	-0.13	-3.16	-4.09
4	PIROCTONE OLAMINE	4.22E-11	5.12	-1.45	-4.29	-2.86
5	THIMEROSAL	1.60E-07	3.79	-2.48	0.61	-3.46
6	CICLOPIROX OLAMINE	5.05E-07	4.10	-0.60	-3.37	-2.90
7	ADAPALENE	1.15E-06	5.94	-3.19	-3.89	-3.86
8	HOMIDIUM BROMIDE	5.59E-06	3.46	-0.43	-2.13	-2.91
9	CYCLOHEXIMIDE	1.38E-05	3.50	-1.44	0.50	-3.74
10	MELPHALAN*	1.38E-04	3.12	-0.10	-2.07	-2.25
11	MYCOPHENOLIC ACID	1.55E-04	3.38	-0.53	-2.37	-2.51
12	PENTAMIDINE ISETHIONATE	1.71E-04	3.22	-0.80	-0.46	-3.21
13	NIFUROXAZIDE	3.74E-04	3.06	-0.95	-1.36	-2.78

there are recent indications that key muscle differentiation mediators such as MyoD may have oncogenic roles (Tenente et al., 2017). Thus, differentiation therapy still needs to be thoroughly tested in RMS and future experiments could explore the potential of niclosamide, piroctone olamine and pyrvinium pamoate to induce RMS cell differentiation. This could involve determining the effect of these drugs on the expression of MyoD target genes such as *LMOD2*, *TNNI2*, *ACTA1* and *CKM* which are highly downregulated in RMS cells (Zhang, Truscott, and Davie 2013). Furthermore, detection of terminally differentiated muscle cells after treatment can be detected by immunofluorescence using a differentiation muscle cell marker such as an antibody to sarcomeric myosin heavy chain as well as identifying multi-nucleated myotubes (Miyake, Mcdermott, & Gramolini, 2011).

In the experiments investigating whether the anti-cancer activity of niclosamide, piroctone olamine and pyrvinium pamoate may be through inhibiting TBX2/3 no significant effect on cell viability was observed when TBX2/3 levels were rescued (Fig. 4.19). This raises the question as to whether cell viability assays are an accurate readout of the impact of the drugs on the oncogenic roles of TBX2/3. TBX2 and TBX3 have been implicated in promoting senescence bypass, cell proliferation and migration and therefore future experiments should evaluate the effect of drug-induced TBX2/3 inhibition on these processes. This will be an important avenue of investigation especially since light microscopy images show that, after piroctone olamine and pyrvinium pamoate treatment, RMS cells assume a morphology typical of senescent cells i.e. they become flatter and larger (Fig. 4.21C). This is exciting as senescence induced therapy is a rapidly growing field with profound biological implications in the field of oncology (Fan & Schmitt, 2017).

Although the high throughput screen was conducted successfully with the identification of 'hit' drugs that could be validated, there were several technical challenges that should be noted for the improvement of similar such experiments in the future. For example, as a positive control for the screen we needed an agent known to negatively regulate TBX2/3 levels and nuclear localisation. Based on previous work in the Goding and Prince laboratories, several compounds have been shown to negatively regulate TBX2/3 including the PI3K inhibitors LY294002 and GDC0941 and the nucleolin aptamer AS1411 which was shown to block TBX3 nuclear localisation. These compounds were tested but none of them provided a

large enough dynamic range for the robust detection of 'hit' drugs and thus the experiment proceeded without positive controls. While this is not uncommon, it was risky, and it is highly recommended for more confident identification of 'hits' that future screens utilize positive controls. In this regard, the current screen has revealed niclosamide, piroctone olamine and pyrvinium pamoate as potential positive controls. Although the use of the Tet-On system to express inducible FLAG-tagged TBX2/3 proteins allowed for better detection of TBX2/3 levels by immunofluorescence with an antibody to FLAG, this system was flawed. For example, only 'hits' that posttranscriptionally regulate TBX2/3 could be identified and it presented with the risk of identifying false positive 'hits' such as tacrolimus that interfere with the Tet-On system. Therefore, the use of the Tet-On system or similar systems in such a drug screen should only be used if a better alternative is not available. Lastly, although the use of experimental endpoint z-scores is a commonly used method to successfully identify 'hits' during this study it became clear that there are more powerful multiparametric approaches such as HC StratoMineR that can be utilized. Indeed, with hindsight, HC StratoMineR is a better analyses tool and future screens should alter the experimental design and feature extraction to maximise the power of HC StratoMineR.

In summary, in this chapter a target-based drug repurposing strategy was adopted to identify FDA-approved drugs that can negatively regulate the oncogenic TBX2 and TBX3 transcription factors. While several challenges were encountered in designing and developing the screen, the screen was successfully run and 'hits' were identified and selected 'hits' were validated. This study shows for the first time that niclosamide, piroctone olamine and pyrvinium pamoate can negatively regulate the oncogenic TBX2 and TBX3 and it also broadens the anti-cancer activity of these drugs to include efficacy against RMS and melanoma. Although further validation and characterisation of these drugs was very preliminary, niclosamide, piroctone olamine and pyrvinium pamoate show promising repurposing potential for the treatment of TBX2/3 driven cancers including RMS.

CHAPTER 5

Concluding Remarks

This study set out to address the need for more effective and less toxic therapies for the treatment of RMS using a two-pronged approach. The first approach identified the palladium-based compound, AJ-5, and its more water-soluble derivate BTC2, as potent and selective anti-cancer drugs in RMS and other sarcoma subtypes. AJ-5 was shown to mediate its anti-cancer activity in RMS through DSBs, induction of apoptosis and necroptosis markers as well as the reduction of autophagic flux. This study provides an in-depth characterisation of the anti-cancer mechanisms of AJ-5 which contributes novel findings to the anti-cancer mechanisms of palladium-based drugs. Furthermore, the safety and pharmacokinetic profile of AJ-5 in nude mice supports the evidence that AJ-5 is a promising anti-cancer drug and should be taken forward through the drug development pipeline. The second approach exploited our current understanding of the key roles that the transcription factors TBX2 and TBX3 play in rhabdomyosarcomagenesis. Indeed, a target-based drug repurposing strategy was adopted to circumvent the challenge of developing a de novo targeted therapy for TBX2 and TBX3 and to fast track the drug discovery and development pipeline. Niclosamide, piroctone olamine and pyrvinium pamoate were identified and successfully validated as 'hits' that downregulate TBX2 and TBX3 in RMS. While these drugs have been identified to exert anti-cancer activity, their mechanism(s) of action have not been fully elucidated and their activity in melanoma and RMS has not been reported. This study contributes novel findings to shed light on their mechanism(s) of action as well as provide evidence that their therapeutic range may be broadened to include RMS and melanoma. Although, future work is required to elucidate how these drugs are downregulating TBX2/3, this study contributes to the body of work that can drive these drugs to clinical trials to be repurposed for the treatment of cancer.

CHAPTER 6

References

Aaes, T. L., Kaczmarek, A., Delvaeye, T., De Craene, B., De Koker, S., Heyndrickx, L., … Krysko, D. V. (2016). Vaccination with Necroptotic Cancer Cells Induces Efficient Anti-tumor Immunity. *Cell Reports*, *15*(2), 274–287.

Abraham, J., Nuñez-Álvarez, Y., Hettmer, S., Carrió, E., Chen, H.-I. H., Nishijo, K., … Keller, C. (2014). Lineage of origin in rhabdomyosarcoma informs pharmacological response. *Genes & Development*, *28*(14), 1578–1591.

Adams, J. M., & Cory, S. (2007). The Bcl-2 apoptotic switch in cancer development and therapy. *Oncogene*, *26*(9), 1324–1337.

Akdi, K., Vilaplana, R. A., Kamah, S., Navarro, J. A. R., Salas, J. M., & González-Vílchez, F. (2002). Study of the biological effects and DNA damage exerted by a new dipalladium-Hmtpo complex on human cancer cells. *Journal of Inorganic Biochemistry*, *90*(1–2), 51–60.

Aliwaini, S. H. (2017). TBX3 Role in Colorectal Cancer Treatment. *IUG Journal of Natural Studies*, *25*(2), 282–288.

Aliwaini, S., Peres, J., Kröger, W. L., Blanckenberg, A., de la Mare, J., Edkins, A. L., … Prince, S. (2015). The palladacycle, AJ-5, exhibits anti-tumour and anti-cancer stem cell activity in breast cancer cells. *Cancer Letters*, *357*(1), 206–218.

Aliwaini, S., Swarts, A. J., Blanckenberg, A., Mapolie, S., & Prince, S. (2013). A novel binuclear palladacycle complex inhibits melanoma growth in vitro and in vivo through apoptosis and autophagy. *Biochemical Pharmacology*, *86*(12), 1650–1663.

Amankwah, E. K., Conley, A. P., & Reed, D. R. (2013). Epidemiology and therapies for metastatic sarcoma. *Clinical Epidemiology*, *5*, 147–162.

Amaravadi, R. K., Yu, D., Lum, J. J., Bui, T., Christophorou, M. A., Evan, G. I., … Thompson, C. B. (2007). Autophagy inhibition enhances therapy-induced apoptosis in a Myc-induced model of lymphoma. *The Journal of Clinical Investigation*, *117*(2), 326–336.

Anderson, J., Ramsay, A., Gould, S., & Pritchard-Jones, K. (2001). PAX3-FKHR induces morphological change and enhances cellular proliferation and invasion in

rhabdomyosarcoma. *The American Journal of Pathology*, *159*(3), 1089–1096.

Antonarakis, E. S., Heath, E. I., Smith, D. C., Rathkopf, D., Blackford, A. L., Danila, D. C., … Carducci, M. A. (2013). Repurposing Itraconazole as a Treatment for Advanced Prostate Cancer: A Noncomparative Randomized Phase II Trial in Men With Metastatic Castration-Resistant Prostate Cancer. *The Oncologist*, *18*(2), 163–173.

Arend, R. C., Londoño-Joshi, A. I., Samant, R. S., Li, Y., Conner, M., Hidalgo, B., … Buchsbaum, D. J. (2014). Inhibition of Wnt/β-catenin pathway by niclosamide: A therapeutic target for ovarian cancer. *Gynecologic Oncology*, *134*(1), 112–120.

Arndt, C. A. S., Hawkins, D. S., Meyer, W. H., Sencer, S. F., Neglia, J. P., & Anderson, J. R. (2008). Comparison of results of a pilot study of alternating vincristine/doxorubicin/cyclophosphamide and etoposide/ifosfamide with IRS-IV in intermediate risk rhabdomyosarcoma: a report from the Children's Oncology Group. *Pediatric Blood & Cancer*, *50*(1), 33–36.

Arndt, C. A. S., Stoner, J. A., Hawkins, D. S., Rodeberg, D. A., Hayes-Jordan, A. A., Paidas, C. N., … Meyer, W. H. (2009). Vincristine, actinomycin, and cyclophosphamide compared with vincristine, actinomycin, and cyclophosphamide alternating with vincristine, topotecan, and cyclophosphamide for intermediate-risk rhabdomyosarcoma: children's oncology group study D9803. *Journal of Clinical Oncology : Official Journal of the American Society of Clinical Oncology*, *27*(31), 5182–5188.

Arruebo, M., Vilaboa, N., Sáez-Gutierrez, B., Lambea, J., Tres, A., Valladares, M., & González-Fernández, A. (2011). Assessment of the evolution of cancer treatment therapies. *Cancers*, *3*(3), 3279–3330.

Asati, V., Mahapatra, D. K., & Bharti, S. K. (2016). PI3K/Akt/mTOR and Ras/Raf/MEK/ERK signaling pathways inhibitors as anticancer agents: Structural and pharmacological perspectives. *European Journal of Medicinal Chemistry*, *109*, 314–341.

Ashburn, T. T., & Thor, K. B. (2004). Drug repositioning: identifying and developing new uses for existing drugs. *Nature Reviews Drug Discovery*, *3*(8), 673–683.

Astellas Pharma. (2012). *PROGRAF® [package insert]*. Deerfield, Illinois, USA.

Ayalon, D., Glaser, T., & Werner, H. (2001). Transcriptional regulation of IGF-I receptor gene expression by the PAX3–FKHR oncoprotein. *Growth Hormone & IGF Research*, *11*(5), 289–297.

Badisa, R. B., Darling-Reed, S. F., Joseph, P., Cooperwood, J. S., Latinwo, L. M., & Goodman, C.

B. (2009). Selective cytotoxic activities of two novel synthetic drugs on human breast carcinoma MCF-7 cells. *Anticancer Research*, *29*(8), 2993–2996.

Ballif, B. C., Theisen, A., Rosenfeld, J. A., Traylor, R. N., Gastier-Foster, J., Thrush, D. L., … Shaffer, L. G. (2010). Identification of a Recurrent Microdeletion at 17q23.1q23.2 Flanked by Segmental Duplications Associated with Heart Defects and Limb Abnormalities. *The American Journal of Human Genetics*, *86*(3), 454–461.

Bamshad, M., Le, T., Watkins, W. S., Dixon, M. E., Kramer, B. E., Roeder, A. D., … Jorde, L. B. (1999). The Spectrum of Mutations in TBX3: Genotype/Phenotype Relationship in Ulnar-Mammary Syndrome. *The American Journal of Human Genetics*, *64*(6), 1550–1562.

Bamshad, M., Lin, R. C., Law, D. J., Watkins, W. S., Krakowiak, P. A., Moore, M. E., … Jorde, L. B. (1997). Mutations in human TBX3 alter limb, apocrine and genital development in ulnar-mammary syndrome. *Nature Genetics*, *16*(3), 311–315.

Barr, F. G., Duan, F., Smith, L. M., Gustafson, D., Pitts, M., Hammond, S., & Gastier-Foster, J. M. (2009). Genomic and clinical analyses of 2p24 and 12q13-q14 amplification in alveolar rhabdomyosarcoma: A report from the Children's Oncology Group. *Genes, Chromosomes and Cancer*, *48*(8), 661–672.

Basu, A., & Krishnamurthy, S. (2010). Cellular responses to Cisplatin-induced DNA damage. *Journal of Nucleic Acids*, *2010*.

Basu, D., Reyes-Múgica, M., & Rebbaa, A. (2013). Histone acetylation-mediated regulation of the Hippo pathway. *PloS One*, *8*(5), e62478.

Bayer Pharmaceuticals Corporation. (1988). *YOMESAN® [package insert]*. West Haven, Connecticut, USA.

Bayer Pharmaceuticals Corporation. (2007). *LEVITRA® [package insert]*. West Haven, Connecticut, USA.

Bedford Laboratories. (2012). *ADRIAMYCIN® [package insert]*. Bedford, Ohio, USA.

Belyea, B. C., Naini, S., Bentley, R. C., & Linardic, C. M. (2011). Inhibition of the Notch-Hey1 axis blocks embryonal rhabdomyosarcoma tumorigenesis. *Clinical Cancer Research : An Official Journal of the American Association for Cancer Research*, *17*(23), 7324–7336.

Berghe, T. Vanden, Linkermann, A., Jouan-Lanhouet, S., Walczak, H., & Vandenabeele, P. (2014). Regulated necrosis: the expanding network of non-apoptotic cell death pathways. *Nature Reviews Molecular Cell Biology*, *15*(2), 135–147.

Blanckenberg, A. (2016). *Preparation and Characterization of Novel Palladacycles and their*

Evaluation as Anticancer Agents. Stellenbosch University.

Blay, J.-Y. (2011). Updating progress in sarcoma therapy with mTOR inhibitors. *Annals of Oncology*, *22*(2), 280–287.

Boehm, S., Rothermundt, C., Hess, D., & Joerger, M. (2010). Antiangiogenic drugs in oncology: a focus on drug safety and the elderly - a mini-review. *Gerontology*, *56*(3), 303–309.

Bollag, R. J., Siegfried, Z., Cebra-Thomas, J. A., Garvey, N., Davison, E. M., & Silver, L. M. (1994). An ancient family of embryonically expressed mouse genes sharing a conserved protein motif with the T locus. *Nature Genetics*, *7*(3), 383–389.

Boyd, S. C., Mijatov, B., Pupo, G. M., Tran, S. L., Gowrishankar, K., Shaw, H. M., … Becker, T. M. (2013). Oncogenic B-RAFV600E Signaling Induces the T-Box3 Transcriptional Repressor to Repress E-Cadherin and Enhance Melanoma Cell Invasion. *Journal of Investigative Dermatology*, *133*(5), 1269–1277.

Breneman, J. C., Lyden, E., Pappo, A. S., Link, M. P., Anderson, J. R., Parham, D. M., … Crist, W. M. (2003). Prognostic factors and clinical outcomes in children and adolescents with metastatic rhabdomyosarcoma--a report from the Intergroup Rhabdomyosarcoma Study IV. *Journal of Clinical Oncology : Official Journal of the American Society of Clinical Oncology*, *21*(1), 78–84.

Bridge, J. A., Liu, J., Qualman, S. J., Suijkerbuijk, R., Wenger, G., Zhang, J., … Barr, F. G. (2002). Genomic gains and losses are similar in genetic and histologic subsets of rhabdomyosarcoma, whereas amplification predominates in embryonal with anaplasia and alveolar subtypes. *Genes, Chromosomes & Cancer*, *33*(3), 310–321.

Bridge, J. A., Liu, J., Weibolt, V., Baker, K. S., Perry, D., Kruger, R., … Suijkerbuijk, R. (2000). Novel genomic imbalances in embryonal rhabdomyosarcoma revealed by comparative genomic hybridization and fluorescence in situ hybridization: an intergroup rhabdomyosarcoma study. *Genes, Chromosomes & Cancer*, *27*(4), 337–344.

Brody, T. (2011). *Clinical Trials: Study Design, Endpoints and Biomarkers, Drug Safety, and FDA and ICH Guidelines*. Academic Press.

Brummelkamp, T. R., Kortlever, R. M., Lingbeek, M., Trettel, F., MacDonald, M. E., van Lohuizen, M., & Bernards, R. (2002). TBX-3, the Gene Mutated in Ulnar-Mammary Syndrome, Is a Negative Regulator of p19 ^{ARF} and Inhibits Senescence. *Journal of Biological Chemistry*, *277*(8), 6567–6572.

Brunelle, J. K., & Letai, A. (2009). Control of mitochondrial apoptosis by the Bcl-2 family.

Journal of Cell Science, *122*(Pt 4), 437–441.

Buckingham, M., & Relaix, F. (2007). The Role of *Pax* Genes in the Development of Tissues and Organs: *Pax3* and *Pax7* Regulate Muscle Progenitor Cell Functions. *Annual Review of Cell and Developmental Biology*, *23*(1), 645–673.

Burgucu, D., Guney, K., Sahinturk, D., Ozbudak, I. H., Ozel, D., Ozbilim, G., & Yavuzer, U. (2012). Tbx3 represses PTEN and is over-expressed in head and neck squamous cell carcinoma. *BMC Cancer*, *12*(1), 481.

Cai, Z., Jitkaew, S., Zhao, J., Chiang, H.-C., Choksi, S., Liu, J., … Liu, Z.-G. (2014). Plasma membrane translocation of trimerized MLKL protein is required for TNF-induced necroptosis. *Nature Cell Biology*, *16*(1), 55–65.

Calhabeu, F., Hayashi, S., Morgan, J. E., Relaix, F., & Zammit, P. S. (2013). Alveolar rhabdomyosarcoma-associated proteins PAX3/FOXO1A and PAX7/FOXO1A suppress the transcriptional activity of MyoD-target genes in muscle stem cells. *Oncogene*, *32*(5), 651–662.

Calvisi, D. F., Factor, V. M., Loi, R., Thorgeirsson, S. S., Wei, Y., Cairo, S., … Buendia, M.-A. (2007). Activation of beta-catenin during hepatocarcinogenesis in transgenic mouse models: relationship to phenotype and tumor grade. *Cancer Research*, *61*(5), 2085–2091.

Campbell, C., Goodrich, K., Casey, G., & Beatty, B. (1995). Cloning and Mapping of a Human Gene (TBX2) Sharing a Highly Conserved Protein Motif with the Drosophila omb Gene. *Genomics*, *28*(2), 255–260.

Campisi, J. (2013). Aging, Cellular Senescence, and Cancer. *Annual Review of Physiology*, *75*(1), 685–705.

Canner, J. A., Sobo, M., Ball, S., Hutzen, B., DeAngelis, S., Willis, W., … Lin, J. (2009). MI-63: A novel small-molecule inhibitor targets MDM2 and induces apoptosis in embryonal and alveolar rhabdomyosarcoma cells with wild-type p53. *British Journal of Cancer*, *101*(5), 774–781.

Cao, Y., & Klionsky, D. J. (2007). Physiological functions of Atg6/Beclin 1: a unique autophagy-related protein. *Cell Research*, *17*(10), 839–849.

Caretti, G., Di Padova, M., Micales, B., Lyons, G. E., & Sartorelli, V. (2004). The Polycomb Ezh2 methyltransferase regulates muscle gene expression and skeletal muscle differentiation. *Genes & Development*, *18*(21), 2627–2638.

Carlson, B. M. (2014). Integumentary, Skeletal, and Muscular Systems. *Human Embryology*

and Developmental Biology, 156–192.

Carlson, H., Ota, S., Campbell, C. E., & Hurlin, P. J. (2001). A dominant repression domain in Tbx3 mediates transcriptional repression and cell immortalization: relevance to mutations in Tbx3 that cause ulnar-mammary syndrome. *Human Molecular Genetics*, *10*(21), 2403–2413.

Carlson, H., Ota, S., Song, Y., Chen, Y., & Hurlin, P. J. (2002). Tbx3 impinges on the p53 pathway to suppress apoptosis, facilitate cell transformation and block myogenic differentiation. *Oncogene*, *21*(24), 3827–3835.

Carreira, S., Liu, B., & Goding, C. R. (2000). The gene encoding the T-box factor Tbx2 is a target for the microphthalmia-associated transcription factor in melanocytes. *The Journal of Biological Chemistry*, *275*(29), 21920–21927.

Cecchetto, G., Carretto, E., Bisogno, G., Dall'Igna, P., Ferrari, A., Scarzello, G., … Carli, M. (2008). Complete second look operation and radiotherapy in locally advanced non-alveolar rhabdomyosarcoma in children: A report from the AIEOP soft tissue sarcoma committee. *Pediatric Blood & Cancer*, *51*(5), 593–597.

Chalhoub, N., & Baker, S. J. (2009). PTEN and the PI3-Kinase Pathway in Cancer. *Annual Review of Pathology: Mechanisms of Disease*, *4*(1), 127–150.

Chan, F. K.-M., Nailwal, H., & Moriwaki, K. (2019). Targeting Necroptosis in Antitumor Therapy. *Targeting Cell Survival Pathways to Enhance Response to Chemotherapy*, 275–285.

Charytonowicz, E., Matushansky, I., Domingo-Doménech, J., Castillo-Martín, M., Ladanyi, M., Cordon-Cardo, C., & Ziman, M. (2012). PAX7-FKHR fusion gene inhibits myogenic differentiation via NF-kappaB upregulation. *Clinical and Translational Oncology*, *14*(3), 197–206.

Chen, E. Y. (2016). Wnt Signaling in Rhabdomyosarcoma - A Potential Targeted Therapy Option. *Current Drug Targets*, *17*(11), 1245–1251.

Chen, M., Wang, J., Lu, J., Bond, M. C., Ren, X.-R., Lyerly, H. K., … Chen, W. (2009). The Anti-Helminthic Niclosamide Inhibits Wnt/Frizzled1 Signaling. *Biochemistry*, *48*(43), 10267–10274.

Chen, X., Li, W., Ren, J., Huang, D., He, W., Song, Y., … Han, J. (2014). Translocation of mixed lineage kinase domain-like protein to plasma membrane leads to necrotic cell death. *Cell Research*, *24*(1), 105–121.

Chen, X., Stewart, E., Shelat, A. A., Qu, C., Bahrami, A., Hatley, M., … St. Jude Children's Research Hospital–Washington University Pediatric Cancer Genome Project. (2013). Targeting Oxidative Stress in Embryonal Rhabdomyosarcoma. *Cancer Cell*, *24*(6), 710–724.

Chen, Z., Lü, G., & Ji, T. (2009). Expression of TBX3 mRNA and its role in the pathogenesis and metastasis of breast cancer. *Nan Fang Yi Ke Da Xue Xue Bao = Journal of Southern Medical University*, *29*(1), 87–89.

Cheung-Ong, K., Giaever, G., & Nislow, C. (2013). DNA-damaging agents in cancer chemotherapy: serendipity and chemical biology. *Chemistry & Biology*, *20*(5), 648–659.

Chiarle, R., Voena, C., Ambrogio, C., Piva, R., & Inghirami, G. (2008). The anaplastic lymphoma kinase in the pathogenesis of cancer. *Nature Reviews Cancer*, *8*(1), 11–23.

Chinna Babu, P., Sundaraganesan, N., Sudha, S., Aroulmoji, V., & Murano, E. (2012). Molecular structure and vibrational spectra of Irinotecan: a density functional theoretical study. *Spectrochimica Acta. Part A, Molecular and Biomolecular Spectroscopy*, *98*, 1–6.

Chisholm, J. C., Merks, J. H., Casanova, M., Bisogno, G., Orbach, D., Gentet, J.-C., … Oberlin, O. (2016). BERNIE: Open-label, randomized, phase II study of bevacizumab plus chemotherapy in pediatric metastatic rhabdomyosarcoma (RMS) and non-rhabdomyosarcoma soft tissue sarcoma (NRSTS). *Journal of Clinical Oncology*, *34*(15_suppl), 11054–11054.

Cho, Y., Challa, S., Moquin, D., Genga, R., Ray, T. D., Guildford, M., & Chan, F. K.-M. (2009). Phosphorylation-Driven Assembly of the RIP1-RIP3 Complex Regulates Programmed Necrosis and Virus-Induced Inflammation. *Cell*, *137*(6), 1112–1123.

Chong, C. R., Xu, J., Lu, J., Bhat, S., Sullivan, D. J., & Liu, J. O. (2007). Inhibition of Angiogenesis by the Antifungal Drug Itraconazole. *ACS Chemical Biology*, *2*(4), 263–270.

Christofferson, D. E., & Yuan, J. (2010). Necroptosis as an alternative form of programmed cell death. *Current Opinion in Cell Biology*, *22*(2), 263–268.

Christofori, G. (2003). NEW EMBO MEMBER'S REVIEW: Changing neighbours, changing behaviour: cell adhesion molecule-mediated signalling during tumour progression. *The EMBO Journal*, *22*(10), 2318–2323.

Ciarapica, R., De Salvo, M., Carcarino, E., Bracaglia, G., Adesso, L., Leoncini, P. P., … Rota, R. (2014). The Polycomb group (PcG) protein EZH2 supports the survival of PAX3-FOXO1 alveolar rhabdomyosarcoma by repressing FBXO32 (Atrogin1/MAFbx). *Oncogene*,

33(32), 4173–4184.

Ciarapica, R., Russo, G., Verginelli, F., Raimondi, L., Donfrancesco, A., Rota, R., & Giordano, A. (2009). Deregulated expression of miR-26a and Ezh2 in Rhabdomyosarcoma. *Cell Cycle*, *8*(1), 172–175.

Ciardiello, F., Caputo, R., Bianco, R., Damiano, V., Pomatico, G., De Placido, S., … Tortora, G. (2000). Antitumor effect and potentiation of cytotoxic drugs activity in human cancer cells by ZD-1839 (Iressa), an epidermal growth factor receptor-selective tyrosine kinase inhibitor. *Clinical Cancer Research : An Official Journal of the American Association for Cancer Research*, *6*(5), 2053–2063.

Ciavarella, S., Milano, A., Dammacco, F., & Silvestris, F. (2010). Targeted Therapies in Cancer. *BioDrugs*, *24*(2), 77–88.

Cieśla, M., Dulak, J., & Józkowicz, A. (2014). MicroRNAs and epigenetic mechanisms of rhabdomyosarcoma development. *The International Journal of Biochemistry & Cell Biology*, *53*, 482–492.

Cocker, H. A., Hobbs, S. M., Tiffin, N., Pritchard-Jones, K., Pinkerton, C. R., & Kelland, L. R. (2001). High levels of the MDM2 oncogene in paediatric rhabdomyosarcoma cell lines may confer multidrug resistance. *British Journal of Cancer*, *85*(11), 1746–1752.

Cocker, H. A., Pinkerton, C. R., & Kelland, L. R. (2000). Characterization and modulation of drug resistance of human paediatric rhabdomyosarcoma cell lines. *British Journal of Cancer*, *83*(3), 338–345.

Cohen, M. H., Johnson, J. R., Chen, Y.-F., Sridhara, R., & Pazdur, R. (2005). FDA drug approval summary: erlotinib (Tarceva) tablets. *The Oncologist*, *10*(7), 461–466.

Cohen, S. M., & Lippard, S. J. (2001). Cisplatin: from DNA damage to cancer chemotherapy. *Progress in Nucleic Acid Research and Molecular Biology*, *67*, 93–130.

Conti, B., K. Slemmons, K., Rota, R., & M. Linardic, C. (2016). Recent Insights into Notch Signaling in Embryonal Rhabdomyosarcoma. *Current Drug Targets*, *17*(11), 1235–1244.

Cooper, A. (2016). *A tumour suppressor role for the T-box transcription factor TBX3 in fibroblasts*. University of Cape Town.

Crist, W., Gehan, E. A., Ragab, A. H., Dickman, P. S., Donaldson, S. S., Fryer, C., … Heyn, R. (1995). The Third Intergroup Rhabdomyosarcoma Study. *Journal of Clinical Oncology : Official Journal of the American Society of Clinical Oncology*, *13*(3), 610–630.

Crose, L. E. S., Galindo, K. A., Kephart, J. G., Chen, C., Fitamant, J., Bardeesy, N., … Linardic, C.

M. (2014). Alveolar rhabdomyosarcoma–associated PAX3-FOXO1 promotes tumorigenesis via Hippo pathway suppression. *The Journal of Clinical Investigation*, *124*(1), 285–296.

D'Adamo, D. R. (2011). Appraising the current role of chemotherapy for the treatment of sarcoma. *Seminars in Oncology*, *38 Suppl 3*, S19-29.

D'Costa, Z. C., Higgins, C. A., Ong, C. W., Irwin, G., Boyle, D., McArt, D. G., … Mullan, P. B. (2014). TBX2 represses CST6 resulting in uncontrolled legumain activity to sustain breast cancer proliferation: a novel cancer-selective target pathway with therapeutic opportunities. *Oncotarget*, *5*(6), 1609–1620.

Dang, C. V., Reddy, E. P., Shokat, K. M., & Soucek, L. (2017). Drugging the "undruggable" cancer targets. *Nature Reviews Cancer*, *17*(8), 502–508.

Danial, N. N., & Korsmeyer, S. J. (2004). Cell death: critical control points. *Cell*, *116*(2), 205–219.

Darzynkiewicz, Z. (2010). Critical aspects in analysis of cellular DNA content. *Current Protocols in Cytometry / Editorial Board, J. Paul Robinson, Managing Editor ... [et Al.]*, *Chapter 7*, Unit7.2.

Dasgupta, R., & Rodeberg, D. A. (2012). Update on rhabdomyosarcoma. *Seminars in Pediatric Surgery*, *21*(1), 68–78.

Davis, E., Teng, H., Bilican, B., Parker, M. I., Liu, B., Carriera, S., … Prince, S. (2008). Ectopic Tbx2 expression results in polyploidy and cisplatin resistance. *Oncogene*, *27*(7), 976–984.

de Almagro, M. C., & Vucic, D. (2015). Necroptosis: Pathway diversity and characteristics. *Seminars in Cell & Developmental Biology*, *39*, 56–62.

De Giovanni, C., Landuzzi, L., Frabetti, F., Nicoletti, G., Griffoni, C., Rossi, I., … Lollini, P. L. (1996). Antisense epidermal growth factor receptor transfection impairs the proliferative ability of human rhabdomyosarcoma cells. *Cancer Research*, *56*(17), 3898–3901.

De Salvo, M., Raimondi, L., Vella, S., Adesso, L., Ciarapica, R., Verginelli, F., … Rota, R. (2014). Hyper-Activation of Notch3 Amplifies the Proliferative Potential of Rhabdomyosarcoma Cells. *PLoS ONE*, *9*(5), e96238.

Degterev, A., Huang, Z., Boyce, M., Li, Y., Jagtap, P., Mizushima, N., … Yuan, J. (2005). Chemical inhibitor of nonapoptotic cell death with therapeutic potential for ischemic brain injury. *Nature Chemical Biology*, *1*(2), 112–119.

Degterev, A., Maki, J. L., & Yuan, J. (2013). Activity and specificity of necrostatin-1, small-molecule inhibitor of RIP1 kinase. *Cell Death & Differentiation*, *20*(2), 366–366.

Degterev, A., & Yuan, J. (2008). Expansion and evolution of cell death programmes. *Nature Reviews Molecular Cell Biology*, *9*(5), 378–390.

Demicco, E. G., Maki, R. G., Lev, D. C., & Lazar, A. J. (2012). New therapeutic targets in soft tissue sarcoma. *Advances in Anatomic Pathology*, *19*(3), 170–180.

Department of Health. (2015). *Ethics in Health Research: Principles, Processes and Structures. 2nd Edition.* Pretoria.

Desai, J., Solomon, B. J., Davis, I. D., Lipton, L. R., Hicks, R., Scott, A. M., … Finckenstein, F. G. (2010). Phase I dose-escalation study of daily BMS-754807, an oral, dual IGF-1R/insulin receptor (IR) inhibitor in subjects with solid tumors. *Journal of Clinical Oncology*, *28*(15_suppl), 3104–3104.

Di Croce, L., & Helin, K. (2013). Transcriptional regulation by Polycomb group proteins. *Nature Structural & Molecular Biology*, *20*(10), 1147–1155.

Diller, L., Sexsmith, E., Gottlieb, A., Li, F. P., & Malkin, D. (1995). Germline p53 mutations are frequently detected in young children with rhabdomyosarcoma. *The Journal of Clinical Investigation*, *95*(4), 1606–1611.

Dilling, M. B., Dias, P., Shapiro, D. N., Germain, G. S., Johnson, R. K., & Houghton, P. J. (1994). Rapamycin selectively inhibits the growth of childhood rhabdomyosarcoma cells through inhibition of signaling via the type I insulin-like growth factor receptor. *Cancer Research*, *54*(4), 903–907.

Dimova, I., Orsetti, B., Negre, V., Rouge, C., Ursule, L., Lasorsa, L., … Theillet, C. (2009). Genomic markers for ovarian cancer at chromosomes 1, 8 and 17 revealed by array CGH analysis. *Tumori*, *95*(3), 357–366.

Dolcet, X., Llobet, D., Pallares, J., & Matias-Guiu, X. (2005). NF-kB in development and progression of human cancer. *Virchows Archiv*, *446*(5), 475–482.

Dominici, M., Le Blanc, K., Mueller, I., Slaper-Cortenbach, I., Marini, F. ., Krause, D. S., … Horwitz, E. M. (2006). Minimal criteria for defining multipotent mesenchymal stromal cells. The International Society for Cellular Therapy position statement. *Cytotherapy*, *8*(4), 315–317.

Dondelinger, Y., Declercq, W., Montessuit, S., Roelandt, R., Goncalves, A., Bruggeman, I., … Vandenabeele, P. (2014). MLKL Compromises Plasma Membrane Integrity by Binding to

Phosphatidylinositol Phosphates. *Cell Reports*, *7*(4), 971–981.

Dowling, R. J. O., Zakikhani, M., Fantus, I. G., Pollak, M., & Sonenberg, N. (2007). Metformin Inhibits Mammalian Target of Rapamycin–Dependent Translation Initiation in Breast Cancer Cells. *Cancer Research*, *67*(22), 10804–10812.

Du, H. F., Ou, L. P., Yang, X., Song, X. D., Fan, Y. R., Tan, B., … Wu, X. H. (2014). A new PKCα/β/TBX3/E-cadherin pathway is involved in PLCε-regulated invasion and migration in human bladder cancer cells. *Cellular Signalling*, *26*(3), 580–593.

du Toit, A., Hofmeyr, J.-H. S., Gniadek, T. J., & Loos, B. (2018). Measuring autophagosome flux. *Autophagy*, 1–12.

Du, W.-L., Fang, Q., Chen, Y., Teng, J.-W., Xiao, Y.-S., Xie, P., … Wang, J.-Q. (2017). Effect of silencing the T-Box transcription factor TBX2 in prostate cancer PC3 and LNCaP cells. *Molecular Medicine Reports*, *16*(5), 6050–6058.

Dunlop, E. A., & Tee, A. R. (2014). mTOR and autophagy: A dynamic relationship governed by nutrients and energy. *Seminars in Cell & Developmental Biology*.

Eaton, B. R., McDonald, M. W., Kim, S., Marcus, R. B., Sutter, A. L., Chen, Z., & Esiashvili, N. (2013). Radiation therapy target volume reduction in pediatric rhabdomyosarcoma: implications for patterns of disease recurrence and overall survival. *Cancer*, *119*(8), 1578–1585.

Eccles, S. A., Box, C., & Court, W. (2005). Cell migration/invasion assays and their application in cancer drug discovery. *Biotechnology Annual Review*, *11*, 391–421.

Edinger, A. L., & Thompson, C. B. (2004). Death by design: apoptosis, necrosis and autophagy. *Current Opinion in Cell Biology*, *16*(6), 663–669.

Egas-Bejar, D., & Huh, W. W. (2014). Rhabdomyosarcoma in adolescent and young adult patients: current perspectives. *Adolescent Health, Medicine and Therapeutics*, *5*, 115–125.

El-Badry, O. M., Minniti, C., Kohn, E. C., Houghton, P. J., Daughaday, W. H., & Helman, L. J. (1990). Insulin-like growth factor II acts as an autocrine growth and motility factor in human rhabdomyosarcoma tumors. *Cell Growth & Differentiation : The Molecular Biology Journal of the American Association for Cancer Research*, *1*(7), 325–331.

Elmore, S. (2007). Apoptosis: a review of programmed cell death. *Toxicologic Pathology*, *35*(4), 495–516.

Elsebaie, M. A. T., Amgad, M., Elkashash, A., Elgebaly, A. S., Ashal, G. G. E. l., Shash, E., &

Elsayed, Z. (2018). Management of Low and Intermediate Risk Adult Rhabdomyosarcoma: A Pooled Survival Analysis of 553 Patients. *Scientific Reports*, *8*(1), 9337.

Eskelinen, E.-L. (2011). The dual role of autophagy in cancer. *Current Opinion in Pharmacology*, *11*(4), 294–300.

Eskes, R., Desagher, S., Antonsson, B., & Martinou, J. C. (2000). Bid induces the oligomerization and insertion of Bax into the outer mitochondrial membrane. *Molecular and Cellular Biology*, *20*(3), 929–935.

Estep, A. L., Tidyman, W. E., Teitell, M. A., Cotter, P. D., & Rauen, K. A. (2006). HRAS mutations in Costello syndrome: Detection of constitutional activating mutations in codon 12 and 13 and loss of wild-type allele in malignancy. *American Journal of Medical Genetics Part A*, *140A*(1), 8–16.

Esumi, H., Lu, J., Kurashima, Y., & Hanaoka, T. (2004). Antitumor activity of pyrvinium pamoate, 6-(dimethylamino)-2-[2-(2,5-dimethyl-1-phenyl-1H-pyrrol-3-yl)ethenyl]-1-methyl-quinolinium pamoate salt, showing preferential cytotoxicity during glucose starvation. *Cancer Science*, *95*(8), 685–690.

Evans, J. M. M., Donnelly, L. A., Emslie-Smith, A. M., Alessi, D. R., & Morris, A. D. (2005). Metformin and reduced risk of cancer in diabetic patients. *BMJ*, *330*(7503), 1304–1305.

Fan, D. N. Y., & Schmitt, C. A. (2017). Detecting Markers of Therapy-Induced Senescence in Cancer Cells. In *Methods in molecular biology (Clifton, N.J.)* (Vol. 1534, pp. 41–52).

FDA. (2018). *Approved Drug Products With Therapeutic Equivalence Evaluations* (38th ed.). Silver Spring, Maryland, USA.

Fehres, C. M., Unger, W. W. J., Garcia-Vallejo, J. J., & van Kooyk, Y. (2014). Understanding the Biology of Antigen Cross-Presentation for the Design of Vaccines Against Cancer. *Frontiers in Immunology*, *5*, 149.

Felix, C. A., Kappel, C. C., Mitsudomi, T., Nau, M. M., Tsokos, M., Crouch, G. D., … Helman, L. J. (1992). Frequency and Diversity of p53 Mutations in Childhood Rhabdomyosarcoma. *Cancer Res.*, *52*(8), 2243–2247.

Ferrari, A., Sultan, I., Huang, T. T., Rodriguez-Galindo, C., Shehadeh, A., Meazza, C., … Spunt, S. L. (2011). Soft tissue sarcoma across the age spectrum: a population-based study from the Surveillance Epidemiology and End Results database. *Pediatric Blood & Cancer*, *57*(6), 943–949.

Fillmore, C. M., Gupta, P. B., Rudnick, J. A., Caballero, S., Keller, P. J., Lander, E. S., & Kuperwasser, C. (2010). Estrogen expands breast cancer stem-like cells through paracrine FGF/Tbx3 signaling. *Proceedings of the National Academy of Sciences*, *107*(50), 21737–21742.

Fiuza, S. M., Holy, J., Batista de Carvalho, L. A. E., & Marques, M. P. M. (2011). Biologic activity of a dinuclear Pd(II)-spermine complex toward human breast cancer. *Chemical Biology & Drug Design*, *77*(6), 477–488.

Francis, P., Namløs, H. M., Müller, C., Edén, P., Fernebro, J., Berner, J.-M., … Nilbert, M. (2007). Diagnostic and prognostic gene expression signatures in 177 soft tissue sarcomas: hypoxia-induced transcription profile signifies metastatic potential. *BMC Genomics*, *8*, 73.

Frisch, S. M., Schaller, M., & Cieply, B. (2013). Mechanisms that link the oncogenic epithelial–mesenchymal transition to suppression of anoikis. *Journal of Cell Science*, *126*(1), 21–29.

Fuchs, Y., Brunwasser, M., Haif, S., Haddad, J., Shneyer, B., Goldshmidt-Tran, O., … Ron, D. (2012). Sef Is an Inhibitor of Proinflammatory Cytokine Signaling, Acting by Cytoplasmic Sequestration of NF-κB. *Developmental Cell*, *23*(3), 611–623.

Fuchs, Y., & Steller, H. (2015). Live to die another way: modes of programmed cell death and the signals emanating from dying cells. *Nature Reviews Molecular Cell Biology*, *16*(6), 329–344.

Fulda, S. (2009). Caspase-8 in cancer biology and therapy. *Cancer Letters*, *281*(2), 128–133.

Fulda, S. (2012). Autophagy and cell death. *Autophagy*, *8*(8), 1250–1251.

Galili, N., Davis, R. J., Fredericks, W. J., Mukhopadhyay, S., Rauscher, F. J., Emanuel, B. S., … Barr, F. G. (1993). Fusion of a fork head domain gene to PAX3 in the solid tumour alveolar rhabdomyosarcoma. *Nature Genetics*, *5*(3), 230–235.

Gallagher, E. J., & LeRoith, D. (2010). The proliferating role of insulin and insulin-like growth factors in cancer. *Trends in Endocrinology & Metabolism*, *21*(10), 610–618.

Galluzzi, L., Aaronson, S. A., Abrams, J., Alnemri, E. S., Andrews, D. W., Baehrecke, E. H., … Kroemer, G. (2009). Guidelines for the use and interpretation of assays for monitoring cell death in higher eukaryotes. *Cell Death & Differentiation*, *16*(8), 1093–1107.

Galluzzi, L., Kepp, O., Chan, F. K.-M., & Kroemer, G. (2017). Necroptosis: Mechanisms and Relevance to Disease. *Annual Review of Pathology: Mechanisms of Disease*, *12*(1), 103–130.

Galluzzi, L., & Kroemer, G. (2008). Necroptosis: A Specialized Pathway of Programmed Necrosis. *Cell*, *135*(7), 1161–1163.

Galluzzi, L., Maiuri, M. C., Vitale, I., Zischka, H., Castedo, M., Zitvogel, L., & Kroemer, G. (2007). Cell death modalities: classification and pathophysiological implications. *Cell Death and Differentiation*, *14*(7), 1237–1243.

Galluzzi, L., Vitale, I., Abrams, J. M., Alnemri, E. S., Baehrecke, E. H., Blagosklonny, M. V, … Kroemer, G. (2012). Molecular definitions of cell death subroutines: recommendations of the Nomenclature Committee on Cell Death 2012. *Cell Death and Differentiation*, *19*(1), 107–120.

Ganti, R., Skapek, S. X., Zhang, J., Fuller, C. E., Wu, J., Billups, C. A., … Khoury, J. D. (2006). Expression and genomic status of EGFR and ErbB-2 in alveolar and embryonal rhabdomyosarcoma. *Modern Pathology*, *19*(9), 1213–1220.

Geoerger, B., Kieran, M. W., Grupp, S., Perek, D., Clancy, J., Krygowski, M., … Spunt, S. L. (2012). Phase II trial of temsirolimus in children with high-grade glioma, neuroblastoma and rhabdomyosarcoma. *European Journal of Cancer (Oxford, England : 1990)*, *48*(2), 253–262.

Gerber, H. P., Kowalski, J., Sherman, D., Eberhard, D. A., & Ferrara, N. (2000). Complete inhibition of rhabdomyosarcoma xenograft growth and neovascularization requires blockade of both tumor and host vascular endothelial growth factor. *Cancer Research*, *60*(22), 6253–6258.

Gilbertson, R. J. (2005). ERBB2 in Pediatric Cancer: Innocent Until Proven Guilty. *The Oncologist*, *10*(7), 508–517.

Goktug, A. N., Chai, S. C., & Chen, T. (2013). Chapter 7 Data Analysis Approaches in High Throughput Screening.

Gordon, A. T., Brinkschmidt, C., Anderson, J., Coleman, N., Dockhorn-Dworniczak, B., Pritchard-Jones, K., & Shipley, J. (2000). A novel and consistent amplicon at 13q31 associated with alveolar rhabdomyosarcoma. *Genes, Chromosomes & Cancer*, *28*(2), 220–226.

Green, D. R. (2000). Apoptotic pathways: paper wraps stone blunts scissors. *Cell*, *102*(1), 1–4.

Grufferman, S., Delzell, E., & Delong, E. R. (1984). An approach to conducting epidemiologic research within cooperative clinical trials groups. *Journal of Clinical Oncology : Official Journal of the American Society of Clinical Oncology*, *2*(6), 670–675.

Grufferman, S., Lupo, P. J., Vogel, R. I., Danysh, H. E., Erhardt, E. B., & Ognjanovic, S. (2014). Parental military service, agent orange exposure, and the risk of rhabdomyosarcoma in offspring. *The Journal of Pediatrics*, *165*(6), 1216–1221.

Grufferman, S., Ruymann, F., Ognjanovic, S., Erhardt, E. B., & Maurer, H. M. (2009). Prenatal X-ray exposure and rhabdomyosarcoma in children: a report from the children's oncology group. *Cancer Epidemiology, Biomarkers & Prevention : A Publication of the American Association for Cancer Research, Cosponsored by the American Society of Preventive Oncology*, *18*(4), 1271–1276.

Grufferman, S., Schwartz, A. G., Ruymann, F. B., & Maurer, H. M. (1993). Parents' use of cocaine and marijuana and increased risk of rhabdomyosarcoma in their children. *Cancer Causes & Control : CCC*, *4*(3), 217–224.

Gschwind, A., Fischer, O. M., & Ullrich, A. (2004). The discovery of receptor tyrosine kinases: targets for cancer therapy. *Nature Reviews Cancer*, *4*(5), 361–370.

Guenther, M. K., Graab, U., & Fulda, S. (2013). Synthetic lethal interaction between PI3K/Akt/mTOR and Ras/MEK/ERK pathway inhibition in rhabdomyosarcoma. *Cancer Letters*, *337*(2), 200–209.

Guo, J., Lv, J., Chang, S., Chen, Z., Lu, W., Xu, C., … Pang, X. (2016). Inhibiting cytoplasmic accumulation of HuR synergizes genotoxic agents in urothelial carcinoma of the bladder. *Oncotarget*, *7*(29), 45249–45262.

Gou, N., & Peng, Z. (2013). MG132, a proteasome inhibitor, induces apoptosis in tumor cells. *Asia-Pacific Journal of Clinical Oncology*, *9*(1), 6–11.

Guttridge, D. C., Albanese, C., Reuther, J. Y., Pestell, R. G., & Baldwin, A. S. (1999). NF-kappaB controls cell growth and differentiation through transcriptional regulation of cyclin D1. *Molecular and Cellular Biology*, *19*(8), 5785–5799.

Guttridge, D. C., Mayo, M. W., Madrid, L. V, Wang, C. Y., & Baldwin, A. S. (2000). NF-kappaB-induced loss of MyoD messenger RNA: possible role in muscle decay and cachexia. *Science (New York, N.Y.)*, *289*(5488), 2363–2366.

Guzmán, C., Bagga, M., Kaur, A., Westermarck, J., Abankwa, D., Puck, T., … Streibig, J. (2014). ColonyArea: An ImageJ Plugin to Automatically Quantify Colony Formation in Clonogenic Assays. *PLoS ONE*, *9*(3), e92444.

Hadizadeh, S., Najafzadeh, N., Mazani, M., Amani, M., Mansouri-Torshizi, H., & Niapour, A. (2014). Cytotoxic Effects of Newly Synthesized Palladium(II) Complexes of

Diethyldithiocarbamate on Gastrointestinal Cancer Cell Lines. *Biochemistry Research International*, *2014*, 813457.

Hallberg, B., & Palmer, R. H. (2016). The role of the ALK receptor in cancer biology. *Annals of Oncology*, *27*(suppl_3), iii4-iii15.

Han, W., Li, L., Qiu, S., Lu, Q., Pan, Q., Gu, Y., … Hu, X. (2007). Shikonin circumvents cancer drug resistance by induction of a necroptotic death. *Molecular Cancer Therapeutics*, *6*(5), 1641–1649.

Han, Y., Tu, W.-W., Wen, Y.-G., Yan, D.-W., Qiu, G.-Q., Peng, Z.-H., & Zhou, C.-Z. (2013). Increased expression of TBX2 is a novel independent prognostic biomarker of a worse outcome in colorectal cancer patients after curative surgery and a potential therapeutic target. *Medical Oncology*, *30*(4), 688.

Hanna, J. A., Garcia, M. R., Go, J. C., Finkelstein, D., Kodali, K., Pagala, V., … Hatley, M. E. (2016). PAX7 is a required target for microRNA-206-induced differentiation of fusion-negative rhabdomyosarcoma. *Cell Death & Disease*, *7*(6), e2256–e2256.

Harada, Y., Ishii, I., Hatake, K., & Kasahara, T. (2012). Pyrvinium pamoate inhibits proliferation of myeloma/erythroleukemia cells by suppressing mitochondrial respiratory complex I and STAT3. *Cancer Letters*, *319*(1), 83–88.

Hartley, A. L., Birch, J. M., Marsden, H. B., Harris, M., & Blair, V. (1988). Neurofibromatosis in children with soft tissue sarcoma. *Pediatric Hematology and Oncology*, *5*(1), 7–16.

Hatley, M. E., Tang, W., Garcia, M. R., Finkelstein, D., Millay, D. P., Liu, N., … Olson, E. N. (2012). A mouse model of rhabdomyosarcoma originating from the adipocyte lineage. *Cancer Cell*, *22*(4), 536–546.

Haupt, S., Berger, M., Goldberg, Z., & Haupt, Y. (2003). Apoptosis - the p53 network. *Journal of Cell Science*, *116*(Pt 20), 4077–4085.

He, C., & Klionsky, D. J. (2009). Regulation mechanisms and signaling pathways of autophagy. *Annual Review of Genetics*, *43*, 67–93.

He, G.-W., Günther, C., Thonn, V., Yu, Y.-Q., Martini, E., Buchen, B., … Becker, C. (2017). Regression of apoptosis-resistant colorectal tumors by induction of necroptosis in mice. *The Journal of Experimental Medicine*, *214*(6), 1655–1662.

He, S., Wang, L., Miao, L., Wang, T., Du, F., Zhao, L., & Wang, X. (2009). Receptor Interacting Protein Kinase-3 Determines Cellular Necrotic Response to TNF-α. *Cell*, *137*(6), 1100–1111.

Heckman-Stoddard, B. M., DeCensi, A., Sahasrabuddhe, V. V., & Ford, L. G. (2017). Repurposing metformin for the prevention of cancer and cancer recurrence. *Diabetologia*, *60*(9), 1639–1647.

Helman, L. J., & Meltzer, P. (2003). Mechanisms of sarcoma development. *Nature Reviews. Cancer*, *3*(9), 685–694.

Hernández Losa, J., Parada Cobo, C., Guinea Viniegra, J., Sánchez-Arevalo Lobo, V. J., Ramón y Cajal, S., & Sánchez-Prieto, R. (2003). Role of the p38 MAPK pathway in cisplatin-based therapy. *Oncogene*, *22*(26), 3998–4006.

Hettmer, S., & Wagers, A. J. (2010). Muscling in: Uncovering the origins of rhabdomyosarcoma. *Nature Medicine*, *16*(2), 171–173.

Heymann, D., & Rédini, F. (2013). Targeted therapies for bone sarcomas. *BoneKEy Reports*, *2*.

Hinson, A. R. P., Jones, R., Crose, L. E. S., Belyea, B. C., Barr, F. G., & Linardic, C. M. (2013). Human Rhabdomyosarcoma Cell Lines for Rhabdomyosarcoma Research: Utility and Pitfalls. *Frontiers in Oncology*, *3*, 183.

Hitomi, J., Christofferson, D. E., Ng, A., Yao, J., Degterev, A., Xavier, R. J., & Yuan, J. (2008). Identification of a Molecular Signaling Network that Regulates a Cellular Necrotic Cell Death Pathway. *Cell*, *135*(7), 1311–1323.

Hoffmann, J. C., Pappa, A., Krammer, P. H., & Lavrik, I. N. (2009). A new C-terminal cleavage product of procaspase-8, p30, defines an alternative pathway of procaspase-8 activation. *Molecular and Cellular Biology*, *29*(16), 4431–4440.

Holohan, C., Van Schaeybroeck, S., Longley, D. B., & Johnston, P. G. (2013). Cancer drug resistance: an evolving paradigm. *Nature Reviews Cancer*, *13*(10), 714–726.

Hosoi, H. (2016). Current status of treatment for pediatric rhabdomyosarcoma in the USA and Japan. *Pediatrics International*, *58*(2), 81–87.

Hosoi, H., Dilling, M. B., Shikata, T., Liu, L. N., Shu, L., Ashmun, R. A., … Houghton, P. J. (1999). Rapamycin Causes Poorly Reversible Inhibition of mTOR and Induces p53-independent Apoptosis in Human Rhabdomyosarcoma Cells. *Cancer Res.*, *59*(4), 886–894.

Hui, J. Y. C. (2016). Epidemiology and Etiology of Sarcomas. In J. M. Farma & A. S. Porpiglia (Eds.), *New Trends in the Treatment of Sarcoma* (pp. 901–914). Philadelphia: Elsevier Inc.

Humtsoe, J. O., Koya, E., Pham, E., Aramoto, T., Zuo, J., Ishikawa, T., & Kramer, R. H. (2012). Transcriptional profiling identifies upregulated genes following induction of epithelial-mesenchymal transition in squamous carcinoma cells. *Experimental Cell Research*,

318(4), 379–390.

Ichim, G., & Tait, S. W. G. (2016). A fate worse than death: apoptosis as an oncogenic process. *Nature Reviews Cancer*, *16*(8), 539–548.

Ignatius, M. S., Hayes, M. N., Lobbardi, R., Chen, E. Y., McCarthy, K. M., Sreenivas, P., … Langenau, D. M. (2017). The NOTCH1/SNAIL1/MEF2C Pathway Regulates Growth and Self-Renewal in Embryonal Rhabdomyosarcoma. *Cell Reports*, *19*(11), 2304–2318.

Iwatsuki, M., Mimori, K., Yokobori, T., Ishi, H., Beppu, T., Nakamori, S., … Mori, M. (2010). Epithelial-mesenchymal transition in cancer development and its clinical significance. *Cancer Science*, *101*(2), 293–299.

Jahromi, E. Z., Divsalar, A., Saboury, A. A., Khaleghizadeh, S., Mansouri-Torshizi, H., & Kostova, I. (2016). Palladium complexes: new candidates for anti-cancer drugs. *Journal of the Iranian Chemical Society*, *13*(5), 967–989.

Jain, S., Xu, R., Prieto, V. G., & Lee, P. (2010). Molecular classification of soft tissue sarcomas and its clinical applications. *International Journal of Clinical and Experimental Pathology*, *3*(4), 416–428.

Jakacki, R. I., Hamilton, M., Gilbertson, R. J., Blaney, S. M., Tersak, J., Krailo, M. D., … Adamson, P. C. (2008). Pediatric phase I and pharmacokinetic study of erlotinib followed by the combination of erlotinib and temozolomide: a Children's Oncology Group Phase I Consortium Study. *Journal of Clinical Oncology : Official Journal of the American Society of Clinical Oncology*, *26*(30), 4921–4927.

Johnstone, T. C., Suntharalingam, K., & Lippard, S. J. (2016). The Next Generation of Platinum Drugs: Targeted Pt(II) Agents, Nanoparticle Delivery, and Pt(IV) Prodrugs. *Chemical Reviews*, *116*(5), 3436–3486.

JU, H., YANG, Y., SHENG, A., & JIANG, X. (2015). Role of microRNAs in skeletal muscle development and rhabdomyosarcoma (Review). *Molecular Medicine Reports*, *11*(6), 4019–4024.

Judson, R. N., Tremblay, A. M., Knopp, P., White, R. B., Urcia, R., De Bari, C., … Wackerhage, H. (2012). The Hippo pathway member Yap plays a key role in influencing fate decisions in muscle satellite cells. *Journal of Cell Science*, *125*(Pt 24), 6009–6019.

Jung, C. H., Ro, S.-H., Cao, J., Otto, N. M., & Kim, D.-H. (2010). mTOR regulation of autophagy. *FEBS Letters*, *584*(7), 1287–1295.

Kacar, O., Adiguzel, Z., Yilmaz, V. T., Cetin, Y., Cevatemre, B., Arda, N., … Acilan, C. (2014).

Evaluation of the molecular mechanisms of a palladium(II) saccharinate complex with terpyridine as an anticancer agent. *Anti-Cancer Drugs*, *25*(1), 17–29.

Kaczmarek, A., Vandenabeele, P., & Krysko, D. V. (2013). Necroptosis: the release of damage-associated molecular patterns and its physiological relevance. *Immunity*, *38*(2), 209–223.

Kaiser, W. J., Sridharan, H., Huang, C., Mandal, P., Upton, J. W., Gough, P. J., … Mocarski, E. S. (2013). Toll-like Receptor 3-mediated Necrosis via TRIF, RIP3, and MLKL. *Journal of Biological Chemistry*, *288*(43), 31268–31279.

Kakazu, N., Yamane, H., Miyachi, M., Shiwaku, K., & Hosoi, H. (2014). Identification of the 12q15 amplicon within the homogeneously staining regions in the embryonal rhabdomyosarcoma cell line RMS-YM. *Cytogenetic and Genome Research*, *142*(3), 167–173.

Kalebic, T., Tsokos, M., & Helman, L. J. (1994). In vivo treatment with antibody against IGF-1 receptor suppresses growth of human rhabdomyosarcoma and down-regulates p34cdc2. *Cancer Research*, *54*(21), 5531–5534.

Karimian, A., Ahmadi, Y., & Yousefi, B. (2016). Multiple functions of p21 in cell cycle, apoptosis and transcriptional regulation after DNA damage. *DNA Repair*, *42*, 63–71.

Karin, M., & Ben-Neriah, Y. (2000). Phosphorylation Meets Ubiquitination: The Control of NF-κB Activity. *Annual Review of Immunology*, *18*(1), 621–663.

Keller, C., & Guttridge, D. C. (2013). Mechanisms of impaired differentiation in rhabdomyosarcoma. *FEBS Journal*, *280*(17), 4323–4334.

Kelley, R. K., & Ko, A. H. (2008). Erlotinib in the treatment of advanced pancreatic cancer. *Biologics : Targets & Therapy*, *2*(1), 83–95.

Kerns, E. H., & Di, L. (2008). *Drug-like properties : concepts, structure design and methods : from ADME to toxicity optimization*. Academic Press.

Khan, J., Bittner, M. L., Saal, L. H., Teichmann, U., Azorsa, D. O., Gooden, G. C., … Meltzer, P. S. (1999). cDNA microarrays detect activation of a myogenic transcription program by the PAX3-FKHR fusion oncogene. *Proceedings of the National Academy of Sciences of the United States of America*, *96*(23), 13264–13269.

Kikuchi, K., Tsuchiya, K., Otabe, O., Gotoh, T., Tamura, S., Katsumi, Y., … Hosoi, H. (2008). Effects of PAX3-FKHR on malignant phenotypes in alveolar rhabdomyosarcoma. *Biochemical and Biophysical Research Communications*, *365*(3), 568–574.

Kim, D. J., Kim, J., Spaunhurst, K., Montoya, J., Khodosh, R., Chandra, K., … Tang, J. Y. (2014).

Open-Label, Exploratory Phase II Trial of Oral Itraconazole for the Treatment of Basal Cell Carcinoma. *Journal of Clinical Oncology*, *32*(8), 745–751.

Kim, J. K., Samaranayake, M., & Pradhan, S. (2009). Epigenetic mechanisms in mammals. *Cellular and Molecular Life Sciences*, *66*(4), 596–612.

Kim, Y., Alpmann, P., Blaum-Feder, S., Krämer, S., Endo, T., Lu, D., … Schmidt-Wolf, I. G. H. (2011). Increased in vivo efficacy of lenalidomide by addition of piroctone olamine. *In Vivo (Athens, Greece)*, *25*(1), 99–103.

King, M. L., Lindberg, M. E., Stodden, G. R., Okuda, H., Ebers, S. D., Johnson, A., … Hayashi, K. (2015). WNT7A/β-catenin signaling induces FGF1 and influences sensitivity to niclosamide in ovarian cancer. *Oncogene*, *34*(26), 3452–3462.

Kluck, R. M., Bossy-Wetzel, E., Green, D. R., & Newmeyer, D. D. (1997). The release of cytochrome c from mitochondria: a primary site for Bcl-2 regulation of apoptosis. *Science (New York, N.Y.)*, *275*(5303), 1132–1136.

Klug, P., & Kreiling, R. (2004). *Safety and Effectiveness Information for Piroctone Olamine*. Frankfurt/Main, Germany.

Koch, A., Tamez, P., Pezzuto, J., & Soejarto, D. (2005). Evaluation of plants used for antimalarial treatment by the Maasai of Kenya. *Journal of Ethnopharmacology*, *101*(1–3), 95–99.

Kohsaka, S., Shukla, N., Ameur, N., Ito, T., Ng, C. K. Y., Wang, L., … Ladanyi, M. (2014). A recurrent neomorphic mutation in MYOD1 defines a clinically aggressive subset of embryonal rhabdomyosarcoma associated with PI3K-AKT pathway mutations. *Nature Genetics*, *46*(6), 595–600.

Kolb, E. A., Gorlick, R., Lock, R., Carol, H., Morton, C. L., Keir, S. T., … Houghton, P. J. (2011). Initial testing (stage 1) of the IGF-1 receptor inhibitor BMS-754807 by the pediatric preclinical testing program. *Pediatric Blood & Cancer*, *56*(4), 595–603.

Kratz, C. P., Rapisuwon, S., Reed, H., Hasle, H., & Rosenberg, P. S. (2011a). Cancer in Noonan, Costello, cardiofaciocutaneous and LEOPARD syndromes. *American Journal of Medical Genetics Part C: Seminars in Medical Genetics*, *157*(2), 83–89.

Kratz, C. P., Rapisuwon, S., Reed, H., Hasle, H., & Rosenberg, P. S. (2011b). Cancer in Noonan, Costello, cardiofaciocutaneous and LEOPARD syndromes. *American Journal of Medical Genetics Part C: Seminars in Medical Genetics*, *157*(2), 83–89.

Kratz, C. P., Steinemann, D., Niemeyer, C. M., Schlegelberger, B., Koscielniak, E., Kontny, U., &

Zenker, M. (2007). Uniparental disomy at chromosome 11p15.5 followed by HRAS mutations in embryonal rhabdomyosarcoma: lessons from Costello syndrome. *Human Molecular Genetics*, *16*(4), 374–379.

Kroemer, G., Galluzzi, L., Vandenabeele, P., Abrams, J., Alnemri, E. S., Baehrecke, E. H., … Melino, G. (2009). Classification of cell death: recommendations of the Nomenclature Committee on Cell Death 2009. *Cell Death and Differentiation*, *16*(1), 3–11.

Kruszewski, M., Bouzyk, E., Oldak, T., Samochocka, K., Fuks, L., Lewandowski, W., … Priebe, W. (2003). Differential toxic effect of cis-platinum(II) and palladium(II) chlorides complexed with methyl 3,4-diamine-2,3,4,6-tetradeoxy-alpha-L-lyxo-hexopyranoside in mouse lymphoma cell lines differing in DSB and NER repair ability. *Teratogenesis, Carcinogenesis, and Mutagenesis*, *Suppl 1*, 1–11.

Krysko, O., Aaes, T. L., Kagan, V. E., D'Herde, K., Bachert, C., Leybaert, L., … Krysko, D. V. (2017). Necroptotic cell death in anti-cancer therapy. *Immunological Reviews*, *280*(1), 207–219.

Kumar, A., Naaz, A., Prakasham, A. P., Gangwar, M. K., Butcher, R. J., Panda, D., & Ghosh, P. (2017). Potent Anticancer Activity with High Selectivity of a Chiral Palladium N-Heterocyclic Carbene Complex. *ACS Omega*, *2*(8), 4632–4646.

Kumar, P., Emechebe, U., Smith, R., Franklin, S., Moore, B., Yandell, M., … Moon, A. M. (2014). Coordinated control of senescence by lncRNA and a novel T-box3 co-repressor complex. *ELife*, *3*.

Kumar, S., Park, S. H., Cieply, B., Schupp, J., Killiam, E., Zhang, F., … Frisch, S. M. (2011). A Pathway for the Control of Anoikis Sensitivity by E-Cadherin and Epithelial-to-Mesenchymal Transition. *Molecular and Cellular Biology*, *31*(19), 4036–4051.

Lam, P. Y., Sublett, J. E., Hollenbach, A. D., & Roussel, M. F. (1999). The oncogenic potential of the Pax3-FKHR fusion protein requires the Pax3 homeodomain recognition helix but not the Pax3 paired-box DNA binding domain. *Molecular and Cellular Biology*, *19*(1), 594–601.

Law, D. J., Gebuhr, T., Garvey, N., Agulnik, S. I., & Silver, L. M. (1995). Identification, characterization, and localization to Chromosome 17q21-22 of the human TBX2 homolog, member of a conserved developmental gene family. *Mammalian Genome*, *6*(11), 793–797.

Leach, F. S., Tokino, T., Meltzer, P., Burrell, M., Oliner, J. D., Smith, S., … Vogelstein, B. (1993). p53 Mutation and MDM2 amplification in human soft tissue sarcomas. *Cancer Research*,

53(10 Suppl), 2231–2234.

Leaphart, C., & Rodeberg, D. (2007). Pediatric surgical oncology: management of rhabdomyosarcoma. *Surgical Oncology*, *16*(3), 173–185.

Levine, B. (2007). Cell biology: autophagy and cancer. *Nature*, *446*(7137), 745–747.

Li, B., Fei, D. L., Flaveny, C. A., Dahmane, N., Baubet, V., Wang, Z., … Robbins, D. J. (2014). Pyrvinium attenuates Hedgehog signaling downstream of smoothened. *Cancer Research*, *74*(17), 4811–4821.

Li, P., Nijhawan, D., Budihardjo, I., Srinivasula, S. M., Ahmad, M., Alnemri, E. S., & Wang, X. (1997). Cytochrome c and dATP-dependent formation of Apaf-1/caspase-9 complex initiates an apoptotic protease cascade. *Cell*, *91*(4), 479–489.

Li, R., Hu, Z., Sun, S.-Y., Chen, Z. G., Owonikoko, T. K., Sica, G. L., … Deng, X. (2013). Niclosamide Overcomes Acquired Resistance to Erlotinib through Suppression of STAT3 in Non-Small Cell Lung Cancer. *Molecular Cancer Therapeutics*, *12*(10), 2200–2212.

Li, S. Q., Cheuk, A. T., Shern, J. F., Song, Y. K., Hurd, L., Liao, H., … Khan, J. (2013). Targeting Wild-Type and Mutationally Activated FGFR4 in Rhabdomyosarcoma with the Inhibitor Ponatinib (AP24534). *PLoS ONE*, *8*(10), e76551.

Li, X., Ruan, X., Zhang, P., Yu, Y., Gao, M., Yuan, S., … Zhao, L. (2018). TBX3 promotes proliferation of papillary thyroid carcinoma cells through facilitating PRC2-mediated p57KIP2 repression. *Oncogene*, *37*(21), 2773–2792.

Li, Z., Zhang, Y., Ramanujan, K., Ma, Y., Kirsch, D. G., & Glass, D. J. (2013). Oncogenic NRAS, required for pathogenesis of embryonic rhabdomyosarcoma, relies upon the HMGA2-IGF2BP2 pathway. *Cancer Research*, *73*(10), 3041–3050.

Liang, C., Feng, P., Ku, B., Dotan, I., Canaani, D., Oh, B.-H., & Jung, J. U. (2006). Autophagic and tumour suppressor activity of a novel Beclin1-binding protein UVRAG. *Nature Cell Biology*, *8*(7), 688–699.

Linardic, C. M., Downie, D. L., Qualman, S., Bentley, R. C., & Counter, C. M. (2005). Genetic Modeling of Human Rhabdomyosarcoma. *Cancer Research*, *65*(11), 4490–4495.

Lingbeek, M. E., Jacobs, J. J. L., & van Lohuizen, M. (2002). The T-box Repressors *TBX2* and *TBX3* Specifically Regulate the Tumor Suppressor Gene *p14* ^{ARF} via a Variant T-site in the Initiator. *Journal of Biological Chemistry*, *277*(29), 26120–26127.

Linkermann, A., & Green, D. R. (2014). Necroptosis. *New England Journal of Medicine*, *370*(5), 455–465.

Liu, C., Lou, W., Zhu, Y., Nadiminty, N., Schwartz, C. T., Evans, C. P., & Gao, A. C. (2014). Niclosamide inhibits androgen receptor variants expression and overcomes enzalutamide resistance in castration-resistant prostate cancer. *Clinical Cancer Research : An Official Journal of the American Association for Cancer Research*, *20*(12), 3198–3210.

Liu, F., Singh, A., Yang, Z., Garcia, A., Kong, Y., & Meyskens, F. L. (2010). MiTF links Erk1/2 kinase and p21CIP1/WAF1 activation after UVC radiation in normal human melanocytes and melanoma cells. *Molecular Cancer*, *9*(1), 214.

Liu, W.-K., Jiang, X.-Y., & Zhang, Z.-X. (2010). Expression of PSCA, PIWIL1, and TBX2 in endometrial adenocarcinoma. *Onkologie*, *33*(5), 241–245.

Livesey, K. M., Tang, D., Zeh, H. J., & Lotze, M. T. (2009). Autophagy inhibition in combination cancer treatment. *Current Opinion in Investigational Drugs (London, England : 2000)*, *10*(12), 1269–1279.

Longo, L., Platini, F., Scardino, A., Alabiso, O., Vasapollo, G., & Tessitore, L. (2008). Autophagy inhibition enhances anthocyanin-induced apoptosis in hepatocellular carcinoma. *Molecular Cancer Therapeutics*, *7*(8), 2476–2485.

Lu, W., Lin, C., Roberts, M. J., Waud, W. R., Piazza, G. A., & Li, Y. (2011). Niclosamide Suppresses Cancer Cell Growth By Inducing Wnt Co-Receptor LRP6 Degradation and Inhibiting the Wnt/β-Catenin Pathway. *PLoS ONE*, *6*(12), e29290.

Lu, Z., Luo, R. Z., Lu, Y., Zhang, X., Yu, Q., Khare, S., … Bast, R. C. (2008). The tumor suppressor gene ARHI regulates autophagy and tumor dormancy in human ovarian cancer cells. *The Journal of Clinical Investigation*, *118*(12), 3917–3929.

Lukas, J., Lukas, C., & Bartek, J. (2011). More than just a focus: The chromatin response to DNA damage and its role in genome integrity maintenance. *Nature Cell Biology*, *13*(10), 1161–1169.

Lupo, P. J., Danysh, H. E., Plon, S. E., Curtin, K., Malkin, D., Hettmer, S., … Schiffman, J. D. (2015). Family history of cancer and childhood rhabdomyosarcoma: a report from the Children's Oncology Group and the Utah Population Database. *Cancer Medicine*, *4*(5), 781–790.

Lupo, P. J., Danysh, H. E., Skapek, S. X., Hawkins, D. S., Spector, L. G., Zhou, R., … Grufferman, S. (2014). Maternal and birth characteristics and childhood rhabdomyosarcoma: a report from the Children's Oncology Group. *Cancer Causes & Control : CCC*, *25*(7), 905–913.

Lupo, P. J., Zhou, R., Skapek, S. X., Hawkins, D. S., Spector, L. G., Scheurer, M. E., … Grufferman, S. (2014). Allergies, atopy, immune-related factors and childhood rhabdomyosarcoma: a report from the Children's Oncology Group. *International Journal of Cancer*, *134*(2), 431–436.

Lv, Y., Si, M., Chen, N., Li, Y., Ma, X., Yang, H., … Cao, C. (2017). TBX2 over-expression promotes nasopharyngeal cancer cell proliferation and invasion. *Oncotarget*, *8*(32), 52699–52707.

Lye, K. L., Nordin, N., Vidyadaran, S., & Thilakavathy, K. (2016). Mesenchymal stem cells: From stem cells to sarcomas. *Cell Biology International*, *40*(6), 610–618.

MacQuarrie, K. L., Yao, Z., Fong, A. P., Diede, S. J., Rudzinski, E. R., Hawkins, D. S., & Tapscott, S. J. (2013). Comparison of genome-wide binding of MyoD in normal human myogenic cells and rhabdomyosarcomas identifies regional and local suppression of promyogenic transcription factors. *Molecular and Cellular Biology*, *33*(4), 773–784.

MacQuarrie, K. L., Yao, Z., Young, J. M., Cao, Y., & Tapscott, S. J. (2012). miR-206 integrates multiple components of differentiation pathways to control the transition from growth to differentiation in rhabdomyosarcoma cells. *Skeletal Muscle*, *2*(1), 7.

Mahlamäki, E. H., Bärlund, M., Tanner, M., Gorunova, L., Höglund, M., Karhu, R., & Kallioniemi, A. (2002). Frequent amplification of 8q24, 11q, 17q, and 20q-specific genes in pancreatic cancer. *Genes, Chromosomes and Cancer*, *35*(4), 353–358.

Maki, R. G. (2010). Small Is Beautiful: Insulin-Like Growth Factors and Their Role in Growth, Development, and Cancer. *Journal of Clinical Oncology*, *28*(33), 4985–4995.

Makin, G. (2014). Principles of chemotherapy. *Paediatrics and Child Health*, *24*(4), 161–165.

Malempati, S., & Hawkins, D. S. (2012). Rhabdomyosarcoma: review of the Children's Oncology Group (COG) Soft-Tissue Sarcoma Committee experience and rationale for current COG studies. *Pediatric Blood & Cancer*, *59*(1), 5–10.

Marchand, C., Antony, S., Kohn, K. W., Cushman, M., Ioanoviciu, A., Staker, B. L., … Pommier, Y. (2006). A novel norindenoisoquinoline structure reveals a common interfacial inhibitor paradigm for ternary trapping of the topoisomerase I-DNA covalent complex. *Molecular Cancer Therapeutics*, *5*(2), 287–295.

Marchesi, I., Fiorentino, F. P., Rizzolio, F., Giordano, A., & Bagella, L. (2012). The ablation of EZH2 uncovers its crucial role in rhabdomyosarcoma formation. *Cell Cycle*, *11*(20), 3828–3836.

Mathew, R., Karantza-Wadsworth, V., & White, E. (2007). Role of autophagy in cancer. *Nature*

Reviews. Cancer, *7*(12), 961–967.

Mathijssen, R., Loos, W., Verweij, J., & Sparreboom, A. (2002). Pharmacology of Topoisomerase I Inhibitors Irinotecan (CPT-11) and Topotecan. *Current Cancer Drug Targets*, *2*(2), 103–123.

Matushansky, I., Maki, R. G., Cormier, J. N., Pollock, R. E., Singh, H. K., Kilpatrick, S. E., … al., et. (2005). Mechanisms of Sarcomagenesis. *Hematology/Oncology Clinics of North America*, *19*(3), 427–449.

Maurer, H. M., Beltangady, M., Gehan, E. A., Crist, W., Hammond, D., Hays, D. M., … Ortega, J. (1988). The Intergroup Rhabdomyosarcoma Study-I. A final report. *Cancer*, *61*(2), 209–220.

Maurer, H. M., Gehan, E. A., Beltangady, M., Crist, W., Dickman, P. S., Donaldson, S. S., … Herrmann, J. (1993). The Intergroup Rhabdomyosarcoma Study-II. *Cancer*, *71*(5), 1904–1922.

Maurer, H. M., Moon, T., Donaldson, M., Fernandez, C., Gehan, E. A., Hammond, D., … Tefft, M. (1977). The intergroup rhabdomyosarcoma study.A preliminary report. *Cancer*, *40*(5), 2015–2026.

Mauvezin, C., & Neufeld, T. P. (2015). Bafilomycin A1 disrupts autophagic flux by inhibiting both V-ATPase-dependent acidification and Ca-P60A/SERCA-dependent autophagosome-lysosome fusion. *Autophagy*, *11*(8), 1437–1438.

McCulloch, D., Brown, C., & Iland, H. (2017). Retinoic acid and arsenic trioxide in the treatment of acute promyelocytic leukemia: current perspectives. *OncoTargets and Therapy*, *Volume 10*, 1585–1601.

McDowell, H. P., Foot, A. B. M., Ellershaw, C., Machin, D., Giraud, C., & Bergeron, C. (2010). Outcomes in paediatric metastatic rhabdomyosarcoma: results of The International Society of Paediatric Oncology (SIOP) study MMT-98. *European Journal of Cancer (Oxford, England : 1990)*, *46*(9), 1588–1595.

Megiorni, F., Camero, S., Ceccarelli, S., McDowell, H. P., Mannarino, O., Marampon, F., … Dominici, C. (2016). DNMT3B in vitro knocking-down is able to reverse embryonal rhabdomyosarcoma cell phenotype through inhibition of proliferation and induction of myogenic differentiation. *Oncotarget*, *7*(48).

Megiorni, F., McDowell, H. P., Camero, S., Mannarino, O., Ceccarelli, S., Paiano, M., … Dominici, C. (2015). Crizotinib-induced antitumour activity in human alveolar

rhabdomyosarcoma cells is not solely dependent on ALK and MET inhibition. *Journal of Experimental & Clinical Cancer Research*, *34*(1), 112.

Meng, M.-B., Wang, H.-H., Cui, Y.-L., Wu, Z.-Q., Shi, Y.-Y., Zaorsky, N. G., … Wang, P. (2016). Necroptosis in tumorigenesis, activation of anti-tumor immunity, and cancer therapy. *Oncotarget*, *7*(35), 57391–57413.

Miao, Z.-F., Liu, X.-Y., Xu, H.-M., Wang, Z.-N., Zhao, T.-T., Song, Y.-X., … Xu, Y.-Y. (2016). Tbx3 overexpression in human gastric cancer is correlated with advanced tumor stage and nodal status and promotes cancer cell growth and invasion. *Virchows Archiv*, *469*(5), 505–513.

Micheau, O., & Tschopp, J. (2003). Induction of TNF receptor I-mediated apoptosis via two sequential signaling complexes. *Cell*, *114*(2), 181–190.

Millot, C., Millot, J.-M., Morjani, H., Desplaces, A., & Manfait, M. (1997). Characterization of Acidic Vesicles in Multidrug-resistant and Sensitive Cancer Cells by Acridine Orange Staining and Confocal Microspectrofluorometry. *Journal of Histochemistry & Cytochemistry*, *45*(9), 1255–1264.

Min, L., Choy, E., Pollock, R. E., Tu, C., Hornicek, F., & Duan, Z. (2017). Autophagy as a potential target for sarcoma treatment. *Biochimica et Biophysica Acta (BBA) - Reviews on Cancer*, *1868*(1), 40–50.

Miyake, T., Mcdermott, J. C., & Gramolini, A. O. (2011). A Method for the Direct Identification of Differentiating Muscle Cells by a Fluorescent Mitochondrial Dye. *PLoS ONE*, *6*(12), 28628.

Mizushima, N., & Komatsu, M. (2011). Autophagy: renovation of cells and tissues. *Cell*, *147*(4), 728–741.

Mizushima, N., & Yoshimori, T. (2007). How to interpret LC3 immunoblotting. *Autophagy*, *3*(6), 542–545.

Mohamad, T., Kazim, N., Adhikari, A., & Davie, J. K. (2018). EGR1 interacts with TBX2 and functions as a tumor suppressor in rhabdomyosarcoma. *Oncotarget*, *9*(26), 18084–18098.

Mohammad, R. M., Muqbil, I., Lowe, L., Yedjou, C., Hsu, H.-Y., Lin, L.-T., … Azmi, A. S. (2015). Broad targeting of resistance to apoptosis in cancer. *Seminars in Cancer Biology*, *35*, S78–S103.

Molkentin, J. D., Black, B. L., Martin, J. F., & Olson, E. N. (1995). Cooperative activation of

muscle gene expression by MEF2 and myogenic bHLH proteins. *Cell*, *83*(7), 1125–1136.

Moyer, J. D., Barbacci, E. G., Iwata, K. K., Arnold, L., Boman, B., Cunningham, A., … Miller, P. (1997). Induction of apoptosis and cell cycle arrest by CP-358,774, an inhibitor of epidermal growth factor receptor tyrosine kinase. *Cancer Research*, *57*(21), 4838–4848.

Mukherjee, S., Chowdhury, S., Chattapadhyay, A. P., & Bhattacharya, A. (2011). Spectroscopic, cytotoxic and DFT studies of a luminescent palladium(II) complex of a hydrazone ligand that induces apoptosis in human prostate cancer cells. *Inorganica Chimica Acta*, *373*(1), 40–46.

Ndagi, U., Mhlongo, N., & Soliman, M. E. (2017). Metal complexes in cancer therapy - an update from drug design perspective. *Drug Design, Development and Therapy*, *11*, 599–616.

Neidle, S. (2013). *Cancer Drug Design and Discovery* (Third Ed). San Diego, CA, USA: Academic Press.

Netto, G. J., & Kaul, K. L. (2018). *Genomic Applications in Pathology* (2nd Edn). Cham: Springer.

Nimmakayalu, M., Major, H., Sheffield, V., Solomon, D. H., Smith, R. J., Patil, S. R., & Shchelochkov, O. A. (2011). Microdeletion of 17q22q23.2 encompassing TBX2 and TBX4 in a patient with congenital microcephaly, thyroid duct cyst, sensorineural hearing loss, and pulmonary hypertension. *American Journal of Medical Genetics Part A*, *155*(2), 418–423.

Nishijo, K., Chen, Q.-R., Zhang, L., McCleish, A. T., Rodriguez, A., Cho, M. J., … Keller, C. (2009). Credentialing a Preclinical Mouse Model of Alveolar Rhabdomyosarcoma. *Cancer Research*, *69*(7), 2902–2911.

Nosengo, N. (2016). Can you teach old drugs new tricks? *Nature*, *534*(7607), 314–316.

Novák, J., Vinklárek, J., Bienertová-Vašků, J., & Slabý, O. (2013). MicroRNAs involved in skeletal muscle development and their roles in rhabdomyosarcoma pathogenesis. *Pediatric Blood & Cancer*, *60*(11), 1739–1746.

Oberlin, O., Rey, A., Lyden, E., Bisogno, G., Stevens, M. C. G., Meyer, W. H., … Anderson, J. R. (2008). Prognostic factors in metastatic rhabdomyosarcomas: results of a pooled analysis from United States and European cooperative groups. *Journal of Clinical Oncology : Official Journal of the American Society of Clinical Oncology*, *26*(14), 2384–2389.

Oberst, A., Dillon, C. P., Weinlich, R., McCormick, L. L., Fitzgerald, P., Pop, C., … Green, D. R. (2011). Catalytic activity of the caspase-8–FLIPL complex inhibits RIPK3-dependent

necrosis. *Nature*, *471*(7338), 363–367.

Oda, Y., & Tsuneyoshi, M. (2009). Recent advances in the molecular pathology of soft tissue sarcoma: implications for diagnosis, patient prognosis, and molecular target therapy in the future. *Cancer Science*, *100*(2), 200–208.

Ognjanovic, S., Olivier, M., Bergemann, T. L., & Hainaut, P. (2012). Sarcomas in TP53 germline mutation carriers. *Cancer*, *118*(5), 1387–1396.

Ola, M. S., Nawaz, M., & Ahsan, H. (2011). Role of Bcl-2 family proteins and caspases in the regulation of apoptosis. *Molecular and Cellular Biochemistry*, *351*(1–2), 41–58.

Oliver, F. J. (1998). Importance of Poly(ADP-ribose) Polymerase and Its Cleavage in Apoptosis. Lesson from an uncleavable mutant. *Journal of Biological Chemistry*, *273*(50), 33533–33539.

Omta, W. A., van Heesbeen, R. G., Pagliero, R. J., van der Velden, L. M., Lelieveld, D., Nellen, M., … Egan, D. A. (2016). HC StratoMineR: A Web-Based Tool for the Rapid Analysis of High-Content Datasets. *ASSAY and Drug Development Technologies*, *14*(8), 439–452.

Osada, T., Chen, M., Yang, X. Y., Spasojevic, I., Vandeusen, J. B., Hsu, D., … Lyerly, H. K. (2011). Antihelminth Compound Niclosamide Downregulates Wnt Signaling and Elicits Antitumor Responses in Tumors with Activating APC Mutations. *Cancer Research*, *71*(12), 4172–4182.

Osuna, D., & de Alava, E. (2009). Molecular pathology of sarcomas. *Reviews on Recent Clinical Trials*, *4*(1), 12–26.

Packham, E. A., & Brook, J. D. (2003). T-box genes in human disorders. *Human Molecular Genetics*, *12 Spec No 1*, R37-44.

Pammolli, F., Magazzini, L., & Riccaboni, M. (2011). The productivity crisis in pharmaceutical R&D. *Nature Reviews Drug Discovery*, *10*(6), 428–438.

Pankiv, S., Clausen, T. H., Lamark, T., Brech, A., Bruun, J.-A., Outzen, H., … Johansen, T. (2007). p62/SQSTM1 Binds Directly to Atg8/LC3 to Facilitate Degradation of Ubiquitinated Protein Aggregates by Autophagy. *Journal of Biological Chemistry*, *282*(33), 24131–24145.

Papaioannou, V. E. (2014). The T-box gene family: emerging roles in development, stem cells and cancer. *Development*, *141*(20), 3819–3833.

Pappo, A. S., Shapiro, D. N., Crist, W. M., & Maurer, H. M. (1995). Biology and therapy of pediatric rhabdomyosarcoma. *Journal of Clinical Oncology : Official Journal of the*

American Society of Clinical Oncology, *13*(8), 2123–2139.

Pappo, A. S., Vassal, G., Crowley, J. J., Bolejack, V., Hogendoorn, P. C. W., Chugh, R., … Helman, L. J. (2014). A phase 2 trial of R1507, a monoclonal antibody to the insulin-like growth factor-1 receptor (IGF-1R), in patients with recurrent or refractory rhabdomyosarcoma, osteosarcoma, synovial sarcoma, and other soft tissue sarcomas: Results of a Sarcoma Alliance. *Cancer*, *120*(16), 2448–2456.

Paulson, V., Chandler, G., Rakheja, D., Galindo, R. L., Wilson, K., Amatruda, J. F., & Cameron, S. (2011). High-resolution array CGH identifies common mechanisms that drive embryonal rhabdomyosarcoma pathogenesis. *Genes, Chromosomes and Cancer*, *50*(6), 397–408.

Penn, B. H., Bergstrom, D. A., Dilworth, F. J., Bengal, E., & Tapscott, S. J. (2004). A MyoD-generated feed-forward circuit temporally patterns gene expression during skeletal muscle differentiation. *Genes & Development*, *18*(19), 2348–2353.

Peres, J., Davis, E., Mowla, S., Bennett, D. C., Li, J. A., Wansleben, S., & Prince, S. (2010). The Highly Homologous T-Box Transcription Factors, TBX2 and TBX3, Have Distinct Roles in the Oncogenic Process. *Genes & Cancer*, *1*(3), 272–282.

Peres, J., Mowla, S., & Prince, S. (2015). The T-box transcription factor, TBX3, is a key substrate of AKT3 in melanomagenesis. *Oncotarget*, *6*(3), 1821–1833.

Peres, J., & Prince, S. (2013). The T-box transcription factor, TBX3, is sufficient to promote melanoma formation and invasion. *Molecular Cancer*, *12*(1), 117.

Perez, E. A., Kassira, N., Cheung, M. C., Koniaris, L. G., Neville, H. L., & Sola, J. E. (2011). Rhabdomyosarcoma in children: a SEER population based study. *The Journal of Surgical Research*, *170*(2), e243-51.

Perkins, S. M., Shinohara, E. T., DeWees, T., & Frangoul, H. (2014). Outcome for children with metastatic solid tumors over the last four decades. *PloS One*, *9*(7), e100396.

Peron, M., Bonvini, P., & Rosolen, A. (2012). Effect of inhibition of the ubiquitin-proteasome system and Hsp90 on growth and survival of rhabdomyosarcoma cells in vitro. *BMC Cancer*, *12*, 233.

Perry, R. L., & Rudnick, M. A. (2000). Molecular mechanisms regulating myogenic determination and differentiation. *Frontiers in Bioscience : A Journal and Virtual Library*, *5*, D750-67.

Peterson, J. M., Bakkar, N., & Guttridge, D. C. (2011). NF-κB Signaling in Skeletal Muscle Health

and Disease. *Current Topics in Developmental Biology*, *96*, 85–119.

Pierzyńska-Mach, A., Janowski, P. A., & Dobrucki, J. W. (2014). Evaluation of acridine orange, LysoTracker Red, and quinacrine as fluorescent probes for long-term tracking of acidic vesicles. *Cytometry Part A*, *85*(8), 729–737.

Pillay, K., Govender, D., & Chetty, R. (2002). ALK protein expression in rhabdomyosarcomas. *Histopathology*, *41*(5), 461–467.

Platonova, N., Scotti, M., Babich, P., Bertoli, G., Mento, E., Meneghini, V., … Merlo, G. R. (2007). TBX3, the gene mutated in ulnar-mammary syndrome, promotes growth of mammary epithelial cells via repression of p19ARF, independently of p53. *Cell and Tissue Research*, *328*(2), 301–316.

Pollak, M. (2008). Insulin and insulin-like growth factor signalling in neoplasia. *Nature Reviews Cancer*, *8*(12), 915–928.

Potthoff, M. J., & Olson, E. N. (2007). MEF2: a central regulator of diverse developmental programs. *Development*, *134*(23), 4131–4140.

Pounds, R., Leonard, S., Dawson, C., & Kehoe, S. (2017). Repurposing itraconazole for the treatment of cancer. *Oncology Letters*, *14*(3), 2587–2597.

Pownall, M. E., Gustafsson, M. K., & Emerson, C. P. (2002). Myogenic Regulatory Factors and the Specification of Muscle Progenitors in Vertebrate Embryos. *Annual Review of Cell and Developmental Biology*, *18*(1), 747–783.

Prager, G. W., Braga, S., Bystricky, B., Qvortrup, C., Criscitiello, C., Esin, E., … Ilbawi, A. (2018). Global cancer control: responding to the growing burden, rising costs and inequalities in access. *ESMO Open*, *3*(2), e000285.

Presta, L. G., Chen, H., O'Connor, S. J., Chisholm, V., Meng, Y. G., Krummen, L., … Ferrara, N. (1997). Humanization of an anti-vascular endothelial growth factor monoclonal antibody for the therapy of solid tumors and other disorders. *Cancer Research*, *57*(20), 4593–4599.

Preuss, E., Hugle, M., Reimann, R., Schlecht, M., & Fulda, S. (2013). Pan-mammalian target of rapamycin (mTOR) inhibitor AZD8055 primes rhabdomyosarcoma cells for ABT-737-induced apoptosis by down-regulating Mcl-1 protein. *The Journal of Biological Chemistry*, *288*(49), 35287–35296.

Prince, S., Carreira, S., Vance, K. W., Abrahams, A., & Goding, C. R. (2004). Tbx2 directly represses the expression of the p21(WAF1) cyclin-dependent kinase inhibitor. *Cancer Research*, *64*(5), 1669–1674.

Punyko, J. A., Mertens, A. C., Baker, K. S., Ness, K. K., Robison, L. L., & Gurney, J. G. (2005). Long-term survival probabilities for childhood rhabdomyosarcoma. A population-based evaluation. *Cancer*, *103*(7), 1475–1483.

Pushpakom, S., Iorio, F., Eyers, P. A., Escott, K. J., Hopper, S., Wells, A., … Pirmohamed, M. (2018). Drug repurposing: progress, challenges and recommendations. *Nature Reviews Drug Discovery*.

Qu, X., Yu, J., Bhagat, G., Furuya, N., Hibshoosh, H., Troxel, A., … Levine, B. (2003). Promotion of tumorigenesis by heterozygous disruption of the beclin 1 autophagy gene. *The Journal of Clinical Investigation*, *112*(12), 1809–1820.

Raben, D., Helfrich, B., Chan, D. C., Ciardiello, F., Zhao, L., Franklin, W., … Bunn, P. A. (2005). The effects of cetuximab alone and in combination with radiation and/or chemotherapy in lung cancer. *Clinical Cancer Research : An Official Journal of the American Association for Cancer Research*, *11*(2 Pt 1), 795–805.

Ragab, N., Viehweger, F., Bauer, J., Geyer, N., Yang, M., Seils, A., … Simon-Keller, K. (2018). Canonical WNT/β-Catenin Signaling Plays a Subordinate Role in Rhabdomyosarcomas. *Frontiers in Pediatrics*, *6*, 378.

Raimondi, L., Ciarapica, R., De Salvo, M., Verginelli, F., Gueguen, M., Martini, C., … Rota, R. (2012). Inhibition of Notch3 signalling induces rhabdomyosarcoma cell differentiation promoting p38 phosphorylation and p21Cip1 expression and hampers tumour cell growth in vitro and in vivo. *Cell Death & Differentiation*, *19*(5), 871–881.

Ramaglia, M., D'Angelo, V., Iannotta, A., Di Pinto, D., Pota, E., Affinita, M. C., … Caraglia, M. (2016). High EZH2 expression is correlated to metastatic disease in pediatric soft tissue sarcomas. *Cancer Cell International*, *16*(1), 59.

Raney, B., Stoner, J., Anderson, J., Andrassy, R., Arndt, C., Brown, K., … Hayes-Jordan, A. (2010). Impact of tumor viability at second-look procedures performed before completing treatment on the Intergroup Rhabdomyosarcoma Study Group protocol IRS-IV, 1991-1997: a report from the children's oncology group. *Journal of Pediatric Surgery*, *45*(11), 2160–2168.

Rao, R., Balusu, R., Fiskus, W., Mudunuru, U., Venkannagari, S., Chauhan, L., … Bhalla, K. N. (2012). Combination of pan-histone deacetylase inhibitor and autophagy inhibitor exerts superior efficacy against triple-negative human breast cancer cells. *Molecular Cancer Therapeutics*, *11*(4), 973–983.

Redell, M. S., & Tweardy, D. J. (2006). Targeting transcription factors in cancer: Challenges and evolving strategies. *Drug Discovery Today: Technologies*, *3*(3), 261–267.

Redmond, K. L., Crawford, N. T., Farmer, H., D'Costa, Z. C., O'Brien, G. J., Buckley, N. E., … Mullan, P. B. (2010). T-box 2 represses NDRG1 through an EGR1-dependent mechanism to drive the proliferation of breast cancer cells. *Oncogene*, *29*(22), 3252–3262.

Ricci, M. S., & Zong, W.-X. (2006). Chemotherapeutic approaches for targeting cell death pathways. *The Oncologist*, *11*(4), 342–357.

Rikhof, B., de Jong, S., Suurmeijer, A. J., Meijer, C., & van der Graaf, W. T. (2009). The insulin-like growth factor system and sarcomas. *The Journal of Pathology*, *217*(4), 469–482.

Riley, T., Sontag, E., Chen, P., & Levine, A. (2008). Transcriptional control of human p53-regulated genes. *Nature Reviews. Molecular Cell Biology*, *9*(5), 402–412.

Rini, B. I. (2008). Temsirolimus, an Inhibitor of Mammalian Target of Rapamycin. *Clinical Cancer Research*, *14*(5), 1286–1290.

Riss, T. L., Moravec, R. A., Niles, A. L., Benink, H. A., Worzella, T. J., & Minor, L. (2013, May 1). Cell Viability Assays. Eli Lilly & Company and the National Center for Advancing Translational Sciences.

Rodriguez, M., Aladowicz, E., Lanfrancone, L., & Goding, C. R. (2008). Tbx3 Represses E-Cadherin Expression and Enhances Melanoma Invasiveness. *Cancer Research*, *68*(19).

Rodriguez, R., Rubio, R., & Menendez, P. (2012). Modeling sarcomagenesis using multipotent mesenchymal stem cells. *Cell Research*, *22*(1), 62–77.

Roma, J., Masia, A., Reventos, J., Sanchez de Toledo, J., & Gallego, S. (2011). Notch Pathway Inhibition Significantly Reduces Rhabdomyosarcoma Invasiveness and Mobility In Vitro. *Clinical Cancer Research*, *17*(3), 505–513.

Romania, P., Bertaina, A., Bracaglia, G., Locatelli, F., Fruci, D., Rota, R., … Rota, R. (2012). Epigenetic Deregulation of MicroRNAs in Rhabdomyosarcoma and Neuroblastoma and Translational Perspectives. *International Journal of Molecular Sciences*, *13*(12), 16554–16579.

Rudin, C. M., Brahmer, J. R., Juergens, R. A., Hann, C. L., Ettinger, D. S., Sebree, R., … Liu, J. O. (2013). Phase 2 Study of Pemetrexed and Itraconazole as Second-Line Therapy for Metastatic Nonsquamous Non–Small-Cell Lung Cancer. *Journal of Thoracic Oncology*, *8*(5), 619–623.

Rudzinski, E. R., Anderson, J. R., Hawkins, D. S., Skapek, S. X., Parham, D. M., & Teot, L. A.

(2015). The World Health Organization Classification of Skeletal Muscle Tumors in Pediatric Rhabdomyosarcoma: A Report From the Children's Oncology Group. *Archives of Pathology & Laboratory Medicine*, *139*(10), 1281–1287.

Saab, R., Bills, J. L., Miceli, A. P., Anderson, C. M., Khoury, J. D., Fry, D. W., … Skapek, S. X. (2006). Pharmacologic inhibition of cyclin-dependent kinase 4/6 activity arrests proliferation in myoblasts and rhabdomyosarcoma-derived cells. *Molecular Cancer Therapeutics*, *5*(5), 1299–1308.

SABS Standards Division. (2015). *South African Bureau of Standards, South African National Standard: The care and use of animals for scientific purposes (SANS 10386:2008)*. *Groenkloof, Pretoria* (Vol. 1st Ed.).

Sachet, M., Liang, Y. Y., & Oehler, R. (2017). The immune response to secondary necrotic cells. *Apoptosis : An International Journal on Programmed Cell Death*, *22*(10), 1189–1204.

Satoh, K., Zhang, L., Zhang, Y., Chelluri, R., Boufraqech, M., Nilubol, N., … Kebebew, E. (2016). Identification of Niclosamide as a Novel Anticancer Agent for Adrenocortical Carcinoma. *Clinical Cancer Research*, *22*(14), 3458–3466.

Sawyers, C. (2004). Targeted cancer therapy. *Nature*, *432*(7015), 294–297.

Scannell, J. W., Blanckley, A., Boldon, H., & Warrington, B. (2012). Diagnosing the decline in pharmaceutical R&D efficiency. *Nature Reviews Drug Discovery*, *11*(3), 191–200.

Scheidler, S., Fredericks, W. J., Rauscher, F. J., Barr, F. G., & Vogt, P. K. (1996). The hybrid PAX3-FKHR fusion protein of alveolar rhabdomyosarcoma transforms fibroblasts in culture. *Proceedings of the National Academy of Sciences of the United States of America*, *93*(18), 9805–9809.

Schindelin, J., Arganda-Carreras, I., Frise, E., Kaynig, V., Longair, M., Pietzsch, T., … Cardona, A. (2012). Fiji: an open-source platform for biological-image analysis. *Nature Methods*, *9*(7), 676–682.

Schmidt, J. (2015). *Role and regulation of TBX2 and TBX3*. University of Oxford.

Schneider, C. A., Rasband, W. S., & Eliceiri, K. W. (2012). NIH Image to ImageJ: 25 years of image analysis. *Nature Methods*, *9*(7), 671–675.

Schöffski, P., Adkins, D., Blay, J.-Y., Gil, T., Elias, A. D., Rutkowski, P., … Grebennik, D. O. (2013). An open-label, phase 2 study evaluating the efficacy and safety of the anti-IGF-1R antibody cixutumumab in patients with previously treated advanced or metastatic soft-tissue sarcoma or Ewing family of tumours. *European Journal of Cancer*, *49*(15), 3219–

3228.

Schöffski, P., Wozniak, A., Leahy, M. G., Aamdal, S., Rutkowski, P., Bauer, S., … Strauss, S. J. (2018). The tyrosine kinase inhibitor crizotinib does not have clinically meaningful activity in heavily pre-treated patients with advanced alveolar rhabdomyosarcoma with FOXO rearrangement: European Organisation for Research and Treatment of Cancer phase 2 trial 90101 'CREATE.' *European Journal of Cancer*, *94*, 156–167.

Schwab, M. (2004). MYCN in neuronal tumours. *Cancer Letters*, *204*(2), 179–187.

Scrable, H., Cavenee, W., Ghavimi, F., Lovell, M., Morgan, K., & Sapienza, C. (1989). A model for embryonal rhabdomyosarcoma tumorigenesis that involves genome imprinting. *Proceedings of the National Academy of Sciences of the United States of America*, *86*(19), 7480–7484.

Sebé-Pedrós, A., Ariza-Cosano, A., Weirauch, M. T., Leininger, S., Yang, A., Torruella, G., … Ruiz-Trillo, I. (2013). Early evolution of the T-box transcription factor family. *Proceedings of the National Academy of Sciences of the United States of America*, *110*(40), 16050–16055.

Seki, M., Nishimura, R., Yoshida, K., Shimamura, T., Shiraishi, Y., Sato, Y., … Takita, J. (2015). Integrated genetic and epigenetic analysis defines novel molecular subgroups in rhabdomyosarcoma. *Nature Communications*, *6*(1), 7557.

Serrano, F. A., Matsuo, A. L., Monteforte, P. T., Bechara, A., Smaili, S. S., Santana, D. P., … Rodrigues, E. G. (2011). A cyclopalladated complex interacts with mitochondrial membrane thiol-groups and induces the apoptotic intrinsic pathway in murine and cisplatin-resistant human tumor cells. *BMC Cancer*, *11*(1), 296.

Shackelford, D. B., & Shaw, R. J. (2009). The LKB1-AMPK pathway: metabolism and growth control in tumour suppression. *Nature Reviews. Cancer*, *9*(8), 563–575.

Shapiro, D. N., Jones, B. G., Shapiro, L. H., Dias, P., & Houghton, P. J. (1994). Antisense-mediated reduction in insulin-like growth factor-I receptor expression suppresses the malignant phenotype of a human alveolar rhabdomyosarcoma. *Journal of Clinical Investigation*, *94*(3), 1235–1242.

Shen, S., Kepp, O., & Kroemer, G. (2012). The end of autophagic cell death? *Autophagy*, *8*(1), 1–3.

Shern, J. F., Chen, L., Chmielecki, J., Wei, J. S., Patidar, R., Rosenberg, M., … Khan, J. (2014). Comprehensive genomic analysis of rhabdomyosarcoma reveals a landscape of

alterations affecting a common genetic axis in fusion-positive and fusion-negative tumors. *Cancer Discovery*, *4*(2), 216–231.

Shern, J. F., Yohe, M. E., & Khan, J. (2015). Pediatric Rhabdomyosarcoma. *Critical Reviews in Oncogenesis*, *20*(3–4), 227–243.

Shi, Y. (2002). Mechanisms of caspase activation and inhibition during apoptosis. *Molecular Cell*, *9*(3), 459–470.

Shintani, T., & Klionsky, D. J. (2004). Autophagy in health and disease: a double-edged sword. *Science (New York, N.Y.)*, *306*(5698), 990–995.

Shuman, C., Beckwith, J. B., & Weksberg, R. (1993). *Beckwith-Wiedemann Syndrome*. *GeneReviews®*. University of Washington, Seattle.

Silva, M. T. (2010). Secondary necrosis: The natural outcome of the complete apoptotic program. *FEBS Letters*, *584*(22), 4491–4499.

Silverman, R. B., & Holladay, M. W. (2014). *The Organic Chemistry of Drug Design and Drug Action* (Third Ed). San Diego, CA, USA: Academic Press.

Sims, D. A. (2016). *The role of T-box transcription factor TBX3 in rhabdomyosarcoma*. University of Cape Town.

Sionov, R. V, & Haupt, Y. (1999). The cellular response to p53: the decision between life and death. *Oncogene*, *18*(45), 6145–6157.

Skapek, S. X., Ferrari, A., Gupta, A. A., Lupo, P. J., Butler, E., Shipley, J., … Hawkins, D. S. (2019). Rhabdomyosarcoma. *Nature Reviews Disease Primers*, *5*(1), 1.

Skubitz, K. M., & D'Adamo, D. R. (2007). Sarcoma. *Mayo Clinic Proceedings*, *82*(11), 1409–1432.

Smith, H. J., & Williams, H. (2005). *Introduction to the Principles of Drug Design and Action* (4th Ed.). Boca Raton, FL, USA: CRC Press Taylor & Francis Group.

Smith, J. A., Wilson, L., Azarenko, O., Zhu, X., Lewis, B. M., Littlefield, B. A., & Jordan, M. A. (2010). Eribulin Binds at Microtubule Ends to a Single Site on Tubulin To Suppress Dynamic Instability. *Biochemistry*, *49*(6), 1331–1337.

Smith, T. C., Kinkel, A. W., Gryczko, C. M., & Goulet, J. R. (1976). Absorption of pyrvinium pamoate. *Clinical Pharmacology and Therapeutics*, *19*(6), 802–806.

Soerjomataram, I., Lortet-Tieulent, J., Parkin, D. M., Ferlay, J., Mathers, C., Forman, D., & Bray, F. (2012). Global burden of cancer in 2008: a systematic analysis of disability-adjusted life-years in 12 world regions. *The Lancet*, *380*(9856), 1840–1850.

Soldani, C., & Scovassi, A. I. (2002). Poly(ADP-ribose) polymerase-1 cleavage during apoptosis: An update. *Apoptosis*, *7*(4), 321–328.

Soleimani, V. D., & Rudnicki, M. A. (2011). New insights into the origin and the genetic basis of rhabdomyosarcomas. *Cancer Cell*, *19*(2), 157–159.

Song, S., Christova, T., Perusini, S., Alizadeh, S., Bao, R.-Y., Miller, B. W., … Attisano, L. (2011). Wnt Inhibitor Screen Reveals Iron Dependence of -Catenin Signaling in Cancers. *Cancer Research*, *71*(24), 7628–7639.

Srinivasula, S. M., Ahmad, M., Fernandes-Alnemri, T., & Alnemri, E. S. (1998). Autoactivation of procaspase-9 by Apaf-1-mediated oligomerization. *Molecular Cell*, *1*(7), 949–957.

Stevens, M. C. G. (2005). Treatment for childhood rhabdomyosarcoma: the cost of cure. *The Lancet. Oncology*, *6*(2), 77–84.

Storer, N. Y., White, R. M., Uong, A., Price, E., Nielsen, G. P., Langenau, D. M., & Zon, L. I. (2013). Zebrafish rhabdomyosarcoma reflects the developmental stage of oncogene expression during myogenesis. *Development*, *140*(14), 3040–3050.

Su, Z., Yang, Z., Xie, L., DeWitt, J. P., & Chen, Y. (2016). Cancer therapy in the necroptosis era. *Cell Death & Differentiation*, *23*(5), 748–756.

Sui, X., Jin, L., Huang, X., Geng, S., He, C., & Hu, X. (2011). p53 signaling and autophagy in cancer: a revolutionary strategy could be developed for cancer treatment. *Autophagy*, *7*(6), 565–571.

Sun, C., De Mello, V., Mohamed, A., Ortuste Quiroga, H. P., Garcia-Munoz, A., Al Bloshi, A., … Zammit, P. S. (2017). Common and Distinctive Functions of the Hippo Effectors Taz and Yap in Skeletal Muscle Stem Cell Function. *Stem Cells (Dayton, Ohio)*, *35*(8), 1958–1972.

Sun, L., Wang, H., Wang, Z., He, S., Chen, S., Liao, D., … Wang, X. (2012). Mixed Lineage Kinase Domain-like Protein Mediates Necrosis Signaling Downstream of RIP3 Kinase. *Cell*, *148*(1–2), 213–227.

Svalina, M. N., & Keller, C. (2014). YAPping About Differentiation Therapy in Muscle Cancer. *Cancer Cell*, *26*(2), 154–155.

Tada, M., & Smith, J. C. (2001). T-targets: Clues to understanding the functions of T-box proteins. *Development, Growth and Differentiation*, *43*(1), 1–11.

Tan, C.-P., Lu, Y.-Y., Ji, L.-N., & Mao, Z.-W. (2014). Metallomics insights into the programmed cell death induced by metal-based anticancer compounds. *Metallomics : Integrated Biometal Science*, *6*(5), 978–995.

Tanida, I., Ueno, T., & Kominami, E. (2008). LC3 and Autophagy. *Methods in Molecular Biology (Clifton, N.J.)*, *445*, 77–88.

Tapscott, S. J. (2005). The circuitry of a master switch: Myod and the regulation of skeletal muscle gene transcription. *Development*, *132*(12), 2685–2695.

Tapscott, S. J., Thayer, M. J., & Weintraub, H. (1993). Deficiency in rhabdomyosarcomas of a factor required for MyoD activity and myogenesis. *Science (New York, N.Y.)*, *259*(5100), 1450–1453.

Tasaka, R., Fukuda, T., Shimomura, M., Inoue, Y., Wada, T., Kawanishi, M., … Sumi, T. (2017). TBX2 expression is associated with platinum-sensitivity of ovarian serous carcinoma. *Oncology Letters*, *15*(3), 3085–3090.

Taulli, R., Foglizzo, V., Morena, D., Coda, D. M., Ala, U., Bersani, F., … Ponzetto, C. (2014). Failure to downregulate the BAF53a subunit of the SWI/SNF chromatin remodeling complex contributes to the differentiation block in rhabdomyosarcoma. *Oncogene*, *33*(18), 2354–2362.

Taulli, R., Scuoppo, C., Bersani, F., Accornero, P., Forni, P. E., Miretti, S., … Ponzetto, C. (2006). Validation of Met as a Therapeutic Target in Alveolar and Embryonal Rhabdomyosarcoma. *Cancer Research*, *66*(9), 4742–4749.

Teicher, B. A. (2012). Searching for molecular targets in sarcoma. *Biochemical Pharmacology*, *84*(1), 1–10.

Tenente, I. M., Hayes, M. N., Ignatius, M. S., McCarthy, K., Yohe, M., Sindiri, S., … Langenau, D. M. (2017). Myogenic regulatory transcription factors regulate growth in rhabdomyosarcoma. *ELife*, *6*.

The United States Pharmacopeial Convention. (2008). *USP Certificate Piroctone Olamine*. Rockville, Maryland, USA.

Thuault, S., Hayashi, S., Lagirand-Cantaloube, J., Plutoni, C., Comunale, F., Delattre, O., … Gauthier-Rouvière, C. (2013). P-cadherin is a direct PAX3–FOXO1A target involved in alveolar rhabdomyosarcoma aggressiveness. *Oncogene*, *32*(15), 1876–1887.

Tiash, S., & Chowdhury, E. (2015). Growth factor receptors: promising drug targets in cancer. *Journal of Cancer Metastasis and Treatment*, *1*(3), 190.

Tiffin, N., Williams, R. D., Shipley, J., & Pritchard-Jones, K. (2003). PAX7 expression in embryonal rhabdomyosarcoma suggests an origin in muscle satellite cells. *British Journal of Cancer*, *89*(2), 327–332.

Tobinick, E. L. (2009). The value of drug repositioning in the current pharmaceutical market. *Drug News & Perspectives*, *22*(2), 119–125.

Totaro, A., Panciera, T., & Piccolo, S. (2018). YAP/TAZ upstream signals and downstream responses. *Nature Cell Biology*, *20*(8), 888–899.

Tremblay, A. M., Missiaglia, E., Galli, G. G., Hettmer, S., Urcia, R., Carrara, M., … Camargo, F. D. (2014). The Hippo Transducer YAP1 Transforms Activated Satellite Cells and Is a Potent Effector of Embryonal Rhabdomyosarcoma Formation. *Cancer Cell*, *26*(2), 273–287.

Tsubamoto, H., Sonoda, T., & Inoue, K. (2014). Impact of itraconazole on the survival of heavily pre-treated patients with triple-negative breast cancer. *Anticancer Research*, *34*(7), 3839–3844.

Tsubamoto, H., Sonoda, T., Yamasaki, M., & Inoue, K. (2014). Impact of combination chemotherapy with itraconazole on survival of patients with refractory ovarian cancer. *Anticancer Research*, *34*(5), 2481–2487.

Tšuiko, O., Jatsenko, T., Parameswaran Grace, L. K., Kurg, A., Vermeesch, J. R., Lanner, F., … Salumets, A. (2018). A speculative outlook on embryonic aneuploidy: Can molecular pathways be involved? *Developmental Biology*.

Tsumura, H., Yoshida, T., Saito, H., Imanaka-Yoshida, K., & Suzuki, N. (2006). Cooperation of oncogenic K-ras and p53 deficiency in pleomorphic rhabdomyosarcoma development in adult mice. *Oncogene*, *25*(59), 7673–7679.

Turner, J. A., & Johnson, P. E. (1962). Pyrvinium pamoate in the treatment of pinworm infection (enterobiasis) in the bome. *The Journal of Pediatrics*, *60*(2), 243–251.

Ulukaya, E., Ari, F., Dimas, K., Ikitimur, E. I., Guney, E., & Yilmaz, V. T. (2011). Anti-cancer activity of a novel palladium(II) complex on human breast cancer cells in vitro and in vivo. *European Journal of Medicinal Chemistry*, *46*(10), 4957–4963.

Ulukaya, E., Ari, F., Dimas, K., Sarimahmut, M., Guney, E., Sakellaridis, N., & Yilmaz, V. T. (2011). Cell death-inducing effect of novel palladium(II) and platinum(II) complexes on non-small cell lung cancer cells in vitro. *Journal of Cancer Research and Clinical Oncology*, *137*(10), 1425–1434.

Ulukaya, E., Frame, F. M., Cevatemre, B., Pellacani, D., Walker, H., Mann, V. M., … Maitland, N. J. (2013). Differential cytotoxic activity of a novel palladium-based compound on prostate cell lines, primary prostate epithelial cells and prostate stem cells. *PloS One*, *8*(5), e64278.

Ummat, A., Rechkoblit, O., Jain, R., Roy Choudhury, J., Johnson, R. E., Silverstein, T. D., … Aggarwal, A. K. (2012). Structural basis for cisplatin DNA damage tolerance by human polymerase η during cancer chemotherapy. *Nature Structural & Molecular Biology*, *19*(6), 628–632.

Valdiglesias, V., Giunta, S., Fenech, M., Neri, M., & Bonassi, S. (2013). γH2AX as a marker of DNA double strand breaks and genomic instability in human population studies. *Mutation Research*, *753*(1), 24–40.

Van Antwerp, M. E., Chen, D. G., Chang, C., & Prochownik, E. V. (1992). A point mutation in the MyoD basic domain imparts c-Myc-like properties. *Proceedings of the National Academy of Sciences of the United States of America*, *89*(19), 9010–9014.

van der Graaf, W. T. A., Blay, J.-Y., Chawla, S. P., Kim, D.-W., Bui-Nguyen, B., Casali, P. G., … Hohenberger, P. (2012). Pazopanib for metastatic soft-tissue sarcoma (PALETTE): a randomised, double-blind, placebo-controlled phase 3 trial. *Lancet*, *379*(9829), 1879–1886.

van Engeland, M., Nieland, L. J., Ramaekers, F. C., Schutte, B., & Reutelingsperger, C. P. (1998). Annexin V-affinity assay: a review on an apoptosis detection system based on phosphatidylserine exposure. *Cytometry*, *31*(1), 1–9.

van Erp, A. E. M., Hillebrandt-Roeffen, M. H. S., van Houdt, L., Fleuren, E. D. G., van der Graaf, W. T. A., & Versleijen-Jonkers, Y. M. H. (2017). Targeting Anaplastic Lymphoma Kinase (ALK) in Rhabdomyosarcoma (RMS) with the Second-Generation ALK Inhibitor Ceritinib. *Targeted Oncology*, *12*(6), 815–826.

van Gaal, J. C., Flucke, U. E., Roeffen, M. H. S., de Bont, E. S. J. M., Sleijfer, S., Mavinkurve-Groothuis, A. M. C., … Versleijen-Jonkers, Y. M. H. (2012). Anaplastic Lymphoma Kinase Aberrations in Rhabdomyosarcoma: Clinical and Prognostic Implications. *Journal of Clinical Oncology*, *30*(3), 308–315.

Vance, K. W., Carreira, S., Brosch, G., & Goding, C. R. (2005). Tbx2 Is Overexpressed and Plays an Important Role in Maintaining Proliferation and Suppression of Senescence in Melanomas. *Cancer Research*, *65*(6), 2260–2268.

Vandenabeele, P., Galluzzi, L., Vanden Berghe, T., & Kroemer, G. (2010). Molecular mechanisms of necroptosis: an ordered cellular explosion. *Nature Reviews. Molecular Cell Biology*, *11*(10), 700–714.

Vermes, I., Haanen, C., Steffens-Nakken, H., & Reutellingsperger, C. (1995). A novel assay for

apoptosis Flow cytometric detection of phosphatidylserine expression on early apoptotic cells using fluorescein labelled Annexin V. *Journal of Immunological Methods*, *184*(1), 39–51.

Viola, G., Bortolozzi, R., Hamel, E., Moro, S., Brun, P., Castagliuolo, I., … Basso, G. (2012). MG-2477, a new tubulin inhibitor, induces autophagy through inhibition of the Akt/mTOR pathway and delayed apoptosis in A549 cells. *Biochemical Pharmacology*, *83*(1), 16–26.

von Maltzahn, J., Chang, N. C., Bentzinger, C. F., & Rudnicki, M. A. (2012). Wnt signaling in myogenesis. *Trends in Cell Biology*, *22*(11), 602–609.

Wachtel, M., Runge, T., Leuschner, I., Stegmaier, S., Koscielniak, E., Treuner, J., … Schäfer, B. W. (2006). Subtype and prognostic classification of rhabdomyosarcoma by immunohistochemistry. *Journal of Clinical Oncology : Official Journal of the American Society of Clinical Oncology*, *24*(5), 816–822.

Wackerhage, H., Del Re, D. P., Judson, R. N., Sudol, M., & Sadoshima, J. (2014). The Hippo signal transduction network in skeletal and cardiac muscle. *Science Signaling*, *7*(337), re4.

Wajant, H. (2002). The Fas signaling pathway: more than a paradigm. *Science (New York, N.Y.)*, *296*(5573), 1635–1636.

Walters, Z. S., Villarejo-Balcells, B., Olmos, D., Buist, T. W. S., Missiaglia, E., Allen, R., … Shipley, J. (2014). JARID2 is a direct target of the PAX3-FOXO1 fusion protein and inhibits myogenic differentiation of rhabdomyosarcoma cells. *Oncogene*, *33*(9), 1148–1157.

Wan, X., Shen, N., Mendoza, A., Khanna, C., & Helman, L. J. (2006). CCI-779 Inhibits Rhabdomyosarcoma Xenograft Growth by an Antiangiogenic Mechanism Linked to the Targeting of mTOR/Hif-1α/VEGF Signaling. *Neoplasia*, *8*(5), 394–401.

Wang, B., Lindley, L. E., Fernandez-Vega, V., Rieger, M. E., Sims, A. H., & Briegel, K. J. (2012). The T Box Transcription Factor TBX2 Promotes Epithelial-Mesenchymal Transition and Invasion of Normal and Malignant Breast Epithelial Cells. *PLoS ONE*, *7*(7), e41355.

Wang, C. (2012). Childhood rhabdomyosarcoma: recent advances and prospective views. *Journal of Dental Research*, *91*(4), 341–350.

Wang, H., Garzon, R., Sun, H., Ladner, K. J., Singh, R., Dahlman, J., … Guttridge, D. C. (2008). NF-κB–YY1–miR-29 Regulatory Circuitry in Skeletal Myogenesis and Rhabdomyosarcoma. *Cancer Cell*, *14*(5), 369–381.

Wang, H., Sun, L., Su, L., Rizo, J., Liu, L., Wang, L.-F., … Wang, X. (2014). Mixed Lineage Kinase

Domain-like Protein MLKL Causes Necrotic Membrane Disruption upon Phosphorylation by RIP3. *Molecular Cell*, *54*(1), 133–146.

Wang, Q., Na, B., Ou, J. J., Pulliam, L., & Yen, T. S. B. (2012). Hepatitis B Virus Alters the Antioxidant System in Transgenic Mice and Sensitizes Hepatocytes to Fas Signaling. *PLoS ONE*, *7*(5), e36818.

Wang, S., & El-Deiry, W. S. (2003). TRAIL and apoptosis induction by TNF-family death receptors. *Oncogene*, *22*(53), 8628–8633.

Wansleben, S. (2013). *The role of the transcription factor TBX2 in breast cancer and melanoma and its regulation by the UV-induced DNA damage pathway*. University of Cape Town.

Wansleben, S., Davis, E., Peres, J., & Prince, S. (2013). A novel role for the anti-senescence factor TBX2 in DNA repair and cisplatin resistance. *Cell Death & Disease*, *4*(10), e846–e846.

Wansleben, S., Peres, J., Hare, S., Goding, C. R., & Prince, S. (2014). T-box transcription factors in cancer biology. *Biochimica et Biophysica Acta*, *1846*(2), 380–391.

Ward, E., DeSantis, C., Robbins, A., Kohler, B., & Jemal, A. (2014). Childhood and adolescent cancer statistics, 2014. *CA: A Cancer Journal for Clinicians*, *64*(2), 83–103.

Waring, M. J., Arrowsmith, J., Leach, A. R., Leeson, P. D., Mandrell, S., Owen, R. M., … Weir, A. (2015). An analysis of the attrition of drug candidates from four major pharmaceutical companies. *Nature Reviews Drug Discovery*, *14*(7), 475–486.

Watt, K. I., Judson, R., Medlow, P., Reid, K., Kurth, T. B., Burniston, J. G., … Wackerhage, H. (2010). Yap is a novel regulator of C2C12 myogenesis. *Biochemical and Biophysical Research Communications*, *393*(4), 619–624.

Weber-Hall, S., Anderson, J., McManus, A., Abe, S., Nojima, T., Pinkerton, R., … Shipley, J. (1996). Gains, losses, and amplification of genomic material in rhabdomyosarcoma analyzed by comparative genomic hybridization. *Cancer Research*, *56*(14), 3220–3224.

Wei, L., Surma, M., Gough, G., Shi, S., Lambert-Cheatham, N., Chang, J., & Shi, J. (2015). Dissecting the Mechanisms of Doxorubicin and Oxidative Stress-Induced Cytotoxicity: The Involvement of Actin Cytoskeleton and ROCK1. *PLOS ONE*, *10*(7), e0131763.

Wei, M. C., Lindsten, T., Mootha, V. K., Weiler, S., Gross, A., Ashiya, M., … Korsmeyer, S. J. (2000). tBID, a membrane-targeted death ligand, oligomerizes BAK to release cytochrome c. *Genes & Development*, *14*(16), 2060–2071.

Wei, M. C., Zong, W. X., Cheng, E. H., Lindsten, T., Panoutsakopoulou, V., Ross, A. J., …

Korsmeyer, S. J. (2001). Proapoptotic BAX and BAK: a requisite gateway to mitochondrial dysfunction and death. *Science (New York, N.Y.)*, *292*(5517), 727–730.

Weintraub, H., Tapscott, S. J., Davis, R. L., Thayer, M. J., Adam, M. A., Lassar, A. B., & Miller, A. D. (1989). Activation of muscle-specific genes in pigment, nerve, fat, liver, and fibroblast cell lines by forced expression of MyoD. *Proceedings of the National Academy of Sciences of the United States of America*, *86*(14), 5434–5438.

Weiss, A., Gill, J., Goldberg, J., Lagmay, J., Spraker-Perlman, H., Venkatramani, R., & Reed, D. (2014). Advances in therapy for pediatric sarcomas. *Current Oncology Reports*, *16*(8), 395.

Wertz, I. E., O'Rourke, K. M., Zhou, H., Eby, M., Aravind, L., Seshagiri, S., … Dixit, V. M. (2004). De-ubiquitination and ubiquitin ligase domains of A20 downregulate NF-κB signalling. *Nature*, *430*(7000), 694–699.

White, E. (2012). Deconvoluting the context-dependent role for autophagy in cancer. *Nature Reviews. Cancer*, *12*(6), 401–410.

White, E., & DiPaola, R. S. (2009). The double-edged sword of autophagy modulation in cancer. *Clinical Cancer Research : An Official Journal of the American Association for Cancer Research*, *15*(17), 5308–5316.

Wieland, A., Trageser, D., Gogolok, S., Reinartz, R., Hofer, H., Keller, M., … Scheffler, B. (2013). Anticancer Effects of Niclosamide in Human Glioblastoma. *Clinical Cancer Research*, *19*(15), 4124–4136.

Williamson, D., Selfe, J., Gordon, T., Lu, Y.-J., Pritchard-Jones, K., Murai, K., … Shipley, J. (2007). Role for Amplification and Expression of *Glypican-5* in Rhabdomyosarcoma. *Cancer Research*, *67*(1), 57–65.

Willmer, T., Cooper, A., Sims, D., Govender, D., & Prince, S. (2016). The T-box transcription factor 3 is a promising biomarker and a key regulator of the oncogenic phenotype of a diverse range of sarcoma subtypes. *Oncogenesis*, *5*(2), e199.

Wilson, V., & Conlon, F. L. (2002). The T-box family. *Genome Biology*, *3*(6), reviews3008.1.

Wirawan, E., Vanden Berghe, T., Lippens, S., Agostinis, P., & Vandenabeele, P. (2012). Autophagy: for better or for worse. *Cell Research*, *22*(1), 43–61.

Woo, M., Hakem, R., Soengas, M. S., Duncan, G. S., Shahinian, A., Kägi, D., … Mak, T. W. (1998). Essential contribution of caspase 3/CPP32 to apoptosis and its associated nuclear changes. *Genes & Development*, *12*(6), 806–819.

Wood, C. D., Thornton, T. M., Sabio, G., Davis, R. A., & Rincon, M. (2009). Nuclear localization of p38 MAPK in response to DNA damage. *International Journal of Biological Sciences*, *5*(5), 428–437.

Woodburn, J. R. (1999). The epidermal growth factor receptor and its inhibition in cancer therapy. *Pharmacology & Therapeutics*, *82*(2–3), 241–250.

Woods, D., & Turchi, J. J. (2013). Chemotherapy induced DNA damage response: convergence of drugs and pathways. *Cancer Biology & Therapy*, *14*(5), 379–389.

Wright, A., Reiley, W. W., Chang, M., Jin, W., Lee, A. J., Zhang, M., & Sun, S.-C. (2007). Regulation of Early Wave of Germ Cell Apoptosis and Spermatogenesis by Deubiquitinating Enzyme CYLD. *Developmental Cell*, *13*(5), 705–716.

Xiao, W., Mohseny, A. B., Hogendoorn, P. C. W., Cleton-Jansen, A.-M., Friedenstein, A., Chailakhjan, R., … Lira, S. (2013). Mesenchymal stem cell transformation and sarcoma genesis. *Clinical Sarcoma Research*, *3*(1), 10.

Xie, T., Peng, W., Yan, C., Wu, J., Gong, X., & Shi, Y. (2013). Structural Insights into RIP3-Mediated Necroptotic Signaling. *Cell Reports*, *5*(1), 70–78.

Yang, P.-M., Liu, Y.-L., Lin, Y.-C., Shun, C.-T., Wu, M.-S., & Chen, C.-C. (2010). Inhibition of autophagy enhances anticancer effects of atorvastatin in digestive malignancies. *Cancer Research*, *70*(19), 7699–7709.

Yang, P., Grufferman, S., Khoury, M. J., Schwartz, A. G., Kowalski, J., Ruymann, F. B., & Maurer, H. M. (1995). Association of childhood rhabdomyosarcoma with neurofibromatosis type I and birth defects. *Genetic Epidemiology*, *12*(5), 467–474.

Yang, Z. J., Chee, C. E., Huang, S., & Sinicrope, F. A. (2011). The role of autophagy in cancer: therapeutic implications. *Molecular Cancer Therapeutics*, *10*(9), 1533–1541.

Yap, T. A., Garrett, M. D., Walton, M. I., Raynaud, F., de Bono, J. S., & Workman, P. (2008). Targeting the PI3K-AKT-mTOR pathway: progress, pitfalls, and promises. *Current Opinion in Pharmacology*, *8*(4), 393–412.

Yarosh, W., Barrientos, T., Esmailpour, T., Lin, L., Carpenter, P. M., Osann, K., … Huang, T. (2008). TBX3 Is Overexpressed in Breast Cancer and Represses p14ARF by Interacting with Histone Deacetylases. *Cancer Research*, *68*(3), 693–699.

Yatim, N., Jusforgues-Saklani, H., Orozco, S., Schulz, O., Barreira da Silva, R., Reis e Sousa, C., … Albert, M. L. (2015). RIPK1 and NF- B signaling in dying cells determines cross-priming of CD8+ T cells. *Science*, *350*(6258), 328–334.

Yeh, J. E., Toniolo, P. A., & Frank, D. A. (2013). Targeting transcription factors. *Current Opinion in Oncology*, *25*(6), 652–658.

Yu, D.-H., Macdonald, J., Liu, G., Lee, A. S., Ly, M., Davis, T., … Li, Q.-X. (2008). Pyrvinium Targets the Unfolded Protein Response to Hypoglycemia and Its Anti-Tumor Activity Is Enhanced by Combination Therapy. *PLoS ONE*, *3*(12), e3951.

Yu, H., Liu, B. O., Liu, A., Li, K., & Zhao, H. (2015). T-box 2 expression predicts poor prognosis in gastric cancer. *Oncology Letters*, *10*(3), 1689–1693.

Yu, P. Y., & Guttridge, D. C. (2018). Dysregulated Myogenesis in Rhabdomyosarcoma. *Current Topics in Developmental Biology*, *126*, 285–297.

Zhan, T., Rindtorff, N., & Boutros, M. (2017). Wnt signaling in cancer. *Oncogene*, *36*(11), 1461–1473.

Zhang, D.-W., Shao, J., Lin, J., Zhang, N., Lu, B.-J., Lin, S.-C., … Han, J. (2009). RIP3, an Energy Metabolism Regulator That Switches TNF-Induced Cell Death from Apoptosis to Necrosis. *Science*, *325*(5938), 332–336.

Zhang, L., Chen, X., Wu, J., Ding, S., Wang, X., Lei, Q., & Fang, W. (2018). Palladium nanoparticles induce autophagy and autophagic flux blockade in Hela cells. *RSC Advances*, *8*(8), 4130–4141.

Zhang, M., Truscott, J., & Davie, J. (2013). Loss of MEF2D expression inhibits differentiation and contributes to oncogenesis in rhabdomyosarcoma cells. *Molecular Cancer*, *12*(1), 150.

Zhang, M., Zhu, B., & Davie, J. (2015). Alternative splicing of MEF2C pre-mRNA controls its activity in normal myogenesis and promotes tumorigenicity in rhabdomyosarcoma cells. *The Journal of Biological Chemistry*, *290*(1), 310–324.

Zhang, X. D. (2011). Illustration of SSMD, z Score, SSMD*, z* Score, and t Statistic for Hit Selection in RNAi High-Throughput Screens. *Journal of Biomolecular Screening*, *16*(7), 775–785.

Zhou, B. B., & Elledge, S. J. (2000). The DNA damage response: putting checkpoints in perspective. *Nature*, *408*(6811), 433–439.

Zhou, H., Shen, T., Shang, C., Luo, Y., Liu, L., Yan, J., … Huang, S. (2014). Ciclopirox induces autophagy through reactive oxygen species-mediated activation of JNK signaling pathway. *Oncotarget*, *5*(20), 10140–10150.

Zhou, W., & Yuan, J. (2014). Necroptosis in health and diseases. *Seminars in Cell &*

Developmental Biology, *35*, 14–23.

Zhu, B., & Davie, J. K. (2015, January 20). New insights into signalling-pathway alterations in rhabdomyosarcoma. *British Journal of Cancer*. Nature Publishing Group.

Zhu, B., Zhang, M., Byrum, S. D., Tackett, A. J., & Davie, J. K. (2014). TBX2 blocks myogenesis and promotes proliferation in rhabdomyosarcoma cells. *International Journal of Cancer*, *135*(4), 785–797.

Zhu, B., Zhang, M., Williams, E. M., Keller, C., Mansoor, A., & Davie, J. K. (2016). TBX2 represses PTEN in rhabdomyosarcoma and skeletal muscle. *Oncogene*, *35*(32), 4212–4224.

Zi, F., Zi, H., Li, Y., He, J., Shi, Q., & Cai, Z. (2018). Metformin and cancer: An existing drug for cancer prevention and therapy. *Oncology Letters*, *15*(1), 683–690.

Ziegler, U. (2004). Morphological Features of Cell Death. *News in Physiological Sciences*, *19*(3), 124–128.

CHAPTER 7

Appendix

7.1 Mycoplasma test Mounting fluid

20mM citric acid

55mM $Na_2HPO_4.2H_2O$

50% glycerol

pH to 5.5

Store at 4°C

7.2 Cell viability assays

7.2.1 MTT reagent

100mg MTT powder

Dissolve in 20mL autoclaved 1XPBS (see Appendix 7.7)

Vortex and incubate at 37°C for 15min

Filter through 0.2µm filter

Cover in foil and store at 4°C

7.2.2 Solubilising reagent

25g sodium dodecyl sulphate (SDS)

Dissolve in 350mL dH_20 (using stirrer bar)

Add 76.6µL concentrated hydrochloric acid (HCL)

Store at -20°C

7.3 0.5% crystal violet staining solution: 100mL

0.5% crystal violet (w/v), therefore 0.5g

Fill up to 100mL with 100% methanol

Store at RT

7.4 2x boiling blue protein sample loading buffer: 10mL

1.25mL 1M tris-HCl pH 6.8 (see below)

4mL 10% SDS

1mL β-mercaptoethanol

2mL glycerol

1.75mL dH_2O

Pinch of bromophenol blue

Store at -20°C

7.5 SDS-PAGE protein markers

PageRuler™ Prestained Protein Ladder
10 to 180 kDa
Thermo Fisher Scientific

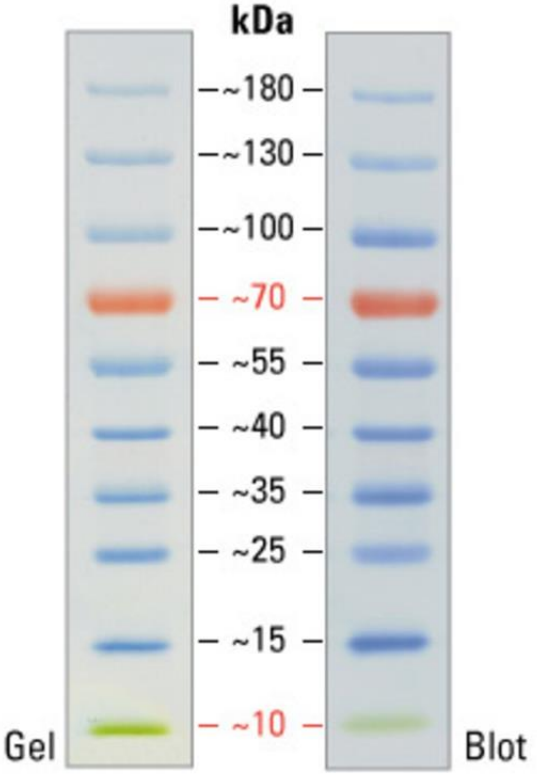

Color Prestained Protein Standard, Broad Range
11–245 kDa
New England BioLabs

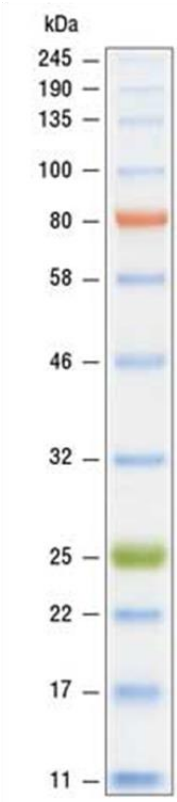

7.6 SDS-PAGE solutions and buffers

7.6.1 Resolving gels

Gel % acrylamide	8%		10%		12%		15%	
Total volume	**10mL**	**20mL**	**10mL**	**20mL**	**10mL**	**20mL**	**10mL**	**20mL**
H_2O	5.3mL	10.6mL	4.8mL	9.6mL	4.3mL	8.6mL	3.5mL	7mL
40% acrylamide	2mL	4mL	2.5mL	5mL	3mL	6mL	3.8mL	7.6mL
1.5M Tris (pH 8.8)	2.5mL	5.0mL	2.5mL	5.0mL	2.5mL	5.0mL	2.5mL	5.0mL
10% SDS	100ul	200ul	100ul	200ul	100ul	200ul	100ul	200ul
10% APS	100ul	200ul	100ul	200ul	100ul	200ul	100ul	200ul
TEMED	10ul	20ul	10ul	20ul	10ul	20ul	10ul	20ul

7.6.2 Stacking gels

Gel % acrylamide	5%	
Total volume	**8mL**	**4mL**
H_2O	5.8mL	2.75mL
40% acrylamide	1mL	650ul
1.5M Tris (pH 6.8)	1mL	500ul
10% SDS	80ul	40ul
10% APS	80ul	40ul
TEMED	8ul	4ul

7.6.3 1.5M Tris pH 8.8: 1L (buffer for resolving gels)

Dissolve 181.65g tris-base in 800mL dH_20 (using a stirrer bar)

Adjust pH to 8.8 with concentrated HCl

Fill up to 1L with dH_20

Store at 4°C

7.6.4 1.5M Tris pH 6.8: 1L (buffer for stacking gels)

Dissolve 181.65g tris-base in 800mL dH_20 (using a stirrer bar)

Adjust pH to 6.8 with concentrated HCl

Fill up to 1L with dH_20

Store at 4°C

7.6.5 10% sodium dodecyl sulphate (SDS): 1L

100g SDS

Dissolve in 800mL dH_20 (using a stirrer bar)

pH to 7.2 with concentrated HCL

Fill up to 1L with dH_20

Store at RT

7.6.6 10% ammonium persulphate (APS): 1mL

0.1g ammonium persulphate

Make solution up to 1mL with dH_2O

Store at 4°C

7.6.7 10x running buffer: 1L

10g SDS

30.3g tris-base

144g glycine

Dissolve in 800mL dH_2O (using a stirrer bar)

Once dissolved fill solution up to 1L with dH_2O

For use dilute to 1x (100mL 10x running buffer + 900mL dH_2O)

Store at RT

7.6.8 10x transfer buffer: 1L

33.3g tris-base

144g glycine

Dissolve in 800mL dH_2O (using a stirrer bar)

Once dissolved fill solution up to 1L with dH_2O

For use dilute to 1x (100mL 10x transfer buffer, 200mL isopropanol and 700mL dH_20)

Store at 4°C

7.7 10x phosphate buffered saline (PBS): 1L

80g NaCl

12.6g Na_2HPO_4 anhydrous

2g KCl

2.4g KH_2PO_4

Dissolve in 800mL dH_20 (using stirrer bar)

pH to 7.4 with concentrated HCl

Fill up to 1L and autoclave

For use dilute to 1x (100mL 10xPBS + 900mL dH_2O)

Store at RT

7.8 10x tris buffered saline (TBS): 1L

60.5g tris-base

87.6g NaCl

Dissolve in 800mL dH_2O (using stirrer bar)

pH to 7.6 with concentrated HCl

Fill up to 1L with dH_2O and autocalve

For use dilute to 1x (100mL 10xTBS + 900mL dH_2O)

Store at RT

7.9 4% Paraformaldehyde (4%): 50mL

2g paraformaldehyde

Dissolve in 100mL 1xPBS at 60°C

Allow to cool and store at 4°C

7.10 Propidium iodide staining solution

Reagent	Stock Concentration	Final Concentration	5mL	10mL	20mL
Triton X-100	100%	0.1%	5µL	10µL	20µL
$MgCl_2$	1M	0.002M	10µL	20µL	40µL
NaCl	5M	0.1M	100µL	200µL	400µL
***PIPES**	0.1M	0.01M	500µL	1mL	2mL
****PI**	1mg/mL	0.01mg/mL	50µL	100µL	200µL
dH_20	-	-	4.335mL	8.67mL	17.34mL

*PIPES buffer made up in 1M NaOH (pH 6.8) **PI stock solution is kept at -20°C (light-sensitive)

7.11 Extracted 'hit' images with z-scores and 'hit' compound descriptions

Pharmakon Library Plate 1

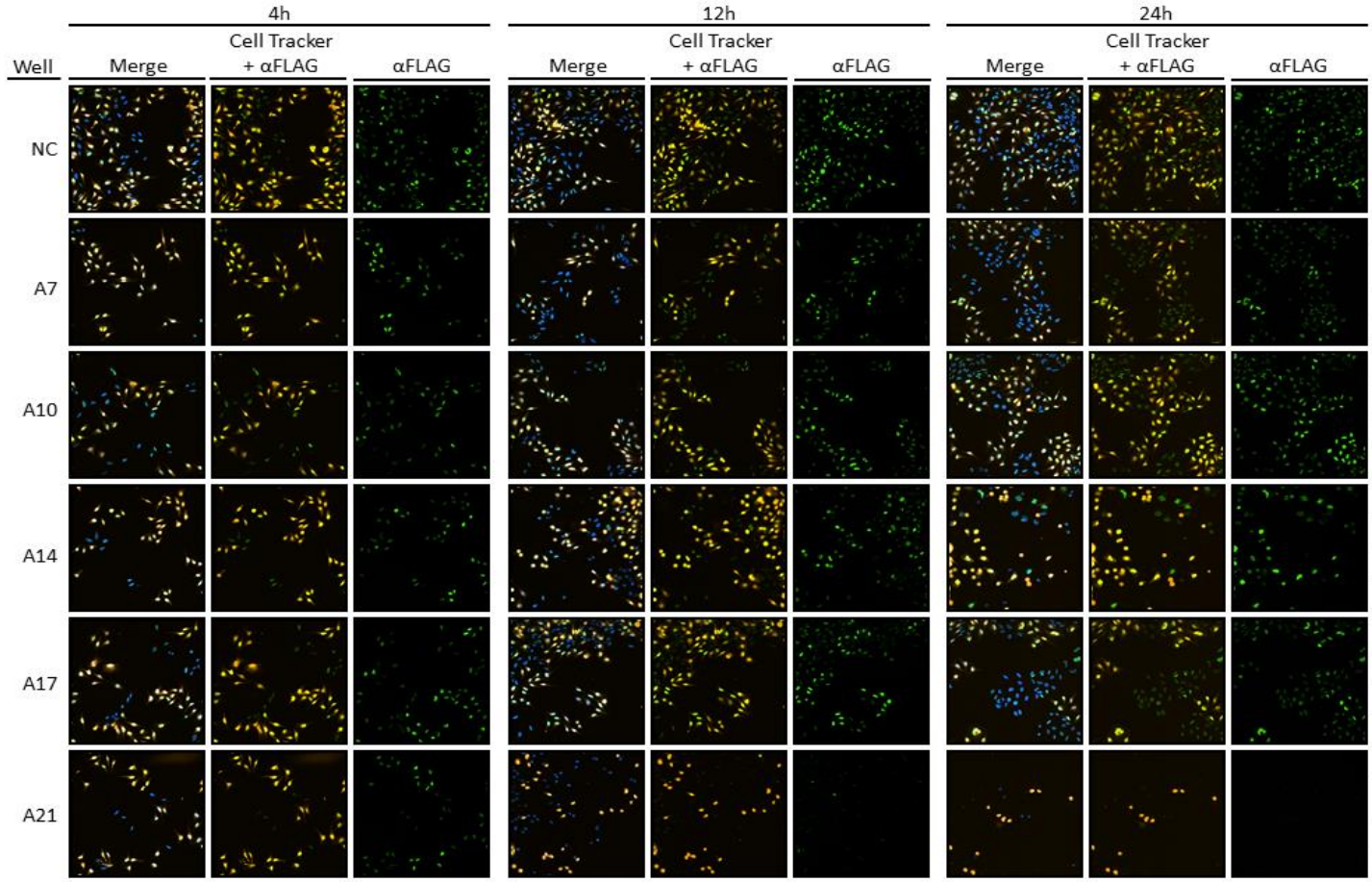

0.16% DMSO
Negative Control

DESVENLAFAXINE SUCCINATE

End-Point	TBX2 (orange)	TBX3
Downregulation	-	-
Translocation	-	4h (2,08)

ZOLMITRIPTAN

End-Point	TBX2 (orange)	TBX3
Downregulation	-	-
Translocation	4h (2,07)	4h (2,05)

DOCETAXEL

End-Point	TBX2 (orange)	TBX3
Downregulation	-	-
Translocation	(2,02) (3,05) (3,10)	4h (2,44), 12h (2,25)

MEGESTROL ACETATE

End-Point	TBX2 (orange)	TBX3
Downregulation		
Translocation	4h (2,09)	4h (2,02)

DACTINOMYCIN

End-Point	TBX2 (orange)	TBX3
Downregulation		
Translocation	4h (2,23)	

Pharmakon Library Plate 1

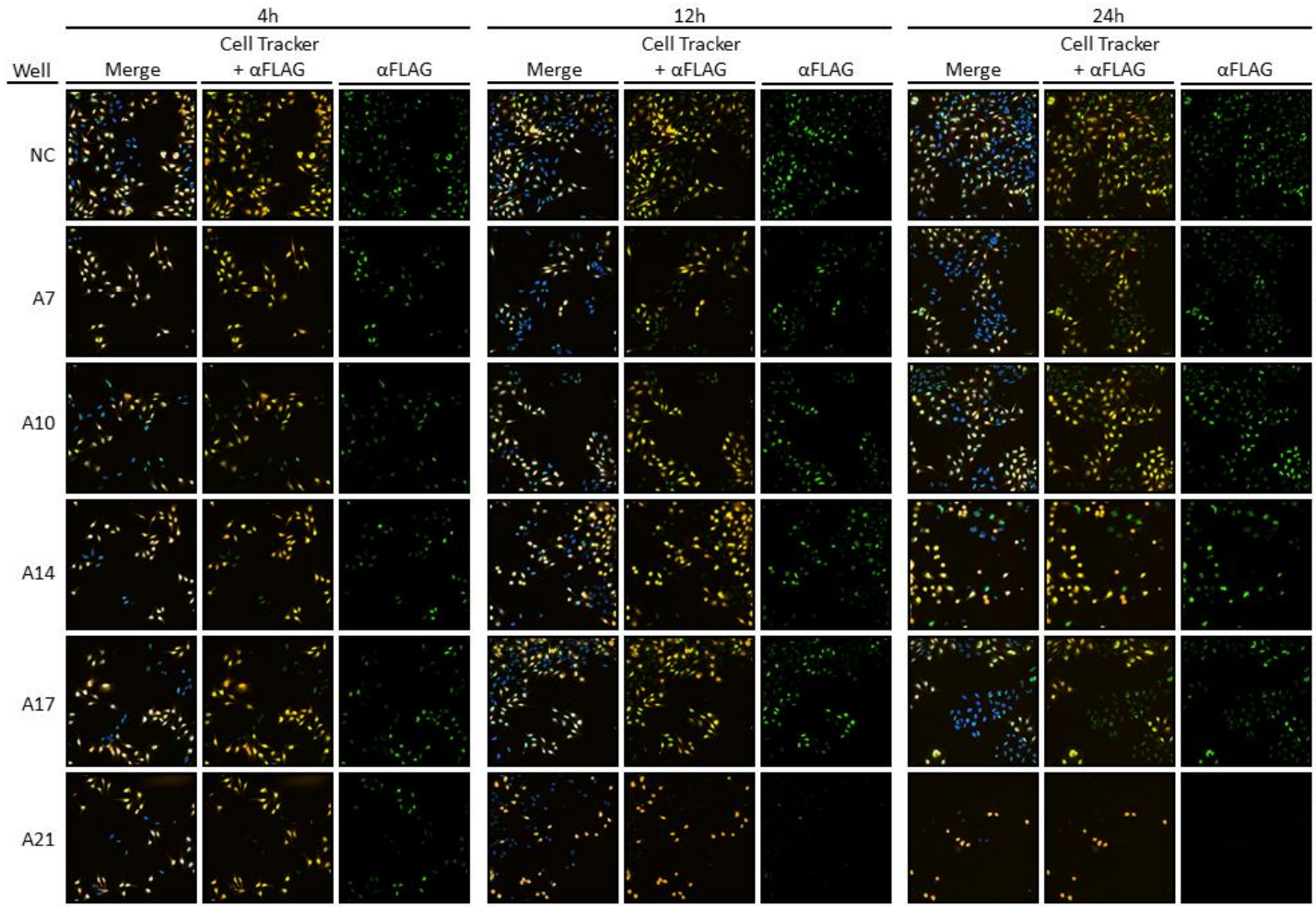

Compound with Z-Score < -2

0.16% DMSO
Negative Control

DESVENLAFAXINE SUCCINATE

End-Point	TBX2 (orange)	TBX3
Downregulation	-	-
Translocation	-	4h (2,08)

ZOLMITRIPTAN

End-Point	TBX2 (orange)	TBX3
Downregulation	-	-
Translocation	4h (2,07)	4h (2,05)

DOCETAXEL

End-Point	TBX2 (orange)	TBX3
Downregulation	-	-
Translocation	(2,02) (3,05) (3,10)	4h (2,44), 12h (2,25)

MEGESTROL ACETATE

End-Point	TBX2 (orange)	TBX3
Downregulation		
Translocation	4h (2,09)	4h (2,02)

DACTINOMYCIN

End-Point	TBX2 (orange)	TBX3
Downregulation		
Translocation	4h (2,23)	

Pharmakon Library Plate 1

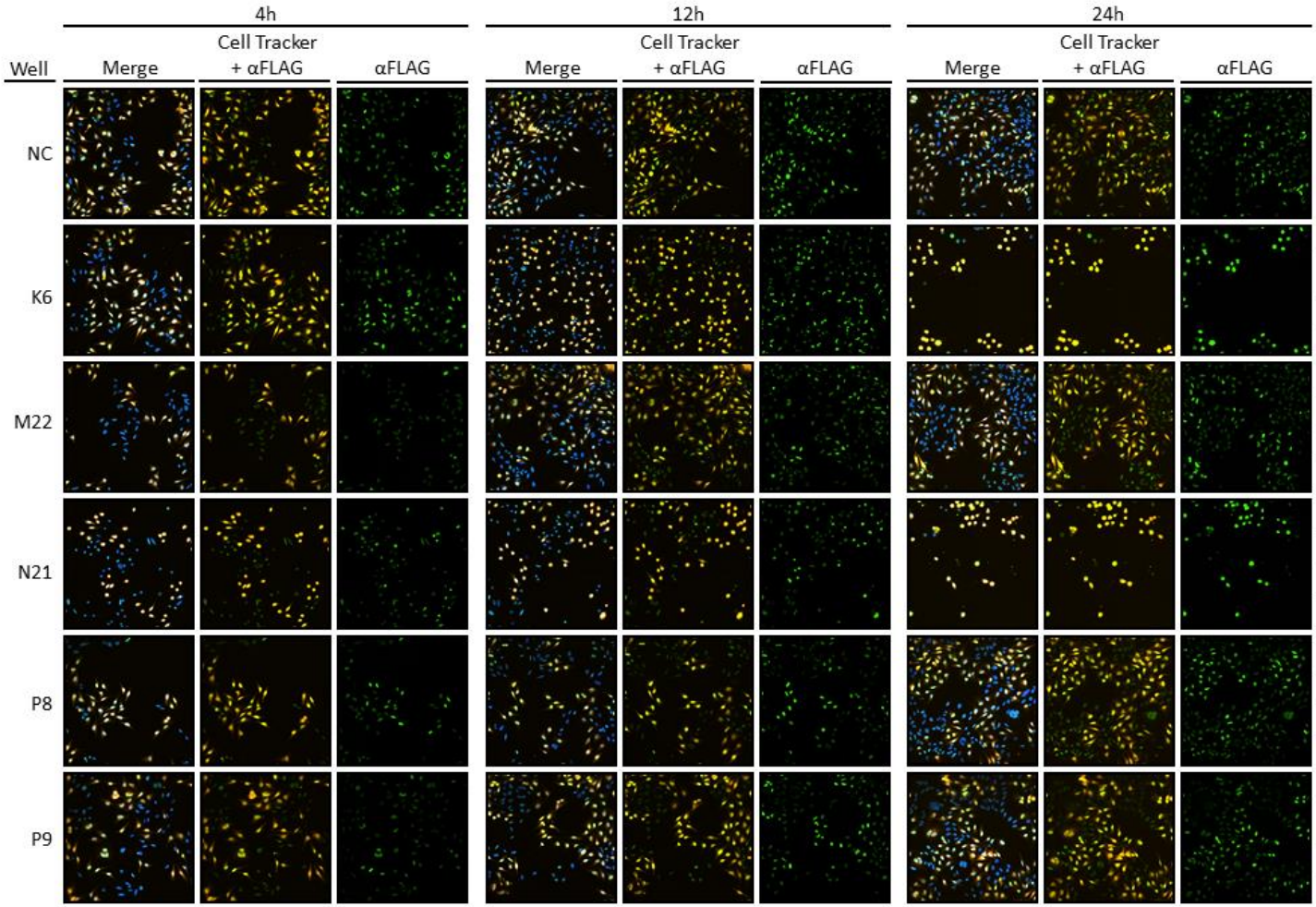

Compound with Z-Score < -2

0.16% DMSO
Negative Control

AUROTHIOGLUCOSE

End-Point	TBX2 (orange)	TBX3
Downregulation	-	-
Translocation	24h (2,87)	24h (4,27)

PREDNISOLONE TEBUTATE

End-Point	TBX2 (orange)	TBX3
Downregulation	4h (2,48)	-
Translocation	-	-

PODOFILOX

End-Point	TBX2 (orange)	TBX3
Downregulation	-	-
Translocation	12h (2,07)	-

CHLORAMPHENICOL PALMITATE

End-Point	TBX2 (orange)	TBX3
Downregulation	-	-
Translocation	12h (2,02)	4h (2,48) 12h (2,14)

SPARTEINE SULFATE

End-Point	TBX2 (orange)	TBX3
Downregulation	-	-
Translocation	4h (2,07)	4h (2,63)

Pharmakon Library Plate 1

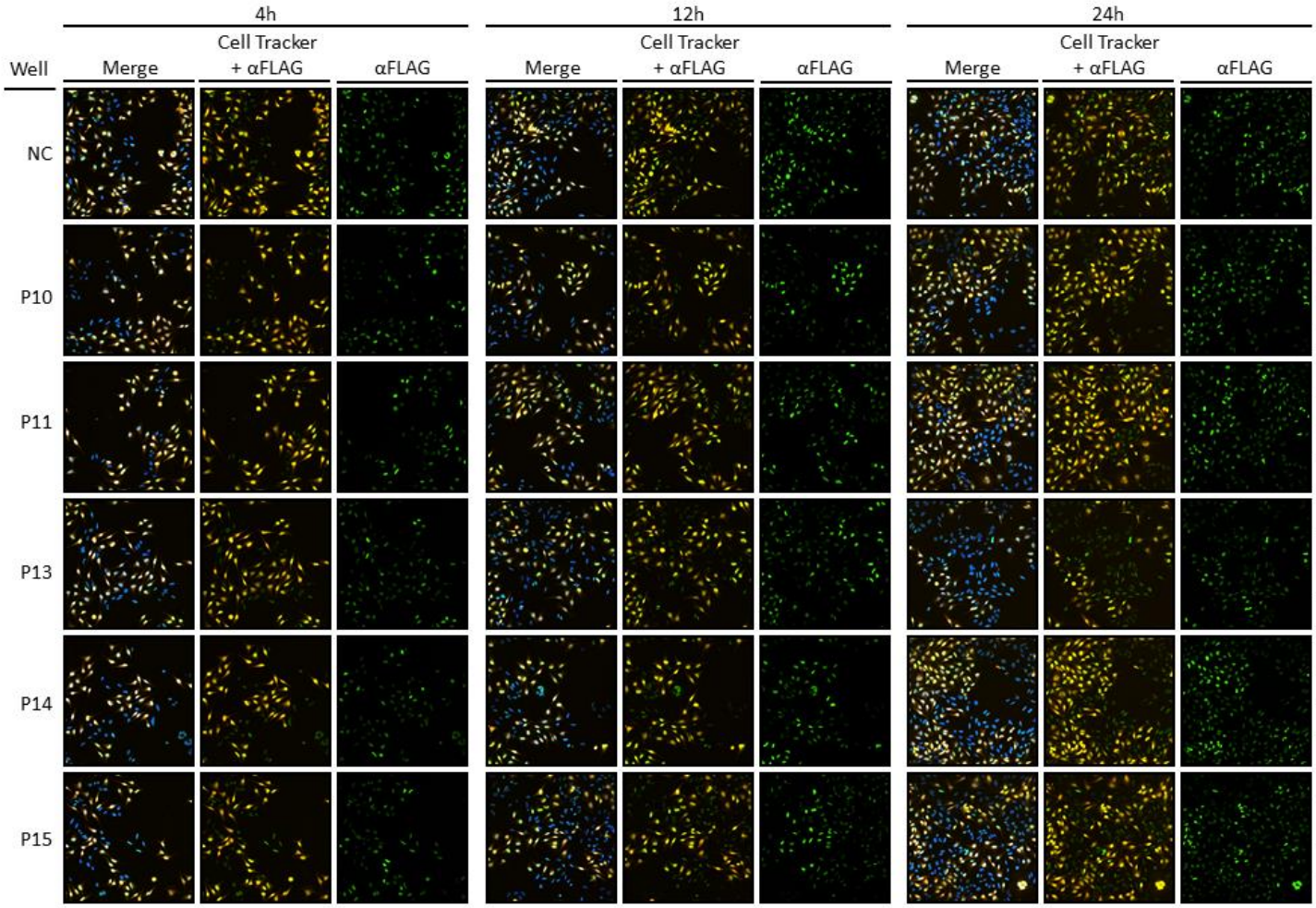

Compound with Z-Score < -2

0.16% DMSO
Negative Control

CHLORAMPHENICOL SODIUM SUCCINATE

End-Point	TBX2 (orange)	TBX3
Downregulation	-	-
Translocation	4h (2,08)	4h (2,34)

TESTOSTERONE PROPIONATE

End-Point	TBX2 (orange)	TBX3
Downregulation	-	-
Translocation	4h (2,28) 12h (2,16)	4h (2,39) 12h (2,42)

PYRIDOSTIGMINE BROMIDE

End-Point	TBX2 (orange)	TBX3
Downregulation	-	-
Translocation	4h (2,03)	4h (2,01)

CHLORCYCLIZINE HYDROCHLORIDE

End-Point	TBX2 (orange)	TBX3
Downregulation	-	-
Translocation	-	4h (2,25)

ENILCONAZOLE SULFATE

End-Point	TBX2 (orange)	TBX3
Downregulation	-	-
Translocation	-	4h (2,04)

Pharmakon Library Plate 1

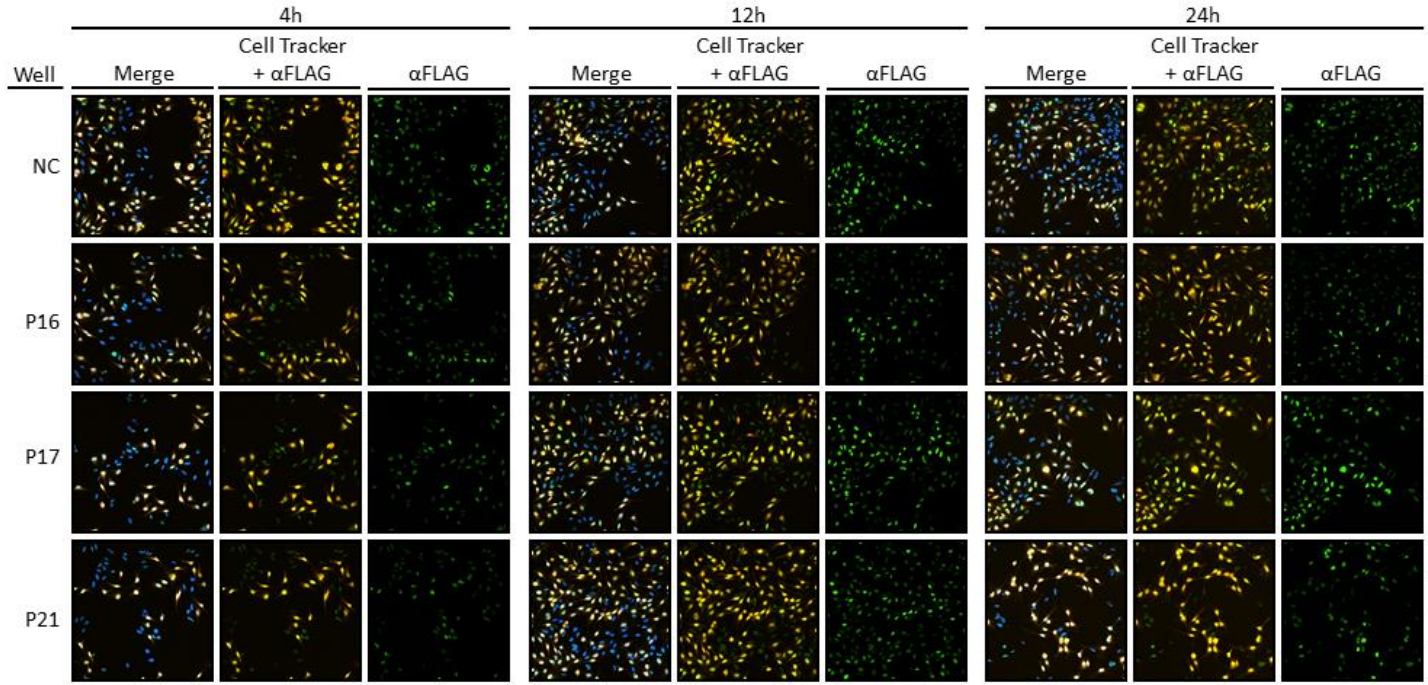

Compound with Z-Score < -2

0.16% DMSO
Negative Control

CHLORHEXIDINE DIHYDROCHLORIDE

End-Point	TBX2 (orange)	TBX3
Downregulation	4h (2,43)	4h (2,33) 12h (2,20)
Translocation	-	-

BETAMETHASONE SODIUM PHOSPHATE

End-Point	TBX2 (orange)	TBX3
Downregulation	-	-
Translocation	-	4h (2,20)

ACRISORCIN

End-Point	TBX2 (orange)	TBX3
Downregulation	-	4h (2,24)
Translocation	-	-

LP1	A	7	DESVENLAFAXINE SUCCINATE	Desvenlafaxine is an antidepressant of the serotonin-norepinephrine reuptake inhibitor (SNRI) class. It is a synthetic form of the major active metabolite of venlafaxine. It is being targeted as the first non-hormonal based treatment for menopause.
LP1	A	10	ZOLMITRIPTAN	Zolmitriptan is a selective serotonin receptor agonist of the 1B and 1D subtypes. It is a triptan, used in the acute treatment of migraine attacks with or without aura and cluster headaches.
LP1	A	14	DOCETAXEL	Docetaxel is a chemotherapy medication used to treat a number of types of cancer. This includes breast cancer, head and neck cancer, stomach cancer, prostate cancer and non small-cell lung cancer.
LP1	A	17	MEGESTROL ACETATE	Megestrol acetate, also known as 17α-acetoxy-6-dehydro-6-methylprogesterone, is a steroidal progestin of the 17α-hydroxyprogesterone group that is used in the treatment of breast and endometrial cancer and as an appetite stimulant.
LP1	A	21	DACTINOMYCIN	Dactinomycin, also known as actinomycin D, is a chemotherapy medication used to treat a number of types of cancer. This includes Wilms tumor, rhabdomyosarcoma, Ewing's sarcoma, trophoblastic neoplasm, testicular cancer, and certain types of ovarian cancer.
LP1	K	6	AUROTHIOGLUCOSE	Aurothioglucose, also known as gold thioglucose, is a chemical compound with the formula AuSC6H11O5. This derivative of the sugar glucose was formerly used to treat rheumatoid arthritis.
LP1	M	22	PREDNISOLONE TEBUTATE	Prednisolone is a steroid medication used to treat certain types of allergies, inflammatory conditions, autoimmune disorders, and cancers. Some of these conditions include adrenocortical insufficiency, high blood calcium, rheumatoid arthritis, dermatitis, eye inflammation, asthma, and multiple sclerosis.
LP1	N	21	PODOFILOX	Podofilox (podofilox) topical solution is an antimitotic drug which can be chemically synthesized or purified from the plant families Coniferae and Berberidaceae (e.g.species of Juniperus and podophyllum). Indicated for topical treatment of external genital warts (Condyloma acuminatum).
LP1	P	8	CHLORAMPHENICOL PALMITATE	Chloramphenicol is an antibiotic useful for the treatment of a number of bacterial infections. This includes as an eye ointment to treat conjunctivitis. By mouth or by injection into a vein, it is used to treat meningitis, plague, cholera, and typhoid fever. Its use by mouth or by injection is only recommended when safer antibiotics cannot be used and if used, monitoring both blood levels of the medication and blood cell levels every two days is recommended during treatment.
LP1	P	9	SPARTEINE SULFATE	Sparteine sulfate is a quinolizidine alkaloid. It has been used as an oxytocic and an anti-arrhythmia agent.
LP1	P	10	CHLORAMPHENICOL SODIUM SUCCINATE	Chloramphenicol is an antibiotic useful for the treatment of a number of bacterial infections. This includes as an eye ointment to treat conjunctivitis. By mouth or by injection into a vein, it is used to treat meningitis, plague, cholera, and typhoid fever. Its use by mouth or by injection is only recommended when safer antibiotics cannot be used and if used, monitoring both blood levels of the medication and blood cell levels every two days is recommended during treatment.
LP1	P	11	TESTOSTERONE PROPIONATE	Testosterone propionate is an androgen and anabolic steroid and a testosterone ester.
LP1	P	13	PYRIDOSTIGMINE BROMIDE	Pyridostigmine bromide has been FDA approved for military use during combat situations as an agent to be given prior to exposure to the nerve agent soman in order to increase survival.
LP1	P	14	CHLORCYCLIZINE HYDROCHLORIDE	Chlorcyclizine is a first-generation antihistamine of the phenylpiperazine class marketed in the United States and certain other countries. It is used primarily to treat allergy symptoms such as rhinitis, urticaria, and pruritus, and may also be used as an antiemetic. In addition to its antihistamine effects, chlorcyclizine also has some anticholinergic, antiserotonergic, and local anesthetic properties. It also has been studied as a potential treatment for hepatitis C.
LP1	P	15	ENILCONAZOLE SULFATE	Enilconazole is a fungicide widely used in agriculture, particularly in the growing of citrus fruits. Enilconazole is also used in veterinary medicine as a topical antimycotic.
LP1	P	16	CHLORHEXIDINE DIHYDROCHLORIDE	Chlorhexidine is a disinfectant and antiseptic that is used for skin disinfection before surgery and to sterilize surgical instruments. It may be used both to disinfect the skin of the patient and the hands of the healthcare providers. It is also used for cleaning wounds, preventing dental plaque, treating yeast infections of the mouth, and to keep urinary catheters from blocking.
LP1	P	17	BETAMETHASONE SODIUM PHOSPHATE	Betamethasone is a corticosteroid with anti-inflammatory and immunosuppressive abilities, used especially where water retention is undesirable. It is applied as a topical cream, ointment, lotion or gel to treat itching (e.g. from eczema). Corticosteroid used to stimulate fetal lung maturation and to decrease the incidence and mortality from intracranial hemorrhage in premature infants.
LP1	P	21	ACRISORCIN	Acrisorcin is a topical anti-infective typically used as a fungicide. It is a combination of the active ingredients 9-aminoacridine and 4-hexylresorcinol.

Pharmakon Library Plate 2

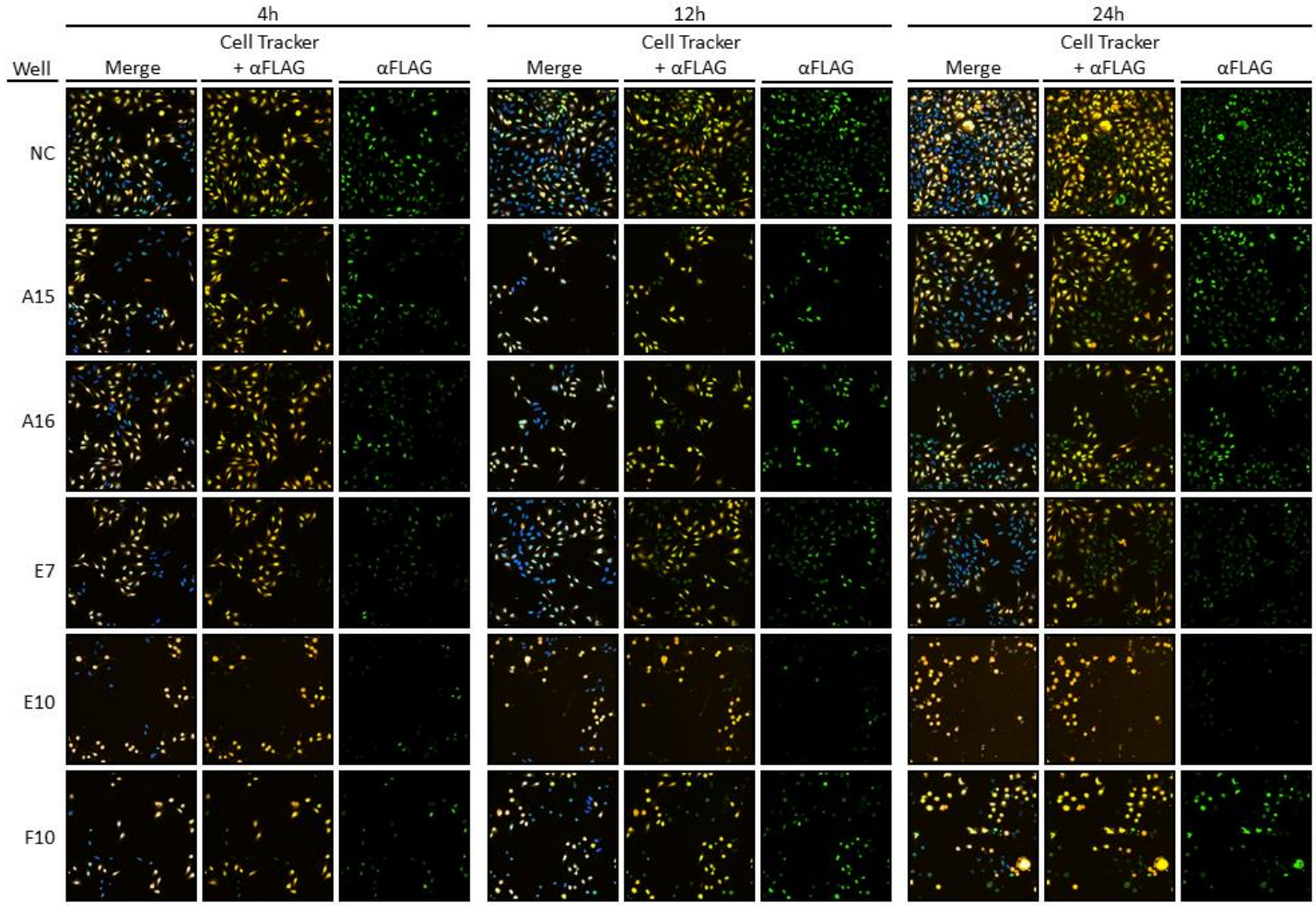

Compound with Z-Score < -2

0.16% DMSO
Negative Control

CHLORTHALIDONE

End-Point	TBX2 (orange)	TBX3
Downregulation	-	-
Translocation	4h (2,23)	-

ETHIONAMIDE

End-Point	TBX2 (orange)	TBX3
Downregulation	4h (2,10)	-
Translocation	-	-

VARDENAFIL HYDROCHLORIDE

End-Point	TBX2 (orange)	TBX3
Downregulation	4h (2,11) 12h (2,49)	-
Translocation	-	-

GENTIAN VIOLET

End-Point	TBX2 (orange)	TBX3
Downregulation	4h (3,95) 12h (3,57)	-
Translocation	-	-

ALBENDAZOLE

End-Point	TBX2 (orange)	TBX3
Downregulation	-	-
Translocation	12h (2,05)	-

Pharmakon Library Plate 2

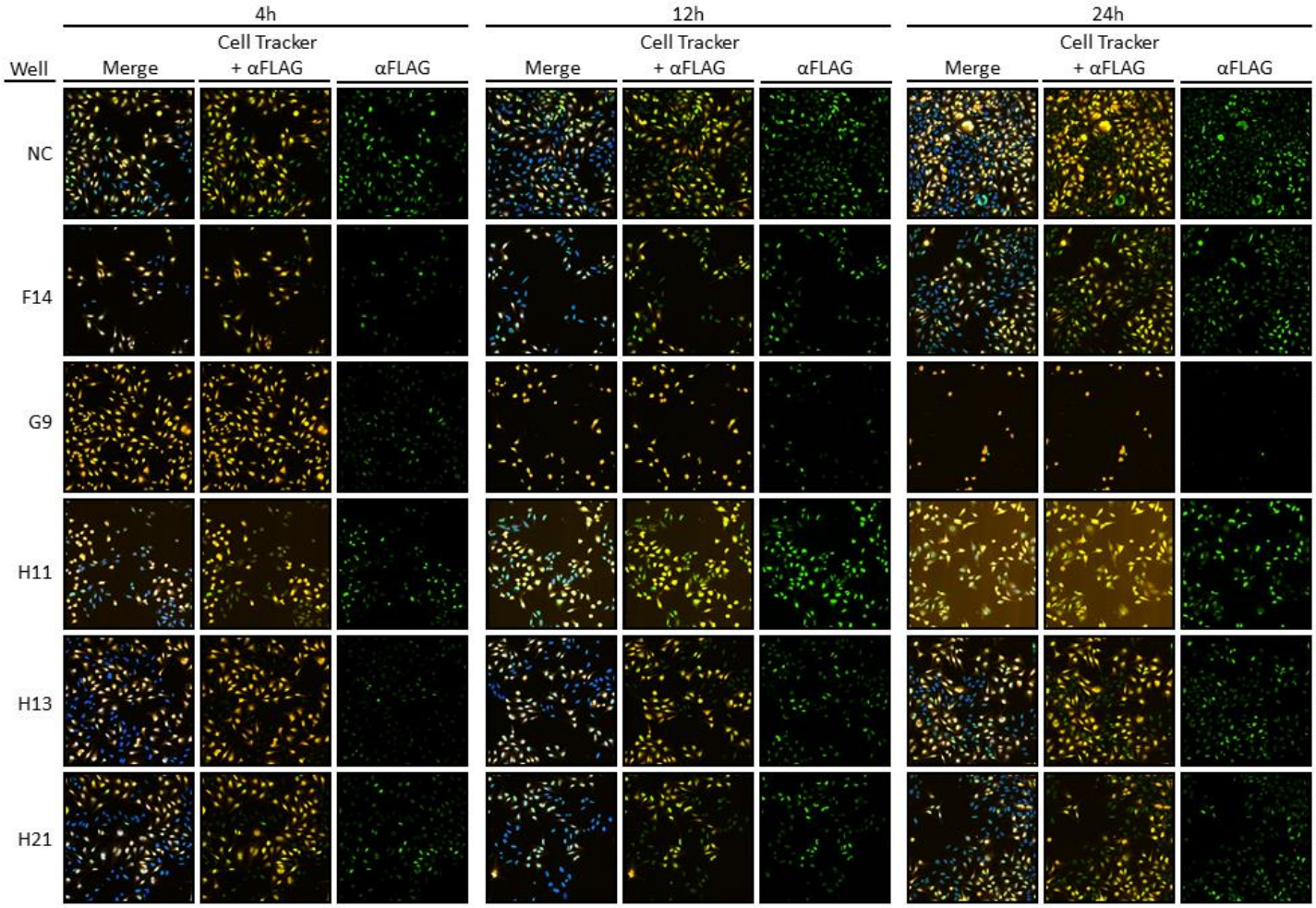

Compound with Z-Score < -2

0.16% DMSO
Negative Control

PHENACETIN

End-Point	TBX2 (orange)	TBX3
Downregulation	·	·
Translocation	4h (2,02)	·

DAUNORUBICIN

End-Point	TBX2 (orange)	TBX3
Downregulation	4h (2,49) 12h (3,09)	·
Translocation	·	·

PYRVINIUM PAMOATE

End-Point	TBX2 (orange)	TBX3
Downregulation	·	(5,92) (5,17) (4,16)
Translocation	·	·

QUINACRINE HYDROCHLORIDE

End-Point	TBX2 (orange)	TBX3
Downregulation	4h (3,32) 12h (2,62)	4h (2,71)
Translocation	·	·

RESERPINE

End-Point	TBX2 (orange)	TBX3
Downregulation	12h (2,09)	·
Translocation	·	·

Pharmakon Library Plate 2

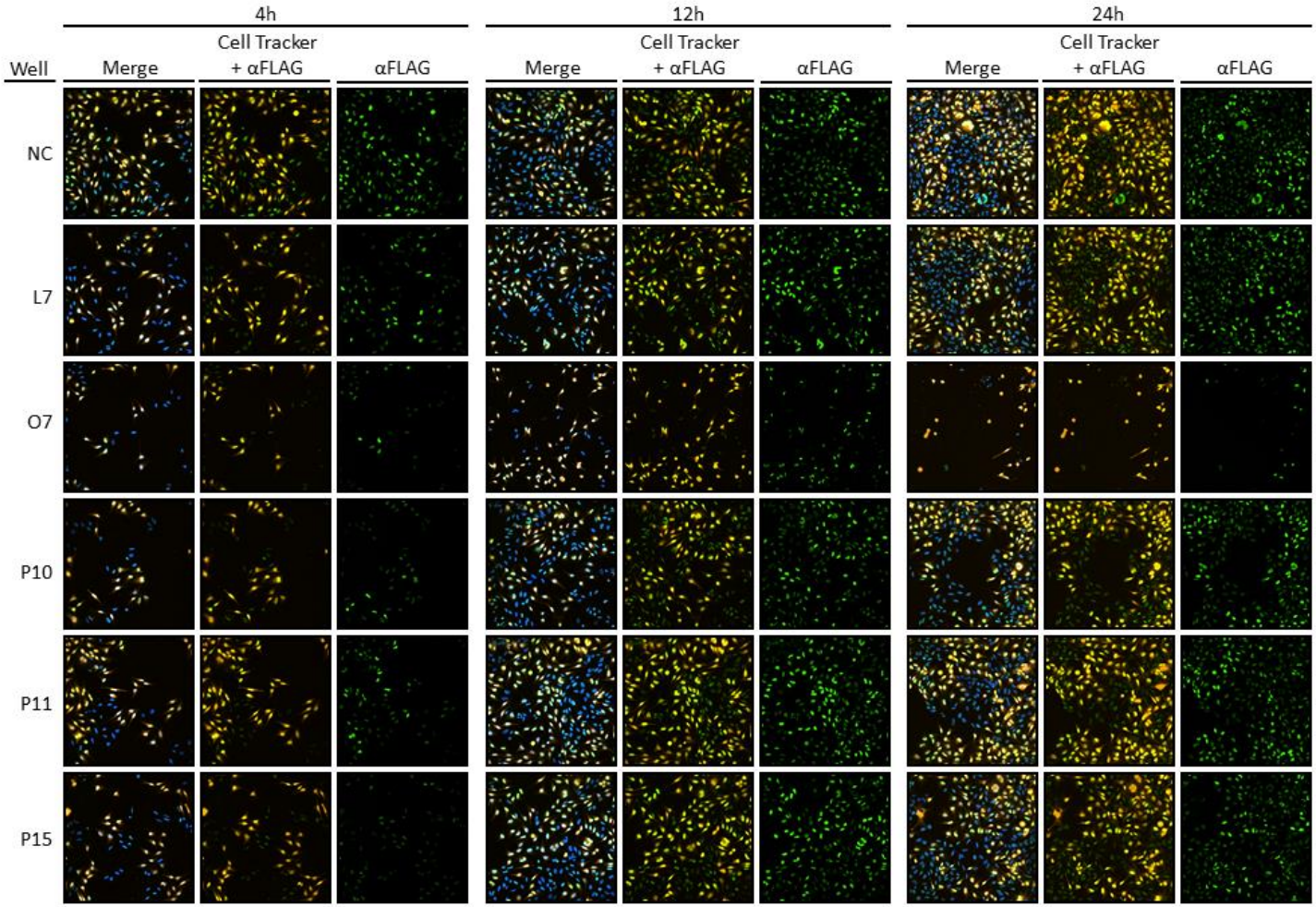

Compound with Z-Score < -2

0.16% DMSO
Negative Control

SULFACETAMIDE

End-Point	TBX2 (orange)	TBX3
Downregulation	-	-
Translocation	-	24h (2,11)

EMETINE DIHYDROCHLORIDE

End-Point	TBX2 (orange)	TBX3
Downregulation	4h (2,65) 12h (2,24)	-
Translocation	-	-

FLUTAMIDE

End-Point	TBX2 (orange)	TBX3
Downregulation	-	-
Translocation	4h (2,42)	4h (2,18)

TIMOLOL MALEATE

End-Point	TBX2 (orange)	TBX3
Downregulation	-	-
Translocation	12h (2,36)	-

TOLAZOLINE HYDROCHLORIDE

End-Point	TBX2 (orange)	TBX3
Downregulation	-	-
Translocation	4h (2,05)	-

Pharmakon Library Plate 2

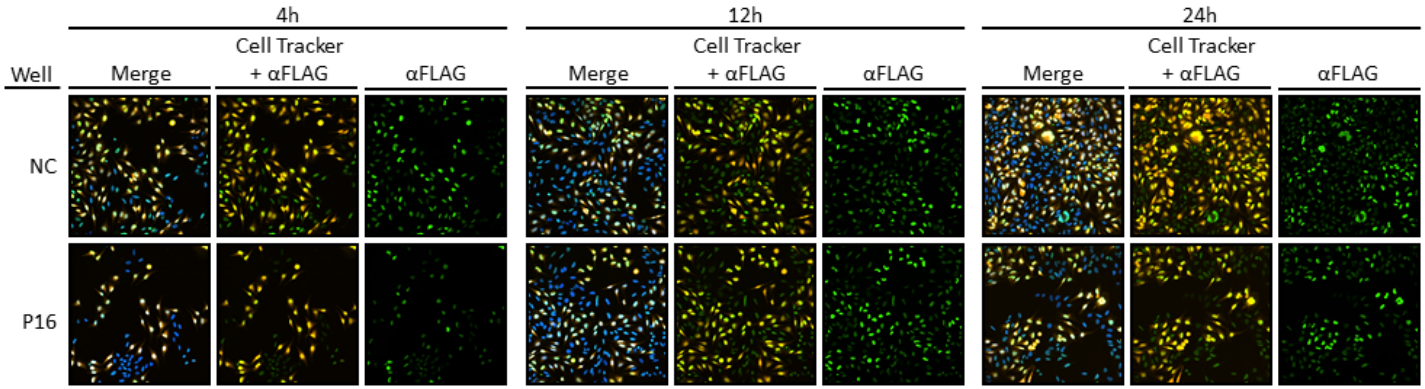

End-Point	TBX2 (orange)	TBX3
Downregulation		
Translocation	4h (2,53) 12h (2,01)	

LP2	A	15	CHLORTHALIDONE	Chlortalidone or chlorthalidone is a diuretic drug used to treat hypertension. It is described as a thiazide diuretic.
LP2	A	16	ETHIONAMIDE	Ethionamide is an antibiotic used to treat tuberculosis. Specifically it is used, along with other antituberculosis medications, to treat active multidrug-resistant tuberculosis.
LP2	E	7	VARDENAFIL HYDROCHLORIDE	Vardenafil is a PDE5 inhibitor used for treating erectile dysfunction.
LP2	E	10	GENTIAN VIOLET	Crystal violet or gentian violet is a triarylmethane dye used as a histological stain and in Gram's method of classifying bacteria. Crystal violet has antibacterial, antifungal, and anthelmintic properties and was formerly important as a topical antiseptic.
LP2	F	10	ALBENDAZOLE	Albendazole is a medication used for the treatment of a variety of parasitic worm infestations. It is useful for giardiasis, trichuriasis, filariasis, neurocysticercosis, hydatid disease, pinworm disease, and ascariasis, among others.
LP2	F	14	PHENACETIN	Phenacetin is a pain-relieving and fever-reducing drug.
LP2	G	9	DAUNORUBICIN	Daunorubicin, also known as daunomycin, is a chemotherapy medication used to treat cancer. Specifically it is used for acute myeloid leukemia (AML), acute lymphocytic leukemia (ALL), chronic myelogenous leukemia (CML), and Kaposi's sarcoma.
LP2	H	11	PYRVINIUM PAMOATE	Pyrvinium is an anthelmintic effective for pinworms. Several forms of pyrvinium have been prepared with variable counter anions, such as halides, tosylate, triflate and pamoate. Pyrvinium salts can also inhibit the growth of cancer cells. More specifically, the pamoate salt has been shown to have preferential toxicity for various cancer cell lines during glucose starvation.
LP2	H	13	QUINACRINE HYDROCHLORIDE	Quinacrine hydrochloride is an acridine derivative formerly widely used as an antimalarial but superseded by chloroquine in recent years. It has also been used as an anthelmintic and in the treatment of giardiasis and malignant effusions. It is used in cell biological experiments as an inhibitor of phospholipase A2. Yellow in colour.
LP2	H	21	RESERPINE	Reserpine is an indole alkaloid, antipsychotic, and antihypertensive drug that has been used for the control of high blood pressure and for the relief of psychotic symptoms.
LP2	L	7	SULFACETAMIDE	Sulfacetamide is approved for the treatment of acne and seborrheic dermatitis.
LP2	O	7	EMETINE DIHYDROCHLORIDE	Emetine is a drug used as both an anti-protozoal and to induce vomiting. It is produced from the ipecac root.
LP2	P	10	FLUTAMIDE	Flutamide is a synthetic, non-steroidal antiandrogen used primarily to treat prostate cancer. It acts as a selective antagonist of the androgen receptor (AR), competing with androgens such as testosterone and its powerful active metabolite dihydrotestosterone (DHT) for binding to ARs in the prostate gland. In addition to its use in prostate cancer, flutamide has been used to treat hyperandrogenism.
LP2	P	11	TIMOLOL MALEATE	Timolol is a medication used either by mouth or as eye drops. As eye drops it is used to treat increased pressure inside the eye such as in ocular hypertension and glaucoma. By mouth it is used for high blood pressure, chest pain due to insufficient blood flow to the heart, to prevent further complications after a heart attack, and to prevent migraines.
LP2	P	15	TOLAZOLINE HYDROCHLORIDE	Tolazoline is a non-selective competitive α-adrenergic receptor antagonist. It is a vasodilator that is used to treat spasms of peripheral blood vessels (as in acrocyanosis). It has also been used (in conjunction with sodium nitroprusside) successfully as an antidote to reverse the severe peripheral vasoconstriction which can occur as a result of overdose with certain 5-HT2A agonist drugs.
LP2	P	16	ETODOLAC	Etodolac is licensed for the treatment of inflammation and pain caused by osteoarthritis and rheumatoid arthritis.

Pharmakon Library Plate 3

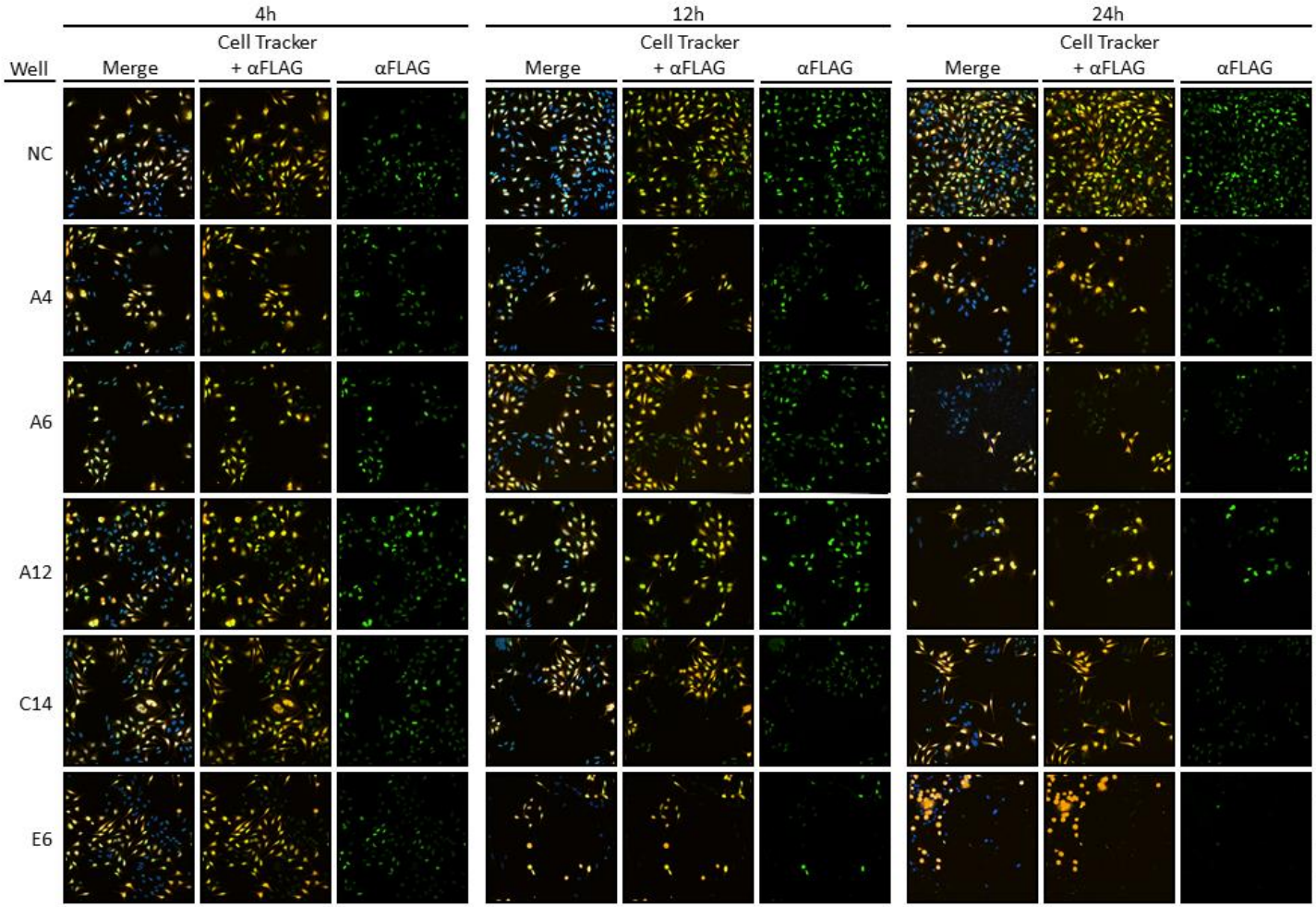

0.16% DMSO
Negative Control

HYCANTHONE

End-Point	TBX2 (orange)	TBX3
Downregulation	-	-
Translocation	12h (2,12) 24h (2,38)	-

NAPHAZOLINE HYDROCHLORIDE

End-Point	TBX2 (orange)	TBX3
Downregulation	-	-
Translocation	-	24h (3,31)

PIROCTONE OLAMINE

End-Point	TBX2 (orange)	TBX3
Downregulation	-	24h (2,58)
Translocation	-	-

NICLOSAMIDE

End-Point	TBX2 (orange)	TBX3
Downregulation	12h (2,21)	-
Translocation	-	-

MITOXANTRONE HYDROCHLORIDE

End-Point	TBX2 (orange)	TBX3
Downregulation	12h (2,17)	-
Translocation	-	-

Pharmakon Library Plate 3

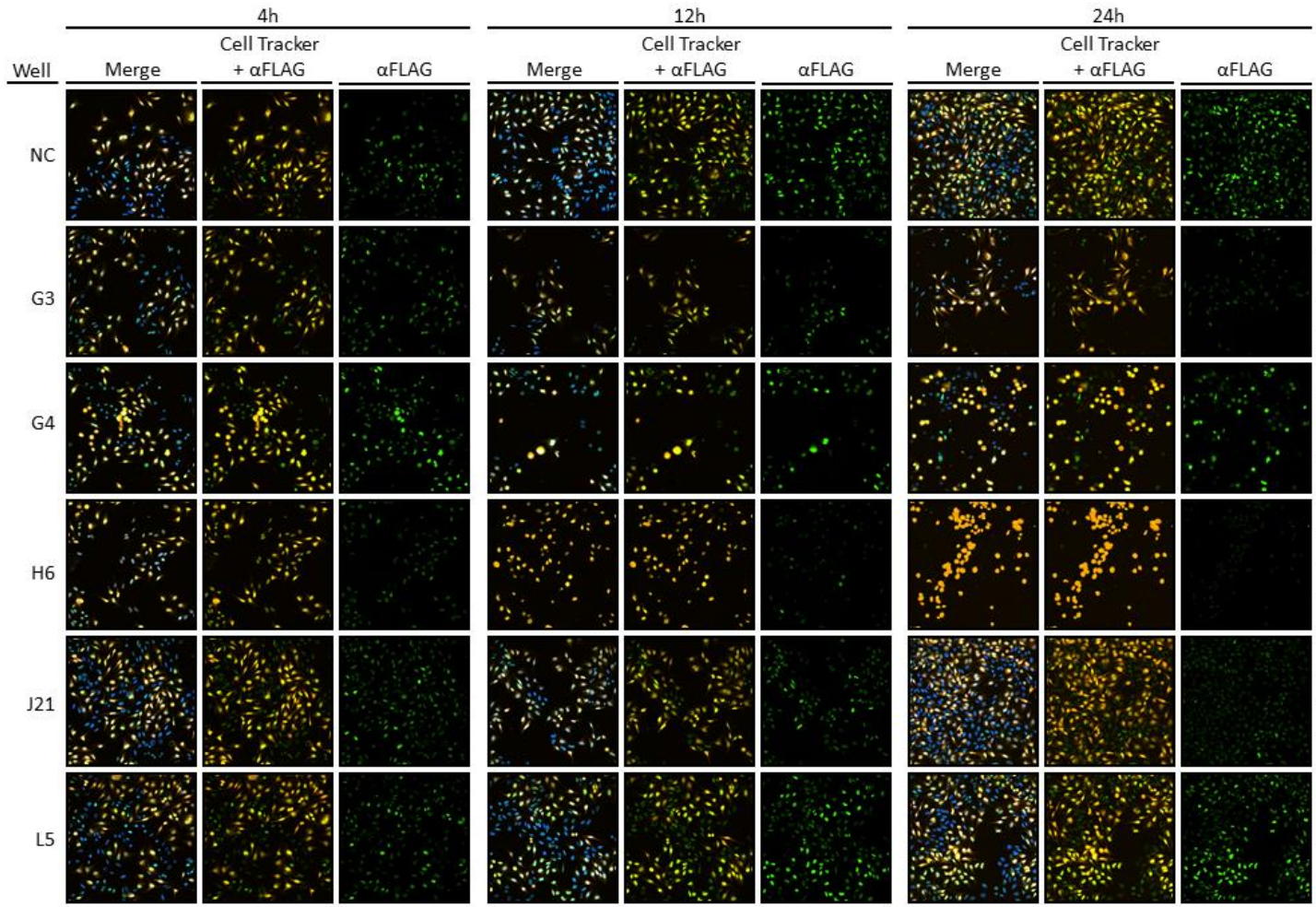

Compound with Z-Score < -2

0.16% DMSO
Negative Control

CYCLOSPORINE

End-Point	TBX2 (orange)	TBX3
Downregulation	-	-
Translocation	24h (-2,25)	-

OXIBENDAZOLE

End-Point	TBX2 (orange)	TBX3
Downregulation	-	-
Translocation	24h (-2,40)	-

DOXORUBICIN

End-Point	TBX2 (orange)	TBX3
Downregulation	(-2,10) (-2,56) (-2,19)	(-2,10) (-2,56) (-2,19)
Translocation	-	-

DERACOXIB

End-Point	TBX2 (orange)	TBX3
Downregulation	12h (-2,30)	
Translocation	-	-

CITICOLINE

End-Point	TBX2 (orange)	TBX3
Downregulation	-	-
Translocation	4h (-2,12)	-

Pharmakon Library Plate 3

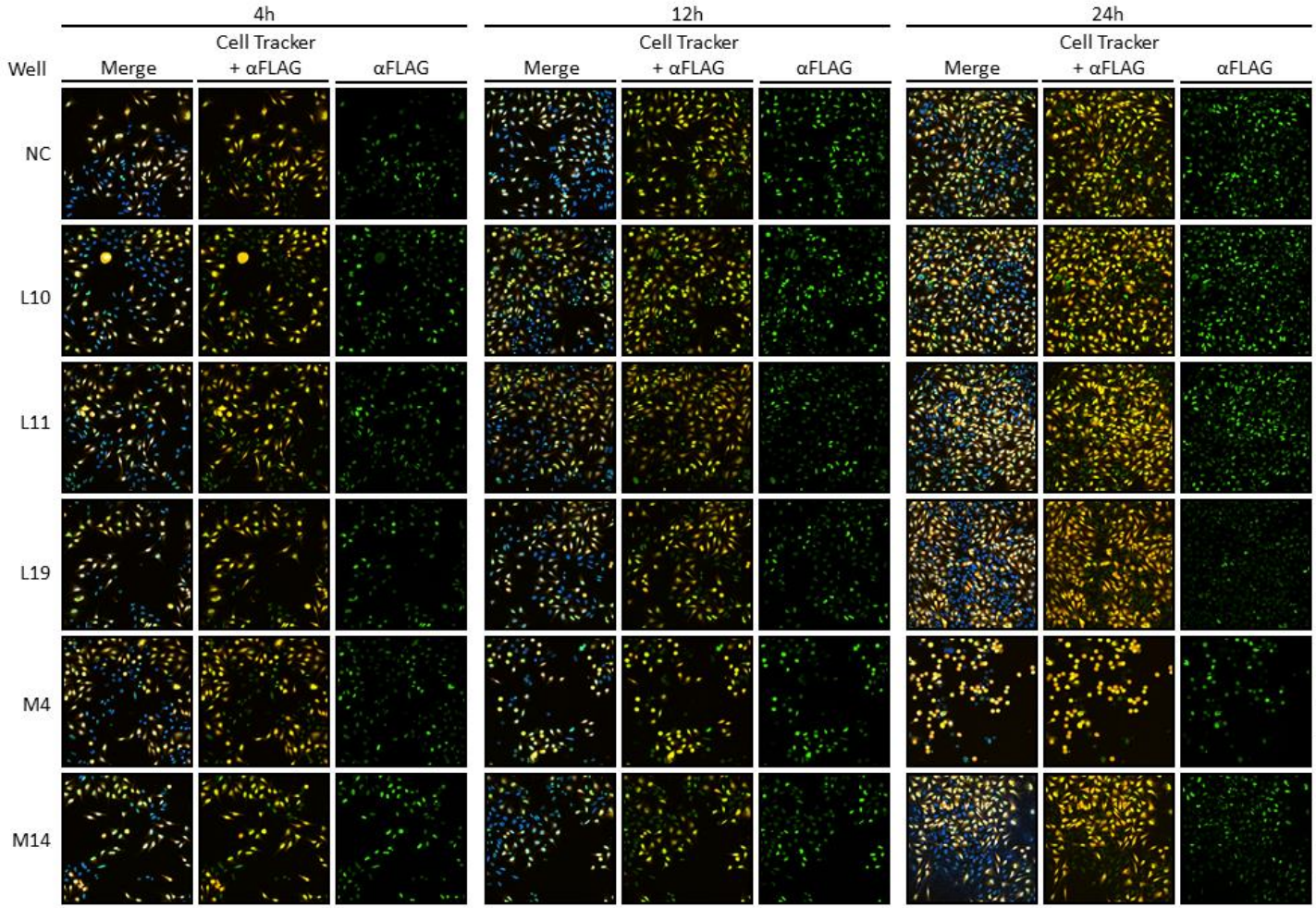

Compound with Z-Score < -2

0.16% DMSO
Negative Control

OXFENDAZOLE

End-Point	TBX2 (orange)	TBX3
Downregulation	-	-
Translocation	-	12h (2,17)

MINOCYCLINE HYDROCHLORIDE

End-Point	TBX2 (orange)	TBX3
Downregulation	-	-
Translocation	12h (2,01)	-

NITAZOXANIDE

End-Point	TBX2 (orange)	TBX3
Downregulation	-	-
Translocation	24h (2,25)	-

PACLITAXEL

End-Point	TBX2 (orange)	TBX3
Downregulation	-	-
Translocation	12h (2,58) 24h (3.10)	12h (2,37) 24h (3,58)

LANSOPRAZOLE

End-Point	TBX2 (orange)	TBX3
Downregulation	-	-
Translocation	-	24h (2,39)

Pharmakon Library Plate 3

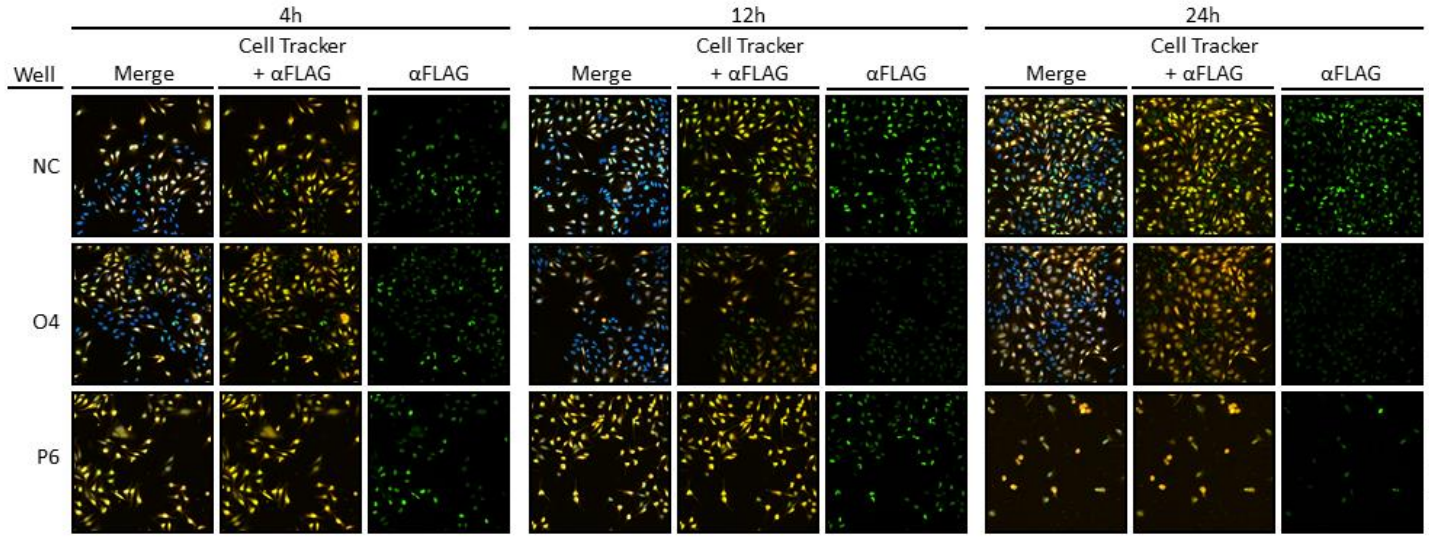

Compound with Z-Score < -2

0.16% DMSO
Negative Control

TACROLIMUS

End-Point	TBX2 (orange)	TBX3
Downregulation	(2,30) (2,66) (2,32)	12h (2,34)
Translocation		

EPIRUBICIN HYDROCHLORIDE

End-Point	TBX2 (orange)	TBX3
Downregulation	12h (2,03)	
Translocation		

LP3	A	4	HYCANTHONE	Hycanthone is an schistosomicide. It is a metabolite of lucanthone. Hycanthone interferes with parasite nerve function, resulting in paralysis and death. Hycanthone is shown to be an effective inhibitor of acetylcholinesterase (AChE) from Schistosoma mansoni, but is less potential against AChE from mammalian origin. This agent also intercalates into DNA and inhibits RNA synthesis in vitro and shows potential antineoplastic activity.
LP3	A	6	NAPHAZOLINE HYDROCHLORIDE	Naphazoline (in the hydrochloride form) is a sympathomimetic agent with marked alpha adrenergic activity. It is a vasoconstrictor with a rapid action in reducing swelling when applied to mucous membrane. It acts on alpha-receptors in the arterioles of the conjunctiva to produce constriction, resulting in decreased congestion.
LP3	A	12	PIROCTONE OLAMINE	Piroctone olamine is a compound sometimes used in the treatment of fungal infections. Piroctone olamine is the ethanolamine salt of the hydroxamic acid derivative piroctone.
LP3	C	14	NICLOSAMIDE	Niclosamide is a medication used to treat tapeworm infestations. Niclosamide inhibits glucose uptake, oxidative phosphorylation, and anaerobic metabolism in the tapeworm.
LP3	E	6	MITOXANTRONE HYDROCHLORIDE	Mitoxantrone is an anthracenedione antineoplastic agent. Mitoxantrone is used to treat certain types of cancer, mostly metastatic breast cancer, acute myeloid leukemia, and non-Hodgkin's lymphoma. It improves the survival rate of children suffering from acute lymphoblastic leukemia relapse.
LP3	G	3	CYCLOSPORINE	Ciclosporin is an immunosuppressant medication and natural product. It is used for rheumatoid arthritis, psoriasis, Crohn's disease, nephrotic syndrome, and in organ transplants to prevent rejection. Ciclosporin lowers the activity of T cells by binding to cyclophilin, a multifunctional protein that facilitates protein folding, acts as a protein chaperone, and regulates the activity of other proteins. The resulting ciclosporin complex inhibits the phosphatase activity of calcineurin which in turn is required for the activation of transcription factors that up regulate the expression of inflammatory cytokines.
LP3	G	4	OXIBENDAZOLE	Oxibendazole is a benzimidazole drug that is used to protect against roundworms, strongyles, threadworms, pinworms and lungworm infestations in horses and some domestic pets.
LP3	H	6	DOXORUBICIN	Doxorubicin is a chemotherapy medication used to treat cancer. This includes breast cancer, bladder cancer, Kaposi's sarcoma, lymphoma, and acute lymphocytic leukemia. It is often used together with other chemotherapy agents.
LP3	J	21	DERACOXIB	Deracoxib is a non-steroidal anti-inflammatory drug of the coxib class used in veterinary medicine to treat osteoarthritis in dogs. Deramaxx received FDA approval in August 2002 for "the control of post operative pain and inflammation associated with orthopedic surgery in dogs."
LP3	L	5	CITICOLINE	Citicoline is an intermediate in the generation of phosphatidylcholine from choline, a common biochemical process in cell membranes. Citicoline is naturally occurring in the cells of human and animal tissue, in particular the organs. Citicoline helps prevent memory impairment resulting from poor environmental conditions.
LP3	L	10	OXFENDAZOLE	Oxfendazole is a broad spectrum benzimidazole anthelmintic. Its main use is for protecting livestock against roundworm, strongyles and pinworms. Oxfendazole is the sulfoxide metabolite of fenbendazole.
LP3	L	11	MINOCYCLINE HYDROCHLORIDE	Minocycline is a broad-spectrum tetracycline antibiotic, and has a broader spectrum than the other members of the group. It is a bacteriostatic antibiotic, classified as a long-acting type.
LP3	L	19	NITAZOXANIDE	Nitazoxanide is a broad-spectrum antiparasitic and broad-spectrum antiviral drug that is used in medicine for the treatment of various helminthic, protozoal, and viral infections.
LP3	M	4	PACLITAXEL	Paclitaxel is a chemotherapy medication used to treat a number of types of cancer. This includes ovarian cancer, breast cancer, lung cancer, Kaposi sarcoma, cervical cancer, and pancreatic cancer.
LP3	M	14	LANSOPRAZOLE	Lansoprazole is a proton-pump inhibitor that inhibits the stomach's production of acid. It is used for the treatment of stomach ulcers, gastroesophageal reflux disease, Zollinger-Ellison syndrome and Helicobacter pylori infection
LP3	O	4	TACROLIMUS	Tacrolimus is an immunosuppressive drug used mainly after allogeneic organ transplant to lower the risk of organ rejection. It achieves this by inhibiting the production of interleukin-2. Tacrolimus is also used in the treatment of other T cell-mediated diseases such as eczema, severe refractory uveitis after bone marrow transplants, exacerbations of minimal change disease, Kimura's disease, and the skin condition vitiligo.
LP3	P	6	EPIRUBICIN HYDROCHLORIDE	Epirubicin is an anthracycline drug used for chemotherapy. It can be used in combination with other medications to treat breast cancer in patients who have had surgery to remove the tumor. Similarly to other anthracyclines, epirubicin acts by intercalating DNA strands. Intercalation results in complex formation which inhibits DNA and RNA synthesis. It also triggers DNA cleavage by topoisomerase II, resulting in mechanisms that lead to cell death.

Pharmakon Library Plate 4

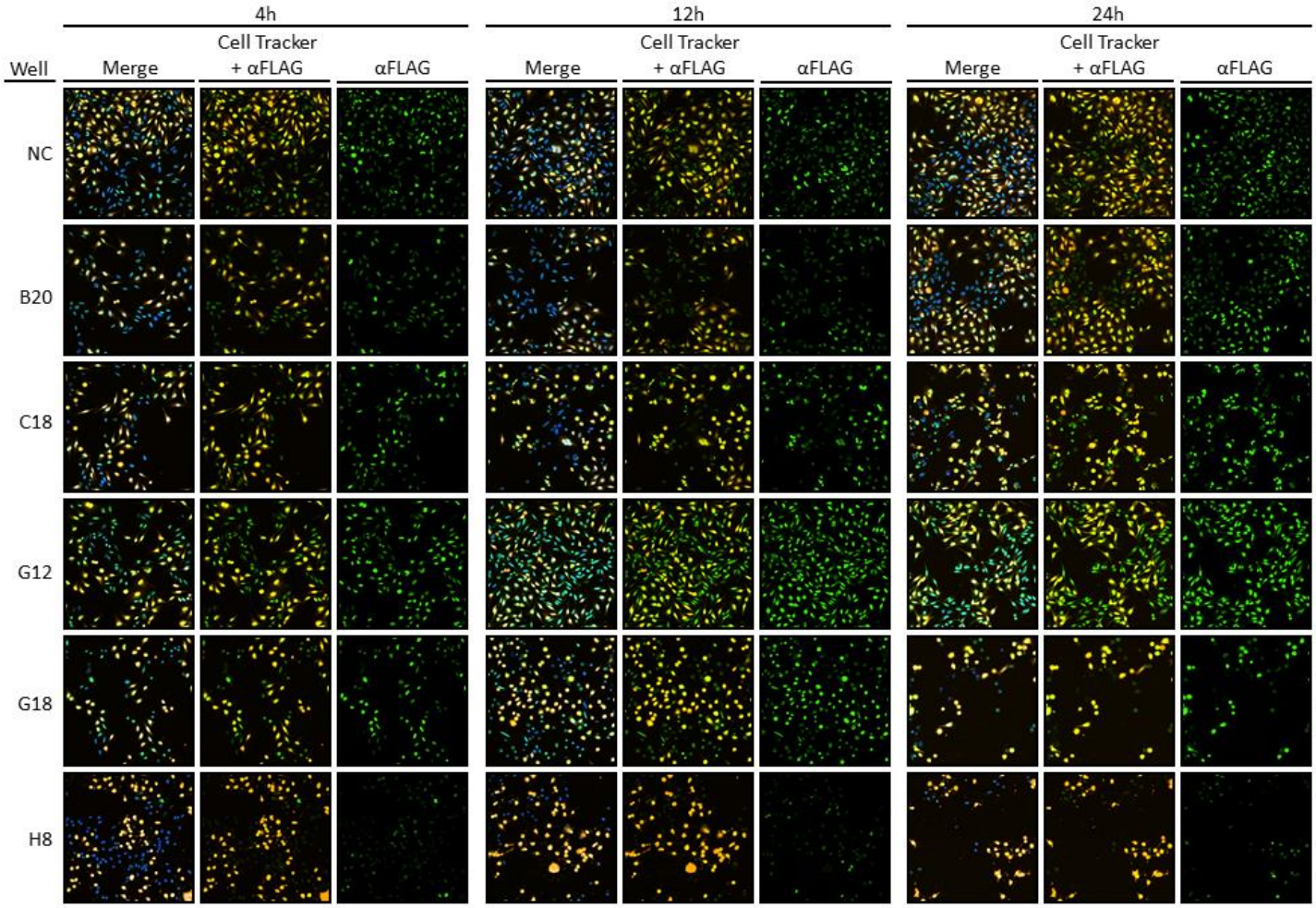

Compound with Z-Score < -2

0.16% DMSO
Negative Control

LEVOSIMENDAN

End-Point	TBX2 (orange)	TBX3
Downregulation	-	-
Translocation	12h (2,41)	-

CEFOXITIN SODIUM

End-Point	TBX2 (orange)	TBX3
Downregulation	-	-
Translocation	-	12h (2,27)

MECLOCYCLINE SULFOSALICYLATE

End-Point	TBX2 (orange)	TBX3
Downregulation	-	-
Translocation	12h (2,05) 24h (2,13)	-

VINCRISTINE SULFATE

End-Point	TBX2 (orange)	TBX3
Downregulation	-	-
Translocation	24h (3,39)	12h (2,81) 24h (4,33)

THIMEROSAL

End-Point	TBX2 (orange)	TBX3
Downregulation	(3,22) (3,22) (2,31)	4h (3,61) 12h (2,36)
Translocation		24h (2,49)

Pharmakon Library Plate 4

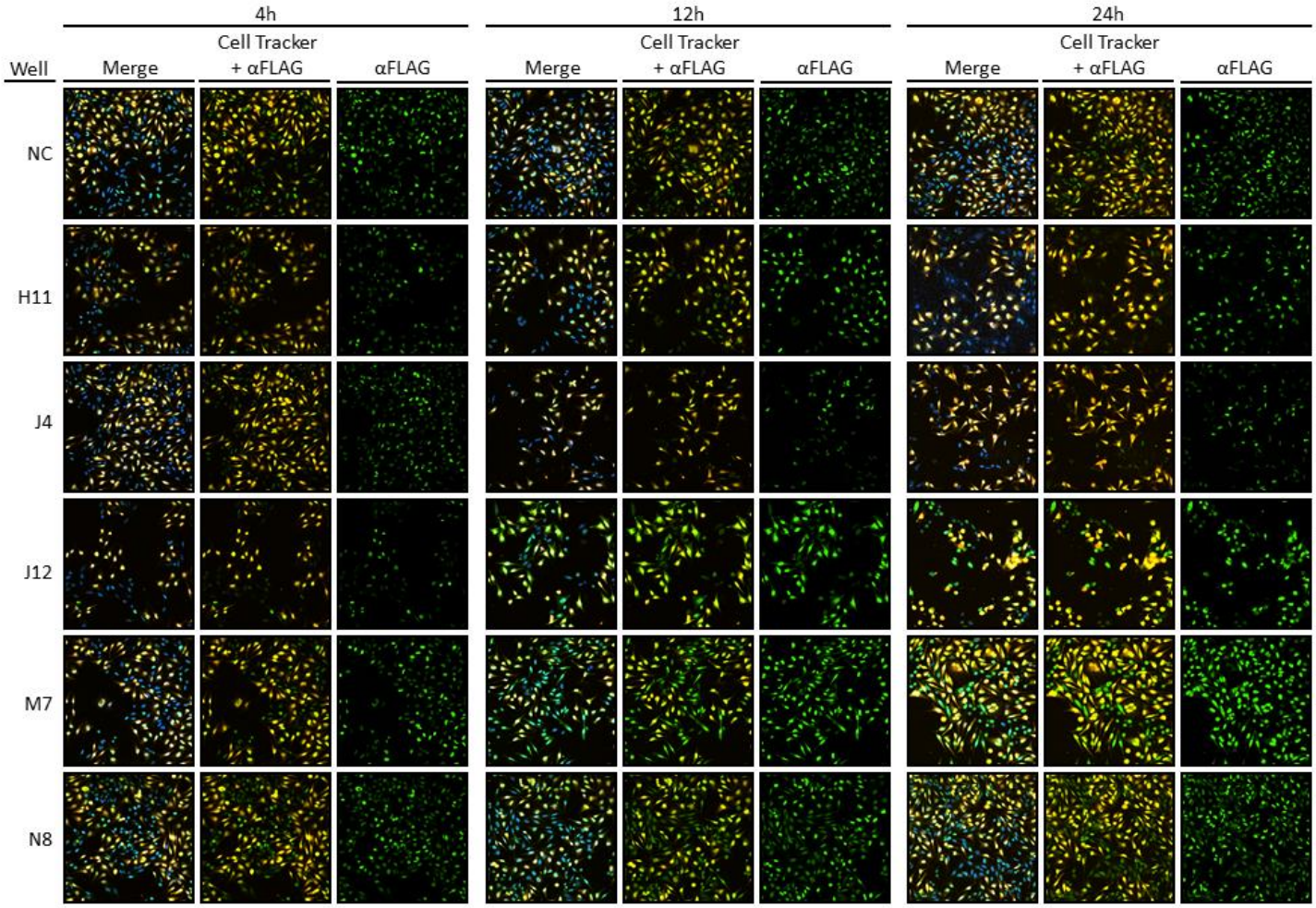

Compound with Z-Score < -2

0.16% DMSO
Negative Control

ADAPALENE

End-Point	TBX2 (orange)	TBX3
Downregulation	-	24h (2,20)
Translocation	-	-

CYCLOHEXIMIDE

End-Point	TBX2 (orange)	TBX3
Downregulation	-	4h (2,12) 12h (2,06)
Translocation	-	-

THIRAM

End-Point	TBX2 (orange)	TBX3
Downregulation	-	-
Translocation	12h (3,85) 24h (3,58)	(2,54) (4,89) (5,03)

THIOSTREPTON

End-Point	TBX2 (orange)	TBX3
Downregulation	-	-
Translocation	24h (3,07)	24h (3,27)

MERBROMIN

End-Point	TBX2 (orange)	TBX3
Downregulation	-	-
Translocation	(4,16) (3,57) (3,45)	(4,54) (3,29) (2,70)

Pharmakon Library Plate 4

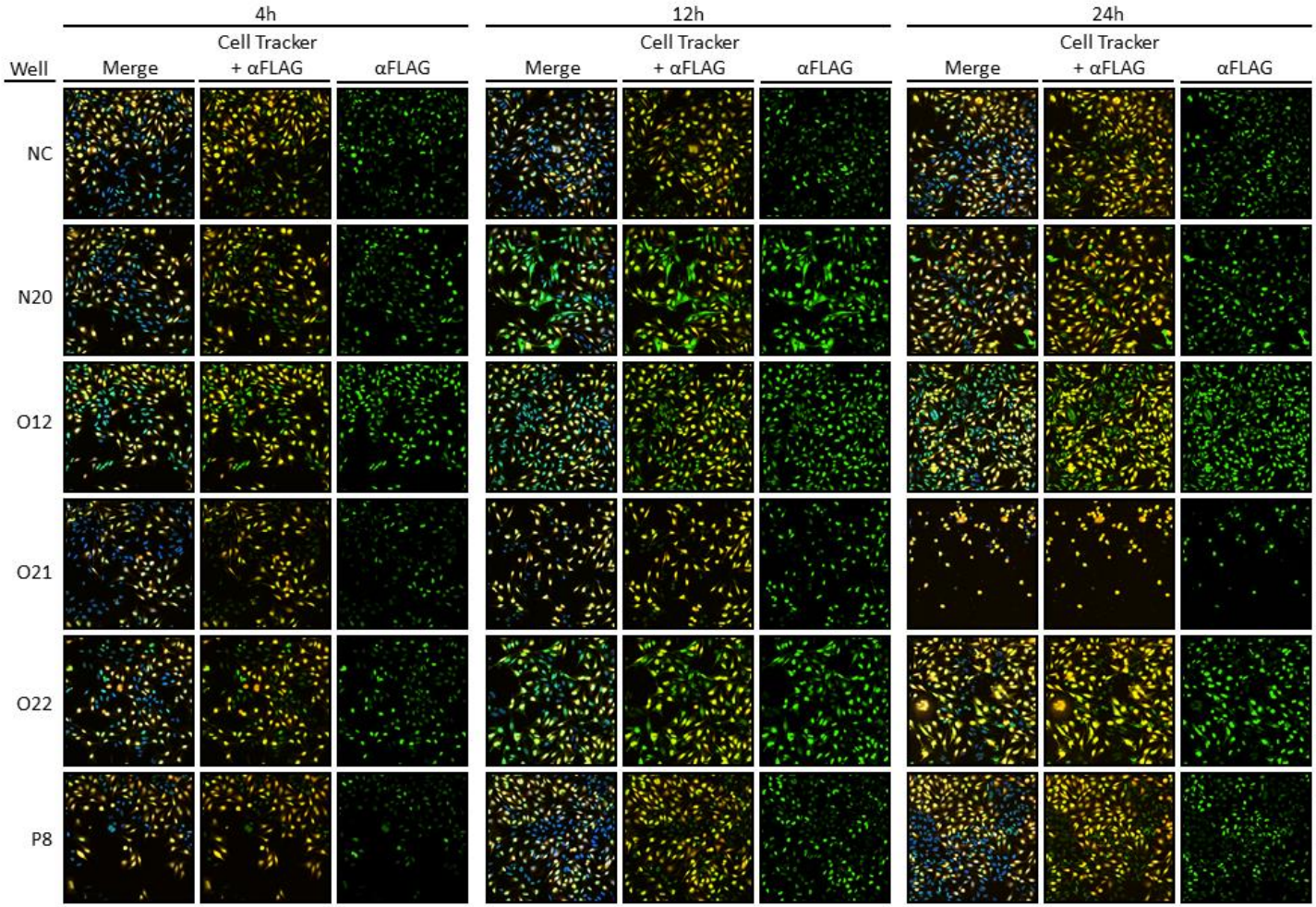

Compound with Z-Score < -2

0.16% DMSO
Negative Control

OXYQUINOLINE SULFATE

End-Point	TBX2 (orange)	TBX3
Downregulation	-	-
Translocation	-	12h (2,98) 24h (2,66)

METHACYCLINE HYDROCHLORIDE

End-Point	TBX2 (orange)	TBX3
Downregulation	-	-
Translocation	12h (2,33) 24h (2,26)	-

PUROMYCIN DIHYDROCHLORIDE

End-Point	TBX2 (orange)	TBX3
Downregulation	-	-
Translocation	24h (3,56)	-

CHLOROACETOXYQUINOLINE

End-Point	TBX2 (orange)	TBX3
Downregulation	-	-
Translocation	12h (2,85)	12h (3,36) 24h (2,85)

FENTHION

End-Point	TBX2 (orange)	TBX3
Downregulation	-	-
Translocation	-	4h (2,08)

LP4	B	20	LEVOSIMENDAN	Levosimendan is a calcium sensitiser used in the management of acutely decompensated congestive heart failure.
LP4	C	18	CEFOXITIN SODIUM	Cefoxitin sodium is a beta-lactam, second-generation cephalosporin antibiotic with bactericidal activity. Cefoxitin sodium binds to and inactivates penicillin-binding proteins (PBP) located on the inner membrane of the bacterial cell wall.
LP4	G	12	MECLOCYCLINE SULFOSALICYLATE	Meclocycline sulfosalicylate is a tetracycline antibiotic with broad-spectrum antibacterial and antiprotozoal activity. Meclocycline sulfosalicylate is bacteriostatic and inhibits bacterial protein synthesis by binding to the 30S ribosomal subunit, thereby preventing the addition of amino acids to the growing peptide chain. This tetracycline is active against a wide range of gram-positive and gram-negative bacteria.
LP4	G	18	VINCRISTINE SULFATE	Vincristine sulphate is a chemotherapy medication used to treat a number of types of cancer.This includes acute lymphocytic leukemia, acute myeloid leukemia, Hodgkin's disease, neuroblastoma, and small cell lung cancer among others.
LP4	H	8	THIMEROSAL	Thiomersal is an organomercury compound. This compound is a well established antiseptic and antifungal agent.
LP4	H	11	ADAPALENE	Adapalene is a third-generation topical retinoid primarily used in the treatment of mild-moderate acne, and is also used off-label to treat keratosis pilaris as well as other skin conditions.
LP4	J	4	CYCLOHEXIMIDE	Cycloheximide is a eukaryote protein synthesis inhibitor.
LP4	J	12	THIRAM	Thiram is a fungicide, ectoparasiticide, and animal repellent. Is used to prevent fungal diseases in seed and crops. It is also used as an animal repellent to protect fruit trees and ornamentals from damage by rabbits, rodents and deer. Thiram has been used in the treatment of human scabies, as a sun screen and as a bactericide applied directly to the skin or incorporated into soap.
LP4	M	7	THIOSTREPTON	Thiostrepton is a natural cyclic oligopeptide antibiotic of the thiopeptide class, derived from several strains of streptomycetes, such as Streptomyces azureus and Streptomyces laurentii. Thiostrepton is a natural product of the ribosomally synthesized and post-translationally modified peptide class. Thiostrepton has been used in veterinary medicine in mastitis caused by gram-negative organisms and in dermatologic disorders.
LP4	N	8	MERBROMIN	Merbromin is a topical antiseptic used for minor cuts and scrapes. Merbromin is an organomercuric disodium salt compound and a fluorescein.
LP4	N	20	OXYQUINOLINE SULFATE	Oxyquinoline is a heterocyclic phenol and Oxyquinoline Sulfate is its salt, both of which are described as cosmetic biocides for use in cosmetic formulations. Oxyquinoline Sulfate are accepted for use as stabilizers for hydrogen peroxide in rinse-off and leave-on hair care preparations, with concentration limitations.
LP4	O	12	METHACYCLINE HYDROCHLORIDE	Methacycline hydrochloride is a tetracycline antibiotic with broad-spectrum antibacterial and antiprotozoal activity. Methacycline hydrochloride is bacteriostatic and inhibits bacterial protein synthesis by binding to the 30S ribosomal subunit, thereby preventing the addition of amino acids to the growing peptide chain. This tetracycline is active against a wide range of gram-positive and gram-negative bacteria.
LP4	O	21	PUROMYCIN DIHYDROCHLORIDE	Puromycin Dihydrochloride is an aminonucleoside antibiotic produced by Streptomyces alboniger. Puromycin works by inhibiting peptidyl transfer on both prokaryotic and eukaryotic ribosomes.
LP4	O	22	CHLOROACETOXYQUINOLINE	Chloroacetoxyquinoline is a derivative of 8-hydroxyquinoline . These organic compounds exhibit antiseptic, disinfectant, and pesticide properties and can function as a transcription inhibitor. Its solution in alcohol is used in liquid bandages. It once was of interest as an anti-cancer drug.
LP4	P	8	FENTHION	Fenthion is an organothiophosphate insecticide, avicide, and acaricide. Like most other organophosphates, its mode of action is via cholinesterase inhibition. Fenthion is a contact and stomach insecticide used against many biting insects. It is particularly effective against fruit flies, leaf hoppers, cereal bugs, stem borers, mosquitoes, animal parasites, mites, aphids, codling moths, and weaver birds. It has been widely used in sugar cane, rice, field corn, beets, pome and stone fruit, citrus fruits, pistachio, cotton, olives, coffee, cocoa, vegetables, and vines.

Pharmakon Library Plate 5

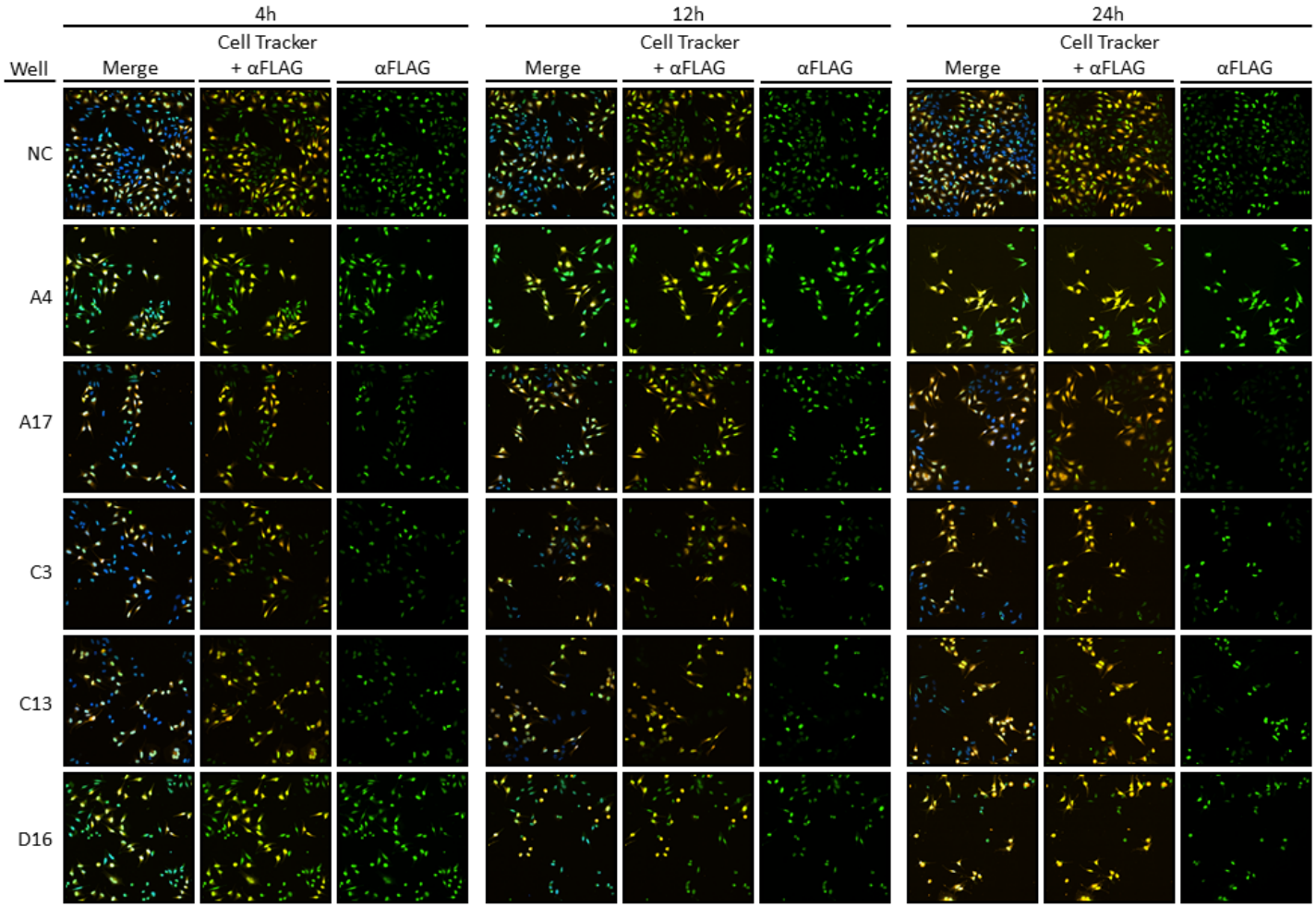

Compound with Z-Score < -2

0.16% DMSO
Negative Control

ACRIFLAVINIUM HYDROCHLORIDE

End-Point	TBX2 (orange)	TBX3
Downregulation	·	·
Translocation	4h (4,34) 12h (3,03)	4h (2,26)

PENTAMIDINE ISETHIONATE

End-Point	TBX2 (orange)	TBX3
Downregulation	12h (2,25) 24h (2,71)	·
Translocation	·	24h (2,01)

ETHACRIDINE LACTATE

End-Point	TBX2 (orange)	TBX3
Downregulation	4h (2,03)	·
Translocation	·	·

BROXALDINE

End-Point	TBX2 (orange)	TBX3
Downregulation	12h (2,29)	12h (2,91)
Translocation	·	·

PROFLAVINE HEMISULFATE

End-Point	TBX2 (orange)	TBX3
Downregulation	·	·
Translocation	4h (3,63)	·

Pharmakon Library Plate 5

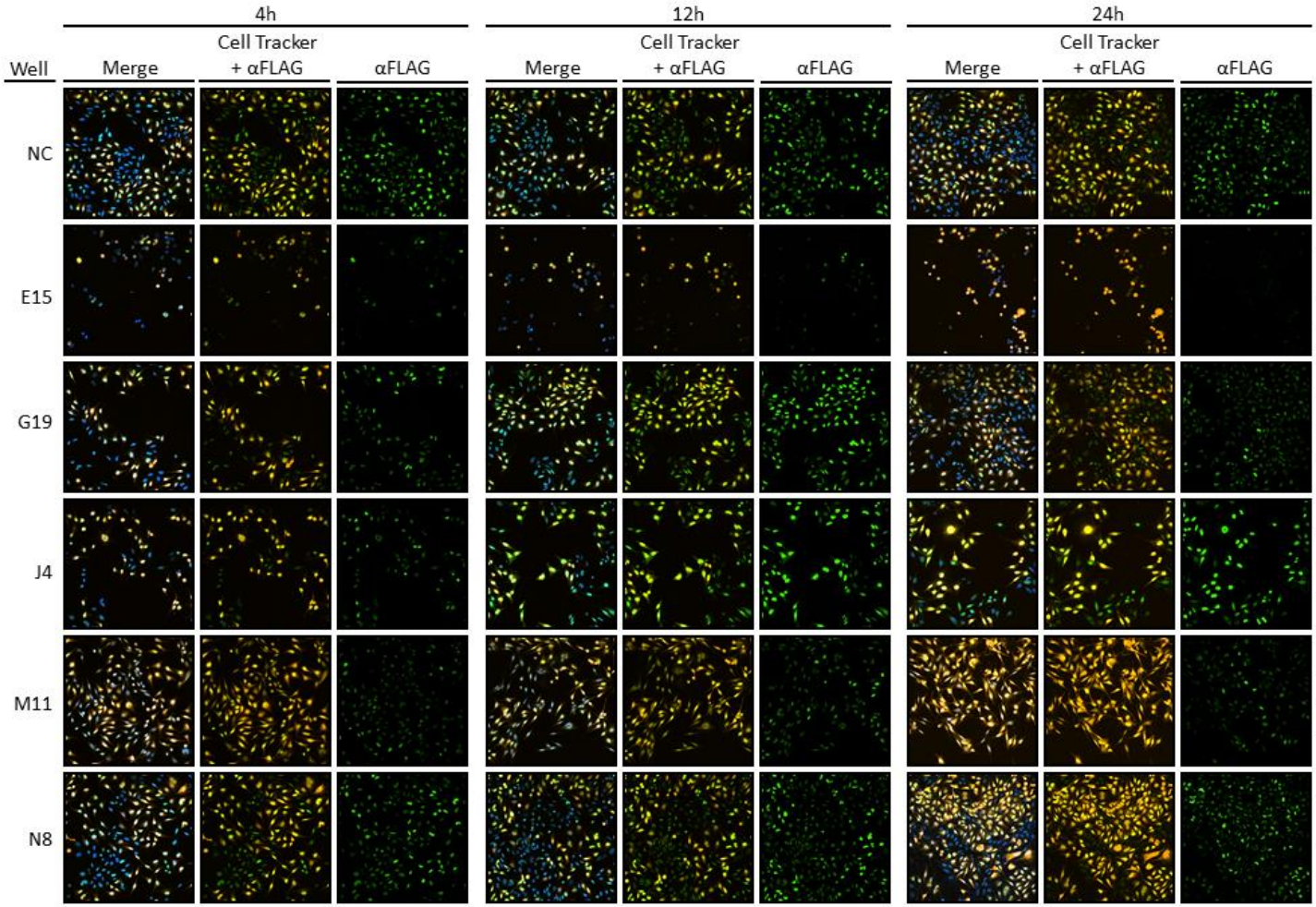

Compound with Z-Score < -2

0.16% DMSO
Negative Control

CETRIMONIUM BROMIDE

End-Point	TBX2 (orange)	TBX3
Downregulation	12h (3,50)	-
Translocation	-	-

CLEMIZOLE HYDROCHLORIDE

End-Point	TBX2 (orange)	TBX3
Downregulation	12h (2,37) 24h (2,09)	-
Translocation	-	-

DISULFIRAM

End-Point	TBX2 (orange)	TBX3
Downregulation	-	-
Translocation	-	24h (2,23)

HOMIDIUM BROMIDE

End-Point	TBX2 (orange)	TBX3
Downregulation	(2,11) (3,04) (2,49)	-
Translocation	-	-

CARGLUMIC ACID

End-Point	TBX2 (orange)	TBX3
Downregulation	-	-
Translocation	-	24h (2,15)

Pharmakon Library Plate 5

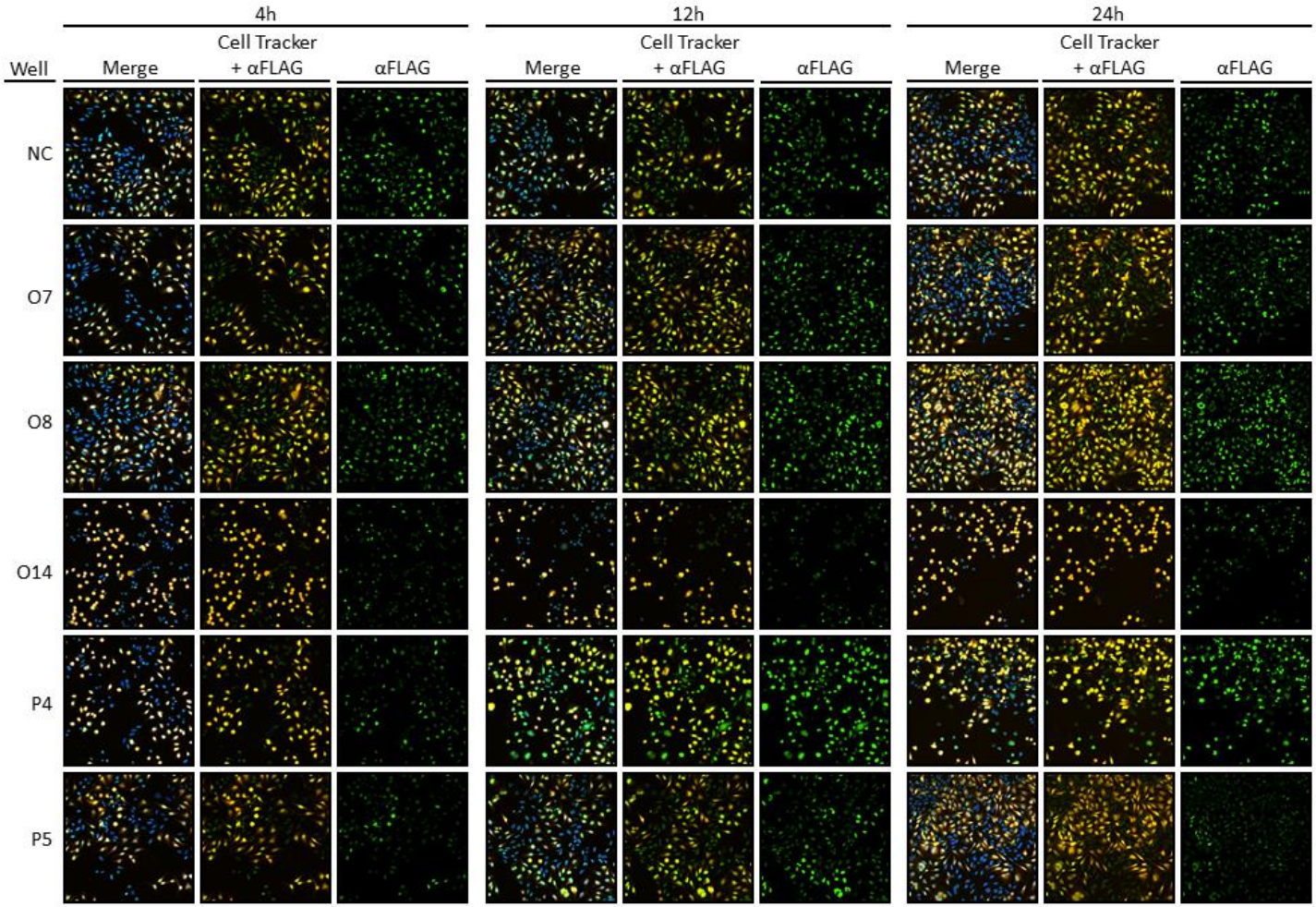

LP5	A	4	ACRIFLAVINIUM HYDROCHLORIDE	Acriflavine hydrochloride is a topical antiseptic. It has the form of an orange or brown powder. Acriflavine is used in biochemistry for fluorescently labeling high molecular weight RNA. In an animal model, acriflavine has been shown to inhibit HIF-1, which prevents blood vessels growing to supply tumors with blood and interferes with glucose uptake and use. Acriflavine might be effective in fighting common cold virus, and also aid the fight against increasingly antibiotic resistant bacteria.
LP5	A	17	PENTAMIDINE ISETHIONATE	Pentamidine isethionate is antimicrobial medication used to treat African trypanosomiasis, leishmaniasis, babesiosis, and to prevent and treat pneumocystis pneumonia .
LP5	C	3	ETHACRIDINE LACTATE	Ethacridine lactate is an aromatic organic compound based on acridine. It forms orange-yellow crystals. Its primary use is as an antiseptic. It is effective against mostly gram-positive species like Streptococci and Staphylococci and ineffective against gram-negative.
LP5	C	13	BROXALDINE	Broxaldine is an antiprotozoal drug.
LP5	D	16	PROFLAVINE HEMISULFATE	Proflavine hemisulfate is a small, amphipathic, acridine-derived fluorescent dye.Proflavine hemisulfate is used as a rapid stain for cytological studies of biological specimens. It stains cytoplasmic structures and nuclei. Proflavine has the capability to intercalate double stranded DNA.
LP5	E	15	CETRIMONIUM BROMIDE	Cetrimonium bromide is a quaternary ammonium surfactant. It is one of the components of the topical antiseptic cetrimide. Identified as a potential apoptogenic quaternary ammonium compound possessing in vitro and in vivo efficacy against head and neck cancers.
LP5	G	19	CLEMIZOLE HYDROCHLORIDE	Clemizole is a potent and selective H1 histamine receptor antagonist.
LP5	J	4	DISULFIRAM	Disulfiram is used to support the treatment of chronic alcoholism by producing an acute sensitivity to ethanol (drinking alcohol). Disulfiram works by inhibiting the enzyme acetaldehyde dehydrogenase. Disulfiram is also being studied as a treatment for cocaine dependence. Several studies have reported that it has antiprotozoal activity, as well. Disulfiram is the subject of research for treatment of cancer and HIV.
LP5	M	11	HOMIDIUM BROMIDE	Homidium bromide is used for the treatment of Trypanosomiasis in cattle
LP5	N	8	CARGLUMIC ACID	Carglumic acid is an orphan drug used for the treatment of hyperammonaemia in patients with N-acetylglutamate synthase deficiency.
LP5	O	7	DEFERIPRONE	Deferiprone is a drug that chelates iron and is used to treat iron overload in thalassaemia major.
LP5	O	8	HYDROXYTOLUIC ACID	Hydroxytoluic acid is a long-acting salicylate derivative with antilipidemic properties. Hydroxytoluic acid has been shown to lower plasma free fatty acid and cholesterol levels.
LP5	O	14	BRONOPOL	Bronopol is an organic antimicrobial. Bronopol is used in consumer products as an effective preservative agent, as well as a wide variety of industrial applications.
LP5	P	4	BENZYL ISOTHIOCYANATE	Benzyl isothiocyanate is a naturally-occurring constituent of cruciferous vegetables. It has antibacterial properties and its metabolism in man has been investigated. It inhibits chemically induced cancer in animal models
LP5	P	5	DICLAZURIL	Antiprotozoal agent that acts upon Coccidia parasites.

7.12 TBX2 HC StratoMineR ranked 'hits'

Ranked 'Hits': TBX2 4h							
Plate	**Well**	**Pharmakon Compound**	**Factor 1**	**Factor 2**	**Factor 3**	**Distance Score**	**p-value**
5	d06	HEXETIDINE	8.38	-5.41	2.06	10.55	2.02E-106
5	p17	CLOFOCTOL	-4.31	-7.82	-6.19	10.54	3.30E-101
3	h21	AMLODIPINE BESYLATE	7.58	-6.10	1.02	9.74	6.63E-81
1	h12	BENZETHONIUM CHLORIDE	-4.22	-8.09	-2.95	9.49	1.78E-78
1	p04	CETYLPYRIDINIUM CHLORIDE	-1.33	-7.85	-3.74	8.87	3.51E-70
1	a11	SANGUINARIUM CHLORIDE	-4.27	-7.23	-0.89	8.22	6.65E-61
5	o14	BRONOPOL	-1.77	-7.99	-0.81	8.11	2.37E-60
2	e10	GENTIAN VIOLET	-3.75	-7.24	1.62	8.06	5.14E-59
5	o05	ESCIN	-2.78	-7.13	-4.15	8.42	1.69E-58
2	p07	THIORIDAZINE HYDROCHLORIDE	6.50	-5.51	1.16	8.67	6.80E-55
4	f08	PYRITHIONE ZINC	-0.85	-7.68	2.70	7.86	7.90E-55
5	n09	METERGOLINE	1.48	-7.17	0.87	7.69	1.80E-50
3	k04	TERFENADINE	-3.28	-6.79	3.00	7.74	2.53E-45
2	h11	PYRVINIUM PAMOATE	2.94	-6.61	1.11	7.29	6.59E-43
2	g09	DAUNORUBICIN	-2.68	-1.06	-9.04	9.63	6.99E-41
1	l14	BROMOCRIPTINE MESYLATE	6.51	1.38	-1.20	7.00	1.80E-38
2	m17	DOXYCYCLINE HYDROCHLORIDE	6.28	-1.28	-0.45	6.63	2.00E-38
2	g08	HEXACHLOROPHENE	-1.80	-6.24	3.24	6.99	2.15E-37
2	d11	PRAZOSIN HYDROCHLORIDE	6.19	-0.48	-0.57	6.46	5.14E-35
3	c04	AMSACRINE	6.24	-0.82	0.45	6.47	1.33E-34
3	a20	METHYLBENZETHONIUM CHLORIDE	-1.37	-6.28	1.61	6.33	1.61E-34
3	h06	DOXORUBICIN	-2.28	-1.24	-6.58	7.07	1.62E-34
3	m20	PERPHENAZINE	3.34	-5.59	1.24	6.44	4.51E-32
2	e14	GRAMICIDIN (gramicidin A shown)	-1.15	-6.47	-0.15	6.38	2.74E-31
5	e15	CETRIMONIUM BROMIDE	-3.29	-3.46	-4.92	6.44	6.94E-30
3	g13	ASTEMIZOLE	3.33	-4.33	2.99	6.05	2.44E-29
3	a13	ERYTHROMYCIN ESTOLATE	5.80	0.49	0.22	6.06	5.47E-28
4	h08	THIMEROSAL	-2.03	-5.68	0.44	5.73	1.08E-27
4	o11	CANDICIDIN	-1.41	-4.75	-2.71	5.63	5.29E-27
1	i08	MOXIDECTIN	4.82	2.94	-0.50	6.07	1.69E-25
5	h18	CAPTAMINE	5.02	0.88	0.45	5.59	4.36E-24
2	b14	TRIFLUOPERAZINE HYDROCHLORIDE	2.99	-5.22	0.51	6.18	4.50E-24
5	a03	METITEPINE MALEATE	0.53	-4.63	2.17	5.27	2.80E-23
4	e21	IVERMECTIN	-1.00	-5.48	-0.70	5.40	6.09E-22
5	n13	TOLONIUM CHLORIDE	-1.12	-5.06	1.08	5.25	1.51E-21
3	o13	PERHEXILINE MALEATE	3.60	-4.11	1.08	5.45	1.60E-21
3	l18	THONZONIUM BROMIDE	-0.09	-5.37	0.62	5.11	2.01E-20
4	g14	PENFLURIDOL	-0.73	-5.36	1.16	5.31	4.50E-20
2	m22	PROGESTERONE	1.98	-4.03	2.23	4.91	5.85E-19
4	d03	TOREMIPHENE CITRATE	3.62	-3.98	1.35	5.49	8.14E-19
3	j18	RALOXIFENE HYDROCHLORIDE	4.57	0.94	0.06	4.91	8.16E-18
1	m17	LASALOCID SODIUM	5.05	-1.35	-0.24	5.30	1.10E-16

5	p04	BENZYL ISOTHIOCYANATE	-1.43	-4.69	0.59	4.82	1.91E-16
2	p08	FLUPHENAZINE HYDROCHLORIDE	1.77	-4.13	-0.91	4.77	3.59E-16
1	c08	SULOCTIDIL	3.74	-2.93	-0.25	4.70	4.04E-16
5	j15	ALEXIDINE HYDROCHLORIDE	0.83	-4.27	1.27	4.65	8.35E-16
3	i14	BENZALKONIUM CHLORIDE	-3.02	-3.84	-2.78	5.35	1.26E-14
1	n21	PODOFILOX	1.57	-4.30	1.04	4.39	2.60E-14
1	a09	ANTIMONY POTASSIUM TARTRATE TRIHYDRATE	0.21	0.22	-3.93	4.38	3.15E-14
1	a16	SULFADIMETHOXINE	-1.74	-1.55	-3.32	4.27	4.20E-14
5	j04	DISULFIRAM	-0.58	-3.91	0.92	4.03	1.70E-12
1	a15	MEDRYSONE	-1.67	-1.73	-2.95	3.99	3.14E-12
4	p19	BENAZEPRIL HYDROCHLORIDE	1.61	-3.69	0.90	4.03	8.13E-12
4	g22	DESLORATIDINE	2.25	-3.30	0.03	3.92	1.21E-11
2	h13	QUINACRINE HYDROCHLORIDE	-3.17	-1.44	2.53	4.09	5.25E-11
1	a08	FLUBENDAZOLE	-1.16	-2.91	-2.15	3.83	5.72E-11
2	c19	COLCHICINE	1.81	-3.41	0.40	3.83	6.30E-11
1	a10	ZOLMITRIPTAN	-1.51	-0.46	-3.16	3.92	6.46E-11
3	l09	SERTRALINE HYDROCHLORIDE	-0.56	-3.87	1.49	3.83	1.43E-10
1	p11	TESTOSTERONE PROPIONATE	-1.99	0.40	-2.74	3.77	2.16E-10
1	a17	MEGESTROL ACETATE	-1.55	-0.98	-2.89	3.73	4.86E-10
5	e13	SALINOMYCIN, SODIUM	3.02	-1.16	1.50	4.03	6.27E-10
5	d16	PROFLAVINE HEMISULFATE	2.56	-0.51	-2.72	3.86	1.18E-09
3	p06	EPIRUBICIN HYDROCHLORIDE	-2.11	-0.04	-3.79	4.36	2.36E-09
4	g12	MECLOCYCLINE SULFOSALICYLATE	3.87	-0.02	-0.13	4.29	3.86E-09
4	c08	QUINESTROL	0.40	2.71	-1.28	3.92	4.58E-09
1	p16	CHLORHEXIDINE DIHYDROCHLORIDE	-2.59	0.08	-2.40	3.81	5.94E-09
4	k22	PROMETHAZINE HYDROCHLORIDE	1.85	-3.27	0.30	3.66	8.76E-09
4	j12	THIRAM	-0.37	-4.21	0.78	4.03	9.27E-09
4	o12	METHACYCLINE HYDROCHLORIDE	3.19	-0.66	-0.06	3.52	3.19E-08
2	o07	EMETINE DIHYDROCHLORIDE	-2.54	-2.78	0.55	3.55	1.28E-07
5	c13	BROXALDINE	-1.48	2.64	-1.83	3.30	1.84E-07
1	a21	DACTINOMYCIN	-2.60	-1.16	-1.37	3.32	8.27E-07
1	a14	DOCETAXEL	-0.86	-1.83	-2.31	3.25	1.28E-06
1	p15	ENILCONAZOLE SULFATE	-1.48	1.18	-1.92	3.13	2.01E-06
5	b16	COUMOPHOS	2.14	1.45	1.27	3.36	2.98E-06
1	m06	TILORONE	-1.39	-2.78	1.80	3.16	3.66E-06
3	o10	PAROXETINE HYDROCHLORIDE	0.77	-3.29	1.09	3.25	4.89E-06
1	a12	SULFACHLORPYRIDAZINE	-1.39	-0.96	-2.21	3.02	5.18E-06
1	p10	CHLORAMPHENICOL SODIUM SUCCINATE	-1.73	0.12	-2.09	3.05	7.02E-06
5	a04	ACRIFLAVINIUM HYDROCHLORIDE	0.90	-1.43	-3.23	3.55	7.21E-06
1	o16	CROTAMITON	-0.60	0.06	-2.04	2.91	1.44E-05
1	o03	MEBENDAZOLE	-0.17	-3.27	0.71	3.00	2.47E-05
3	o04	TACROLIMUS	-2.44	0.54	-1.39	2.96	3.08E-05
4	f17	HYDROXYPROGESTERONE CAPROATE	2.34	-0.55	1.20	2.82	3.66E-05
1	p08	CHLORAMPHENICOL PALMITATE	-1.57	0.47	-1.84	2.82	3.92E-05
1	i22	ALGESTONE ACETOPHENIDE	3.06	-0.11	0.52	3.18	4.44E-05
1	h07	CLARITHROMYCIN	2.77	0.32	0.37	2.93	5.84E-05

3	e06	MITOXANTRONE HYDROCHLORIDE	-1.94	-1.81	-2.10	3.23	7.00E-05
1	p13	PYRIDOSTIGMINE BROMIDE	-1.87	0.43	-1.76	2.92	8.19E-05
1	p12	CHLORAMPHENICOL	-1.67	0.50	-1.83	2.94	8.44E-05
3	g11	MONENSIN SODIUM (monensin A is shown)	2.41	-1.22	0.31	2.75	9.23E-05
4	h13	CANDESARTAN CILEXTIL	0.46	2.23	0.49	2.70	9.23E-05
1	i21	NORTRIPTYLINE HYDROCHLORIDE	2.09	-2.15	0.65	2.86	9.56E-05
1	m22	PREDNISOLONE TEBUTATE	-2.55	1.23	-0.34	3.08	9.79E-05

Ranked 'Hits': TBX2 12h

Plate	Well	Pharmakon Compound	Factor 1	Factor 2	Factor 3	Distance Score	p-value
2	g09	DAUNORUBICIN	-6.13	-3.19	-10.80	13.09	0.00E+00
4	f08	PYRITHIONE ZINC	-10.75	-2.13	-1.35	10.99	4.30E-200
5	p17	CLOFOCTOL	-9.41	-3.46	-5.76	11.79	2.41E-195
3	h06	DOXORUBICIN	-6.80	-2.52	-8.62	10.99	1.90E-145
2	h11	PYRVINIUM PAMOATE	-2.48	8.25	1.25	9.26	1.89E-141
5	o05	ESCIN	-8.85	-2.75	-2.58	9.84	2.28E-141
5	o14	BRONOPOL	-9.07	-1.75	0.55	9.38	6.80E-131
5	n09	METERGOLINE	-7.76	2.70	1.00	8.74	6.67E-128
2	e10	GENTIAN VIOLET	-8.58	-3.54	-0.36	9.43	8.33E-128
3	h21	AMLODIPINE BESYLATE	-5.98	5.27	0.47	8.20	7.97E-113
4	h08	THIMEROSAL	-8.15	-2.49	-0.75	8.46	3.21E-107
3	g13	ASTEMIZOLE	-4.73	5.18	2.98	7.89	7.85E-97
2	g08	HEXACHLOROPHENE	-6.73	-2.22	5.14	8.87	1.36E-83
1	a09	ANTIMONY POTASSIUM TARTRATE TRIHYDRATE	-4.25	6.37	-2.92	8.71	1.65E-83
4	g14	PENFLURIDOL	-7.62	0.39	-2.42	8.12	4.21E-83
3	c04	AMSACRINE	2.29	5.96	-1.43	6.98	1.78E-78
2	e14	GRAMICIDIN (gramicidin A shown)	-3.43	5.13	1.98	7.01	3.81E-71
1	k06	AUROTHIOGLUCOSE	-6.68	1.85	0.84	7.13	5.49E-71
2	d11	PRAZOSIN HYDROCHLORIDE	1.41	6.30	-1.15	7.07	5.23E-68
3	a20	METHYLBENZETHONIUM CHLORIDE	-6.86	-1.34	-0.03	6.77	2.80E-66
3	k04	TERFENADINE	-7.00	-2.79	-1.48	7.39	8.97E-66
1	a11	SANGUINARIUM CHLORIDE	-6.07	-3.71	-0.67	6.85	1.49E-64
4	d03	TOREMIPHENE CITRATE	-4.77	4.25	0.92	6.77	3.36E-63
1	h12	BENZETHONIUM CHLORIDE	-6.79	-2.12	-0.85	7.02	2.77E-62
1	i08	MOXIDECTIN	-0.05	5.67	-0.23	6.31	1.29E-61
3	i14	BENZALKONIUM CHLORIDE	-6.18	-2.49	-2.41	6.77	1.80E-60
1	i19	OXYPHENBUTAZONE	4.08	4.82	-1.11	6.96	8.34E-60
4	o09	PROSCILLARIDIN	-6.25	-0.98	1.15	6.50	1.27E-59
5	d06	HEXETIDINE	-3.72	4.92	0.99	6.65	2.51E-58
2	p07	THIORIDAZINE HYDROCHLORIDE	-5.37	3.43	0.71	6.97	5.59E-57
4	e21	IVERMECTIN	-7.59	-2.10	-2.73	8.33	2.51E-56
2	p08	FLUPHENAZINE HYDROCHLORIDE	-5.05	0.33	-1.64	5.94	2.92E-55
3	m20	PERPHENAZINE	-4.46	4.06	0.30	6.25	1.89E-54
2	m17	DOXYCYCLINE HYDROCHLORIDE	-2.89	4.35	0.88	5.86	8.64E-54
4	g18	VINCRISTINE SULFATE	-5.44	1.64	1.18	5.99	9.58E-53

1	p04	CETYLPYRIDINIUM CHLORIDE	-6.23	-1.89	-2.99	7.04	1.37E-52
2	o07	EMETINE DIHYDROCHLORIDE	-5.79	-2.16	0.03	6.39	1.27E-51
2	b14	TRIFLUOPERAZINE HYDROCHLORIDE	-5.00	1.74	0.16	5.79	1.11E-50
4	j12	THIRAM	-2.62	4.54	-0.05	5.67	5.29E-49
2	c19	COLCHICINE	-4.95	1.85	0.89	5.82	3.90E-46
5	j15	ALEXIDINE HYDROCHLORIDE	-4.24	2.67	0.75	5.43	3.07E-44
3	e06	MITOXANTRONE HYDROCHLORIDE	-4.57	-2.15	-4.14	6.22	4.16E-42
5	n13	TOLONIUM CHLORIDE	-5.60	-0.36	-0.92	5.88	1.20E-41
4	k20	POTASSIUM p-AMINOBENZOATE	-4.97	-0.41	1.72	5.34	1.89E-40
3	p06	EPIRUBICIN HYDROCHLORIDE	-1.69	-2.08	-5.26	5.62	1.69E-39
1	l14	BROMOCRIPTINE MESYLATE	-1.30	4.92	-0.29	5.72	2.57E-39
5	a03	METITEPINE MALEATE	-4.52	-0.38	2.11	5.14	2.99E-39
1	f05	TENIPOSIDE	0.45	4.65	-0.64	5.37	1.04E-38
5	e15	CETRIMONIUM BROMIDE	-4.28	-2.99	-2.75	6.11	5.39E-38
3	o13	PERHEXILINE MALEATE	-4.36	2.66	0.20	5.27	8.15E-38
4	o11	CANDICIDIN	-4.49	2.43	0.99	5.46	1.98E-37
3	a13	ERYTHROMYCIN ESTOLATE	-1.97	5.01	0.41	5.78	4.96E-36
4	g22	DESLORATIDINE	-3.52	3.19	1.57	5.35	1.18E-34
1	g03	VINBLASTINE SULFATE	-5.18	-0.87	1.36	5.30	1.80E-33
4	o22	CHLOROACETOXYQUINOLINE	2.00	3.54	-2.10	4.83	4.19E-33
2	j04	OUABAIN	-4.47	-0.87	1.71	5.04	7.45E-33
5	j04	DISULFIRAM	2.71	3.84	-1.93	5.33	1.09E-32
2	e21	CYTARABINE	4.96	-1.76	-2.17	5.39	1.74E-32
1	a05	ETOPOSIDE	5.12	-1.57	-1.12	5.42	8.45E-32
2	k09	DIGOXIN	-4.56	-0.77	1.33	5.01	1.18E-31
1	m17	LASALOCID SODIUM	-2.19	3.42	-0.29	4.64	1.53E-31
2	o21	ESTRADIOL CYPIONATE	-4.23	2.03	-1.23	5.65	1.63E-31
1	a21	DACTINOMYCIN	-4.52	-2.82	-1.00	5.12	3.67E-30
4	o18	BLEOMYCIN (bleomycin B2 shown)	4.59	-0.81	-1.42	4.77	6.84E-30
4	o21	PUROMYCIN DIHYDROCHLORIDE	-4.85	1.61	0.43	5.31	2.19E-29
3	l18	THONZONIUM BROMIDE	-4.31	-1.34	1.71	4.63	3.68E-29
3	a11	SPIPERONE	-2.46	3.84	-0.64	4.89	5.32E-29
1	n09	TOPOTECAN HYDROCHLORIDE	0.02	3.38	-2.00	4.54	6.29E-29
3	l09	SERTRALINE HYDROCHLORIDE	-4.42	-0.19	1.90	4.74	3.35E-28
1	c08	SULOCTIDIL	-1.39	3.51	0.44	4.39	3.83E-27
5	i10	ANCITABINE HYDROCHLORIDE	3.55	-1.42	-2.94	4.68	1.56E-26
3	a12	PIROCTONE OLAMINE	2.04	2.38	-2.58	4.42	1.94E-26
2	m22	PROGESTERONE	-4.06	0.22	1.80	4.71	1.20E-25
4	g12	MECLOCYCLINE SULFOSALICYLATE	-2.54	3.30	0.46	4.64	4.18E-22
2	k07	DIGITOXIN	-4.14	-0.63	1.14	4.57	5.21E-22
2	a16	ETHIONAMIDE	-0.23	-1.77	-3.55	4.04	2.08E-21
1	n21	PODOFILOX	-3.80	-0.13	0.76	3.84	1.32E-19
3	g07	MENADIONE	-0.60	3.40	-0.39	3.89	1.50E-19
4	o12	METHACYCLINE HYDROCHLORIDE	-2.96	2.03	-0.28	3.96	4.55E-19
4	f04	CICLOPIROX OLAMINE	2.66	1.75	-2.68	4.26	1.39E-18
3	o10	PAROXETINE HYDROCHLORIDE	-3.82	0.30	0.06	3.86	2.08E-18
2	h15	QUINIDINE GLUCONATE	-1.51	2.69	0.36	3.71	2.20E-18

3	b09	TRIFLURIDINE	2.94	-0.99	-2.15	3.76	2.73E-18
3	d11	CARVEDILOL	-2.23	2.64	0.56	3.81	8.34E-18
5	j17	GALLIC ACID	3.35	1.35	-0.49	3.64	9.28E-18
5	h18	CAPTAMINE	0.64	3.15	0.75	3.60	1.74E-17
5	p14	CARBIDOPA	3.98	1.32	-1.11	4.32	5.04E-17
2	a10	ETHACRYNIC ACID	0.06	-0.38	-3.45	3.75	5.21E-17
4	n20	OXYQUINOLINE SULFATE	2.94	0.98	-1.91	3.67	6.52E-17
4	h11	ADAPALENE	3.22	0.36	-1.44	3.54	1.12E-16
2	g13	DEMECLOCYCLINE HYDROCHLORIDE	-0.44	2.91	0.67	3.56	6.82E-16
4	g13	DOXAZOSIN MESYLATE	-2.18	2.78	0.86	4.01	8.69E-16
2	a15	CHLORTHALIDONE	-0.52	-0.75	-3.19	3.57	1.01E-14
5	i07	DEQUALINIUM CHLORIDE	-3.28	0.74	0.89	3.84	1.24E-14
2	p05	THIOGUANINE	-2.00	1.70	-0.62	3.32	2.02E-14
2	a09	CHLORPROMAZINE	-0.73	-0.97	-2.90	3.36	9.28E-14
2	a08	ESTRONE	-0.38	-0.94	-2.89	3.26	1.76E-13
5	j22	LANATOSIDE C	-3.65	-0.97	1.15	4.05	6.71E-13
2	p09	THIOTHIXENE	-2.29	-0.66	-1.44	3.15	1.19E-12
5	j10	BROXYQUINOLINE	1.83	0.67	-1.96	3.14	2.35E-12
4	c05	ITRACONAZOLE	-2.54	0.52	1.72	3.31	3.25E-12
1	i13	IRINOTECAN HYDROCHLORIDE	3.03	0.53	-0.95	3.47	5.07E-12
1	o19	PIMOZIDE	-1.01	2.45	-0.41	3.27	6.87E-12
3	d05	SIMVASTATIN	-3.12	0.16	1.30	3.40	7.02E-12
2	k11	DIHYDROERGOTAMINE MESYLATE	-1.11	2.63	0.31	3.46	2.30E-11
3	o04	TACROLIMUS	0.97	-2.81	-1.59	3.05	3.47E-11
3	j18	RALOXIFENE HYDROCHLORIDE	-1.38	2.49	0.63	3.27	6.82E-11
3	m04	PACLITAXEL	-2.91	-0.73	1.27	3.12	9.80E-11
4	k22	PROMETHAZINE HYDROCHLORIDE	-2.96	0.49	1.24	3.44	1.01E-10
4	b14	OXALIPLATIN	2.97	-0.72	-0.86	3.06	1.76E-10
5	p04	BENZYL ISOTHIOCYANATE	-1.02	2.76	-0.42	3.34	2.02E-10
4	d10	GRISEOFULVIN	-1.87	2.19	0.97	3.42	2.52E-10
2	p11	TIMOLOL MALEATE	-0.74	-1.36	-2.35	2.98	2.55E-10
2	a14	ETHINYL ESTRADIOL	-0.82	0.04	-2.22	2.88	3.59E-10
5	p03	CEPHARANTHINE	-1.44	2.58	-0.38	3.39	4.82E-10
1	b07	ERYTHROMYCIN	-0.01	2.24	0.05	2.90	7.34E-10
2	a11	CHLORPROPAMIDE	-0.18	-0.86	-2.88	3.21	9.45E-10
4	c18	CEFOXITIN SODIUM	-2.68	-0.07	0.67	2.85	1.05E-09
1	g08	TEPOXALIN	1.61	1.56	-0.41	2.80	1.73E-09
1	p06	CHLORAMBUCIL	2.24	-1.60	-1.26	2.84	2.95E-09
2	c10	FLUOCINONIDE	0.37	2.13	-0.52	2.78	3.33E-09
5	a04	ACRIFLAVINIUM HYDROCHLORIDE	-0.20	1.57	-2.13	3.00	5.90E-09
2	a17	CHLORZOXAZONE	-0.21	-0.98	-2.60	3.02	6.18E-09
2	p15	TOLAZOLINE HYDROCHLORIDE	-0.02	-1.23	-2.40	2.84	6.25E-09
4	d17	MAPROTILINE HYDROCHLORIDE	-2.47	0.35	1.83	3.28	7.03E-09
2	h13	QUINACRINE HYDROCHLORIDE	-0.06	-2.74	1.79	2.78	7.31E-09
3	l10	OXFENDAZOLE	-2.39	0.24	-0.16	2.76	9.82E-09

5	m11	HOMIDIUM BROMIDE	-0.55	-2.67	-1.24	2.82	1.03E-08
5	b09	GLAFENINE	-0.11	2.39	0.35	2.76	1.73E-08
1	c19	PITAVASTATIN CALCIUM	-3.08	0.80	1.31	3.58	1.86E-08
2	b18	TRIMEPRAZINE TARTRATE	-2.35	0.05	0.78	2.78	2.52E-08
2	a13	CHLORTETRACYCLINE HYDROCHLORIDE	-0.36	0.11	-2.15	2.65	2.61E-08
5	c13	BROXALDINE	0.04	-2.06	-3.06	3.73	2.91E-08
2	p14	FAMOTIDINE	-0.48	-0.96	-2.45	2.93	2.93E-08
2	b09	LEVOTHYROXINE	0.20	0.06	-2.38	2.83	3.96E-08
3	g04	OXIBENDAZOLE	-2.41	-0.16	1.48	2.78	6.03E-08
1	b05	BETAMETHASONE VALERATE	0.12	1.93	-0.06	2.74	7.11E-08
3	f11	FLUVASTATIN	-2.33	0.13	1.43	2.73	1.08E-07
2	c12	FLUOROMETHOLONE	0.40	1.87	-0.54	2.55	1.65E-07
4	g07	TRETINOIN	0.28	2.03	0.65	2.58	1.72E-07
1	j13	HYDROCORTISONE	0.37	1.92	0.09	2.59	2.16E-07
5	m08	PAMABROM	-0.74	-1.18	-2.13	2.60	2.38E-07
2	o18	OXIDOPAMINE HYDROCHLORIDE	2.53	0.12	-0.77	2.51	2.69E-07
1	d11	ATORVASTATIN CALCIUM	-2.45	0.21	0.77	2.64	3.49E-07
4	n05	MECHLORETHAMINE	2.75	-0.50	-1.55	3.08	4.21E-07
4	j07	ESTRAMUSTINE	-2.33	0.83	-0.02	2.68	4.87E-07
2	p17	TOLBUTAMIDE	-0.59	-1.03	-2.09	2.61	6.02E-07
3	p15	NISOLDIPINE	1.88	-1.36	-1.53	2.69	6.04E-07
1	h07	CLARITHROMYCIN	0.00	1.79	0.35	2.49	6.84E-07
2	c08	FLUOCINOLONE ACETONIDE	0.59	2.15	-0.51	2.86	7.36E-07
2	b16	TRIHEXYPHENIDYL HYDROCHLORIDE	-0.63	0.15	-1.83	2.43	9.62E-07
5	e13	SALINOMYCIN, SODIUM	-1.34	1.44	0.67	2.45	1.05E-06
4	d14	VERAPAMIL HYDROCHLORIDE	-0.31	2.18	0.32	2.65	1.51E-06
2	i08	HYDROFLUMETHIAZIDE	0.06	1.84	0.39	2.38	2.36E-06
1	b16	MITOMYCIN	0.43	0.70	-1.88	2.57	2.79E-06
2	b10	TRIAMTERENE	-0.46	-0.17	-2.15	2.55	3.03E-06
2	p16	ETODOLAC	-0.39	-1.22	-2.02	2.51	3.16E-06
1	p16	CHLORHEXIDINE DIHYDROCHLORIDE	-0.67	-1.87	-1.83	2.40	3.39E-06
4	h13	CANDESARTAN CILEXTIL	-0.46	2.02	0.47	2.55	3.61E-06
2	p10	FLUTAMIDE	0.09	-0.75	-2.23	2.52	4.50E-06
2	b08	TRIAMCINOLONE DIACETATE	0.69	1.14	-1.18	2.33	5.45E-06
3	j21	DERACOXIB	1.08	-2.41	-0.24	2.37	6.74E-06
1	c03	METAPROTERENOL	-1.23	1.47	0.46	2.45	7.37E-06
2	f10	ALBENDAZOLE	-2.19	-0.74	1.34	2.77	7.65E-06
2	a12	ETHAMBUTOL HYDROCHLORIDE	-0.29	-0.26	-2.15	2.54	8.06E-06
4	h12	PHENYLMERCURIC ACETATE	1.42	1.18	-0.86	2.36	8.40E-06
1	e10	FLUMETHASONE	1.03	1.46	0.14	2.37	9.75E-06
1	j21	NONOXYNOL-9	-1.77	0.74	-0.33	2.35	1.26E-05
3	g03	CYCLOSPORINE	-1.86	-1.90	-0.38	2.26	1.32E-05
3	c07	AMIODARONE HYDROCHLORIDE	-2.11	0.71	0.71	2.43	1.43E-05
2	o09	EPINEPHRINE BITARTRATE	0.90	-0.66	-1.83	2.33	1.55E-05
5	i19	NIFUROXAZIDE	2.37	0.03	-0.58	2.35	1.65E-05

3	g11	MONENSIN SODIUM (monensin A is shown)	-0.13	1.69	0.32	2.23	1.81E-05
5	c03	ETHACRIDINE LACTATE	1.18	-1.73	-1.30	2.22	2.07E-05
1	p08	CHLORAMPHENICOL PALMITATE	-0.03	-1.55	-1.88	2.21	2.16E-05
3	k10	SELAMECTIN	0.63	0.08	-1.89	2.29	2.99E-05
4	b20	LEVOSIMENDAN	1.40	-2.04	0.04	2.19	3.19E-05
2	f18	NOSCAPINE HYDROCHLORIDE	-0.89	0.86	1.48	2.26	3.24E-05
3	d18	PREDNISOLONE HEMISUCCINATE	1.06	1.28	0.63	2.27	3.48E-05
2	d13	PREDNISOLONE	0.92	1.81	0.09	2.41	3.59E-05
2	c06	FLUMETHAZONE PIVALATE	0.32	1.74	0.16	2.32	3.63E-05
4	j04	CYCLOHEXIMIDE	-1.39	-2.04	-0.61	2.22	3.68E-05
1	d19	LOVASTATIN	-2.02	0.12	1.12	2.38	4.42E-05
5	p08	VINCAMINE	-1.22	0.39	-0.95	2.27	4.64E-05
2	g22	HYDROCORTISONE ACETATE	0.25	1.62	0.21	2.19	4.70E-05
3	m21	BETAMETHASONE 17,21-DIPROPIONATE	-0.91	0.89	0.16	2.15	5.05E-05
1	p11	TESTOSTERONE PROPIONATE	-0.20	-1.49	-1.84	2.21	5.16E-05
2	i06	HYDROCORTISONE PHOSPHATE TRIETHYLAMINE	0.32	1.53	-0.19	2.21	5.22E-05
1	p10	CHLORAMPHENICOL SODIUM SUCCINATE	0.18	-1.40	-2.19	2.45	5.78E-05
5	p10	DIXANTHOGEN	-0.62	-1.05	-2.14	2.51	6.16E-05
4	n10	ABAMECTIN (avermectin B1a shown)	-0.92	2.28	-0.74	3.00	6.76E-05
2	d10	TRYPTOPHAN	-1.02	1.11	0.80	2.20	7.59E-05
2	i04	HYDROCORTISONE HEMISUCCINATE	0.03	1.60	0.08	2.15	7.67E-05
1	m11	FENBENDAZOLE	-2.10	-0.05	-0.15	2.15	7.75E-05
2	i12	HYDROXYUREA	2.65	-0.73	-1.32	2.84	7.85E-05
2	p12	DROPERIDOL	-0.56	-0.98	-1.67	2.17	8.02E-05
3	c14	NICLOSAMIDE	-1.18	-2.24	0.26	2.11	8.78E-05
2	e07	VARDENAFIL HYDROCHLORIDE	0.93	-2.63	0.39	2.28	9.28E-05
1	a08	FLUBENDAZOLE	-1.69	-1.69	-0.59	2.13	9.77E-05

Ranked 'Hits': TBX2 24h

Plate	Well	Pharmakon Compound	Factor 1	Factor 2	Factor 3	Distance Score	p-value
1	a09	ANTIMONY POTASSIUM TARTRATE TRIHYDRATE	13.98	-3.09	-5.79	16.12	0.00E+00
1	f05	TENIPOSIDE	13.57	-0.57	-2.40	14.40	1.95E-288
1	k06	AUROTHIOGLUCOSE	10.68	-6.25	-0.64	12.99	2.39E-257
1	n09	TOPOTECAN HYDROCHLORIDE	11.42	0.21	-2.83	12.37	2.09E-224
2	g09	DAUNORUBICIN	-3.30	6.75	-7.43	15.28	2.65E-216
2	h11	PYRVINIUM PAMOATE	10.46	-2.67	1.33	11.09	5.80E-173
1	a21	DACTINOMYCIN	-4.80	-6.09	-6.29	10.11	4.69E-142
3	a13	ERYTHROMYCIN ESTOLATE	9.28	-2.19	-0.15	10.12	1.07E-132
5	p17	CLOFOCTOL	-3.97	-5.36	-6.85	9.46	6.92E-118
1	l14	BROMOCRIPTINE MESYLATE	7.95	-2.67	0.67	8.99	9.48E-112
1	n21	PODOFILOX	8.45	-2.68	1.27	9.52	2.60E-100
3	h06	DOXORUBICIN	-3.39	-5.35	-8.47	10.24	2.18E-98
1	i13	IRINOTECAN HYDROCHLORIDE	-1.16	7.94	-2.12	8.11	5.91E-91
3	g13	ASTEMIZOLE	5.27	-4.99	1.09	7.83	7.70E-89

1	a11	SANGUINARIUM CHLORIDE	-4.08	-4.61	-4.96	8.01	2.30E-87
4	f08	PYRITHIONE ZINC	-2.49	-7.50	-1.32	7.95	3.28E-86
2	m17	DOXYCYCLINE HYDROCHLORIDE	6.57	-3.31	0.58	7.59	2.77E-82
2	e14	GRAMICIDIN (gramicidin A shown)	6.45	-3.12	1.18	7.47	1.90E-77
4	n05	MECHLORETHAMINE	-1.30	7.34	-0.48	7.35	3.77E-77
5	i10	ANCITABINE HYDROCHLORIDE	-1.22	6.95	-2.83	7.56	1.41E-76
2	e10	GENTIAN VIOLET	-2.18	-7.39	-1.21	8.00	3.19E-76
3	e06	MITOXANTRONE HYDROCHLORIDE	-3.57	-5.46	-6.46	8.84	1.39E-75
4	o21	PUROMYCIN DIHYDROCHLORIDE	3.11	-6.59	-0.38	7.59	2.77E-75
4	j12	THIRAM	6.21	-2.24	-0.66	7.27	1.37E-74
1	a05	ETOPOSIDE	-1.51	6.92	-2.71	7.45	6.37E-71
1	h12	BENZETHONIUM CHLORIDE	-2.29	-5.87	-3.07	7.29	1.45E-70
1	p04	CETYLPYRIDINIUM CHLORIDE	-2.06	-6.55	-0.04	7.04	3.74E-70
2	c19	COLCHICINE	6.13	-2.61	0.88	6.95	1.18E-68
3	i14	BENZALKONIUM CHLORIDE	-3.22	-5.85	-4.30	7.63	2.80E-66
5	o05	ESCIN	-3.20	-5.36	-3.52	7.04	3.24E-66
5	d06	HEXETIDINE	5.94	-3.53	1.39	7.44	8.98E-66
5	a04	ACRIFLAVINIUM HYDROCHLORIDE	4.89	0.52	-4.01	6.77	1.98E-62
5	n09	METERGOLINE	3.63	-5.16	0.28	6.60	1.33E-61
4	g12	MECLOCYCLINE SULFOSALICYLATE	5.59	-3.09	0.84	6.97	1.99E-60
1	a19	MELPHALAN	-2.22	6.03	-2.05	6.49	4.85E-60
4	h08	THIMEROSAL	-2.08	-6.61	0.08	6.84	9.40E-60
2	e21	CYTARABINE	-1.04	6.82	-2.49	7.18	2.07E-59
1	c19	PITAVASTATIN CALCIUM	1.62	-5.82	-1.02	6.63	5.54E-59
4	o18	BLEOMYCIN (bleomycin B2 shown)	-0.54	7.58	-0.47	7.55	4.38E-57
3	k04	TERFENADINE	-2.09	-5.97	-1.85	6.57	1.94E-55
1	b16	MITOMYCIN	3.07	-0.98	-4.83	6.46	1.01E-54
1	o03	MEBENDAZOLE	5.49	-2.47	1.18	6.71	2.22E-54
4	o12	METHACYCLINE HYDROCHLORIDE	4.05	-4.03	-0.12	6.18	2.94E-54
5	o14	BRONOPOL	-1.57	-6.18	-0.30	6.36	3.78E-54
2	o07	EMETINE DIHYDROCHLORIDE	-0.99	-6.21	-0.35	6.52	3.28E-49
3	a12	PIROCTONE OLAMINE	2.64	4.13	-3.05	6.04	1.12E-48
4	o09	PROSCILLARIDIN	-0.49	-6.00	0.52	6.07	2.62E-48
3	a20	METHYLBENZETHONIUM CHLORIDE	-0.91	-5.82	-0.65	6.00	3.24E-47
1	m11	FENBENDAZOLE	3.94	-2.77	-1.78	5.84	2.47E-46
3	b09	TRIFLURIDINE	0.01	5.24	-2.63	5.87	2.88E-45
4	f04	CICLOPIROX OLAMINE	1.38	5.24	-1.81	5.81	4.31E-45
4	k20	POTASSIUM p-AMINOBENZOATE	-0.03	-5.89	0.47	6.01	4.94E-44
3	d05	SIMVASTATIN	0.90	-5.19	-0.24	5.62	1.00E-43
5	e15	CETRIMONIUM BROMIDE	-3.01	-5.06	-1.37	5.95	1.02E-43
2	p08	FLUPHENAZINE HYDROCHLORIDE	0.89	-5.09	-1.48	5.73	1.31E-43
3	c04	AMSACRINE	4.42	3.19	-1.42	6.11	1.48E-43
3	h21	AMLODIPINE BESYLATE	3.39	-4.24	-0.30	5.86	3.19E-42
2	g08	HEXACHLOROPHENE	1.27	-5.33	-0.51	5.87	3.81E-41
4	g14	PENFLURIDOL	2.31	-4.79	-0.72	5.78	2.39E-40
2	k09	DIGOXIN	-0.01	-5.53	1.11	5.84	5.77E-40
2	p07	THIORIDAZINE HYDROCHLORIDE	1.70	-4.78	0.56	5.35	2.29E-38

3	m20	PERPHENAZINE	1.98	-4.39	-1.75	5.40	2.43E-38
3	o13	PERHEXILINE MALEATE	1.58	-4.98	-0.51	5.50	3.06E-38
4	g18	VINCRISTINE SULFATE	3.80	-3.29	1.27	5.65	2.79E-37
1	c11	METHOTREXATE(+/-)	-2.14	3.99	-3.02	5.29	7.33E-37
2	f10	ALBENDAZOLE	4.29	-2.15	1.21	5.15	5.98E-36
3	f11	FLUVASTATIN	0.72	-4.99	0.72	5.38	2.29E-34
1	a15	MEDRYSONE	-0.80	-1.55	-4.30	5.01	7.47E-34
4	j05	PEMETREXED	-1.06	4.99	-1.11	5.07	1.13E-33
2	b14	TRIFLUOPERAZINE HYDROCHLORIDE	0.56	-4.76	0.06	5.11	2.00E-32
4	c18	CEFOXITIN SODIUM	2.78	-4.21	0.10	5.42	4.05E-32
2	j04	OUABAIN	-0.11	-5.10	1.16	5.41	4.90E-32
5	d11	NIMUSTINE	-0.35	5.11	0.20	5.12	4.15E-31
1	a08	FLUBENDAZOLE	2.07	-2.44	-3.07	5.09	8.96E-31
1	c03	METAPROTERENOL	4.01	-0.83	-1.01	4.86	1.44E-30
3	a11	SPIPERONE	3.28	-2.89	0.15	4.85	8.91E-30
3	g04	OXIBENDAZOLE	2.70	-3.46	-0.05	4.78	1.66E-29
4	e21	IVERMECTIN	-1.39	-4.27	-1.90	4.81	5.12E-29
1	d11	ATORVASTATIN CALCIUM	1.51	-4.48	1.28	5.24	6.86E-29
1	g03	VINBLASTINE SULFATE	1.45	-4.20	1.22	4.95	1.75E-28
1	m17	LASALOCID SODIUM	3.63	-2.41	-0.41	5.01	7.39E-28
1	a16	SULFADIMETHOXINE	-0.03	-1.38	-4.07	4.75	1.45E-26
1	p09	SPARTEINE SULFATE	-1.83	0.48	-4.00	4.54	2.39E-26
4	d03	TOREMIPHENE CITRATE	0.69	-4.04	1.37	4.53	2.96E-26
4	g22	DESLORATIDINE	1.10	-3.92	1.21	4.49	9.91E-26
2	k07	DIGITOXIN	0.07	-4.32	0.90	4.60	2.76E-25
3	p06	EPIRUBICIN HYDROCHLORIDE	-2.32	-3.03	-5.47	6.24	4.76E-24
4	j07	ESTRAMUSTINE	2.46	-2.97	0.21	4.27	2.48E-23
4	b14	OXALIPLATIN	-1.55	4.17	0.11	4.25	7.68E-23
4	o22	CHLOROACETOXYQUINOLINE	2.79	2.07	-1.64	4.23	5.65E-21
1	j14	BECLOMETHASONE DIPROPIONATE	3.53	0.39	-0.03	4.09	8.94E-21
3	a21	ISOTRETINON	3.74	-0.71	-0.35	4.37	2.74E-20
4	g07	TRETINOIN	2.95	-1.88	0.99	4.16	1.15E-19
1	b05	BETAMETHASONE VALERATE	3.04	-1.17	-0.49	3.99	2.08E-19
1	d19	LOVASTATIN	0.81	-3.36	1.37	3.98	2.52E-19
4	e10	IDOXURIDINE	3.06	-1.37	1.50	4.22	7.84E-19
4	o03	AZACITIDINE	2.52	-2.63	-0.77	4.20	2.22E-18
4	m07	THIOSTREPTON	1.98	2.92	-1.50	4.13	3.51E-18
2	g21	DEFEROXAMINE MESYLATE	-0.35	3.92	-1.04	3.94	3.49E-17
5	p04	BENZYL ISOTHIOCYANATE	3.57	-1.72	0.28	4.54	3.83E-17
5	j04	DISULFIRAM	3.20	2.40	-0.53	4.39	1.07E-16
1	e10	FLUMETHASONE	3.25	0.50	-0.46	3.88	1.12E-16
1	p15	ENILCONAZOLE SULFATE	-1.79	-0.02	-3.16	3.73	1.81E-15
5	h07	AMINOPTERIN	-1.42	3.61	-1.47	4.03	2.14E-15
5	j22	LANATOSIDE C	-0.33	-3.47	1.05	3.63	2.35E-15
3	m04	PACLITAXEL	0.55	-3.36	-0.38	3.70	2.86E-15

1	c08	SULOCTIDIL	2.29	-1.74	-1.01	3.74	7.09E-15
1	b07	ERYTHROMYCIN	2.92	-0.75	-0.67	3.73	6.20E-14
1	a17	MEGESTROL ACETATE	-1.36	-0.20	-2.88	3.49	8.55E-14
1	p10	CHLORAMPHENICOL SODIUM SUCCINATE	-1.62	-0.01	-3.24	3.77	1.08E-13
1	a10	ZOLMITRIPTAN	-1.44	0.01	-2.96	3.57	1.25E-13
4	h13	CANDESARTAN CILEXTIL	2.30	-1.47	0.79	3.37	1.69E-13
3	g07	MENADIONE	2.50	1.23	0.72	3.57	8.00E-13
1	a14	DOCETAXEL	1.31	-0.53	-2.38	3.40	1.25E-12
5	a03	METITEPINE MALEATE	-0.90	-3.00	1.34	3.36	1.26E-12
4	c05	ITRACONAZOLE	0.20	-2.68	1.75	3.38	1.48E-12
1	i22	ALGESTONE ACETOPHENIDE	3.29	-0.20	0.76	3.89	1.50E-12
3	m08	CLOBETASOL PROPIONATE	1.66	-2.08	-0.95	3.26	1.97E-12
2	d11	PRAZOSIN HYDROCHLORIDE	2.92	1.50	0.00	3.33	2.42E-12
5	i19	NIFUROXAZIDE	-1.56	3.06	-0.69	3.33	2.80E-12
1	p16	CHLORHEXIDINE DIHYDROCHLORIDE	-1.72	-1.88	-1.93	3.33	2.98E-12
3	o10	PAROXETINE HYDROCHLORIDE	-0.67	-3.47	0.05	3.54	9.34E-12
3	l09	SERTRALINE HYDROCHLORIDE	-0.07	-3.02	1.16	3.46	1.25E-11
5	a17	PENTAMIDINE ISETHIONATE	-2.51	2.35	-0.43	3.17	1.27E-11
1	e08	FLUNISOLIDE	2.82	0.73	-0.03	3.44	1.74E-11
1	i19	OXYPHENBUTAZONE	4.95	0.97	-1.06	5.75	3.45E-11
2	d10	TRYPTOPHAN	1.89	-2.15	0.32	3.16	1.00E-10
1	p06	CHLORAMBUCIL	-1.83	3.42	-0.33	3.57	4.22E-10
1	p11	TESTOSTERONE PROPIONATE	-1.62	-0.34	-2.85	3.44	5.62E-10
2	p05	THIOGUANINE	1.38	-2.94	-0.19	3.60	6.03E-10
5	i07	DEQUALINIUM CHLORIDE	1.86	-1.85	0.24	2.96	6.52E-10
4	g16	ACEBUTOLOL HYDROCHLORIDE	1.75	-1.68	0.52	2.95	8.50E-10
1	c21	METHYLPREDNISOLONE	2.42	0.01	-0.39	3.10	9.42E-10
1	p08	CHLORAMPHENICOL PALMITATE	-1.66	0.17	-2.75	3.30	1.05E-09
1	o12	HYDROCORTISONE VALERATE	2.11	-1.44	-0.10	3.34	1.41E-09
3	d11	CARVEDILOL	1.63	-1.58	0.75	2.92	1.57E-09
3	l18	THONZONIUM BROMIDE	-0.87	-2.98	1.00	3.33	3.50E-09
1	j13	HYDROCORTISONE	2.72	0.05	-0.11	3.29	5.73E-09
1	p17	BETAMETHASONE SODIUM PHOSPHATE	0.26	-0.23	-2.50	3.02	6.69E-09
2	l07	SULFACETAMIDE	-0.38	-2.21	0.19	2.91	7.28E-09
4	d17	MAPROTILINE HYDROCHLORIDE	0.37	-2.05	1.59	2.87	1.13E-08
2	d13	PREDNISOLONE	2.58	0.97	0.08	2.83	2.03E-08
5	n13	TOLONIUM CHLORIDE	-0.82	-2.24	-1.93	3.05	2.33E-08
2	b10	TRIAMTERENE	-0.92	2.72	-1.14	2.95	2.58E-08
3	l13	TELITHROMYCIN	1.06	-1.73	1.16	2.82	2.68E-08
4	h11	ADAPALENE	-0.29	4.97	0.06	4.96	3.35E-08
2	c12	FLUOROMETHOLONE	2.56	0.02	0.05	2.72	4.91E-08
5	p03	CEPHARANTHINE	0.80	-2.43	-0.08	2.84	5.34E-08
1	h07	CLARITHROMYCIN	2.42	-0.23	0.45	3.01	9.30E-08
4	e18	GRANISETRON HYDROCHLORIDE	1.90	-1.09	0.40	2.75	1.13E-07
2	c08	FLUOCINOLONE ACETONIDE	2.60	0.41	0.03	2.79	1.48E-07

3	o08	SIROLIMUS	1.83	-1.43	-0.41	2.87	1.87E-07
4	g13	DOXAZOSIN MESYLATE	0.46	-2.41	0.25	2.68	2.10E-07
4	n10	ABAMECTIN (avermectin B1a shown)	0.94	-1.25	-1.26	2.61	2.47E-07
3	g18	THIOTEPA	-0.55	2.78	0.27	2.93	2.59E-07
3	j15	ROSUVASTATIN CALCIUM	0.44	-1.77	1.24	2.60	3.22E-07
1	b09	CYPROHEPTADINE HYDROCHLORIDE	-0.96	-0.25	-1.85	2.66	4.53E-07
2	g13	DEMECLOCYCLINE HYDROCHLORIDE	2.47	-1.57	0.59	3.28	6.13E-07
1	b15	TOLNAFTATE	0.13	-0.48	-1.93	2.60	6.78E-07
2	h20	MYCOPHENOLIC ACID	-1.44	2.42	-1.28	2.92	8.35E-07
2	o09	EPINEPHRINE BITARTRATE	-1.02	-0.83	-2.23	2.72	1.06E-06
1	a18	SULFAMONOMETHOXINE	-1.61	-0.46	-1.73	2.51	1.11E-06
4	e07	RISEDRONATE SODIUM	2.01	-0.08	0.40	2.63	1.14E-06
5	c13	BROXALDINE	1.25	1.89	-1.24	2.85	1.15E-06
2	m22	PROGESTERONE	-0.40	-2.70	0.32	2.95	1.26E-06
5	j15	ALEXIDINE HYDROCHLORIDE	2.02	-1.33	0.77	2.91	2.14E-06
1	a07	DESVENLAFAXINE SUCCINATE	-1.62	-0.61	-1.53	2.51	2.55E-06
4	o11	CANDICIDIN	1.80	-2.01	-0.64	3.31	2.59E-06
5	m11	HOMIDIUM BROMIDE	-2.39	0.74	-1.15	2.49	2.84E-06
1	a06	GANCICLOVIR	-1.87	-0.13	-1.74	2.72	3.48E-06
4	i11	RIBAVIRIN	1.87	-0.51	0.22	2.51	3.99E-06
3	d18	PREDNISOLONE HEMISUCCINATE	2.02	0.31	0.26	2.65	4.17E-06
1	b08	MEQUINOL	-1.23	1.08	-1.97	2.59	5.00E-06
1	l06	BETAMETHASONE	1.80	-0.71	-0.59	2.72	5.60E-06
2	p09	THIOTHIXENE	-0.74	-2.04	-0.18	2.37	8.18E-06
3	c22	HYDROCORTISONE BUTYRATE	1.84	0.88	-0.09	2.54	8.89E-06
5	j10	BROXYQUINOLINE	1.90	-0.47	-0.22	2.41	9.83E-06
1	b10	alpha-TOCHOPHEROL	-0.88	-0.14	-2.49	2.92	1.28E-05
2	h09	PYRIMETHAMINE	-0.70	2.50	-1.16	2.71	1.74E-05
4	d10	GRISEOFULVIN	1.61	-0.66	0.66	2.44	1.89E-05
1	o11	PROGLUMIDE	-0.86	-1.18	-1.33	2.30	1.95E-05
3	l10	OXFENDAZOLE	0.93	-1.72	0.01	2.35	2.32E-05
2	n17	TETRACYCLINE HYDROCHLORIDE	1.87	-0.77	-0.11	2.27	3.27E-05
1	c22	FLURANDRENOLIDE	1.61	-0.05	-0.32	2.28	3.38E-05
1	a13	MECLOFENAMATE SODIUM	-1.46	-0.39	-1.58	2.34	4.17E-05
5	o06	QUININE ETHYL CARBONATE	-1.01	-1.56	-1.22	2.25	4.32E-05
3	k18	AMCINONIDE	1.63	-1.00	-0.44	2.44	4.35E-05
1	d13	OXYPHENCYCLIMINE HYDROCHLORIDE	1.47	0.83	-0.26	2.25	4.71E-05
4	m13	MYCOPHENOLATE MOFETIL	-1.68	1.81	-1.48	2.52	4.90E-05
2	k11	DIHYDROERGOTAMINE MESYLATE	1.26	-1.46	-0.40	2.51	4.99E-05
1	p14	CHLORCYCLIZINE HYDROCHLORIDE	-1.43	-0.51	-1.93	2.60	5.15E-05
3	c12	METHYLPHENIDATE HYDROCHLORIDE	1.56	0.20	0.49	2.29	5.68E-05
1	b11	LIOTHYRONINE	-0.98	0.48	-2.12	2.52	6.28E-05
2	l09	SULFADIAZINE	-0.57	-1.73	-1.41	2.51	6.28E-05
4	i06	FLUTICASONE PROPIONATE	1.75	-0.34	0.47	2.48	6.28E-05
5	h18	CAPTAMINE	1.69	-0.88	0.21	2.36	6.30E-05

5	j17	GALLIC ACID	0.28	2.09	0.19	2.22	7.50E-05
1	g08	TEPOXALIN	0.99	1.62	-0.65	2.31	8.08E-05
4	f17	HYDROXYPROGESTERONE CAPROATE	1.47	-0.85	0.84	2.41	8.34E-05
2	o21	ESTRADIOL CYPIONATE	2.30	-1.66	-0.80	3.23	8.93E-05

7.13 TBX3 HC StratoMineR ranked 'Hits'

Ranked 'Hits': TBX3 4h

Plate	Well	Pharmakon Compound	Factor 1	Factor 2	Factor 3	Distance Score	p-value
3	p06	EPIRUBICIN HYDROCHLORIDE	-9.58	-11.40	-12.16	19.26	3.71E-250
3	h06	DOXORUBICIN	-4.52	-8.78	-8.83	13.26	2.47E-121
5	p17	CLOFOCTOL	-5.89	-5.94	-6.34	10.19	1.32E-67
2	g09	DAUNORUBICIN	-1.31	-9.15	-9.47	13.31	2.56E-60
5	e15	CETRIMONIUM BROMIDE	-5.05	-5.97	-6.11	9.52	1.10E-47
3	i14	BENZALKONIUM CHLORIDE	-5.45	-3.70	-3.96	7.72	1.35E-28
4	o11	CANDICIDIN	-3.88	-5.03	-5.24	8.07	3.49E-28
3	k04	TERFENADINE	-6.58	2.61	2.17	7.43	1.35E-26
1	a09	ANTIMONY POTASSIUM TARTRATE TRIHYDRATE	-1.54	-4.01	-3.98	6.14	1.83E-19
5	d16	PROFLAVINE HEMISULFATE	-0.16	-4.32	-4.73	6.01	8.31E-19
2	e14	GRAMICIDIN (gramicidin A shown)	-4.16	-2.30	-2.70	5.71	2.83E-17
3	e06	MITOXANTRONE HYDROCHLORIDE	-3.62	-2.84	-2.94	5.49	5.96E-15
1	a10	ZOLMITRIPTAN	-1.58	-3.16	-3.19	5.03	1.31E-13
5	o14	BRONOPOL	-3.39	-3.03	-3.48	5.34	1.60E-13
4	h08	THIMEROSAL	-4.53	0.78	0.45	5.45	1.97E-13
1	a08	FLUBENDAZOLE	-2.33	-2.79	-2.95	4.94	3.39E-13
1	a11	SANGUINARIUM CHLORIDE	-4.15	-1.24	-1.64	4.78	3.16E-12
5	c13	BROXALDINE	0.91	-3.59	-3.40	4.72	4.14E-12
1	a16	SULFADIMETHOXINE	-1.66	-3.08	-3.16	4.98	7.22E-12
1	l14	BROMOCRIPTINE MESYLATE	5.27	-1.14	-1.21	5.65	2.37E-11
3	j18	RALOXIFENE HYDROCHLORIDE	4.28	-0.27	-0.44	4.31	3.10E-10
1	p04	CETYLPYRIDINIUM CHLORIDE	-3.73	-3.01	-3.41	6.11	5.26E-10
1	p11	TESTOSTERONE PROPIONATE	-2.40	-2.37	-2.36	4.36	3.37E-09
1	p09	SPARTEINE SULFATE	-2.73	-1.93	-1.96	4.11	2.95E-08
2	a16	ETHIONAMIDE	-1.64	-2.90	-2.97	4.61	6.69E-08
1	b16	MITOMYCIN	-0.86	-2.33	-2.41	3.78	1.48E-07
1	p10	CHLORAMPHENICOL SODIUM SUCCINATE	-2.38	-1.84	-1.88	3.78	2.54E-07
1	p08	CHLORAMPHENICOL PALMITATE	-2.36	-1.87	-1.86	3.76	4.02E-07
1	a21	DACTINOMYCIN	-3.13	-1.15	-1.23	3.70	4.63E-07
1	p14	CHLORCYCLIZINE HYDROCHLORIDE	-2.23	-2.13	-2.18	4.08	5.26E-07
1	a15	MEDRYSONE	-1.24	-2.18	-2.31	3.72	1.10E-06
1	p16	CHLORHEXIDINE DIHYDROCHLORIDE	-2.23	-2.09	-2.04	3.91	1.16E-06
2	h13	QUINACRINE HYDROCHLORIDE	-1.68	2.53	2.57	4.04	1.48E-06
1	a18	SULFAMONOMETHOXINE	-1.15	-2.10	-2.09	3.46	3.60E-06
1	b10	alpha-TOCHOPHEROL	-0.71	-2.08	-2.13	3.37	6.11E-06
1	a14	DOCETAXEL	-1.48	-2.22	-2.31	3.80	6.22E-06

1	c08	SULOCTIDIL	-3.41	-0.01	-0.35	3.46	9.18E-06
1	o10	NIKETHAMIDE	-1.64	-2.13	-2.20	3.75	9.80E-06
1	a17	MEGESTROL ACETATE	-1.79	-2.15	-2.20	3.81	1.12E-05
1	a13	MECLOFENAMATE SODIUM	-1.10	-2.13	-2.14	3.49	1.63E-05
1	o16	CROTAMITON	-1.16	-1.96	-2.05	3.33	2.14E-05
1	a12	SULFACHLORPYRIDAZINE	-1.17	-2.03	-2.03	3.37	2.85E-05
1	b11	LIOTHYRONINE	-0.83	-2.15	-2.18	3.51	3.12E-05
4	f08	PYRITHIONE ZINC	-2.70	1.84	1.44	3.74	4.27E-05
5	p04	BENZYL ISOTHIOCYANATE	-3.13	1.34	1.01	3.69	6.55E-05
1	a07	DESVENLAFAXINE SUCCINATE	-1.88	-1.72	-1.75	3.34	6.70E-05
1	b14	PANTOTHENIC ACID(d) Na salt	-0.66	-1.93	-1.88	3.08	8.06E-05
1	m17	LASALOCID SODIUM	-2.38	-1.09	-1.40	3.18	1.41E-04
1	b09	CYPROHEPTADINE HYDROCHLORIDE	-1.40	-1.63	-1.69	2.98	1.77E-04
2	e10	GENTIAN VIOLET	-2.93	1.09	0.93	3.53	2.37E-04
4	g14	PENFLURIDOL	-3.23	-0.18	-0.50	3.15	2.56E-04
1	p12	CHLORAMPHENICOL	-2.00	-1.66	-1.73	3.39	3.01E-04
2	a11	CHLORPROPAMIDE	-0.41	-2.40	-2.40	3.54	3.30E-04
5	o05	ESCIN	-3.36	-1.22	-1.61	4.06	3.40E-04
2	a14	ETHINYL ESTRADIOL	-1.07	-1.98	-2.03	3.18	8.42E-04
5	a04	ACRIFLAVINIUM HYDROCHLORIDE	0.15	-3.78	-4.09	5.19	1.04E-03
1	o15	ATENOLOL	-1.04	-1.61	-1.63	2.79	1.27E-03
1	p17	BETAMETHASONE SODIUM PHOSPHATE	-2.08	-1.36	-1.37	3.04	1.38E-03
4	n08	MERBROMIN	-2.46	-1.15	-1.31	2.83	1.63E-03
1	h12	BENZETHONIUM CHLORIDE	-1.93	-0.94	-1.26	2.70	2.04E-03
3	l09	SERTRALINE HYDROCHLORIDE	-1.64	1.64	1.40	2.71	2.15E-03
5	h12	NIFENAZONE	0.05	1.52	1.55	2.64	2.18E-03
2	m17	DOXYCYCLINE HYDROCHLORIDE	2.78	-0.31	-0.61	2.71	2.78E-03
2	o07	EMETINE DIHYDROCHLORIDE	-2.02	-0.41	-0.55	2.63	2.89E-03
3	a13	ERYTHROMYCIN ESTOLATE	3.10	-0.17	-0.30	3.10	2.99E-03
5	n13	TOLONIUM CHLORIDE	-0.82	-2.16	-2.17	2.74	3.07E-03
1	a19	MELPHALAN	-0.25	-1.64	-1.65	2.64	3.59E-03
3	o04	TACROLIMUS	-1.65	-1.59	-1.57	2.84	3.98E-03
1	p15	ENILCONAZOLE SULFATE	-1.88	-0.99	-0.99	2.52	4.31E-03
3	g04	OXIBENDAZOLE	-0.72	1.84	1.55	2.52	4.34E-03
2	a09	CHLORPROMAZINE	-0.95	-2.75	-2.89	4.20	4.63E-03
1	p13	PYRIDOSTIGMINE BROMIDE	-2.09	-1.23	-1.25	2.93	4.78E-03

Ranked 'Hits': TBX3 12h

Plate	Well	Pharmakon Compound	Factor 1	Factor 2	Factor 3	Distance Score	p-value
3	p06	EPIRUBICIN HYDROCHLORIDE	-6.35	-11.59	-10.81	17.00	0.00E+00
4	n20	OXYQUINOLINE SULFATE	-3.00	13.20	-2.78	14.18	0.00E+00
2	m17	DOXYCYCLINE HYDROCHLORIDE	-0.57	11.96	0.53	12.17	5.43E-272
5	a04	ACRIFLAVINIUM HYDROCHLORIDE	0.38	12.49	-3.35	13.16	1.35E-226
5	p04	BENZYL ISOTHIOCYANATE	-1.39	15.11	0.16	15.39	8.81E-224
4	g12	MECLOCYCLINE SULFOSALICYLATE	-0.97	10.75	0.55	11.23	2.48E-219
4	o22	CHLOROACETOXYQUINOLINE	-3.37	10.83	-3.43	12.19	1.94E-218

2	g09	DAUNORUBICIN	-2.25	-3.44	-11.18	12.07	8.12E-199
4	j12	THIRAM	-4.73	8.98	-0.99	10.53	8.00E-190
4	o12	METHACYCLINE HYDROCHLORIDE	-1.98	9.44	0.18	10.06	1.41E-182
2	h11	PYRVINIUM PAMOATE	0.12	10.22	-0.49	10.44	7.26E-181
3	h06	DOXORUBICIN	-3.08	-3.20	-9.64	10.59	5.87E-177
1	a09	ANTIMONY POTASSIUM TARTRATE TRIHYDRATE	-2.56	8.58	-3.66	9.86	1.27E-171
3	a13	ERYTHROMYCIN ESTOLATE	0.54	9.35	0.09	9.68	3.70E-154
4	m07	THIOSTREPTON	-0.19	8.82	0.01	9.25	1.51E-132
3	e06	MITOXANTRONE HYDROCHLORIDE	-4.34	-5.98	-4.86	8.78	6.23E-128
4	g14	PENFLURIDOL	-5.80	-6.41	-3.27	8.85	1.88E-121
5	c13	BROXALDINE	-4.01	-7.16	-5.98	10.10	1.22E-112
5	p17	CLOFOCTOL	-4.23	-6.53	-3.39	8.44	2.85E-104
1	l14	BROMOCRIPTINE MESYLATE	-0.29	7.59	-0.17	7.75	2.36E-103
1	a21	DACTINOMYCIN	-2.71	-6.57	-1.99	7.31	3.34E-86
4	n08	MERBROMIN	-3.37	5.92	-0.22	7.18	5.48E-81
3	k04	TERFENADINE	-4.95	-6.18	-0.80	7.83	2.58E-78
4	o09	PROSCILLARIDIN	-4.33	-4.93	-2.98	6.84	9.40E-77
2	k09	DIGOXIN	-2.98	-5.68	-2.17	6.70	7.60E-75
4	k20	POTASSIUM p-AMINOBENZOATE	-4.21	-5.03	-3.42	7.00	1.01E-72
1	i19	OXYPHENBUTAZONE	-0.83	7.17	-0.78	7.42	1.04E-68
1	a11	SANGUINARIUM CHLORIDE	-1.99	-6.19	-0.63	6.46	4.67E-65
3	h21	AMLODIPINE BESYLATE	0.89	6.42	-0.60	6.80	5.20E-63
1	n09	TOPOTECAN HYDROCHLORIDE	2.47	5.00	-2.48	6.21	2.98E-62
2	j04	OUABAIN	-2.83	-5.31	-1.84	6.22	1.83E-59
4	o03	AZACITIDINE	-0.38	5.39	-1.57	6.00	2.04E-55
3	g13	ASTEMIZOLE	-1.34	5.18	-0.30	5.68	3.67E-52
5	d06	HEXETIDINE	-0.38	6.37	0.06	6.66	1.81E-48
1	f05	TENIPOSIDE	0.72	5.71	-0.30	5.89	4.10E-46
2	e10	GENTIAN VIOLET	-3.95	-4.69	0.70	6.00	1.63E-45
2	o07	EMETINE DIHYDROCHLORIDE	-2.23	-5.30	-1.05	5.70	2.09E-45
5	o05	ESCIN	-3.35	-5.16	-3.44	7.00	1.37E-42
4	o21	PUROMYCIN DIHYDROCHLORIDE	-4.53	0.59	-2.31	5.09	7.94E-40
2	k07	DIGITOXIN	-2.61	-4.23	-1.43	5.06	6.97E-38
4	f08	PYRITHIONE ZINC	-5.06	-0.84	-0.94	5.23	4.86E-36
1	p04	CETYLPYRIDINIUM CHLORIDE	-2.27	-3.86	-3.04	5.43	8.69E-36
4	g18	VINCRISTINE SULFATE	-2.73	3.55	-0.59	4.81	1.04E-34
4	h08	THIMEROSAL	-4.00	-3.69	-0.90	5.17	1.29E-34
5	j22	LANATOSIDE C	-2.86	-4.39	-2.33	5.70	3.58E-34
2	e14	GRAMICIDIN (gramicidin A shown)	-2.11	4.01	1.27	4.82	4.45E-34
5	m11	HOMIDIUM BROMIDE	-0.72	-4.39	-2.30	4.87	4.32E-31
4	e21	IVERMECTIN	-0.62	4.09	-0.84	4.71	1.01E-28
5	i10	ANCITABINE HYDROCHLORIDE	-0.01	-2.84	-3.60	4.48	2.09E-26
5	e15	CETRIMONIUM BROMIDE	-3.32	-4.09	-3.26	6.26	5.22E-25
5	d16	PROFLAVINE HEMISULFATE	-1.50	4.57	-1.16	5.17	5.22E-22
2	c19	COLCHICINE	-0.84	3.75	-1.01	4.22	6.57E-22
2	a09	CHLORPROMAZINE	-0.44	-1.94	-3.75	4.39	1.58E-21
2	h13	QUINACRINE HYDROCHLORIDE	-0.71	-3.73	1.47	3.81	3.54E-21

4	n10	ABAMECTIN (avermectin B1a shown)	0.22	5.21	-0.39	5.68	6.48E-21
1	p16	CHLORHEXIDINE DIHYDROCHLORIDE	-1.64	-2.99	-1.97	3.93	6.96E-21
4	j04	CYCLOHEXIMIDE	-2.77	-3.61	0.06	4.29	1.64E-20
2	a10	ETHACRYNIC ACID	-0.55	-2.17	-4.18	4.85	3.87E-19
4	h13	CANDESARTAN CILEXTIL	-0.23	2.91	1.26	3.64	2.29E-18
5	o14	BRONOPOL	-3.18	-0.05	-2.50	4.16	2.53E-18
2	p09	THIOTHIXENE	-1.11	-2.21	-2.54	3.65	1.32E-17
3	i14	BENZALKONIUM CHLORIDE	-3.35	-3.55	-0.06	4.77	2.20E-17
5	j04	DISULFIRAM	-0.52	4.12	-1.68	4.69	1.45E-16
1	a16	SULFADIMETHOXINE	-1.08	-3.07	-1.73	3.66	1.82E-16
4	e10	IDOXURIDINE	-1.12	0.91	-2.12	4.53	2.27E-16
3	g07	MENADIONE	0.78	2.77	-1.37	3.59	1.33E-15
5	c03	ETHACRIDINE LACTATE	0.11	-3.57	-1.26	3.62	1.38E-15
3	m08	CLOBETASOL PROPIONATE	-0.52	3.16	-0.35	3.53	2.72E-15
4	o11	CANDICIDIN	-3.32	-0.50	-4.00	5.26	3.09E-15
1	k06	AUROTHIOGLUCOSE	-0.74	3.43	0.06	3.69	7.27E-15
1	n21	PODOFILOX	-0.76	3.07	0.01	3.34	2.45E-14
3	b09	TRIFLURIDINE	0.77	-1.80	-2.75	3.32	2.60E-14
1	a10	ZOLMITRIPTAN	-0.59	-2.57	-2.20	3.40	2.75E-14
3	a04	HYCANTHONE	-1.03	-3.18	0.05	3.17	1.01E-13
3	o04	TACROLIMUS	-1.32	-3.42	-0.63	3.56	3.65E-13
5	e07	NITROXOLINE	1.11	2.90	-0.54	3.32	4.44E-13
1	i08	MOXIDECTIN	0.90	3.01	0.05	3.25	4.74E-13
4	f04	CICLOPIROX OLAMINE	0.24	-1.46	-3.06	3.12	4.79E-13
3	l13	TELITHROMYCIN	-1.32	2.65	0.68	3.30	6.51E-13
3	o13	PERHEXILINE MALEATE	-1.40	2.24	-1.13	3.24	1.52E-12
2	a16	ETHIONAMIDE	-0.68	-2.20	-2.73	3.65	3.62E-12
2	p10	FLUTAMIDE	-1.80	-0.43	-2.68	3.45	8.32E-12
2	p15	TOLAZOLINE HYDROCHLORIDE	-1.42	-1.53	-2.27	3.20	1.07E-11
4	g07	TRETINOIN	-0.02	2.83	-0.02	3.27	5.74E-11
1	p11	TESTOSTERONE PROPIONATE	-1.88	-1.49	-2.20	3.31	7.83E-11
2	a15	CHLORTHALIDONE	-0.76	-1.84	-2.81	3.52	1.98E-10
2	p08	FLUPHENAZINE HYDROCHLORIDE	-0.47	-0.46	-2.62	2.96	8.37E-10
3	l10	OXFENDAZOLE	-2.16	1.44	0.81	3.01	1.13E-09
2	g13	DEMECLOCYCLINE HYDROCHLORIDE	0.76	2.30	0.80	2.81	1.36E-09
3	o08	SIROLIMUS	1.59	1.89	-0.48	2.81	3.80E-09
2	e21	CYTARABINE	0.32	-2.28	-2.68	3.62	1.02E-08
5	n09	METERGOLINE	-0.63	3.17	1.77	3.99	1.49E-08
2	p16	ETODOLAC	-1.65	-0.97	-1.67	2.61	1.67E-08
4	f17	HYDROXYPROGESTERONE CAPROATE	1.04	1.64	0.88	2.58	2.50E-08
2	p11	TIMOLOL MALEATE	-2.12	-0.40	-1.52	2.75	2.85E-08
1	a14	DOCETAXEL	-1.05	-2.29	-1.00	2.68	3.12E-08
1	p09	SPARTEINE SULFATE	-1.32	-0.99	-1.89	2.61	5.79E-08
4	g10	RAMOPLANIN [A2 shown; 2mM]	1.05	2.28	0.00	2.93	6.99E-08
2	p17	TOLBUTAMIDE	-1.62	-0.98	-1.86	2.85	8.27E-08
3	c14	NICLOSAMIDE	0.44	-2.80	-0.55	2.66	8.69E-08

1	p12	CHLORAMPHENICOL	-1.26	-1.32	-1.69	2.51	9.09E-08
1	p15	ENILCONAZOLE SULFATE	-1.20	-1.23	-2.27	2.91	1.00E-07
1	a05	ETOPOSIDE	-0.53	-2.67	-0.79	2.79	1.38E-07
1	o12	HYDROCORTISONE VALERATE	-0.99	2.14	-0.96	2.77	2.32E-07
3	j19	PREDNICARBATE	0.45	2.17	0.20	2.55	2.61E-07
1	p10	CHLORAMPHENICOL SODIUM SUCCINATE	-1.33	-0.91	-2.18	2.86	5.11E-07
1	p17	BETAMETHASONE SODIUM PHOSPHATE	-1.34	0.15	-1.92	2.48	6.54E-07
1	a12	SULFACHLORPYRIDAZINE	-0.08	-2.14	-1.29	2.44	7.00E-07
2	d11	PRAZOSIN HYDROCHLORIDE	0.32	1.08	-1.73	2.38	8.72E-07
3	a12	PIROCTONE OLAMINE	0.13	-1.09	-2.53	2.69	1.01E-06
1	p13	PYRIDOSTIGMINE BROMIDE	-1.16	-1.36	-1.65	2.47	1.13E-06
1	p08	CHLORAMPHENICOL PALMITATE	-1.68	-0.97	-1.71	2.84	1.14E-06
4	g22	DESLORATIDINE	0.54	2.00	-0.17	2.53	1.34E-06
5	n13	TOLONIUM CHLORIDE	-1.13	-1.87	-1.42	2.54	1.71E-06
1	b05	BETAMETHASONE VALERATE	0.85	2.27	-0.32	2.56	1.80E-06
2	p12	DROPERIDOL	-2.04	-0.25	-0.99	2.35	1.96E-06
4	d03	TOREMIPHENE CITRATE	1.19	1.81	-0.61	2.68	3.13E-06
1	a08	FLUBENDAZOLE	-1.20	-2.00	-1.63	2.88	3.22E-06
2	f10	ALBENDAZOLE	-0.82	1.96	0.25	2.30	3.86E-06
3	k18	AMCINONIDE	0.54	2.26	0.02	2.68	4.09E-06
5	o07	DEFERIPRONE	-1.64	0.34	-0.41	2.30	4.15E-06
1	m17	LASALOCID SODIUM	-0.64	-1.37	-1.83	2.38	4.26E-06
1	o09	PROPIOLACTONE	-1.43	-0.55	-1.57	2.31	4.42E-06
2	a11	CHLORPROPAMIDE	-0.25	-1.37	-3.09	3.58	5.65E-06
2	a13	CHLORTETRACYCLINE HYDROCHLORIDE	-0.22	0.35	-2.29	2.70	5.85E-06
2	a06	ESTRIOL	-0.36	-2.36	-1.95	3.09	7.06E-06
3	d10	METHYLENE BLUE	0.68	-1.85	-1.76	2.51	8.96E-06
2	a08	ESTRONE	-0.27	-1.90	-2.72	3.41	9.32E-06
2	a17	CHLORZOXAZONE	-0.81	-1.93	-2.76	3.54	9.56E-06
1	l06	BETAMETHASONE	-0.85	1.71	-0.15	2.23	1.21E-05
3	g04	OXIBENDAZOLE	-1.57	1.88	-0.24	2.74	1.37E-05
5	p10	DIXANTHOGEN	-0.76	-0.89	-1.78	2.18	1.52E-05
1	b16	MITOMYCIN	0.69	0.57	-2.31	2.57	1.54E-05
4	d14	VERAPAMIL HYDROCHLORIDE	1.30	1.22	-0.32	2.15	2.15E-05
2	e07	VARDENAFIL HYDROCHLORIDE	0.05	-2.49	0.19	2.31	2.15E-05
4	m16	OXYTETRACYCLINE	-0.06	1.57	-0.08	2.15	2.29E-05
3	d11	CARVEDILOL	1.85	1.12	-0.57	2.38	2.34E-05
2	o16	NITROMIDE	-1.51	-0.33	-1.25	2.25	2.44E-05
3	c04	AMSACRINE	0.72	1.44	-1.08	2.17	2.54E-05
4	k13	CEFORANIDE	-0.17	1.56	0.44	2.19	2.89E-05
2	p05	THIOGUANINE	-0.77	-0.01	-1.86	2.22	3.01E-05
3	k15	MEBEVERINE HYDROCHLORIDE	-0.62	1.74	1.01	2.35	3.12E-05
5	p09	HYDROXYPROGESTERONE	-1.18	-1.00	-1.40	2.14	3.21E-05
4	c18	CEFOXITIN SODIUM	-2.07	0.03	-0.14	2.14	3.43E-05
4	k08	SILDENAFIL CITRATE	0.76	1.63	0.08	2.32	3.66E-05

2	o14	NEOMYCIN SULFATE	-1.61	0.04	-0.92	2.16	3.99E-05
3	a11	SPIPERONE	-0.06	1.48	-1.04	2.11	4.14E-05
3	l07	APRAMYCIN SULFATE	-1.54	1.25	0.85	2.35	4.66E-05
2	p14	FAMOTIDINE	-1.66	-0.89	-1.44	2.47	5.12E-05
3	*l14*	TICLOPIDINE HYDROCHLORIDE	-1.66	0.74	0.58	2.40	5.51E-05
4	k19	AZATADINE MALEATE	0.08	1.80	0.05	2.31	6.03E-05
3	l15	OXAPROZIN	-1.50	1.25	1.12	2.52	6.40E-05
4	f16	CYACETACIDE	0.63	0.97	1.14	2.10	6.45E-05
3	m20	PERPHENAZINE	0.66	1.56	-0.34	2.06	8.73E-05

Ranked 'Hits': TBX3 24h

Plate	Well	Pharmakon Compound	Factor 1	Factor 2	Factor 3	Distance Score	p-value
5	a04	ACRIFLAVINIUM HYDROCHLORIDE	7.73	-4.34	12.54	15.52	6.56E-160
4	m07	THIOSTREPTON	-1.91	-2.47	14.78	15.57	7.00E-143
2	m17	DOXYCYCLINE HYDROCHLORIDE	0.03	0.55	11.56	11.73	5.33E-82
4	g12	MECLOCYCLINE SULFOSALICYLATE	0.74	1.25	10.78	11.41	1.67E-80
3	p06	EPIRUBICIN HYDROCHLORIDE	-4.20	-7.09	-7.35	10.99	2.79E-72
1	f05	TENIPOSIDE	1.09	-1.87	9.92	10.42	9.65E-69
1	n09	TOPOTECAN HYDROCHLORIDE	6.15	-3.00	7.19	10.23	5.87E-67
4	o12	METHACYCLINE HYDROCHLORIDE	-0.51	-0.50	9.96	10.49	3.25E-63
4	j12	THIRAM	-3.92	-2.33	9.40	10.80	7.43E-57
2	g09	DAUNORUBICIN	-3.24	-8.70	-2.44	9.65	3.25E-54
4	n20	OXYQUINOLINE SULFATE	-2.26	-2.53	8.75	9.82	4.50E-53
1	a09	ANTIMONY POTASSIUM TARTRATE TRIHYDRATE	0.09	-5.86	6.37	9.01	1.28E-46
4	o09	PROSCILLARIDIN	-4.87	-2.85	-6.44	8.09	2.39E-40
3	h06	DOXORUBICIN	-1.78	-8.75	-2.09	8.98	6.52E-40
1	a21	DACTINOMYCIN	-3.62	-3.39	-5.94	7.72	1.35E-36
4	o03	AZACITIDINE	0.54	-0.28	7.04	7.60	8.73E-35
1	a11	SANGUINARIUM CHLORIDE	-1.85	-5.09	-5.29	7.65	9.32E-33
3	e06	MITOXANTRONE HYDROCHLORIDE	-3.73	-5.96	-4.64	8.25	1.57E-32
4	k20	POTASSIUM p-AMINOBENZOATE	-4.88	-2.48	-5.61	7.38	2.90E-29
3	a13	ERYTHROMYCIN ESTOLATE	1.30	-0.88	8.21	8.63	4.68E-28
5	p17	CLOFOCTOL	-2.79	-4.70	-5.11	7.31	2.24E-27
1	l14	BROMOCRIPTINE MESYLATE	-0.09	-0.35	6.74	6.98	4.25E-26
3	a06	NAPHAZOLINE HYDROCHLORIDE	-2.74	-5.56	-3.35	6.86	6.79E-26
4	o22	CHLOROACETOXYQUINOLINE	-2.39	-3.16	4.88	6.60	2.91E-24
1	k06	AUROTHIOGLUCOSE	-3.59	-2.55	5.19	7.05	1.06E-23
5	j22	LANATOSIDE C	-2.91	-2.88	-4.74	6.06	2.23E-21
4	e10	IDOXURIDINE	-0.53	0.42	5.88	6.41	2.51E-21
2	h11	PYRVINIUM PAMOATE	-0.77	-0.84	6.06	6.30	3.07E-20
2	k09	DIGOXIN	-3.66	-1.02	-5.22	6.40	5.80E-20
2	j04	OUABAIN	-3.62	-0.89	-4.61	5.83	2.24E-19
5	d16	PROFLAVINE HEMISULFATE	2.00	-1.59	4.99	5.76	4.07E-18
4	g18	VINCRISTINE SULFATE	-3.39	-1.35	3.70	5.44	4.21E-17
1	a16	SULFADIMETHOXINE	-0.77	-4.77	-1.78	5.36	7.37E-17

2	c19	COLCHICINE	-1.73	-2.23	4.49	5.43	7.50E-17
4	n08	MERBROMIN	-2.49	-0.64	5.50	6.44	1.58E-16
2	k07	DIGITOXIN	-3.59	-0.20	-4.54	5.59	7.25E-16
3	i14	BENZALKONIUM CHLORIDE	-3.24	-1.74	-4.67	5.79	8.51E-15
4	c18	CEFOXITIN SODIUM	-1.65	-1.00	4.59	5.39	2.17E-13
1	p04	CETYLPYRIDINIUM CHLORIDE	-2.08	-1.58	-4.11	4.93	3.05E-13
4	m13	MYCOPHENOLATE MOFETIL	-0.13	-3.16	-4.09	4.76	8.92E-13
1	a15	MEDRYSONE	-0.86	-4.29	-1.66	4.87	7.25E-12
3	k04	TERFENADINE	-3.31	-0.89	-4.41	5.76	2.05E-11
4	o21	PUROMYCIN DIHYDROCHLORIDE	-5.39	0.23	0.06	5.18	3.54E-11
3	a12	PIROCTONE OLAMINE	-1.45	-4.29	-2.86	5.12	4.22E-11
1	b16	MITOMYCIN	1.41	-4.02	0.29	4.58	5.17E-11
5	o05	ESCIN	-2.37	-1.87	-3.80	4.65	1.37E-10
1	a14	DOCETAXEL	0.01	-4.09	0.74	4.47	3.86E-10
2	o07	EMETINE DIHYDROCHLORIDE	-2.31	-0.33	-3.93	4.37	7.03E-10
1	a08	FLUBENDAZOLE	-0.53	-4.20	-1.42	4.66	1.72E-09
1	n21	PODOFILOX	-1.06	-2.04	3.42	4.49	2.41E-09
1	c11	METHOTREXATE(+/-)	1.34	-3.39	-1.49	4.12	4.11E-09
5	p04	BENZYL ISOTHIOCYANATE	-1.32	-1.85	3.48	4.24	6.65E-09
2	e10	GENTIAN VIOLET	-2.65	-2.26	-3.18	4.70	1.36E-08
2	e21	CYTARABINE	1.04	-4.19	-0.85	4.45	1.52E-08
5	i10	ANCITABINE HYDROCHLORIDE	1.09	-3.80	-0.87	3.96	2.52E-08
4	f08	PYRITHIONE ZINC	-4.31	0.72	-1.59	4.29	2.90E-08
5	e15	CETRIMONIUM BROMIDE	-2.54	0.40	-2.68	3.87	3.83E-08
4	g07	TRETINOIN	-0.70	0.52	3.60	4.20	3.96E-08
4	g14	PENFLURIDOL	-3.36	-1.00	-4.39	5.11	1.06E-07
4	h08	THIMEROSAL	-2.48	0.61	-3.46	3.79	1.60E-07
1	a05	ETOPOSIDE	0.02	-3.08	-1.85	3.77	1.76E-07
2	e14	GRAMICIDIN (gramicidin A shown)	1.79	0.19	3.26	4.01	2.72E-07
4	f04	CICLOPIROX OLAMINE	-0.60	-3.37	-2.90	4.10	5.05E-07
2	f10	ALBENDAZOLE	-1.64	0.01	3.05	3.67	7.18E-07
4	h11	ADAPALENE	-3.19	-3.89	-3.86	5.94	1.15E-06
3	b09	TRIFLURIDINE	1.95	-3.64	0.18	4.03	1.15E-06
4	j07	ESTRAMUSTINE	0.09	-0.70	2.94	3.53	1.62E-06
4	g16	ACEBUTOLOL HYDROCHLORIDE	0.05	0.05	2.95	3.51	3.03E-06
3	l13	TELITHROMYCIN	-1.17	0.76	2.86	3.49	3.67E-06
5	m11	HOMIDIUM BROMIDE	-0.43	-2.13	-2.91	3.46	5.59E-06
4	j05	PEMETREXED	2.15	-1.89	-1.86	3.34	1.31E-05
4	j04	CYCLOHEXIMIDE	-1.44	0.50	-3.74	3.50	1.38E-05
4	e07	RISEDRONATE SODIUM	0.89	0.80	2.48	3.33	2.21E-05
3	g13	ASTEMIZOLE	-2.76	-0.06	2.36	3.99	3.11E-05
1	m11	FENBENDAZOLE	-0.24	-3.60	-0.06	3.96	7.70E-05
3	m08	CLOBETASOL PROPIONATE	-0.93	-1.03	3.08	3.65	1.05E-04
1	c03	METAPROTERENOL	1.33	-1.23	2.39	3.32	1.32E-04
1	a19	MELPHALAN	-0.10	-2.07	-2.25	3.12	1.38E-04
2	h20	MYCOPHENOLIC ACID	-0.53	-2.37	-2.51	3.38	1.55E-04
5	a17	PENTAMIDINE ISETHIONATE	-0.80	-0.46	-3.21	3.22	1.71E-04

3	g04	OXIBENDAZOLE	-1.81	-1.37	2.15	3.31	1.87E-04
2	b10	TRIAMTERENE	1.58	-2.25	-1.05	3.06	3.16E-04
1	j14	BECLOMETHASONE DIPROPIONATE	1.44	-0.25	2.21	2.90	3.62E-04
5	i19	NIFUROXAZIDE	-0.95	-1.36	-2.78	3.06	3.74E-04
3	l10	OXFENDAZOLE	-0.67	-0.02	2.82	3.20	4.03E-04
1	h12	BENZETHONIUM CHLORIDE	1.70	-1.82	-0.88	2.85	5.32E-04
1	p09	SPARTEINE SULFATE	-0.94	-2.41	-1.03	2.96	5.36E-04
1	o03	MEBENDAZOLE	0.61	-1.74	1.50	2.87	5.53E-04
5	h07	AMINOPTERIN	0.96	-2.48	-1.26	2.83	6.48E-04
1	b05	BETAMETHASONE VALERATE	0.75	-0.72	2.12	2.79	8.56E-04
5	c13	BROXALDINE	-0.41	-2.58	-1.52	2.88	9.28E-04
4	k19	AZATADINE MALEATE	-0.02	-0.15	2.49	3.03	1.21E-03
1	m17	LASALOCID SODIUM	-0.04	-2.26	-1.67	2.93	1.43E-03
1	c19	PITAVASTATIN CALCIUM	-1.01	-2.22	0.83	2.90	1.73E-03
2	p08	FLUPHENAZINE HYDROCHLORIDE	0.43	-2.25	-1.41	2.68	2.17E-03
3	l14	TICLOPIDINE HYDROCHLORIDE	-1.50	0.64	1.72	2.63	2.55E-03
1	a10	ZOLMITRIPTAN	-0.02	-2.01	-1.31	2.58	3.23E-03
1	b08	MEQUINOL	0.30	-2.03	-1.41	2.63	3.33E-03
4	i06	FLUTICASONE PROPIONATE	0.54	-0.20	2.03	2.69	3.36E-03
1	l06	BETAMETHASONE	-0.20	0.05	2.45	2.67	3.65E-03
4	b14	OXALIPLATIN	0.09	-1.32	-3.01	2.83	3.76E-03
2	l20	BUDESONIDE	-0.72	-0.28	2.30	2.54	4.19E-03
1	p10	CHLORAMPHENICOL SODIUM SUCCINATE	-1.34	-1.89	-0.50	2.58	4.23E-03
4	e18	GRANISETRON HYDROCHLORIDE	-0.08	-0.46	2.08	2.64	4.99E-03

7.14 High throughput screen immunofluorescence images for doxorubicin treated cells

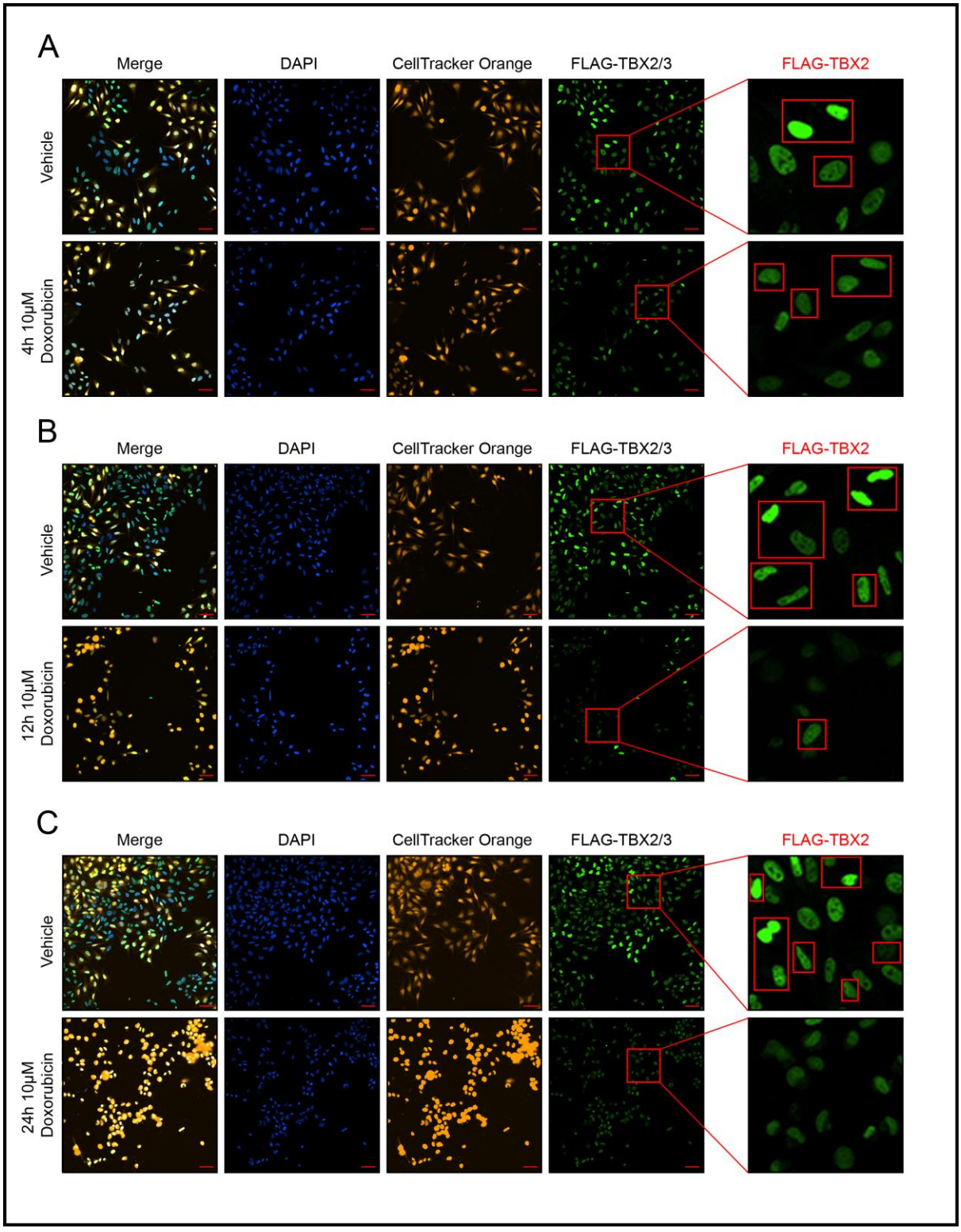

Supplementary Fig. 7.1 High throughput screen immunofluorescence images for doxorubicin treated cells. *Representative IN Cell Analyzer 6000 images of inducible TBX2-FLAG 501mel and inducible TBX3-FLAG 501mel co-cultured cells treated for 24h with 20ng/mL doxycycline followed by 10μM doxorubicin or vehicle for 4h (A), 12h (B) and 24h (C). The TBX2-FLAG population was pre-stained with CellTracker Orange and a FLAG antibody with an Alexa Fluor 488 conjugated secondary antibody was used to*

detect FLAG-tagged TBX2 and TBX3. Nuclei were stained with DAPI. The scale bar is 60µm. Close up images in the far right panel show TBX2-FLAG expressing cells in red outlined boxes (identified from CellTracker Orange staining) with unboxed cells expressing TBX3-FLAG except for the bottom right hand corner image (24h doxorubicin) where all cells express TBX2-FLAG.

7.15 Turnitin Originality Report

Turnitin Originality Report

blljen010:JENNA_PhD_Thesis_FINAL_1.pdf by Jenna Bleloch

From For TurnItIn Submission (99e58091-4ed3-452e-ae8f-f82d0b847550)

- Processed on 11-Feb-2019 04:30 SAST
- ID: 1075992382
- Word Count: 75705

Similarity Index
28%
Similarity by Source

Internet Sources:
21%
Publications:
22%
Student Papers:
3%

Approximately 16% match with Jenna Bleloch publications (highlighted in red boxes)

sources:

1 7% match (Internet from 31-Jan-2019)
https://www.nature.com/articles/s41420-019-0139-9?code=d956fb80-b46c-4f2c-8463-63fd2d1341d9&error=cookies_not_supported

2 6% match (publications)
Jenna Susan Bleloch, André du Toit, Liezl Gibhard, Serah Kimani et al. "The palladacycle complex AJ-5 induces apoptotic cell death while reducing autophagic flux in rhabdomyosarcoma cells", Cell Death Discovery, 2019

3 2% match (publications)
Peter Y. Yu, Denic C. Guttridge. "Dysregulated Myogenesis in Rhabdomyosarcoma", Elsevier BV, 2017

4 1% match ()
Cell Death Discov. 2019 Jan 28; 5:60

5 1% match (publications)
Fuchs, Yaron, and Hermann Steller. "Live to die another way: modes of programmed cell death and the signals emanating from dying cells", Nature Reviews Molecular Cell Biology, 2015.

6 < 1% match (publications)
Aliwaini, Saeb, Jenna Bleloch, Serah Kimani, and Sharon Prince. "Induction of Autophagy and Apoptosis in Melanoma Treated With Palladacycle Complexes", Autophagy Cancer Other Pathologies Inflammation Immunity Infection and Aging, 2016.

7 < 1% match (publications)
Stephen X. Skapek, Andrea Ferrari, Abha A. Gupta, Philip J. Lupo et al. "Rhabdomyosarcoma", Nature Reviews Disease Primers, 2019

8 < 1% match (student papers from 11-Apr-2016)
Submitted to University of Cape Town on 2016-04-11

9 < 1% match (publications)
Jenna S. Bleloch, Reyna D. Ballim, Serah Kimani, Jeannette Parkes, Eugenio Panieri, Tarryn Willmer, Sharon Prince. "Managing sarcoma: where have we come from and where are we going?", Therapeutic Advances in Medical Oncology, 2017